THE UNIVERSITY OF READING

Department of Mathematics and Statistics
Department of Food and Nutritional Sciences

Mathematical Modelling of Low Density Lipoprotein Metabolism. Intracellular Cholesterol Regulation

---

Bonhi Shikha Bhattacharya

May, 2011

Thesis submitted for the degree of Doctor of Philosophy

Abstract

In this thesis we study the biological problem of high plasma cholesterol levels. These levels are widely acknowledged as a major risk factor in the development of coronary heart disease. For this purpose we study the genetic regulatory mechanism responsible for liver cell cholesterol homeostasis. Cellular cholesterol concentration has important ramifications on the ability of the liver to clear cholesterol containing low density lipoprotein particles from the plasma efficiently. Failure to do so results in elevated plasma cholesterol.

We present a mathematical model involving nonlinear ordinary differential equations describing the genetic regulation of enzyme synthesis. This regulation is effected via a two step feedback inhibition mechanism specifically applicable to biochemical pathways involved in the maintenance of cell cholesterol. The inhibitory process involves end product repression mediated by a transcription factor and is described by a Hill function. The Hill coefficients of the model we derive are biologically feasible, in contrast with other models derived in a similar manner. Model analysis and results illustrate that this model system can generate self sustained, small amplitude limit cycles. These results suggest that the process of homeostasis may be dynamic, characterised by oscillatory solutions, as opposed to the traditional steady state viewpoint.

We conclude by integrating the genetic regulation model with a previously derived model of low density lipoprotein receptor mediated uptake. Numerical solutions of this integrated model demonstrate that oversimplification of the subcellular processes may obscure behaviour at the cellular level. The integrated model is used to investigate and make conclusions on the regulatory response of the cell for a number of genetic mutations responsible for the condition familial hypercholesterolaemia.

Declaration

I confirm that this is my own work and the use of all material from other sources has been properly and fully acknowledged.

Bonhi Bhattacharya

Acknowledgements

First and foremost my sincere thanks to all of my academic supervisors at the University of Reading. I thank Dr. Kim Jackson and Dr. Anne-Marie Minihane from the Department of Food and Nutritional Sciences for their valuable guidance and biological expertise.

I would also like to thank all who have participated from Unilever Research Colworth (Biosciences) for their helpful suggestions throughout the course of this thesis. I acknowledge the generous financial support of both Unilever and the BBSRC.

I would like to thank Dr. Marcus Tindall from the Department of Mathematics and Statistics for his infectious enthusiasm about mathematical biology and for his exemplary supervision. I would also like to thank Dr. Peter Sweby from the Department of Mathematics and Statistics, not only for his excellent academic supervision, but for additionally going above and beyond that which one would normally expect from a supervisor. And, to all my supervisors, for their remarkable support and patience through some difficult times, I am incredibly grateful.

Many thanks also to all the wonderful friends, my surrogate family, I have made during my time here. Thanks to all those at the University of Reading, especially Stewart, for helping me enjoy the world of mathematics. And thanks to all those away from acadaemia, especially Lauren, for reminding me that there is a world outside of mathematics!

Finally, I would like to thank those whom I love, and for whom this thesis is written. You have been unarguably the reason for all that I have achieved so far and all that I will continue to achieve. I thank my sister, Millie, for all her help and more than occasional medical expertise which, given my natural affinity for calamity, has been invaluable! I thank Alex, for all his love, for all his support, and for all the anxiety, irritability and unreasonableness he has so patiently endured. I thank him for making me smile when I didn't think I could, for making me work when I tried so desperately to avoid it, and for the sacrifices he has so willingly made.

And, most importantly, I thank my mother, Manju, and my father, Jnan, who have been there for every step of my seemingly endless university studies; thank you is not enough. Not one word here could have been written without the significant encouragement and support they have given me. **This is for you**.

Contents

Figures

Tables

Abbreviations

APO-B100	Apolipoprotein B100
CHD	Coronary Heart Disease
CM	Chylomicron
CVD	Cardiovascular Disease
ER	Endoplasmic Reticulum
FFA	Free Fatty Acid
FH	Familial Hypercholesterolaemia
HDL	High Density Lipoprotein
HMG-CoA	3-hydroxy-3-methylglutaryl coenzyme A
HMGR	3-hydroxy-3-methylglutaryl coenzyme A Reductase
IDL	Intermediate Density Lipoprotein
LDLR	Low Density Lipoprotein Receptor
LDL	Low Density Lipoprotein
RME	Receptor Mediated Endocytosis
SCAP	SREBP Cleavage Activating Protein
SREBP	Sterol Regulatory Element Binding Proteins
SSD	Sterol Sensing Domain
TG	Triglyceride
VLDL	Very Low Density Lipoprotein

1

Introduction

The aim of this thesis is to create and investigate a mathematical model which describes the biological mechanism of cellular cholesterol homeostasis (physiological regulation to ensure stability in response to fluctuations in the outside environment) within hepatocytes (liver cells). Why is this particular mechanism of significance? Abnormal control of cholesterol levels within hepatocytes can lead to aberrant processing of dietary cholesterol by the liver. Consequential high levels of circulating plasma cholesterol are widely acknowledged as a major risk factor for coronary heart disease (CHD).

CHD refers to the failure of the coronary circulation to adequately supply blood (and therefore nutrients and oxygen) to the cardiac muscle and surrounding tissue. Disruption of blood flow to the heart clinically manifests itself in symptoms of worsening severity. This ranges from re-

duced flow (ischaemia) causing angina pectoris (chest pain), to a complete blockage of blood flow where the resultant death of heart muscle can lead to myocardial infarction (heart attack). If severe enough, complete cessation of blood flow to an area of the heart can lead to sudden death. CHD falls within the general class of disorders of the heart and blood circulatory system (the cardiovascular system) known as cardiovascular disease (CVD). In addition to CHD, CVD describes some major clinical conditions, including hypertension (raised blood pressure) and cerebrovascular disease (disruption of blood supply to the brain causing stroke).

Both CVD and CHD are a significant concern for health. Each year, over 4.3 million deaths in Europe are caused by CVD accounting for nearly half of all mortality (European Heart Network). As illustrated in Figure 1.1, CVD is also the main cause of mortality in the UK, resulting in more than one in three deaths each year.

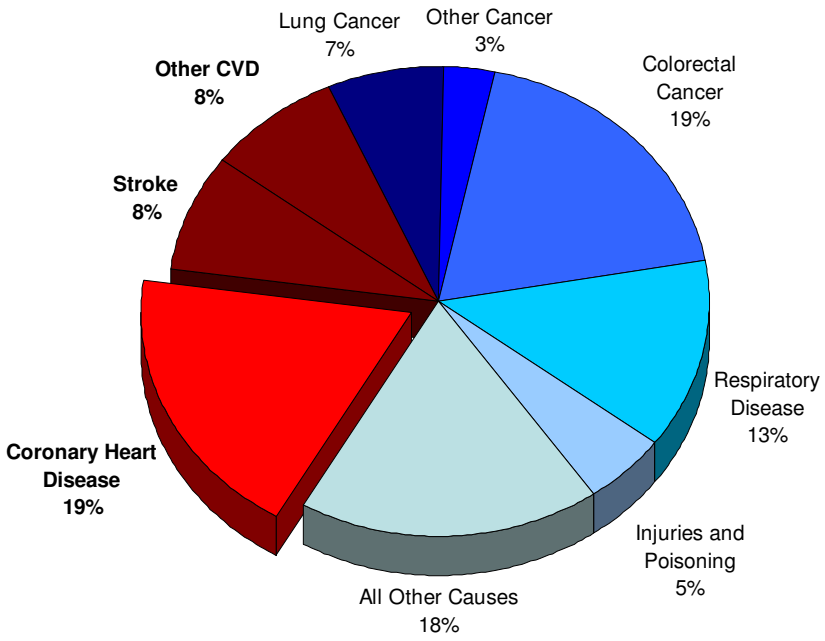

Fig. 1.1: Mortality by cause in 2006 for men in the United Kingdom. The red segments represent deaths as a result of cardiovascular disease, of which deaths from coronary heart disease constitute the majority. (Data adapted from British Heart Foundation Statistics (British Heart Foundation, b)).

In particular, approximately 45% of all deaths from CVD are directly attributable to CHD. CHD by itself is the most common cause of both mortality and premature mortality (death before the age of 75) in the UK, with statistics indicating that one in five men and one in seven women die

as a result of the disease (British Heart Foundation, b).

Aside from these major human costs, the economic consequences of CVD for the UK are substantial. In 2006 alone, CHD was estimated to have cost the UK economy approximately nine billion pounds, in terms of direct and indirect health care and productivity loss due to associated mortality and morbidity in those of working age (British Heart Foundation, a).

Statistics from the World Health Organisation suggest that since 1990 more people have died from CHD than from any other single cause (World Health Organisation). CHD risk is determined by a range of non-modifiable and modifiable risk factors which contribute to the development of underlying pathology leading to morbidity. Non-modifiable risk factors include genetic predisposition, age, gender and ethnicity. Modifiable risk factors include, for example, body weight, blood lipids and blood pressure which can be influenced by lifestyle choices such as smoking, exercise levels and diet. Of particular concern are plasma cholesterol levels which can be altered by changing dietary fat composition including dietary cholesterol intake.

The bulk of dietary cholesterol is delivered to the liver in the form of complex molecules called lipoproteins. Lipoproteins enter hepatocytes via a specialised uptake pathway known as receptor mediated endocytosis (RME). Once within the cell, lipoproteins are catabolised (broken down) to release their cholesterol content. This clearance pathway of lipoprotein from the plasma, and hence circulating plasma cholesterol level, is controlled by the intracellular concentration of cholesterol.

Understanding the mechanisms involved in the biological process described above is therefore crucial to understanding how plasma cholesterol levels are determined. This in turn can lead to a better understanding of how to reduce these levels which may contribute to more effective intervention against the initial development of CHD.

In conjunction with the inaccessibility of the liver as an organ, the importance of the liver in whole body metabolism complicates *in vivo* (within a living organism) biological investigation. While *in vitro* (within a controlled environment e.g. test tube) experiments can provide us with significant insight, the advantage of mathematical modelling lies in the provision of an approach

whereby the effects of certain system parameters, and their perturbation, can be examined both quickly and cost effectively. This approach can help to clarify the underlying mechanisms of a biological process, and further, can be used to identify and investigate parameters which would not be easily isolated by experimental means. These methods can also provide direction for future biological investigation.

1.1 Thesis outline

In Chapter 2 of this thesis we review the biology underlying cholesterol, lipoproteins and CHD. This chapter begins with a description of the role of high plasma cholesterol in the development of CHD. The structure and function of lipoproteins is discussed and the link between lipoprotein cholesterol and CHD risk is emphasised. This is followed by a brief overview of lipoprotein metabolism in which we describe the formation of lipoproteins, their transport through the plasma and their eventual uptake and metabolism by the liver. The subsequent alteration in intracellular cholesterol concentration, and the means by which this is managed by the cell completes the biological discussion. The chapter concludes with a review of the existing mathematical models in this area.

The regulation of intracellular cholesterol, which controls both cholesterol uptake via lipoprotein and *de novo* (from new) cholesterol synthesis within the cell, occurs at the level of the gene. Chapter 3 introduces the fundamental biological concepts of gene expression or protein synthesis, as well as reviewing some primary mathematical approaches related to modelling of gene regulatory networks. Notable modelling approaches including Boolean networks, Hill functions and ordinary differential equations (ODEs).

This provides a prelude to the development of an ODE model of gene expression in the context of cholesterol and lipoprotein metabolism. In the second part of this chapter, the concept of transcription factors in relation to cholesterol homeostasis is introduced. The gene expression model derived in the first part of this chapter is then extended to take into account the processes involved in transcriptional control of protein synthesis. Hence, we create a three variable ODE

model of regulated gene expression which is used to describe cholesterol biosynthesis within the cell; this model is parameterised, where possible, using predominantly *in vitro* experimental data.

In Chapter 4 we consider an analytic investigation of the cholesterol biosynthesis model. The stability of the unique, physiologically valid, steady state of the system is analysed and we consider firstly the case in which the steady state may be stable; either the system tends directly to this steady state or undergoes oscillatory convergence to steady state. Secondly, we consider the case in which the system exhibits limit cycle behaviour giving rise to oscillatory solutions. This indicates the existence of a local bifurcation, in the dynamics of the system, called a Hopf bifurcation and its existence is proved for critical parameter values.

The oscillatory solution is further analysed by the reduction of the three variable model to two variables using Centre Manifold Theory. The resulting two dimensional model is then expressed in polar coordinates and, using averaging, we identify the stability of the oscillations. Expressions describing the amplitude and period of the oscillations are also derived. The analytic results obtained here are discussed in the biological context of homeostasis and of existing gene expression models.

In Chapter 5 we present numerical solutions of the cholesterol biosynthesis model. The first half of this chapter contains numerical results which support the analytical findings of Chapter 4. In the second half of this chapter we explore the regions of parameter space for the parameters which were not able to be derived from experimental data. For these undetermined parameters, the results indicate that the genetic regulation model is much more sensitive to degradation rates than to parameters which reflect the chemical structure of the reactions.

In Chapter 6 the genetic regulation model that has been the subject of this thesis thus far, is integrated with an existing model of the receptor mediated uptake of low density lipoprotein structure, previously discussed in Chapter 3. The lack of experimental data available in this area for both parameter estimation and validation make quantitative analysis problematic. However, we use the integrated model to make qualitative conclusions about the nature of cellular response to incoming lipoprotein cholesterol. These results suggest that the oversimplification of

the genetic pathways regulating these processes may mask behaviour occurring at long times. In the final part of this chapter, we use our integrated model to investigate cellular responses to disease states, in particular those pertaining to the disease familial hypercholesterolaemia.

Finally in Chapter 7 we summarise the overall implications of this work and discuss avenues for further investigation. The appendices provide details on mathematical results employed in this thesis together with calculations used in deriving the parameter values of the models contained within.

A glossary of the major biological terms appearing throughout the thesis is included as a reference for the reader.

2

Coronary Heart Disease, Lipoproteins and Cholesterol Metabolism

In order to develop our mathematical model we must first fully understand the biological processes we wish to model. In this chapter we begin by summarising the principal physiological processes involved in lipoprotein and cholesterol metabolism. Following this, some of the existing mathematical models in this area are briefly reviewed. We begin by describing how high plasma cholesterol levels are linked to the development of CHD.

High levels of circulating cholesterol predispose human blood vessels to atherosclerosis, the accumulation of cholesterol deposits within the walls of the vessels. Proliferation of these deposits in the walls of arteries is the pathological basis of this progressive, chronic inflammatory process.

The inner surfaces of arteries are lined by a single layer of semi-permeable endothelial cells, the principal function of which is to form a physical barrier between the artery wall and blood flowing through the artery lumen. Damage to the endothelial wall increases its permeability and allows larger, cholesterol containing molecules to enter the space between the artery lumen and the arterial wall. Endothelial injury also causes vascular inflammation, and the interaction between the inflammatory response mechanism, increased permeability and numerous other factors, eventually results in the formation of lesions known as plaques. These plaques grow and expand outward into the lumen of the artery, gradually causing occlusion as illustrated in Figure 2.1(a). As a result, blood flow through these arteries is reduced compromising oxygen supply to organs supplied by the affected blood vessels (Falk, 2006; Ross, 1999).

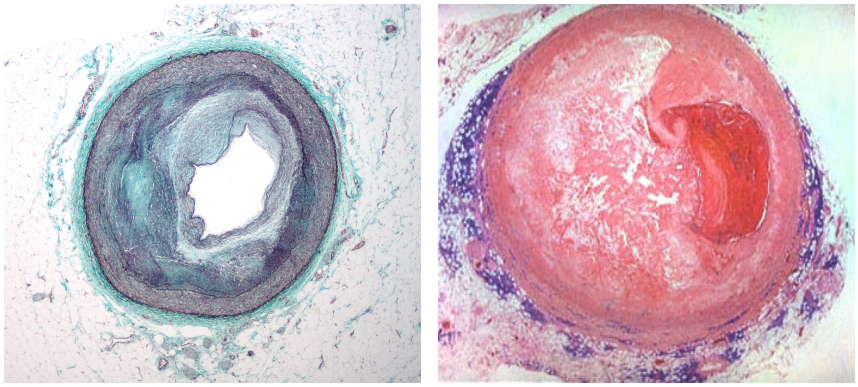

(a) Partial occlusion of an artery lumen. (b) Complete occlusion of an artery lumen.

Fig. 2.1: Microscopic arterial cross sections illustrating lumen stenosis occurring due to atherogenesis. Figure 2.1(a) illustrates a partial blockage of the artery lumen due to plaque formation, the section of the artery shown has only 25% - 35% of the area it once had (Image courtesy of Nephron). In Figure 2.1(b) the mottled white region indicates the plaque while the dark red area to the right of the artery lumen illustrates a thrombus causing complete blockage of the artery (`http://pathcuric1.swmed.edu/PathDemo/cvd1/cvd130.htm`).

During the final stages of atherogenesis (the development of atherosclerosis), disruption of the plaques can initiate a series of coagulation events causing thrombus (blood clot) formation (Davies et al., 1993). This may lead to the complete blockage of arteries as seen in Figure 2.1(b). Atherosclerosis is the most common cause of disturbance to blood flow in CHD and estimates have indicated that over 60% of CHD in developed countries is due to total plasma cholesterol levels in excess of a theoretical recommended value.

Current European medical guidelines for blood lipids advise that the total plasma cholesterol level should be no more than 5.0 mmol/l. In conjunction with this, explicit recommendations are made for levels of *low density lipoprotein* (LDL) cholesterol levels, which should ideally fall under 3.0 mmol/l (Graham et al., 2007).

What is a lipoprotein? In the next section we discuss the structure and biological function of lipoproteins and highlight the reason why LDL cholesterol levels are such a concern for cardiovascular health.

2.1 Lipoproteins and lipoprotein metabolism

Owing to the insoluble nature of cholesterol and other lipids in the plasma, their redistribution throughout the body requires specialised carriers which are capable of solubilising and transporting them. This is the function of the lipoproteins; macromolecular aggregates of lipid and proteins held together by noncovalent forces, as illustrated in Figure 2.2.

Lipids, mainly triglycerides (TGs), and sometimes smaller amounts of esterified cholesterol, are packaged into a core surrounded by a monolayer surface unique to lipoproteins. This surface is composed mainly of phospholipids and smaller amounts of free cholesterol and protein.

Phospholipids have a dual or amphipathic nature. Their hydrophobic tails, which are repelled by water, are positioned toward the core of the particle. Their hydrophilic heads, which are attracted by water, are aligned toward the surface. This creates a spherical particle by which insoluble lipids are thus able to move through the plasma.

The protein molecules interwoven within the monolayer surface are known as apolipoproteins. Apolipoproteins have three major roles as part of lipoprotein structure. Firstly, they act as ligands (binding agents) for various lipoprotein receptors found on the surface of cells. As such they are involved in the transport and redistribution of lipids amongst tissues by allowing the delivery of a particular lipoprotein to the location required for its metabolism. Secondly, they act as cofactors or activators for lipolytic enzymes involved in lipoprotein metabolism.

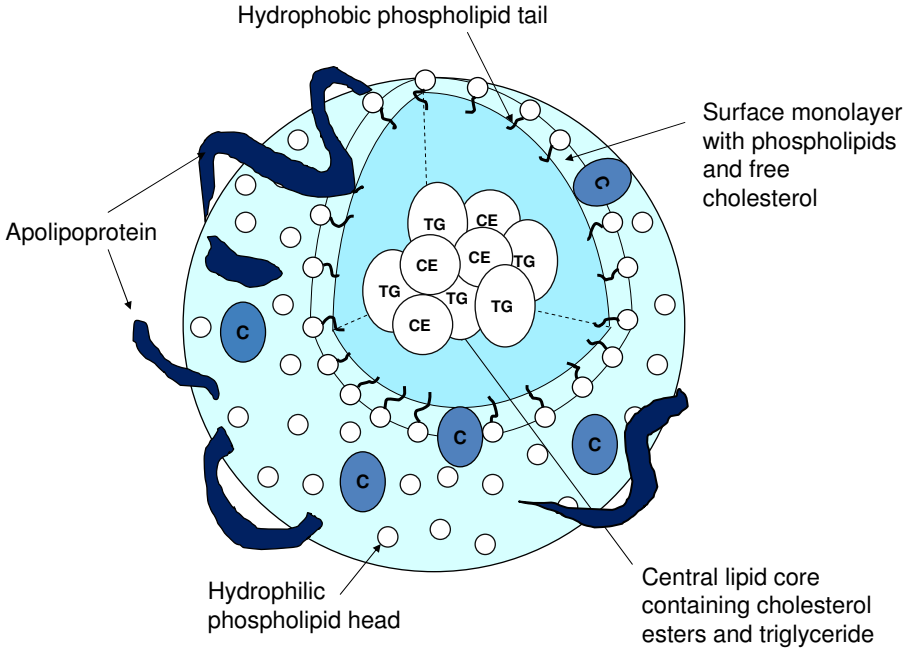

Fig. 2.2: A schematic illustration of the structure of a lipoprotein molecule. The inner lipid core of triglyceride (**TG**) and cholesterol esters (**CE**) is surrounded by a surface layer of phospholipids (**P**), free cholesterol (**C**) and interwoven apolipoproteins.

Apolipoproteins are also amphipathic in nature; their hydrophobic sections interact chemically with TGs and cholesterol ester within the lipoprotein core whilst their hydrophilic sections bind with the surface phospholipids. In doing so they fulfil their third role, which is to confer structural stability to the lipoprotein molecule.

Lipoproteins have traditionally been separated into operational fractions dependent on their physical properties, for eexample, density, size and electrophoretic mobility (which reflects the electric surface charge of the particle). It is important to note that divisions are arbitrary; heterogeneity exists within lipoprotein classes due to differing amounts and types of lipids. This separation results in a widely accepted division of lipoproteins into five major classes, chylomicrons (CM), very low density lipoproteins (VLDL), intermediate density lipoproteins (IDL), low density lipoproteins (LDL), and high density lipoproteins (HDL). The average composition of each type of lipoprotein with respect to the major lipids, together with average sizes and densities, is illustrated in Figure 2.3.

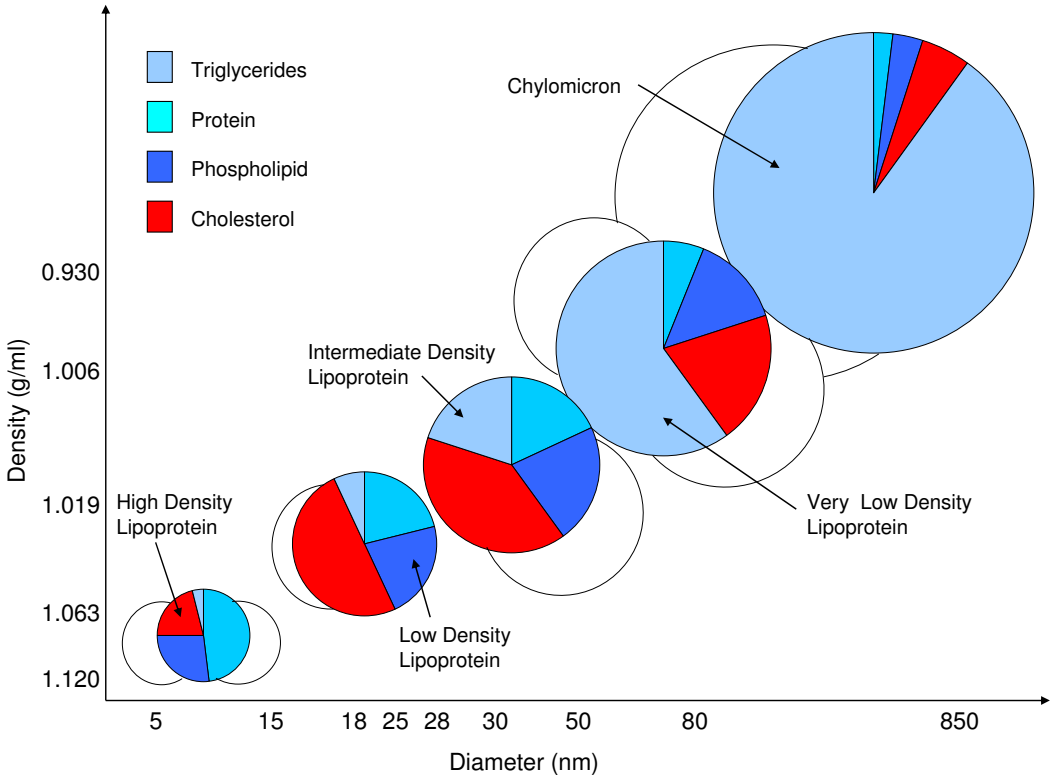

Fig. 2.3: Major lipoprotein classes, their physical properties and composition. Densities are measured in g/ml and size is calculated in nm. The fraction of average protein and lipid amounts present in each particle is illustrated as a percentage of the total composition.

2.1.1 LDL cholesterol and CHD risk

Figure 2.3 illustrates that cholesterol is the predominant lipid in LDL and accounts for approximately 50% of the particle composition. The role of LDL as the major cholesterol carrying lipoprotein identifies plasma LDL-cholesterol levels as a serious risk factor in the development of CHD (Tabas, 2008).

Epidemiological cohort studies have consistently demonstrated that LDL-cholesterol levels are related to CHD risk. These include, for example, the Framingham Heart Study, a long term (three generation) cardiovascular study of the residents of the town of Framingham, Massachussetts (Framingham Heart Study).

The Multiple Risk Factor Intervention Trial, a CHD prevention study designed to assess the combined influence of various risk factors has also provided valuable insight (Stamler et al., 1986).

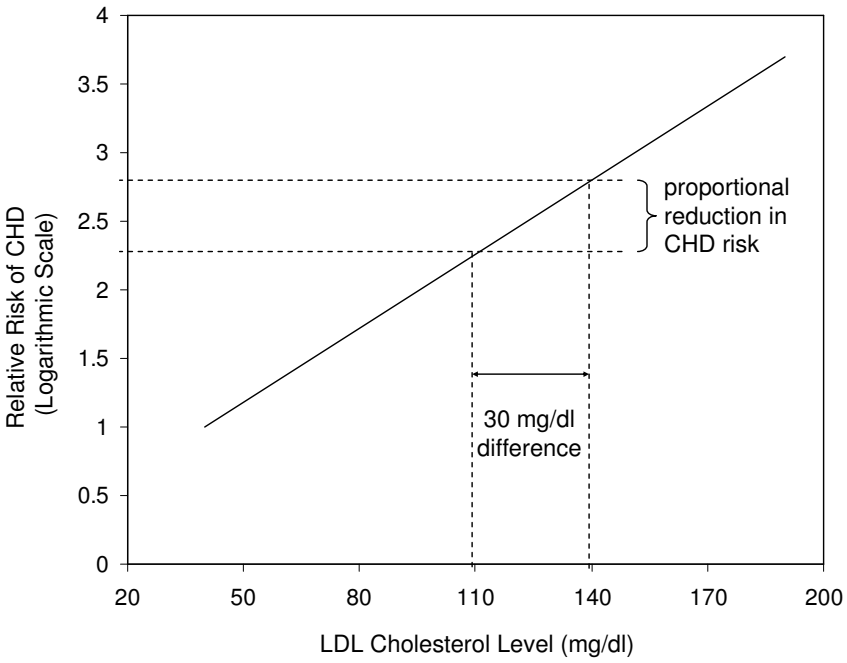

Fig. 2.4: Log-linear relationship between LDL cholesterol levels and relative risk for CHD as reported in Grundy et al. (2004). Every 30 mg/dl increase or decrease in LDL cholesterol corresponds to the relative risk for CHD increasing or decreasing in proportion by roughly 30%. The relative risk is set at 1.0 for an LDL cholesterol concentration of 40 mg/dl.

Figure 2.4 illustrates the log-linear correlation between plasma LDL cholesterol levels and the relative risk for CHD as demonstrated in both epidemiologic data and LDL cholesterol lowering therapy clinical trial data (Grundy et al., 2004).

This relationship suggests that a given absolute reduction in plasma LDL cholesterol levels will produce an equivalent reduction in the relative risk of CHD. For this reason quantities of circulating LDL are a major target for improving cardiovascular health and the primary focus for lipid lowering therapies.

Lifestyle education and pharmaceutical treatments, all developed to aid reduction of both total and LDL cholesterol levels, have achieved some success in decreasing the prevalence of raised

cholesterol. However, proportions of the population with cholesterol levels at or above the recommended levels remain substantially high. Effective interventions for the lowering of plasma LDL cholesterol levels thus remain an important strategy for reducing the burden of CVD and CHD internationally.

To understand how LDL cholesterol levels in the plasma are determined requires an understanding of how LDL is metabolised. LDL concentration within the plasma is determined by the balance of its entry to and removal from the circulation; this forms part of the lipoprotein metabolic pathway.

Conceptually the metabolism of lipoproteins is divided into three non distinct pathways dealing with the transport of dietary lipids (exogenous pathway), the transport of endogenously synthesised lipids (endogenous pathway), and finally reverse cholesterol transport.

2.1.2 Lipoprotein metabolism

In this section we provide further biological details of the lipoprotein metabolic process. We begin with a description of the mechanisms resulting in dietary cholesterol uptake, more commonly known as the exogenous pathway of lipoprotein metabolism.

Exogenous lipoprotein metabolism

Exogenous lipoprotein metabolism describes the transport of dietary lipids, that is, lipids originating from outside the liver. The bulk of these take the form of TGs whilst the remainder are composed of cholesterol, free fatty acids (FFAs) and phospholipids. These lipids undergo various biochemical processes to create micelles that can be directly absorbed from the lumen of the small intestine into the blood.

Here, these lipids are incorporated with apolipoprotein B48 and their amalgamation synthesises nascent CMs. Nascent CMs are secreted into the lymphatic system before entering the bloodstream where they accept other apolipoproteins to become mature CMs (van Greevenbroek and

de Bruin, 1998). Immediately on maturation, these newly acquired apolipoproteins, in particular apolipoprotein CII, activate lipoprotein lipase. This lipolytic enzyme catalyses the hydrolysis of TGs in the lipoprotein core producing FFAs which are taken up by the surrounding tissue (e.g. skeletal muscle or adipose tissue).

The subsequent decrease in core size leads to the formation of cholesterol enriched CM remnants (Goldberg, 1996). These remnants then travel to the liver to undergo clearance as shown in Figure 2.5. Following uptake by the liver, the remaining CM lipids are hydrolysed to liberate FFAs, and cholesterol which is ultimately utilised in the synthesis of VLDL (Redgrave, 2004).

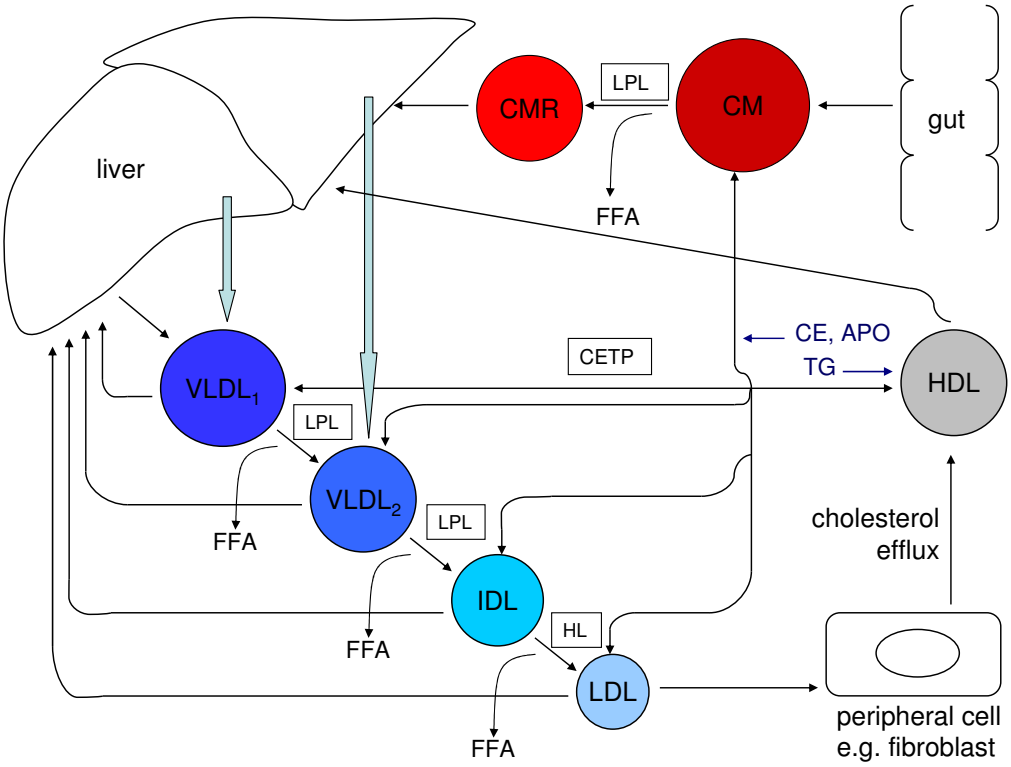

Fig. 2.5: The pathways of lipoprotein metabolism. Exogenous lipoprotein metabolism describes the fate of dietary cholesterol via the chylomicron pathway (red molecules); endogenous lipoprotein metabolism deals with the metabolism of VLDL synthesised within the liver (blue molecules); reverse cholesterol transport describes the HDL pathway (grey molecule) which explains the movement of cholesterol from the peripheral cells. (**CMR**: chylomicron remnant; **HL**: hepatic lipase; **LPL**: lipoprotein lipase; **CETP**: cholesterol ester transfer protein; **CE**: cholesterol ester; **APO**: apolipoprotein; **TG**: triglyceride; **FFA**: free fatty acids).

Endogenous lipoprotein metabolism

The endogenous pathway of lipoprotein metabolism refers to the hepatic secretion and subsequent metabolism of VLDL, that is, lipids which originate in the liver. The process of VLDL synthesis is similar to that of CMs, but in contrast to CMs, VLDL carry only apolipoprotein B100 (APO-B100) on their surface. They also have a significantly higher ratio of cholesterol to TG content. The liver is generally thought to give rise to two major subfractions of nascent VLDL, one of which is the initially assembled $VLDL_2$ particle, TG poor but high in cholesterol ester (CE) (Olofsson et al., 1999). $VLDL_1$ is produced from $VLDL_2$ by bulk lipidation. This addition of an extra TG load is dependent on hepatic TG availability. $VLDL_1$ thus has a smaller ratio of cholesterol to TG than $VLDL_2$.

Nascent VLDL particles secreted by the liver acquire other apolipoproteins on their release into the bloodstream and become mature VLDL. Almost immediately, this results in the activation of lipoprotein lipase, leading to a depletion of the VLDL TG content. The resulting decrease in the size of the VLDL particle causes its density to increase and the TG depleted VLDL falls into the density range of IDL particles.

Approximately half of the IDL thus produced is cleared by the liver. The remaining IDL is subject to the action of hepatic lipase, another lipolytic enzyme, causing further depletion of both TG core content and core cholesterol esters (Nicoll and Lewis, 1980). This creates LDL particles with a high cholesterol to TG content ratio, whose primary function is the delivery of cholesterol to peripheral cells.

The delipidation cascade described above does not consistently occur via a single pathway, instead parallel routes exist (Millar and Packard, 1998). $VLDL_1$ does not always completely delipidate to LDL. Cessation can occur in the $VLDL_2$ and IDL ranges where these remnants either persist in the circulation or are slowly converted to LDL. Small amounts of $VLDL_1$ may be cleared by direct removal from the circulation. $VLDL_2$ can be either directly cleared or metabolised quickly to form LDL which is cleared rapidly from the circulation (Packard et al., 1984; Packard and Shepherd, 1997). This occurs either by delivery to the liver or to peripheral cells such as fibroblasts or adrenal tissue, as illustrated in Figure 2.5.

Reverse cholesterol transport

The reverse cholesterol transport pathway describes the movement of cholesterol from the peripheral cells governed by HDL (Tall, 1990). HDL's primary function is as an extracellular cholesterol acceptor, removing excess cholesterol from various tissues and delivering it to the liver (see Figure 2.5). This occurs by one of two possible routes.

Firstly, HDL lipids can be directly taken up by the liver in a selective uptake process in which the lipoprotein is not internalised. Secondly, by the action of the cholesterol ester transfer protein, HDL cholesterol ester may be exchanged for the triglycerides contained in VLDL, IDL and LDL; these particles are subsequently cleared by the liver.

Synonymous to the three pathways described above is the final step of clearance of the relevant lipoproteins. Almost all cells have the capability to do this. However, via the conversion of cholesterol to bile acids, the liver is the only organ through which cholesterol can be eliminated from the body. For this reason, hepatocytes play a major role in whole body LDL metabolism and defective hepatic LDL uptake is associated with elevated circulating LDL cholesterol concentrations.

The next section reviews the major pathway responsible for the hepatic uptake of LDL.

2.1.3 Hepatic lipoprotein uptake and receptor mediated endocytosis

Although nonspecific means of lipoprotein entry exist, the predominant mechanism involved in the uptake of LDL cholesterol by hepatocytes is the receptor mediated endocytosis (RME) pathway, which is regulated by the LDL receptor (LDLR) and is illustrated in Figure 2.6.

LDLRs are biosynthesised in the cell and are surface receptor proteins responsible for specific binding and internalisation of LDL. They were originally identified during studies of the disease familial hypercholesterolaemia by Goldstein and Brown (1977), which led to the identification of the major steps of the RME pathway (Brown and Goldstein, 1979; Goldstein et al., 1979).

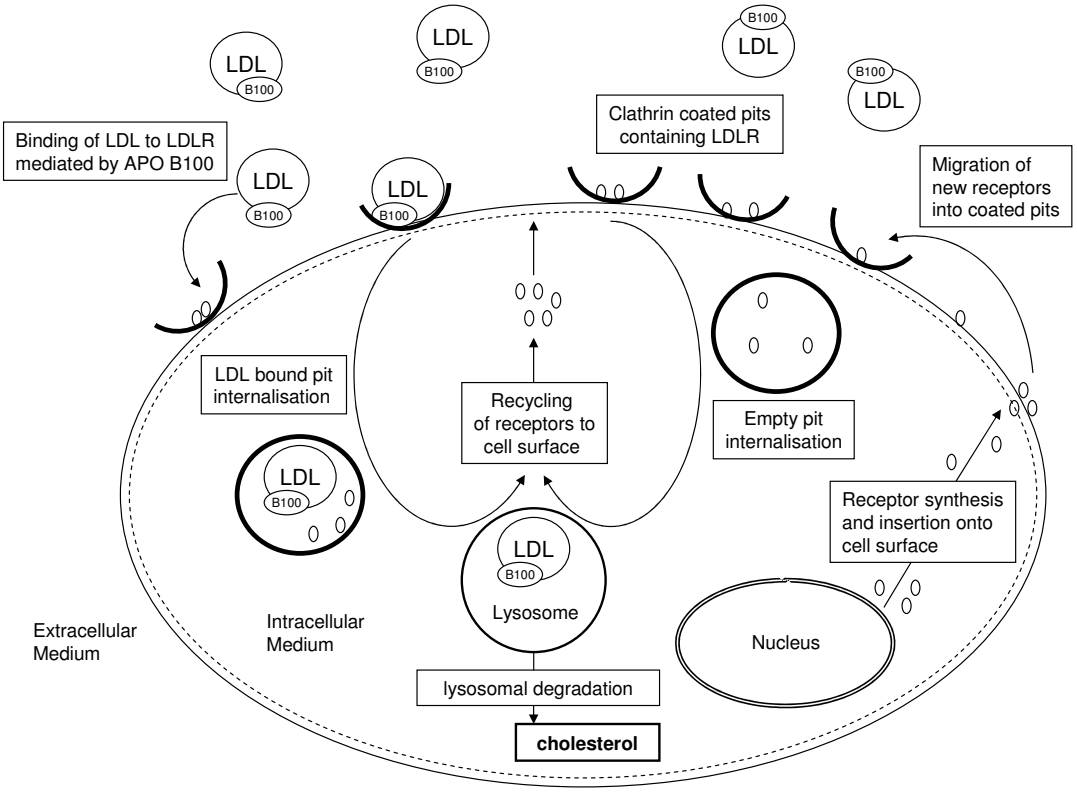

Fig. 2.6: Receptor mediated endocytosis in a hepatocyte illustrating LDL binding, internalisation and its subsequent degradation. LDL binds to the LDLR situated in clathrin coated pits on the cell surface. It is then internalised together with the receptor it is bound to. Within the lysosome LDL is broken down releasing degradation products; the receptor is either also degraded or is recycled to the cell surface. Receptors are newly synthesised within the cell and inserted onto the cell membrane (**B100**: Apolipoprotein B100).

RME is the sequential mechanism of lipoproteins binding to the surface of the cell, and their subsequent internalisation into the cell, where they are eventually degraded. The process begins with the binding of LDL to the LDLR. This binding is mediated by APO-B100, the only apolipoprotein present on the surface of the LDL particle.

Newly synthesised LDLR are inserted directly into the cell surface where they cluster in clathrin coated pits. APO-B100 directs and attaches LDL to the APO-B100 binding site on the LDLR. LDL containing clathrin coated pits then invaginate into the cell, pinch off, and form coated endo-

cytotic vesicles which are internalised. Pits empty of LDL also undergo this process. Following internalisation, the clathrin coat is shed and vesicles fuse together to form larger endosomes, within which the LDL dissociates from the receptor. In the next step, either some receptors are recycled and returned to the cell surface or the receptors remain in the endosome. The endosomes fuse with lysosomes within the cell and and the contents are degraded by lysosomal enzyme hydrolysis (Goldstein et al., 1985). This degradation releases amino acids and cholesterol for use in cellular metabolism.

The mechanisms of lipoprotein metabolism described thus far end at the endocytosis of LDL into the cell, resulting in the entry of exogenous cholesterol. However, this is not the sole contributor to intracellular cholesterol concentration. The next section considers levels of cholesterol within the cell and how they are maintained.

2.2 Intracellular cholesterol

This section begins with a discussion of the endogenous cholesterol production within the cell and reviews the biochemistry of the *de novo* synthesis of cholesterol (synthesis of the complex cholesterol molecule from simpler constituent molecules). Following this, mechanisms by which the cell maintains its cholesterol level are discussed.

2.2.1 Cholesterol biosynthesis

Slightly less than half of the body's cholesterol content derives from *de novo* synthesis of which 10% of the amount produced each day is accounted for by the liver. It is the major contributor to the hepatocyte cholesterol content. The process itself begins with substrates of acetyl-CoA and acetoacetyl-CoA. These substrates are commonly found in all cells as the products of various cellular metabolic reactions. As an example, they are derivatives of fatty acid metabolism (Bloch, 1965).

The initial step of cholesterol synthesis consists of the formation of 3-hydroxy-3-methylglutaryl

coenzyme A (HMG-CoA) controlled by the enzyme HMG-CoA synthase.

$$2\ \text{acetyl-CoA} + \text{acetoacetyl-CoA} \xrightarrow{\text{HMG-CoA synthase}} \text{HMG-CoA}\,.$$

The next step in the reaction involves the formation of mevalonic acid from HMG-CoA in a reaction catalysed by the enzyme HMG-CoA reductase (HMGR).

$$\text{HMG-CoA} \xrightarrow{\text{HMG-CoA reductase (HMGR)}} \text{Mevalonate}\,.$$

Mevalonate is subsequently converted, via a number of intermediate reactions to squalene. This last reaction is catalysed by squalene synthase, the first enzyme in the pathway strictly devoted to the formation of sterol. Squalene is eventually converted to cholesterol, which requires a series of twenty additional steps (Myant, 1981).

The rate-limiting, or slowest step of this thirty step biosynthetic pathway, is the reduction of HMG-CoA in the step catalysed by HMGR. As such this enzyme is subject to complex regulatory controls. The rate of cholesterol production is therefore governed by the rate of production of mevalonic acid; HMGR thus being the key protein involved in endogenous cholesterol production.

In view of the fact that a cell can both produce its own cholesterol and receive it from endogenous sources, we may now ask whether there exists an upper bound on the concentration of cholesterol that a cell can contain.

2.2.2 Intracellular cholesterol homeostasis

Cholesterol is an essential constituent of the plasma membrane of mammalian cells and is used for the maintenance of both membrane structural integrity and selective permeability. In addition, it is vital for the proper function of membrane transport processes and enzyme activities (Simons and Iknonen, 2000).

In mammalian cells cholesterol is a metabolic end product; aside from transport reactions,

cholesterol serves only as a reaction product and does not participate in any other biochemical processes. Consequently, cholesterol can accumulate in cells and its overaccumulation results in cellular toxicity. Direct ramifications of excess cholesterol induced toxicity include loss of membrane fluidity (Yeagle, 1991), induction of apoptosis (a process of programmed cell death) (Tabas, 1997), and intracellular cholesterol crystallisation (in which the precipitation of needle-shaped cholesterol crystals damage cells by physically disrupting the integrity of intracellular structures (Tangirala et al., 1994)).

All cells have the capacity to esterify free cholesterol. The esterification reaction, catalysed by the rate-limiting enzyme acyl-CoA cholesterol acyltransferase, produces cholesterol ester from cholesterol and fatty acyl coenzyme A. Cholesterol ester, a neutral lipid stored as droplets in the cell cytosol (the intracellular fluid enclosed by the cell membrane but not held within cellular organelles), allows for a non toxic method of excess cellular cholesterol storage.

Specialised cell types may also channel cholesterol into other pathways. One such example is steroidogenesis; the synthesis of steroid hormones by the adrenal glands and gonads. In particular, hepatic cells can incorporate cholesterol into newly formed lipoproteins or utilise it in the synthesis of bile acids.

Levels of cholesterol which are too low are also cytotoxic; they result in compromised membrane structure and permeability which can be fatal for the cell. It is therefore crucial that cholesterol levels are strictly regulated. Cellular cholesterol homeostasis, the property to keep cholesterol concentration to within narrow ranges results from a balance of three pathways. These are cholesterol influx to the cell, utilisation and efflux of cholesterol from the cell, see Figure 2.7.

Over accumulation or excessive depletion of free cholesterol is prevented by a negative feedback loop that responds to elevations or depressions in intracellular cholesterol (Figure 2.7). This feedback loop exerts the majority of its control by regulating the two key contributors to cellular cholesterol, HMGR and LDLR.

Thus far the biological aspects of lipoprotein metabolism, intracellular cholesterol homeostasis and high levels of plasma cholesterol have been introduced. However, our intention is to cre-

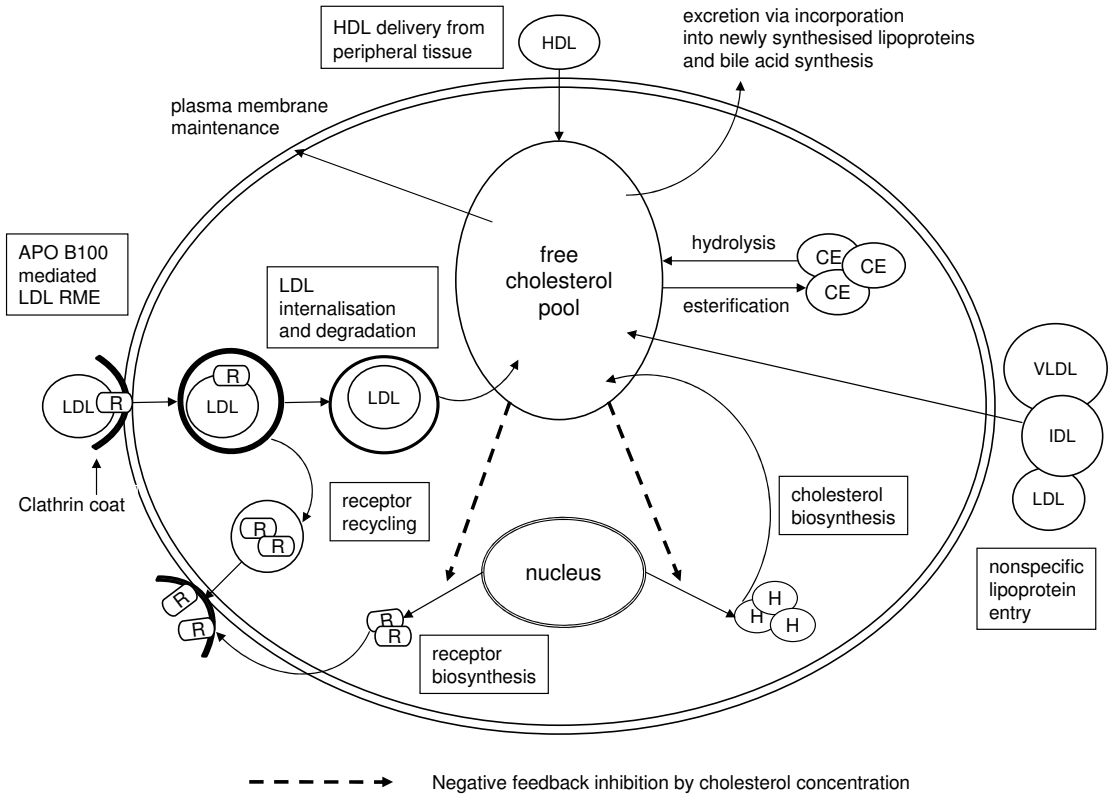

Fig. 2.7: Factors effecting cholesterol balance in the hepatocyte. This diagram illustrates the influx and efflux pathways from a hypothetical pool of free cholesterol within the cell; homeostasis is the balance of these mechanisms. (**CE**: cholesterol ester; **H**: HMGR; **R**: receptor).

ate a mathematical model pertaining to these pathways. Consequently, the literature regarding mathematical modelling in this area is briefly reviewed in the next section.

2.3 Mathematical modelling of lipoprotein metabolism

Previous mathematical modelling of lipoprotein metabolism has varied in both scope and modelling formalism. Extensive modelling has led to an in depth understanding of the processes involved in RME in the context of cell surface receptors and coated pits.

For example, a considerable amount of work exists on the mechanisms by which receptors in-

teract with coated pits on the cell surface. Receptors are inserted randomly on the cell surface following synthesis and must then diffuse until bounded in clathrin coated pits.

The significance of this process lies in the concentration of receptors located in the pits which determine how much LDL can be bound and internalised at any given time.

Goldstein et al. (1981) modelled this mechanism to derive estimates for the diffusion limits of k_{d+}, the forward rate constant for the trapping of LDLRs by coated pits and t_{dc}, the mean time from random insertion of an LDLR into the plasma membrane to its capture by a coated pit.

They considered coated pits as absorbing discs, with radius s, having exponentially distributed lifetimes with mean lifetime $1/\lambda$, and calculated $p(r,t)$, the probability density associated with the LDLR's first arrival at the coated pit's location.

Using $q(r,t)$, the probability density associated with capture at time t of an LDLR initially at distance r from the centre of the coated pit, they arrived at

$$\frac{\partial p(r,t)}{\partial t} = D\blacktriangledown^2 p(r,t), \tag{2.1a}$$

$$q(r,t) = p(r,t)e^{-\lambda t}, \tag{2.1b}$$

where D is the two-dimensional diffusion coefficient for an LDL particle.

Boundary conditions for $p(r,t)$, where b is the outer boundary of the coated pit, are given by

$$p(r,0) = 0 \quad \text{for} \quad s < r \leq b, \tag{2.2}$$

$$p(s,t) = \delta(t), \tag{2.3}$$

$$\partial p(r,t)/\partial r = 0 \quad \text{at} \quad r = b, \tag{2.4}$$

where the final condition treats the outer boundary at $r = b$ as a reflecting wall and δ is the Dirac delta function. The solution of system (2.1) provided $p(r,t)$ with which parameter values for k_{d+} and t_{dc} were estimated.

Similar modelling frameworks were considered in other work investigating receptor trapping by

coated pits (Goldstein et al., 1984; Peacock-Lopez and Ramirez, 1986). Keizer et al. (1985) also derived a related model using statistical mechanic theory of nonequilibrium dynamics. They did not consider that the distribution of receptors around coated pits is random, but rather that this distribution increases with distance from the pit with a characteristic length dependent on kinetic rates of other endocytotic processes.

Echavarria-Heras (1988) and Goldstein et al. (1988) extended these diffusion based models by exploring convection as a candidate for the transport mechanism. They assessed the importance of convective flow in the transport of receptors to coated pits by modelling movement of receptors to coated pits, assuming that receptors can both diffuse on the cell surface and be transported by membrane flow. This created a convection-diffusion equation which was then solved in order to determine parameter values such as the mean time, τ, for a diffusing receptor to reach a coated pit in the presence of membrane flow.

The mechanics of RME have also been investigated, for example in the work of Gao et al. (2005). In order to determine how particle size affects the RME process, they studied how a cell membrane containing diffusive mobile receptors wraps around a coated particle. Their approach modified a diffusion equation describing membrane receptor density during the wrapping process. This results in a Stefan problem; a boundary value problem adapted to the case in which a phase boundary can move with time.

In order to evaluate kinetic parameters such as those involved in ligand receptor interaction and ligand receptor internalisation, Wiley and D (1981) and Gex-Fabry and DeLisi (1984) modelled an RME process in which receptors do not recycle, using the epidermal growth factor receptor as an example. They used an enzyme substrate approach whereby the receptor (R) was considered to be the enzyme and the ligand, epidermal growth factor, (L) was considered to be the substrate as illustrated in (2.5),

$$L + R \rightleftharpoons LR \longrightarrow LR_i. \tag{2.5}$$

Thus they took the association of the ligand with the receptor at the cell surface to be analogous to enzyme substrate complex formation and the internalised receptor ligand complex (LR_i) to be analogous to the product. The resulting ODE models, derived using first order kinet-

ics, were evaluated under the assumption of the existence of a cellular steady state. As such they allowed for the determination of parameter values when compared with experimental data. Further work on these models centred on improving the methods of analysis for determining rate constants. For example, Truskey et al. (1984) considered Scatchard analysis and Bayesian parameter estimation techniques and Wiley and Cunningham (1982) developed specialised graphical analysis forms.

Harwood Jr and Pellarin (1997) extended the enzymatic approach to RME model for application to the LDLR system in which receptors recycle. They added a further step in which the internalised receptor ligand complex dissociates intracellularly with the receptor being recycled to the cell surface. This is similar to the release of the enzyme to participate in further reactions following a catalytic reaction, and is illustrated in (2.6),

$$L + R \rightleftharpoons LR \longrightarrow LR_i \longrightarrow L_i + R. \tag{2.6}$$

Their derived kinetic model enabled determination of rate constants for the LDL RME process. Similar models were developed by Chun et al. (1985) and Yuan et al. (1991), who also considered the means by which the LDL RME process results in cholesterol release into the cell. This allowed for specific fitting of parameters to the experimental results of Goldstein et al. (1979).

The models mentioned thus far concentrate on specific aspects involved in the metabolism of lipoproteins and are useful in both elucidating and quantifying mechanisms of the endocytotic process. However, to further understand the effect of uptake processes in the context of lipoprotein metabolism requires modelling which considers, as much as is possible, the larger reactions involved in the metabolic pathway. An example of this is the use of compartmental models.

Lipoprotein kinetic studies can provide data about the dynamics of physiological processes such as lipoprotein production rates. Traditionally these studies are conducted using stable isotope tracer kinetic studies. The main choice of mathematical model to analyse the resulting data is compartmental modelling. Briefly, a compartment is a mathematical abstract defining a well mixed, kinetically homogeneous amount of material which may or may not correspond to any physiological volume. A compartmental model is a system made up of a finite number of such

compartments interconnected in some specific manner, allowing for the transfer of material from one to another. Such models of lipoprotein metabolism have considered lipoprotein density classes (e.g. VLDL, IDL, LDL) as compartments.

Phenomenological transition rates between these compartments are determined by fitting to data. An example compartmental model as applied to VLDL delipidation is illustrated in Figure 2.8 in which compartment 1 represents the precursor pool of VLDL APO-B100, and compartments 2, 3, and 4 represent VLDL, IDL, and LDL, respectively.

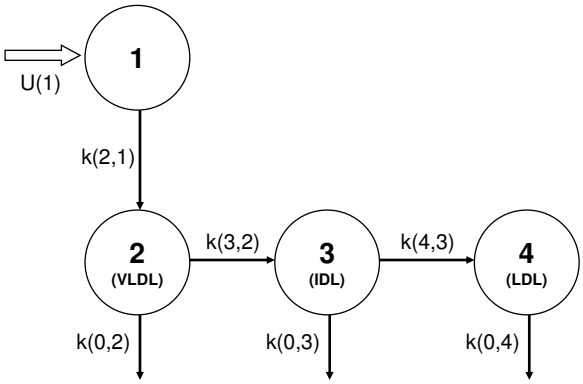

Fig. 2.8: An example three compartmental model illustrating possible application to the VLDL delipidation pathway. Compartments are shown as circles; connectivities are shown as arrows and are labelled with transfer rates (e.g. k(i,j) is the rate of transfer of material from compartment j to compartment i (mass/time)). The rate of input into the system (production rate) is U(1).

With a few exceptions (for example, the comprehensive compartmental model developed by Knoblauch et al. (2000)) most compartmental models are centred on subsets of the lipoprotein metabolism pathway. For example, models developed for the kinetic determination of HDL metabolism or mechanisms of the reverse cholesterol pathway (Cheung and Albers, 1982; Chetiveaux et al., 2004; Packard et al., 1984) or those based on APO-B100 pathways and mechanisms involved in endogenous lipoprotein metabolism (Beltz et al., 1985; Parhofer et al., 1991). More recently work by Packard et al. (2000) and Adiels et al. (2005) has investigated more complex aspects of lipoprotein metabolism related to subfractions of lipoproteins.

However, compartmental models have significant limitations. For example, the labelling of a single lipoprotein density class as a compartment neglects the natural heterogeneity of lipoproteins. Furthermore, the transition from one compartment to another (the delipidation of lipoprotein to another density class) is not a single process but is composed of various reactions such as cholesterol transfer or removal of triglyceride. This simplicity in the empirical transition rates between compartments highlights the lack of dependence on the underlying physiological processes occurring.

In previous sections the importance of elevated LDL cholesterol levels to CHD have been emphasised. In order to investigate hypotheses relating to the mechanisms by which high plasma LDL cholesterol can occur, dynamic models, derived from the physiological and biochemical processes characterising the uptake of LDL from the plasma, are required.

August et al. (2007) developed a dynamic model of the physiological delipidation cascade of endogenous lipoprotein metabolism (VLDL $\rightarrow$ IDL $\rightarrow$ LDL) coupled with cellular receptor mediated uptake of LDL and *de novo* receptor synthesis. This is regulated by negative feedback from intracellular cholesterol concentration creating a system of nonlinear ODEs more tightly linked to the underlying physiological processes. This allows parametric investigation corresponding to various medical and genetic conditions for which they obtain results coinciding with experimental observation. Their model looks in detail at plasma cholesterol levels for which they demonstrate bistability with hysteresis between a high and low cholesterol state.

However, while most processes of this model are based on physiological properties, we note that they make the assumption that all cholesterol in the cell is delivered by lipoproteins. Thus August et al. ignore a significant pathway, that of cholesterol biosynthesis. In the case of zero concentration of extracellular lipoprotein, intracellular cholesterol concentration in their model drops to zero; physiologically a fatal consequence for the cell.

Similarly, the model of Wattis et al. (2008) is a system of nonlinear ODEs derived directly from the biochemical processes. However, their work focuses only on the endocytotic uptake of LDL by a single hepatocyte. Unlike previous models of RME, Wattis et al. explicitly model the presence of receptors within coated pits on the cell surface. This results in equations describing the

evolution of full and empty cell surface pits, intracellular receptors, and extracellular, bound and internalised LDL. Receptor synthesis is modelled as a function of cholesterol content whereby low levels lead to high receptor density and high cholesterol causes low receptor density (negative feedback).

By extending their model to include new variables analogous to variables measured in biological LDL binding studies, Wattis et al. have been able to demonstrate a very good fit of internalised LDL and LDL degradation time evolution to *in vitro* experimental data from Goldstein et al. (1979), as illustrated in Figure 2.9.

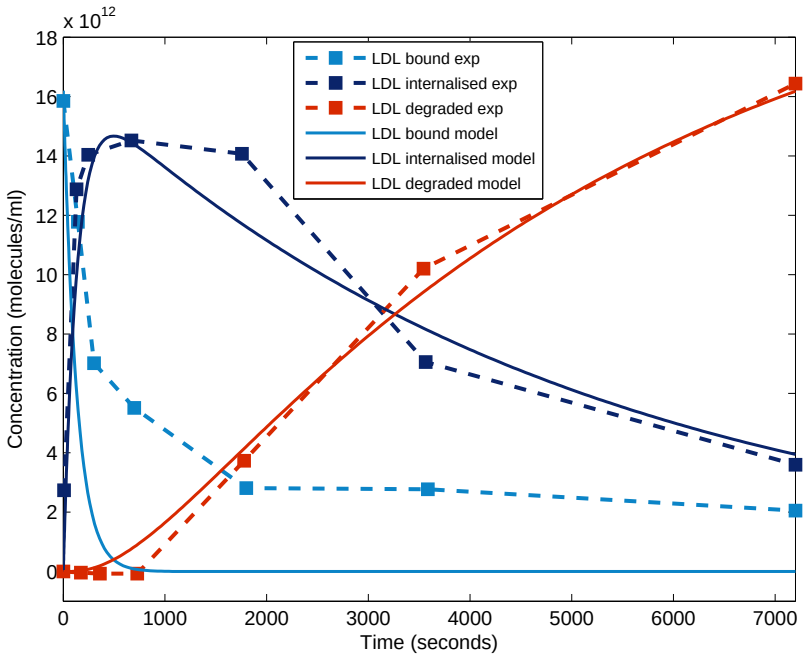

Fig. 2.9: Comparison of the experimental results of Goldstein et al. (1979) with the theoretical predictions of the Wattis et al. (2008) ODE model. The dashed lines indicate experimentally measured variables and the solid lines represent the respective numerical solutions for those variables.

However, simulations for the amount of bound LDL show a discrepancy with the experimental data at long times. Wattis et al. have postulated that this may be due to the nonspecific binding of LDL to other parts of the cell membrane; this results in a nonzero steady state value for this parameter and is in contrast with the simulation result which decays to zero.

This issue is considered in the work of Ratushny (2006) whose approach is to consider a more biologically accurate scenario in which not all receptors are present in coated pits. Instead, some receptors are located on other parts of the cell membrane in the process of diffusing to coated pits. This results in a nonzero steady state of bound LDL since LDL bound outside of coated pits is not internalised.

We also note that, as in the model of August et al. (2007), cholesterol biosynthesis is not treated explicitly. The rate of change of cholesterol with time is modelled as

$$\frac{dc}{dt} = f(l_i) - \lambda(c - c_e), \tag{2.7}$$

where incoming LDL cholesterol is modelled by a function, f, of l_i, internalised LDL. Other cholesterol influx or efflux is modelled by the function $\lambda(c - c_e)$, where λ is a rate constant and c_e is the equilibrium level of cholesterol in the cell. This ensures that if $c < c_e$, that is, cholesterol concentration is too low in the cell then intracellular cholesterol concentration will increase. However, if $c > c_e$, that is, cholesterol is too high then this function ensures intracellular cholesterol concentration will decrease.

While this results in qualitatively correct behaviour, this term does not completely account for the underlying biological mechanisms. In particular the interplay between cholesterol biosynthesis, receptor mediated uptake and cholesterol mediated negative feedback is not fully appreciated. Furthermore, this also results in a bound on the cholesterol concentration within the cell given by the value of c_e.

A consequence of this is that intracellular cholesterol concentration in the model reaches equilibrium rapidly (on a timescale of the order of minutes) after extracellular LDL is delivered to the cell. However, experimental results suggest that this may not be the case, with changes in intracellular cholesterol concentration occurring on timescales of twelve to twenty four hours and resulting in up to a two fold increase in cell cholesterol concentration (Liscum and Faust, 1987; Liscum et al., 1989).

This suggests the possibility that the physiological process of *de novo* cholesterol synthesis not incorporated in the model of Wattis et al. could have a significant effect on intracellular choles-

terol concentration and, as a result, cell surface receptor concentration and LDL internalisation.

Another distinctive feature of the work of both August et al. (2007) and Wattis et al. (2008) is the modelling of the regulation of receptor synthesis as basic reciprocal feedback due to cholesterol concentration. This is the simplest type of mathematical function which represents feedback inhibition, (Murray, 2002). However, the interdependence of the pathways of cholesterol biosynthesis, receptor synthesis and intracellular cholesterol concentration previously discussed suggest that this approach may be too simplistic.

This review of the existing literature indicates a lack of rigorous modelling of both cholesterol biosynthesis and of the feedback regulation of both this pathway and receptor concentration. How important is the cholesterol biosynthesis pathway? As the major contributor to cholesterol concentration within the cell, this pathway is already the basis of the most common form of pharmaceutical treatment for high plasma cholesterol levels. HMGR inhibitors, more commonly known as statins act as competitive inhibitors of the binding site of HMGR. By inhibiting the biosynthesis of cholesterol, statins deplete the intracellular cholesterol pool and promote the transcription of both HMGR and the LDLR, thereby increasing the uptake of plasma LDL. Thus a model of LDL uptake, which aims to describe how changes in the rate of this uptake can affect CHD development, should ideally include this pathway and the receptor related biological mechanisms to which it is linked.

The ultimate aim of this thesis is to develop a model which can describe not only the cellular processes of LDL binding and internalisation, but also the consequential subcellular processes which must respond in order to regulate cell cholesterol content. Therefore, the first aim of this thesis is the development of a model which can describe the cholesterol mediated genetic regulation of cholesterol biosynthesis. This is the subject of the next chapter in which we derive an ODE model of regulated cholesterol biosynthesis directly from the biological mechanisms of protein synthesis from DNA.

3

Regulated Gene Expression and Cholesterol Biosynthesis

In Chapter 2 it was noted that both cell surface LDLR levels and intracellular cholesterol concentration (via HMGR protein levels) are controlled at the level of the gene. This control is exerted by the turning on or off of the process of gene expression which is the biological mechanism of protein synthesis. A brief review of this process is the subject of the first part of this chapter. This is followed by a discussion of the various mathematical approaches adopted in developing models of regulated gene expression. The mathematical models of lipoprotein metabolism reviewed in Section 2.3, whilst acknowledging the influence of intracellular cholesterol concentration on LDLR levels, lack an accurate physiological description of the regulation pathway. Furthermore, they have neglected the significance of cholesterol biosynthesis. The concluding part of this

chapter contains the derivation of the model we will use to describe the process of regulated gene expression, in the context of the cholesterol biosynthetic pathway.

3.1 Gene expression

Gene expression is localised to the cell nucleus and begins at the level of a DNA nucleotide sequence or gene. When the cell requires a particular protein, its nucleotide sequence is copied from the appropriate location in the DNA molecule to produce RNA (a mirror image of the DNA) in a process termed transcription. These RNA copies of DNA segments form templates which direct protein synthesis; this process is known as translation. This principle of flow of genetic information in cells from DNA to RNA to protein is the central dogma of molecular biology. Before we describe protein synthesis, we provide a brief overview of the general structure of a eukaryotic mammal cell as a reference for the cellular organelles which are mentioned in the biology that follows.

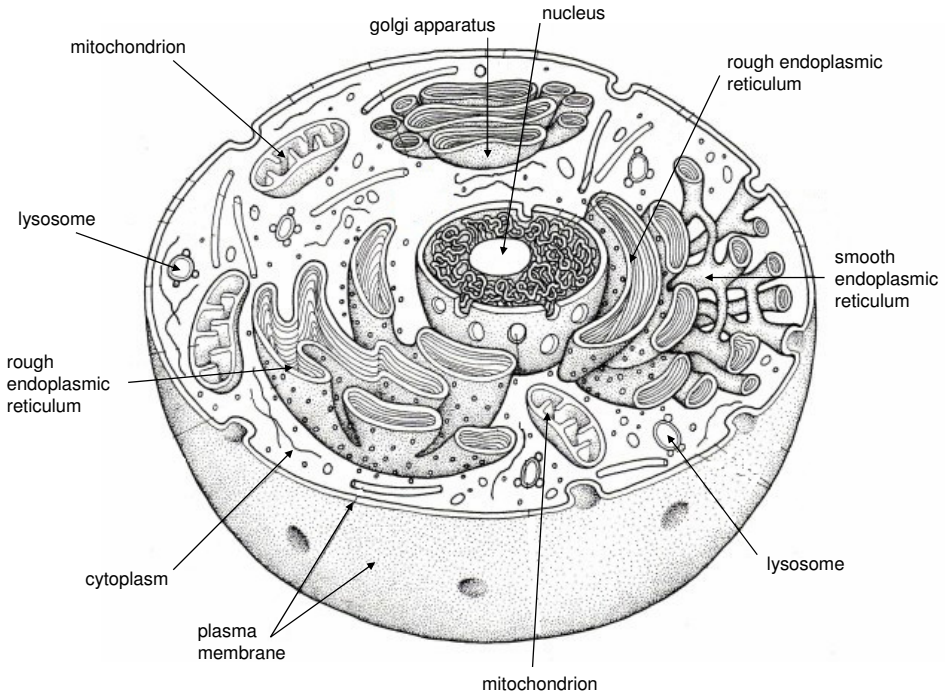

Fig. 3.1: Schematic illustration of a typical eukaryotic cell highlighting the major cellular organelles. Organelle functions are outlined in the list which follows.

The functions of the major eukaryotic cell organelles highlighted in Figure 3.1 are briefly described below.

- **Cytoplasm**: The part of the cell enclosed within the cell membrane.
- **Golgi apparatus**: The organelle responsible for the processing and packaging of macromolecules such as proteins and lipids after their synthesis.
- **Lysosome**: The organelles containing enzymes (hydrolases) which break up waste, engulfed materials and cellular debris.
- **Mitochondrion**: The organelle which converts oxygen and nutrients into ATP to power the cell's metabolic activities.
- **Nucleus**: The regulatory centre of the cell containing most of the cell's genetic material.
- **Plasma membrane**: A semipermeable membrane forming the interface between subcellular components and external environment, controlling the movement of substances in and out of cells.
- **Rough endoplasmic reticulum** : An organelle studded with ribosomes which are the component of the cell responsible for protein synthesis.
- **Smooth endoplasmic reticulum** : The organelle responsible for lipid synthesis, providing surface area for the action and anchoring of enzymes.

We now provide details of the gene expression process necessary for this thesis. For the interested reader further details can be found, for example, in Alberts et al. (2008).

3.1.1 Transcription

The majority of genes carried in a cell's DNA specify the amino acid sequence of proteins; the RNA molecules that are copied from these genes are called messenger RNA (mRNA) molecules. The enzyme responsible for mRNA transcription is RNA polymerase II (RNAP II) which initiates

transcription at a region of the gene known as the promoter (see Figure 3.2). This initiation is mediated by transcription factors; RNAP II will only bind to the promoter following attachment of the relevant transcription factors. Once attached, RNAP II must clear the promoter, and during this time there is a tendency for abortive initiation to occur, when truncated transcripts are produced and released. Once the promoter is cleared, elongation occurs, whereby RNAP II traverses the DNA template region to create an mRNA copy (the polymerase is subject to pauses during this period). Transcription halts at a terminator site and both the DNA and completed mRNA molecule are released from the RNAP II enzyme. These mRNAs then pass through nuclear pores into the cell cytoplasm.

3.1.2 Translation

Located in the cell cytoplasm are large protein assemblies known as ribosomes, on which the nucleotide sequence of the mRNA molecule is translated into a protein. Translation is initiated by the binding of a ribosome to mRNA. The ribosomes synthesise or elongate proteins by catalysing the assembly of individual amino acids into polypeptide chains. Sequences of three nucleotides in the mRNA sequence form the code for inserting a particular amino acid. The complete mRNA molecule acts as a template for the correct amino acid sequence for the protein.

Elongation is followed by termination and the release of the completed polypeptide. The final step of protein synthesis is the folding of the newly synthesised protein into its correct three-dimensional conformation.

In principle, all of the steps from DNA to protein production can be regulated, the main control points are shown in Figure 3.2. A cell can control the protein it makes by controlling how often a gene is transcribed or by selecting which mRNAs in the cytoplasm are translated. Control may also be exerted through the degradation of mRNA molecules. Following protein synthesis, selective activation, inactivation or degradation of protein molecules allows further regulation.

Paramount for most genes is regulation of the first step, that is, control at the transcriptional level. Transcriptional regulatory networks continuously sense a set of certain intracellular sig-

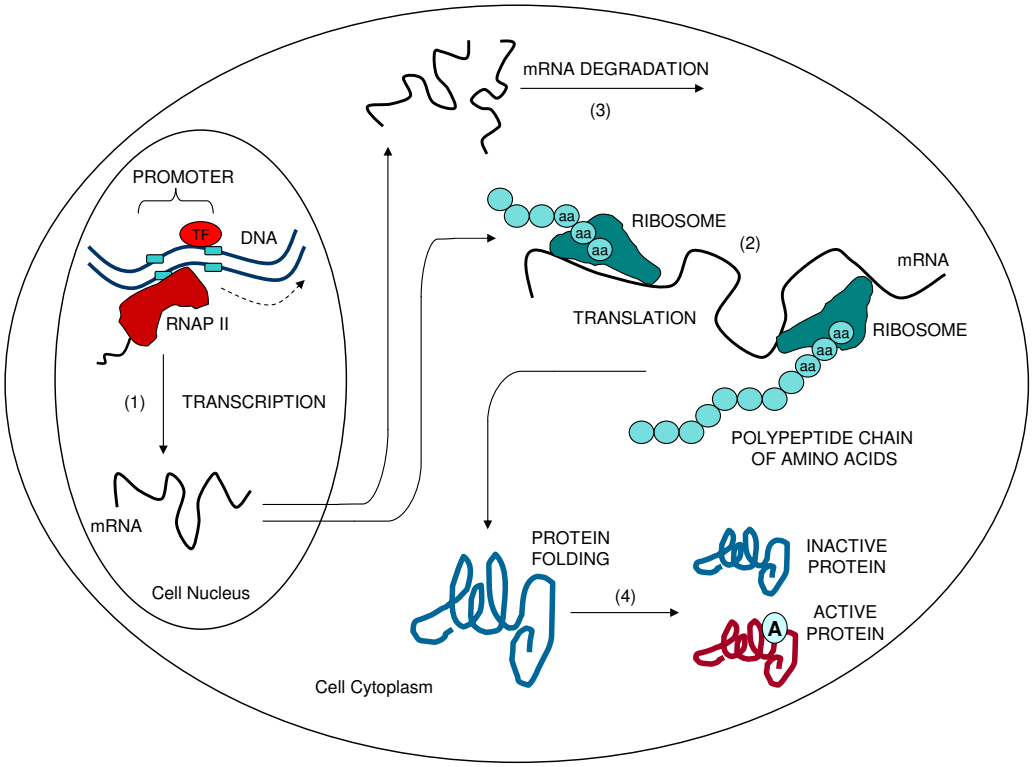

Fig. 3.2: Pathways controlling gene expression in a eukaryotic cell. (1) Transcriptional control; (2) Translational control; (3) mRNA degradation control; and (4) Protein activity control. (**TF**: Transcription Factor; **aa**: Amino Acid; **A**: Active).

nals, for example the concentration of a particular molecule within the cell. This information is then relayed to the cell nucleus in order to adjust transcription appropriately. Sensing these signals is often a fundamental problem for the cell. This is overcome by the action of a particular type of protein known as a transcription factor, which binds to sites on the cell's DNA to control gene expression and the transfer of genetic information to mRNA. Transcription factors usually contain a signal sensing domain which on interaction with the signal allows activation or deactivation of the transcription factor.

Having characterised the essential biological features of gene expression our next step is to translate these into a mathematical model which we will use to describe regulated gene expression. Before doing so, we will give a brief overview of mathematical modelling approaches of transcriptional control in genetic networks.

3.2 Mathematical models of regulated gene expression

Mathematical models used to describe regulated gene expression differ both in their underlying assumptions and in the level of resolution (how many biological variables) they contain. In this section we consider time dependent mathematical approaches; a broad classification of these approaches separates the resulting models into two classes depending on how the time variable is treated. Discrete in time models are designed to describe the state of the physical system at a selected set of distinct times whereas continuous in time mathematical models are valid for any value of the time variable. Continuous models can be further divided into stochastic and deterministic models.

Discrete in time models, also known as Boolean or logical network methods, use relatively simple levels of detail, and were introduced by Kauffman (1969). The assumptions of this approach, due to Somogyi and Sniegoski (1996), can be summarised in the following manner:

(i) the expression of a gene is either *on* (active, (1)) or *off* (inactive, (0));

(ii) no intermediate activity levels are considered; and

(iii) the dynamic behavior of each variable, that is, whether it will be *on* or *off* at the next moment, is governed by a Boolean function. In general, a Boolean or logical function is written as a statement acting on the inputs using the logical operators 'and', 'or' and 'not' and its output is 1 if the statement is true and 0 if false.

We demonstrate the use of Boolean models by means of a simple example. Figure 3.3 illustrates a Boolean network, G(V,F), of three nodes, $V = a, b, c$, where a node may represent either a gene or a biological stimulus, for example, a chemical factor which influences the network and is itself not a gene or gene product.

A node has an associated steady-state expression level representing the amount of gene product (in the case of a gene) or the amount of stimulus present in the cell. This level is approximated as high or low and represented by the binary value 1 or 0, respectively.

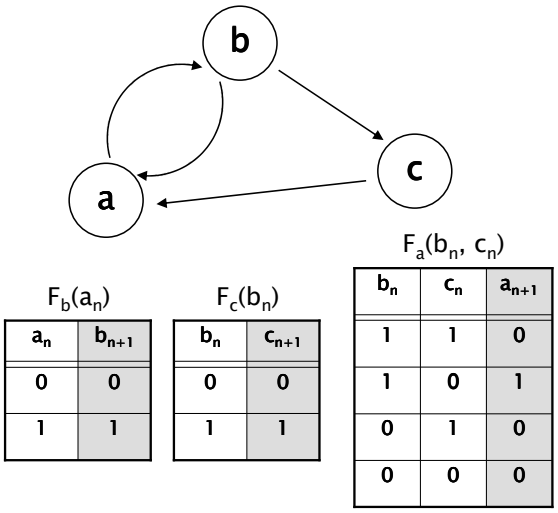

Fig. 3.3: An example of a Boolean network containing three nodes. Each of the entities a, b and c in the network can be in state 0 or 1. State transitions obey the regulation functions shown in the diagram, which describe the rules of the model. For example, if b is in state 1 and c is in state 0, at the next time step the state of a will be 1. Arrows indicate the regulators of each node.

The set $\mathrm{F} = (\mathrm{F}_a, \mathrm{F}_b, \mathrm{F}_c)$ of Boolean functions assigned to the nodes, defines the value of a node on the next step depending on values of other nodes which influence it. The functions F are uniquely defined using the Boolean function truth tables in Figure 3.3, for example, the value of the node b at time $n+1$ depends on the value of a at time n, that is, $b_{n+1} = \mathrm{F}_b(a_n)$.

For the network depicted in Figure 3.3, expression of c directly depends on expression of b, which directly depends on a. However, the influence of b and c on a is more complex; for example, a high level of expression of both b and c leads to inhibition of a.

This approach is useful when modelling molecular concentration changes associated with gene activity which are often characterised by rapid change (Bornholdt, 2008). The switch-like dynamics produced by Boolean networks are not unlike the steep changes and plateaus that are typically observed in cellular protein concentrations.

The work of Kervizic and Corcos (2008) has applied the Boolean network modelling method to the cholesterol biosynthesis pathway and its regulation. Whilst their work has shown qualitative

agreement with the known biochemical features of the pathway, there are obvious limitations of a method which assumes a gene as being either on or off, since gene expression rates are continuous in time (Glass and Kauffman, 1973). This limited level of detail cannot, for example, correctly model the dynamics of a transcription factor that downregulates its own expression (Kauffman et al., 2003).

A further problem lies in the computational expense of analysing large networks; however, when the number of nodes is small and only qualitative knowledge is available, Boolean networks can provide important insights, such as the existence and nature of steady states. More importantly this approach cannot, for example, identify the key physiological parameters to which the behavior of the genetic regulatory system is sensitive. We require an approach which models fundamentally the underlying biological reactions governing the gene network, thus allowing us to investigate the response of the system to biological parameters.

Continuous in time models generally use (linear or nonlinear) differential equations to describe the rate of change of gene product (mRNA and protein) concentrations. Stochastic differential equations are an example of a continuous model often used to model genetic systems. The governing philosophy is that molecular populations are whole numbers and when they change, they do so by discrete amounts. Furthermore, the low average number of important molecules in some cells (i.e. low intracellular concentrations) can lead to randomness in the times of synthesis or degradation of individual molecules.

This level of detail can be incorporated by modelling stochastic fluctuations. Stochastic models address deviations from population homogeneity by considering numbers of molecules rather than concentrations and modelling reaction rates as probabilities (Smolen et al., 1999; McAdams and Arkin, 1997). However, stochastic modelling introduces considerable complexity. More specifically, algorithms for the solution of stochastic models involve procedures that simulate every reaction event which requires considerable computational power.

Cellular processes such as transcription and translation may be considered as systems of distinct chemical reactions. These can be described using the law of mass action (see Section 3.2.1) to yield a set of ODEs which describe the successive concentrations of model species over time.

Generally, these equations take the form

$$\frac{dx_i}{dt} = f_i(\mathbf{x}), \quad 1 \leq i \leq n, \tag{3.1}$$

$$\mathbf{x} = [x_1, x_2, \ldots, x_{n-1}, x_n]^T, \tag{3.2}$$

with the arbitrary initial conditions given by

$$x_1 \neq 0, \;\; x_2 = 0, \;\; \ldots, \;\; x_{n-1} = 0, \;\; x_n = 0, \tag{3.3}$$

where $\mathbf{x}$ is a vector of nonnegative real numbers which describes the concentrations of reacting species, and f_i is some function describing the interaction (reactions) between them.

ODEs are arguably the most common formalism for modelling regulated gene expression and it is this approach that will be used in this thesis.

One of the first instances of the use of ODEs in modelling gene transcription is based on the *operon* models postulated by Jacob and Monod (1961), describing the mechanism of enzyme induction and repression. The early work of Goodwin (1963, 1965) used the Jacob and Monod model to provide a general multistep ODE framework for modelling regulated transcription of mRNA.

We now provide a brief description of Goodwin's model as the basis for the derivation of our model in Section 3.3. The reaction mechanism described in the work of Goodwin (1963), which considers the mediation of mRNA synthesis by an end product it synthesises, is reproduced in the following diagram

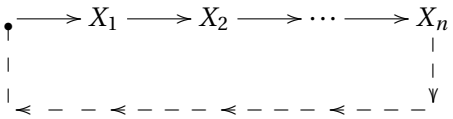

(3.4)

Reaction (3.4) describes a multistep process in which the final product of the reaction, X_n influences its own synthesis by affecting the production of the first reactant in the pathway, X_1. The simplest model equations that can be used to describe the above reaction mechanism as derived

in the work of Goodwin (1963), are given by

$$\frac{dx_1}{dt} = f(x_n) - k_1 x_1, \tag{3.5a}$$
$$\frac{dx_j}{dt} = x_{j-1} - k_j x_j, \quad j = 2, \ldots, n, \tag{3.5b}$$

where lowercase letters denote concentration and n is the number of variables of the multistep reaction. The function $f(x_n)$ is always positive and is the feedback function which describes the effect of x_n on x_1. If $f(x_n)$ is an increasing function of x_n then $f'(x_n) > 0$ and system (3.5) describes a positive feedback loop. If, however, $f(x_n)$ is a monotonically decreasing function of x_n then $f'(x_n) < 0$ and system (3.5) represents a negative feedback loop.

As an example we consider the simple case with $n = 3$ given by,

$$\frac{dx_1}{dt} = \frac{\alpha_1}{1+\beta x_3} - k_1 x_1, \tag{3.6a}$$
$$\frac{dx_2}{dt} = \alpha_2 x_1 - k_2 x_2, \tag{3.6b}$$
$$\frac{dx_3}{dt} = \alpha_3 x_2 - k_3 x_3, \tag{3.6c}$$

which has the initial conditions

$$x_1 \neq 0, \quad x_2 = 0, \quad x_3 = 0. \tag{3.7}$$

Since $f(x_3) = \alpha_1 / \left(1 + \beta x_3\right)$ is monotonically decreasing with $f'(x_3) < 0$, this is a negative feedback loop in which the metabolite x_3 directly represses its own synthesis. The α_i are rates of synthesis, k_i are rates of degradation and β is an equilibrium constant for the reaction between x_3 and x_1.

This model can describe the process whereby a structural gene codes for mRNA (x_1), which then goes on to produce a protein (x_2) which is responsible for metabolite production (x_3). The metabolite may directly influence its own transcription via the function $f(x_3)$. This is a repression function in which one molecule of x_3 can inactivate mRNA transcription.

A further modification proposed by Griffith (1968) was to incorporate the reaction mechanism whereby m molecules of the repressor are required to inactivate transcription; in this case (3.6a)

is given by the modified equation

$$\frac{dx_1}{dt} = \frac{\alpha_1}{1+\beta\,(x_3)^m} - k_1 x_1. \tag{3.8}$$

The parameter m, which here represents the number of binding sites on the gene available to the repressor is also known as a Hill coefficient. Hill coefficients are commonly used in mathematical models of gene expression, however, the use of this coefficient in the form of (3.8) is valid only under certain conditions. To understand these conditions, it is first necessary to give a description of the rationale behind the formulation of ODEs from chemical reactions.

3.2.1 The law of mass action

The mass action kinetic formula is the most fundamental type of kinetic formula. It results from the empirical observation that the rate of an elementary reaction is proportional to the product of the concentrations of the chemical species participating in that reaction (Segel, 1984). This observation is known as the **law of mass action**. An elementary chemical reaction corresponds to a fundamental, instantaneous physical event, for example the collision of two molecules to form a product.

Suppose that two chemicals A and B react to form a chemical product C in a reaction described by

$$A + B \longrightarrow C. \tag{3.9}$$

This reaction will proceed with a speed dictated by the thermodynamics of the chemical reaction, known as the kinetic rate constant. Since thermodynamically all reactions are reversible in principle, a more accurate representation of (3.9) is

$$A + B \underset{k_r}{\overset{k_f}{\rightleftharpoons}} C, \tag{3.10}$$

where k_f is the rate constant for the forward reaction and k_r is the rate constant for the reverse reaction.

The law of mass action states that the rate of increase of c (which we use to denote the concentration of product C) is proportional to the product of the concentrations of A and B with proportionality constant k_f. The rate of decrease of c is proportional to its own concentration with proportionality constant k_r.

The total rate of change of c is then given by the difference between the rate of its creation and the rate of its depletion,

$$\frac{dc}{dt} = k_f ab - k_r c, \tag{3.11}$$

where a, b represent the concentrations of the chemicals of A, B respectively. Similarly the law of mass action allows us to write equations for the time derivatives of the reactant concentrations a and b,

$$\frac{da}{dt} = -k_f ab + k_r c, \qquad \frac{db}{dt} = -k_f ab + k_r c. \tag{3.12}$$

(3.11) together with (3.12) comprise the system of ODEs which describe the chemical reaction occurring in (3.10). We note that

$$\frac{d}{dt}(a+c) = 0 \quad \text{and} \quad \frac{d}{dt}(b+c) = 0, \tag{3.13}$$

and integrating,

$$a + c = a_0 \quad \text{and} \quad b + c = b_0, \tag{3.14}$$

where a_0 and b_0 are the concentrations of a and b at initial time. Since one molecule of each reactant is converted into one molecule of product, each reactant, original and converted to product, is conserved.

These ideas can also be extended to generalised chemical reactions composed of a number of elementary reactions

$$a_1 X_1 + a_2 X_2 + a_3 X_3 + \ldots + a_m X_m \underset{k_r}{\overset{k_f}{\rightleftharpoons}} b_1 Y_1 + b_2 Y_2 + b_3 Y_3 + \ldots + b_n Y_n, \tag{3.15}$$

where the a_i and b_i are the stoichiometric coefficients which describe how many molecules of a particular chemical species is taking part in that particular reaction. The system of ODEs

representing (3.15) is given by

$$\frac{dx_i}{dt} = k_r \prod_{i=1}^{n} y_i^{b_i} - k_f \prod_{i=1}^{m} x_i^{a_i}, \tag{3.16a}$$

$$\frac{dy_i}{dt} = k_f \prod_{i=1}^{m} x_i^{a_i} - k_r \prod_{i=1}^{n} y_i^{b_i}. \tag{3.16b}$$

We note that the law of mass action described above assumes chemical reactions are occurring in a homogeneous, well mixed environment, and that reactions are continuous and deterministic, that is, there is no randomness involved in the occurrence of a chemical reaction event.

However, it is well known that chemical reactions involve discrete, random collisions between individual molecules, which can be continuously approximated given a high enough concentration of molecules involved in the collisions.

The validity of this approach ceases to hold as smaller intracellular environments are considered and stochastic effects become more significant (Cai et al., 2006).

Furthermore, intracellular environments are significantly different from the homogeneous environment chemical reactions are assumed to occur in. They are characterised by a high degree of macromolecular crowding, especially in cell cytoplasm; this can have important consequences in cell thermodynamics and also on diffusion processes, with resultant effects on reaction rates and enzyme activity (Grima and Schnell, 2006; Schnell and Turner, 2004).

In deriving our model, we will assume the reactants are present in high enough concentrations to allow the approximation of continuity and that the cellular environment is essentially homogeneous.

3.2.2 The Hill function

Hill functions were introduced by Hill (1913) to describe the binding of oxygen to haemoglobin, and have been employed in the mathematical models of gene repressor interaction since the

work of Goodwin (1963) and Griffith (1968). Traditionally the Hill coefficient is used to describe the number of molecules that are required to bind to a gene in order to produce a functional effect.

The Hill equation is readily derived from a binding reaction scheme in which m molecules of, for example, repressor (R) bind to a gene (G), i.e.

$$G + mR \underset{k_r}{\overset{k_f}{\rightleftharpoons}} GR_m. \tag{3.17}$$

At equilibrium, the following relation, derived using the law of mass action, holds

$$[G][R]^m = \frac{k_r}{k_f}[GR_m], \tag{3.18}$$

and, given that the number of genes in a cell is inherently constant, we also have that,

$$[G] + [GR_m] = [G_{tot}]. \tag{3.19}$$

mRNA transcription is traditionally taken to be proportional to the fraction of active genes, that is, the fraction of genes not bound to a repressor,

$$\frac{[G]}{[G_{tot}]} = \frac{[G]}{[G]+[GR_m]} = \frac{[G]}{[G]+\dfrac{k_f}{k_r}[G][R]^m} = \frac{1}{1+\left(\dfrac{[R]}{\kappa_D}\right)^m}, \tag{3.20}$$

where κ_D is the dissociation constant for reaction (3.17) and is given by ${\kappa_D}^m = {k_r}/{k_f}$.

Then the rate of mRNA synthesis is given by

$$\frac{\alpha}{1+\beta[R]^m}, \tag{3.21}$$

where α is a proportionality constant representing the maximum transcription rate, $\beta = {1}/{{\kappa_D}^m}$, and we have recovered the form of (3.8) with mRNA $= x_1$ and repressor, [R] $= x_3$.

Although the above reaction is mathematically possible, it is not biologically plausible except in the case $m = 1$. For $m > 1$ the reaction implies the *simultaneous* interaction of multiple

molecules in which no intermediate states occur.

A more realistic binding scheme for genes with multiple individual binding sites is given by the reaction,

$$\begin{aligned} G+mR \quad & \underset{k_{r1}}{\overset{mk_{f1}}{\rightleftharpoons}} \quad GR+(m-1)R \quad \underset{2k_{r2}}{\overset{(m-1)k_{f2}}{\rightleftharpoons}} \quad GR_2+(m-2)R \quad \rightleftharpoons \quad \dots \\ \dots \quad & \underset{(m-1)k_{r(m-1)}}{\overset{2k_{f(m-1)}}{\rightleftharpoons}} \quad GR_{m-1}+R \quad \underset{mk_{rm}}{\overset{k_{fm}}{\rightleftharpoons}} \quad GR_m, \end{aligned} \tag{3.22}$$

in which any binding site can be occupied independently of another.

Here, for example, the first forward rate of reaction represents the fact that when the G is unbound, any of the m binding sites for R are available to be filled and so the total forward rate from the unbound gene is m times the individual forward rate constant k_{f1}. The converse applies to the coefficients of the backward rate constants.

In this case, the fraction of active genes at equilibrium is given by

$$\frac{[G]}{[G_{tot}]} = \frac{1}{1+\sum_{i=1}^{m}\left(\frac{m!}{(m-i)!\,i!}\prod_{j=1}^{i}\frac{1}{\kappa_{Dj}}\,[R]^i\right)}, \tag{3.23}$$

where $\kappa_{Dj} = {}^{k_{rj}}/_{k_{fj}}$ is the dissociation constant for the step forming GR_j (Segel, 1993).

The only condition under which reaction (3.22) can be approximated by reaction (3.17) is when the intermediate states, $GR, GR_2 \dots GR_{m-1}$, never accumulate significantly. This can occur only when $\kappa_{D1} >> \kappa_{D2} >> \dots >> \kappa_{D(m-1)} >> \kappa_{Dm}$, that is, when marked positive cooperativity is present, in which case reaction (3.23) reduces to

$$\frac{[G]}{[G_{tot}]} = \frac{1}{1+\hat{\beta}[R]^m}, \tag{3.24}$$

where

$$\hat{\beta} = \left(\frac{1}{\kappa_{D1}}\right)\left(\frac{1}{\kappa_{D2}}\right)\dots\left(\frac{1}{\kappa_{D(m-1)}}\right)\left(\frac{1}{\kappa_{Dm}}\right), \tag{3.25}$$

that is, to the form of the simultaneous binding approximation in reaction (3.17).

Thus, the Hill coefficient is strictly used as a means of quantification of the enhancement of binding affinity of a ligand to a receptor, in the case where other ligands are already bound to the receptor. The conditions under which the Hill coefficient provides an accurate estimate of the number of binding sites are very specific.

It is solely appropriate in the limiting case when the only possible binding configurations are either all binding sites to be empty or all to be occupied, known as extreme positive cooperativity, (Hill, 1985). Under these conditions, the constant κ_D of reaction (3.17) is also an approximation to the actual dissociation constant of the actual reaction (3.22), given by $\hat{\beta}$.

In the next section we will derive an ODE model of regulated protein synthesis using reasoning congruous to that of Goodwin (1963, 1965) and Griffith (1968). In these models, it has been considered that the end product of the reaction represses mRNA synthesis. However, we will derive our model to consider the case in which mRNA synthesis occurs as a result of gene activation via a transcription factor.

This transcription factor interacts with the end product of the mRNA reaction to become inactivated and in including this biological process, which is not present in the models discussed above, we arrive at a model in which we account explicitly for the Hill coefficient characterising the interaction between gene and transcription factor in the cholesterol biosynthesis pathway.

3.3 Regulated gene expression model formulation

As the first step in our model development we describe the derivation of a general process of regulated protein synthesis (illustrated in Figure 3.4) using the law of mass action described in Section 3.2.1. This results in a system of nonlinear ODEs describing the rate of mRNA production. The system is modified by an efficiency factor reflecting the binding equilibria between the transcription factor and DNA promoter and subsequent protein synthesis from mRNA. We derive our model in a manner similar to Goodwin (1965). However, we adapt the model to include

processes related to transcription factor activity. In particular, we consider the case where the transcription factor can activate mRNA synthesis.

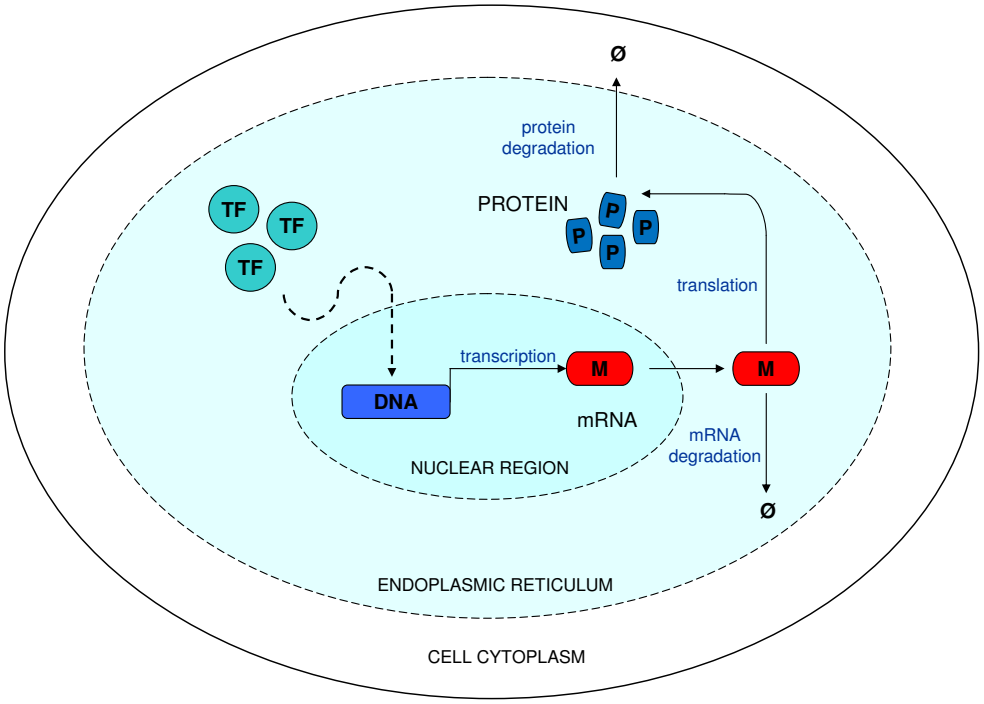

Fig. 3.4: General gene expression and regulation. Transcription of mRNA, **M**, occurs from DNA. This mRNA can continue to participate in translation, the synthesis of protein, **P**; this is the central dogma of molecular biology. Both mRNA and protein are also subject to degradation, (pathways leading to $\emptyset$). The complete reaction can be influenced by the action of transcription factors, **TF** interacting with the gene.

We begin with the central dogma of molecular biology,

$$\text{DNA} \xrightarrow{\text{transcription}} \text{mRNA} \xrightarrow{\text{translation}} \text{protein}, \tag{3.26}$$

and rewrite (3.26) as a reaction mechanism,

$$\text{DNA} \xrightarrow{\bar{\mu}_d} \bar{M} \xrightarrow{\bar{\mu}_p} \bar{P}, \tag{3.27}$$

where $\bar{\mu}_d$ is the rate of transcription of mRNA, $\bar{M}$, and $\bar{\mu}_p$ is the rate of translation of protein, $\bar{P}$.

In our simplified representations of transcription and translation in (3.27), we have not included the separate mechanistic steps of these processes (see Section 3.1), but group them together as immediate effects on the overall rate at which mRNA and protein are produced. This is because we would like to create a mathematical representation which can reproduce as far as possible the underlying physiological mechanism, whilst reducing the model complexity and minimising the number of parameters required.

For this reason, we also ignore the presence of basal transcription levels, and assume that transcription rates may be downregulated to zero. To complete our reaction pathway we include degradation pathways for variables which describe the biological half life of these molecules, as shown in Figure 3.4.

Thus we arrive at the reaction mechanism, shown below, describing gene expression,

$$\begin{array}{ccccc} \text{DNA} & \xrightarrow{\bar{\mu}_d} & \bar{M} & \xrightarrow{\bar{\mu}_p} & \bar{P}, \\ & & \downarrow{\scriptstyle \bar{\delta}_m} & & \downarrow{\scriptstyle \bar{\delta}_p} \\ & & \emptyset & & \emptyset \end{array} \tag{3.28}$$

where $\bar{\delta}_m$ represents the degradation rate of mRNA, $\bar{M}$, and $\bar{\delta}_p$ represents the degradation rate of protein, $\bar{P}$. The empty set, $\emptyset$, is used to indicate that after degradation, the molecule is assumed to play no further part in the reaction mechanism.

We note that this pathway models a case of constant protein production (as mRNA production is simply the copying of the DNA strand; DNA is not used up in this reaction). The gene (or DNA) in (3.28) is modelled by a constitutive promoter, that is, an unregulated promoter allowing for continuous transcription of its associated gene. Herein, we consider any reference to DNA as being analogous to the gene promoter region.

However, most genes are not constitutively expressed; as we have previously discussed, their expression is dependent on the presence of regulatory transcription factors which can activate or inhibit the promoter of the gene in question. Consequently the system must be extended to take into account the presence of the transcription factor.

We consider a model of regulated transcription in which a transcription factor ($\bar{T}_f$) activates mRNA production by interacting with the gene. For our model, we consider the simplest case of interaction which assumes reversible binding of $\bar{T}_f$ to DNA,

$$\text{DNA} + n\bar{T}_f \underset{\bar{k}_r}{\overset{\bar{k}_f}{\rightleftharpoons}} \text{DNA} : n\bar{T}_f, \tag{3.29}$$

where n is the number of binding sites available for $\bar{T}_f$ on the DNA promoter region. (Further details on the interaction between DNA and transcription factor may be found in Appendix A.) Since our model describes activation by a transcription factor, [DNA : $n\bar{T}_f$] represents the concentration of activated DNA capable of creating mRNA, and [DNA] the concentration of inactivated DNA. Including this in the reaction pathway we arrive at the following

$$\begin{array}{ccccccc} \text{DNA} + n\bar{T}_f & \underset{\bar{k}_r}{\overset{\bar{k}_f}{\rightleftharpoons}} & \text{DNA} : n\bar{T}_f & \xrightarrow{\bar{\mu}_d} & \bar{M} & \xrightarrow{\mu_p} & \bar{P}. \\ & & & & \downarrow{\scriptstyle \delta_m} & & \downarrow{\scriptstyle \bar{\delta}_p} \\ & & & & \emptyset & & \emptyset \end{array} \tag{3.30}$$

Before we apply the law of mass action to (3.30) we reiterate two important biological concepts, introduced in Section 3.1 ,which will affect the derived ODEs.

- [DNA : $n\bar{T}_f$] represents the concentration of activated DNA. From Section 3.1.1, we recall that activated DNA is copied by the action of an enzyme to produce mRNA, and as the concentration of DNA is an inherent constant within the cell, mRNA, $\bar{M}$, production does not affect the concentration of [DNA : $n\bar{T}_f$]. That is, synthesis of $\bar{M}$ will *not* deplete [DNA : $n\bar{T}_f$].

- Similarly, from Section 3.1.2, we recall that mRNA synthesises protein via the action of ribosomes. Following protein synthesis, mRNA detaches from the ribosome and is free to participate in further synthesis reactions until it is degraded according to its half life. Therefore, protein, $\bar{P}$, synthesis does not affect the concentration of $\bar{M}$. That is, synthesis of $\bar{P}$ will *not* deplete $\bar{M}$.

Together with the points made above, application of the law of mass action to (3.30) results in the following system of nonlinear ODEs describing regulated protein synthesis

$$\begin{aligned}
\frac{d\bar{d}}{d\bar{t}} &= \bar{k}_r \bar{t}_c - \bar{k}_f \bar{t}_f{}^n \bar{d}, && \text{(3.31a)}\\
\frac{d\bar{t}_f}{d\bar{t}} &= n\bar{k}_r \bar{t}_c - n\bar{k}_f \bar{t}_f{}^n \bar{d}, && \text{(3.31b)}\\
\frac{d\bar{t}_c}{d\bar{t}} &= \bar{k}_f \bar{t}_f{}^n \bar{d} - \bar{k}_r \bar{t}_c, && \text{(3.31c)}\\
\frac{d\bar{m}}{d\bar{t}} &= \bar{\mu}_d \bar{t}_c - \bar{\delta}_m \bar{m}, && \text{(3.31d)}\\
\frac{d\bar{p}}{d\bar{t}} &= \bar{\mu}_p \bar{m} - \bar{\delta}_p \bar{p}, && \text{(3.31e)}
\end{aligned}$$

which has the initial conditions

$$\bar{t}_f(0) = t_0, \qquad \bar{d}(0) = d_0, \qquad \bar{t}_c(0) = 0, \qquad \bar{m}(0) = m_0, \qquad \bar{p}(0) = p_0. \tag{3.32}$$

Here $\bar{d} = [\text{DNA}]$, $\bar{t}_f = [\bar{T}_f]$, $\bar{t}_c = [\text{DNA} : n\bar{T}_f]$, $\bar{m} = [\bar{M}]$ and $\bar{p} = [\bar{P}]$ where square brackets denote concentration and $\bar{k}_f$ and $\bar{k}_r$ are, respectively, the forward and reverse reaction rates for the binding of DNA to $\bar{T}_f$. $\bar{\mu}_d$ and $\bar{\mu}_p$ represent the rates of synthesis, and $\bar{\delta}_m$, $\bar{\delta}_p$ represent the rates of degradation of $\bar{m}$ and $\bar{p}$ respectively. We note the multiplicative factor of n in the right hand side of (3.31b); this results from the fact that dissociation of the complex t_c releases n molecules of t_f whilst the creation of t_c requires n DNA binding sites.

We wish to arrive at a functional form for $\bar{t}_c$ in conjunction with reducing the dimensions of the ODE system. To do so we consider (3.29) in greater detail. The number of genes within a cell is always constant. This conservation law also comes immediately on adding (3.31a) and (3.31c) to obtain

$$\frac{d\bar{d}}{d\bar{t}} + \frac{d\bar{t}_c}{d\bar{t}} = 0 \quad \Rightarrow \quad \bar{d}(t) + \bar{t}_c(t) = d_0, \tag{3.33}$$

on using the initial conditions (3.32). Thus we can reduce the three equations of (3.31a) to (3.31c) to two equations given by

$$\begin{aligned}
\frac{d\bar{t}_f}{d\bar{t}} &= n\bar{k}_r \bar{t}_c - n\bar{k}_f \bar{t}_f{}^n (d_0 - \bar{t}_c), && \text{(3.34a)}\\
\frac{d\bar{t}_c}{d\bar{t}} &= \bar{k}_f \bar{t}_f{}^n (d_0 - \bar{t}_c) - \bar{k}_r \bar{t}_c, && \text{(3.34b)}
\end{aligned}$$

with the initial conditions

$$\bar{t}_f(0) = t_0, \qquad \bar{t}_c(0) = 0. \tag{3.35}$$

We now assume that (3.34b) reaches equilibrium rapidly (see Appendix A) and so we make a quasi-steady-state approximation in which $d\bar{t}_c/dt \approx 0$ such that

$$\bar{k}_f \bar{t}_f{}^n d_0 - \bar{k}_f \bar{t}_f{}^n \bar{t}_c = \bar{k}_r \bar{t}_c, \tag{3.36}$$

and thus

$$\bar{t}_c = \frac{d_0 \bar{t}_f{}^n}{\left(\bar{k}_r/\bar{k}_f\right) + \bar{t}_f{}^n} = \frac{d_0 \bar{t}_f{}^n}{\bar{\kappa}_T + \bar{t}_f{}^n} \tag{3.37}$$

where $\kappa_T = \bar{k}_r/\bar{k}_f$ defines the complex dissociation constant for reaction (3.29).

We note that if we consider the concentration of variables in units of molecules ml^{-1}, and time in units of seconds, then $\bar{k}_r$ has units of s^{-1} and $\bar{k}_f$ has units of ml ^{n} molecules^{-n} s^{-1}.

Therefore, $\bar{\kappa}_T$ has units of molecules ^{n} ml^{-n}. We now define the new quantity $\bar{\kappa}_D$, where

$$\bar{\kappa}_D = \left(\bar{\kappa}_T\right)^{\frac{1}{n}} = \left(\frac{\bar{k}_r}{\bar{k}_f}\right)^{\frac{1}{n}}, \tag{3.38}$$

such that $\bar{\kappa}_D$ has units of molecules ml^{-1} and we write

$$\bar{t}_c = \frac{d_0 \bar{t}_f{}^n}{\bar{\kappa}_D{}^n + \bar{t}_f{}^n}. \tag{3.39}$$

We substitute the value of $\bar{t}_c$ in (3.39) into the now reduced system (3.31). Upon using the conservation law in (3.33) the system of equations becomes

$$\frac{d\bar{t}_f}{dt} = n\bar{k}_r \left(\frac{d_0 \bar{t}_f{}^n}{\bar{\kappa}_D{}^n + \bar{t}_f{}^n}\right) - n\bar{k}_f \bar{t}_f{}^n \left(d_0 - \frac{d_0 \bar{t}_f{}^n}{\bar{\kappa}_D{}^n + \bar{t}_f{}^n}\right), \tag{3.40a}$$

$$\frac{d\bar{m}}{dt} = \bar{\mu}_d \left(\frac{d_0 \bar{t}_f{}^n}{\bar{\kappa}_D{}^n + \bar{t}_f{}^n}\right) - \bar{\delta}_m \bar{m}, \tag{3.40b}$$

$$\frac{d\bar{p}}{dt} = \bar{\mu}_p \bar{m} - \bar{\delta}_p \bar{p}. \tag{3.40c}$$

Expanding equation (3.40a), we find that

$$\frac{d\bar{t}_f}{dt} = \left(n\bar{k}_r + n\bar{k}_f{\bar{t}_f}^n\right)\left(\frac{d_0{\bar{t}_f}^n}{\bar{\kappa}_D^n + {\bar{t}_f}^n}\right) - n\bar{k}_f d_0{\bar{t}_f}^n. \tag{3.41}$$

Using the definition of κ_D given in (3.38) we have that

$$n\left(\frac{\bar{k}_r + \bar{k}_f{\bar{t}_f}^n}{\bar{\kappa}_D^n + {\bar{t}_f}^n}\right) = n\left(\frac{\bar{k}_r + \bar{k}_f{\bar{t}_f}^n}{\bar{k}_r/\bar{k}_f + {\bar{t}_f}^n}\right) = n\bar{k}_f. \tag{3.42}$$

Thus (3.41) becomes

$$\frac{d\bar{t}_f}{dt} = n\bar{k}_f d_0{\bar{t}_f}^n - n\bar{k}_f d_0{\bar{t}_f}^n = 0, \tag{3.43}$$

and we see that the total concentration of $\bar{t}_f$ within the cell is conserved. Using the initial condition in (3.32), $\bar{t}_f$ is constant and given by $\bar{t}_f = t_0$.

We also note that equations (3.31b) and (3.31c) provide a conservation law for the total concentration of transcription factor within the cell given by

$$\frac{d\bar{t}_f}{dt} + n\frac{d\bar{t}_c}{dt} = 0, \tag{3.44a}$$

$$\Rightarrow \quad \bar{t}_f(t) + \bar{t}_c(t) = t_0. \tag{3.44b}$$

As we have shown above from (3.43) $\bar{t}_f$ is constant, and so (3.44a) becomes

$$n\frac{d\bar{t}_c}{dt} = 0 \quad \Rightarrow \quad \bar{t}_c(t) = 0, \tag{3.45}$$

on using the initial condition in (3.32). From (3.44b), we now have

$$\bar{t}_f(t) = t_0 - \bar{t}_c(t) \quad \Rightarrow \quad \bar{t}_f = t_0, \tag{3.46}$$

Thus we may reduce the original system (3.31) of five equations to the two dimensional system

$$\frac{d\bar{m}}{dt} = \bar{\mu}_m\left(\frac{{t_0}^n}{\bar{\kappa}_D^n + {t_0}^n}\right) - \bar{\delta}_m\bar{m}, \tag{3.47a}$$

$$\frac{d\bar{p}}{dt} = \bar{\mu}_p\bar{m} - \bar{\delta}_p\bar{p}, \tag{3.47b}$$

together with the initial conditions

$$\bar{m}(0) = m_0, \qquad \bar{p}(0) = p_0. \tag{3.48}$$

In the system above, we have expressed the function which describes mRNA synthesis as

$$\bar{m}_{(\mathtt{synth})} = \bar{\mu}_m \left(\frac{{t_0}^n}{\bar{\kappa}_D^{\,n} + {t_0}^n} \right) \quad \text{where} \quad \bar{\mu}_m = \bar{\mu}_d d_0. \tag{3.49}$$

We refer to $\bar{\mu}_m$ as the *maximal* rate of transcription; in the case of no transcription factor ($t_0 = 0$) $\bar{m}_{(\mathtt{synth})} = 0$, whereas when transcription factor is present at a maximum (t_0), $\bar{\mu}_m$ describes the maximum number of molecules/ml the DNA can transcribe per second. The action of the transcription factor is described by the term in brackets, which we refer to as a gene activation function. This can only have a value of between zero and one; thus it describes the fraction of genes capable of producing mRNA. This gene activation function is plotted in Figure 3.5 using arbitrary values.

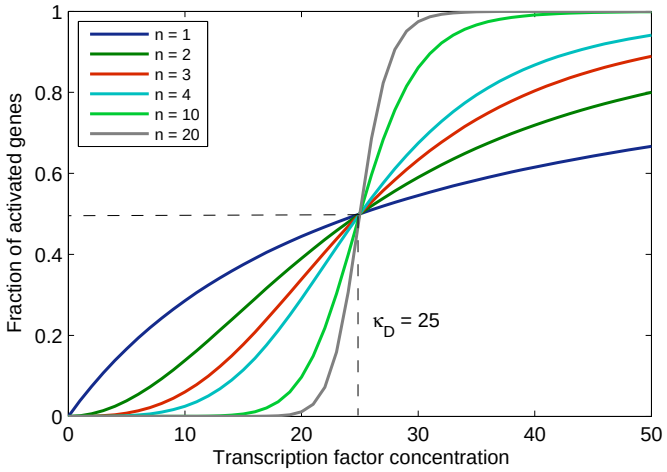

Fig. 3.5: Response of gene activation to the number of transcription factor binding sites, n, with $\bar{s}_0 = 50$. Dashed line illustrates the value of $\bar{\kappa}_D$.

From Figure 3.5, we can see that as the number of binding sites on the gene, n, increases from 1, the behaviour of the activation function changes from being hyperbolic to sigmoidal in shape. Thus the greater the number of binding sites, the greater the sensitivity of the concentration of activated genes to the concentration of transcription factor. Higher values of n confer better

levels of control by the gene; the sigmoidal behaviour suggests a switch-like behaviour for activation of the gene. This is the type of behaviour we would expect given that the role of the transcription factor is to activate or deactivate gene expression, as discussed in Section 3.1.

Information from the work of Vallett et al. (1996), that the HMGR gene contains one main binding site for its transcription factor and two additional binding sites in the promoter region, indicates that the value of $n = 3$. The dashed line in Figure 3.5 illustrates that the value of $\bar{\kappa}_D$ is equivalent to the concentration of transcription factor at which half of the gene binding sites are occupied. Figure 3.6 demonstrates the effect of varying $\bar{\kappa}_D$ on the gene activation function for the case $n = 3$.

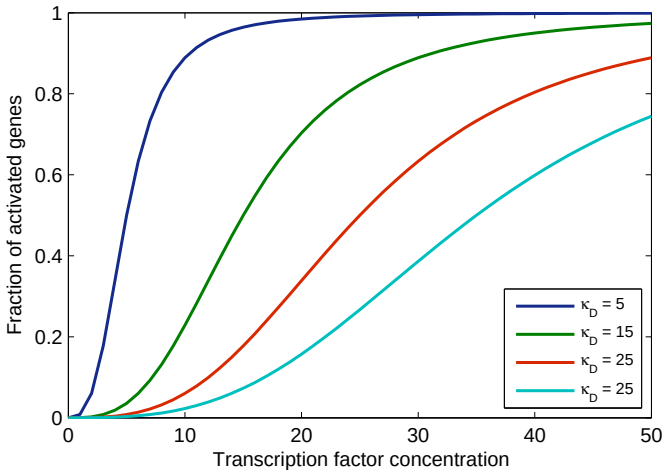

Fig. 3.6: Sensitivity of gene activation to various values of the binding affinity parameter, $\bar{\kappa}_D$, for the case $n = 3$ with $\bar{s}_0 = 50$.

We see that smaller values of $\bar{\kappa}_D$ confer greater sensitivity to transcription factor concentration, and this sensitivity decreases as $\bar{\kappa}_D$ increases. Figure 3.6 also illustrates that for $\bar{\kappa}_D >> t_0$, the gene activation function $\to 0$; in this case the gene is unlikely to ever reach full activation state, and the action of the transcription factor becomes redundant. Similarly, for $\bar{\kappa}_D << t_0$, the gene activation function $\to 1$; here the gene will reach full activation very quickly regardless of how much transcription factor is available. This is better understood by considering the constant $\bar{\kappa}_D$ in greater detail,

$$\bar{\kappa}_D^{\,n} = \frac{\bar{k}_r}{\bar{k}_f} = \frac{\text{dissociation rate}}{\text{association rate}}, \tag{3.50}$$

Smaller values of $\bar{\kappa}_D$ occur when the rate of association is large compared with the rate of dissociation, that is, the higher the binding affinity between the transcription factor and DNA. Higher affinity binding implies that a relatively low concentration of transcription factor is adequate to maximally occupy the transcription factor binding sites on the gene and trigger a physiological response. Similarly, for larger values of $\bar{\kappa}_D$, when the rate of association is small compared with the rate of dissociation, the resulting low affinity binding implies that a relatively high concentration of a ligand is required before the binding sites are maximally occupied and any response in gene expression is seen.

The underlying reason for the development of a model of regulated gene expression was to describe the synthesis of HMGR and LDLR. For both these proteins, cholesterol is the signal molecule whose concentration regulates synthesis. It does so via the action of a family of transcription factors known as sterol regulatory element binding proteins (SREBPs). Before attempting a mathematical formulation of this transcription factor pathway we give a brief review of SREBP biology.

3.4 The SREBP pathway and transcriptional regulation

Three SREBP proteins exist, encoded by two genes present in humans. Of these three isoforms, SREBP2 is responsible for enhancing the transcription of the LDLR (Horton et al., 2002). SREBPs are found in the membranes of the cellular organelle called the endoplasmic reticulum (ER), (see Figure 3.1), where they are inserted following their own synthesis. Here, they exist in a tight complex with the SREBP cleavage activating protein (SCAP). SCAP consists of two domains, one of which is responsible for the association with SREBP. The other domain contains a region known as the sterol sensing domain (SSD).

When the cellular cholesterol concentration becomes depleted, SCAP escorts SREBP to the Golgi apparatus of the cell, where it undergoes sequential cleavage by proteases. The net effect of this is to liberate the transcription factor, nuclear SREBP (nSREBP) which can then enter the cell nucleus (Eberlé et al., 2004; Brown and Goldstein, 1997). Here it binds to a regulatory binding

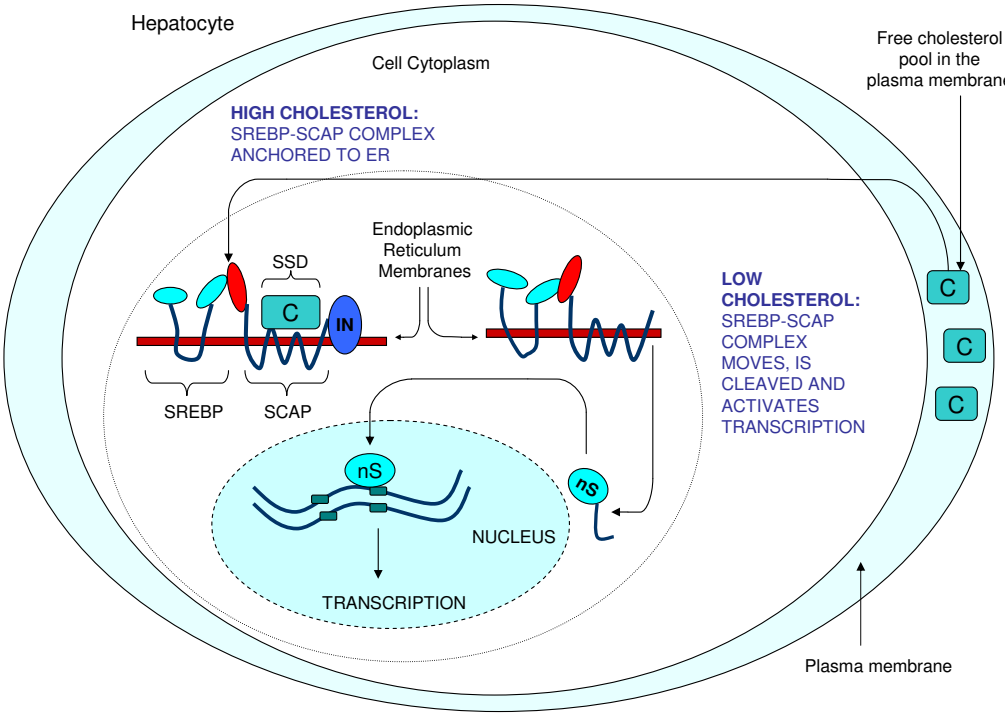

Fig. 3.7: The action of the SREBP transcription factor. In low cholesterol situations the SREBP-SCAP complex is active and free to move, undergoing sequential cleavage to form nSREBP which eventually reaches the nucleus to influence transcription. In replete cholesterol conditions, cholesterol binds to the SSD of the SREBP-SCAP complex forming an anchored inactive complex with INSIG proteins.(**C**: cholesterol; **SSD**: sterol sensing domain; **nS**: nuclear SREBP; **IN**: INSIG).

site (a short sequence of DNA) on the promoter region of the LDLR gene known as the sterol regulatory element (SRE) and activates its transcription (Soutar and Knight, 1990). In addition to activating the LDLR gene, SREBP2 preferentially activates the genes involved in cholesterol biosynthesis (Horton et al., 2002). The SRE site on the HMGR gene is structurally analogous to the SRE site on the LDLR gene and indeed the gene activation process for HMGR by nSREBP is identical to that for the LDLR (Osborne, 1995). Thus the regulation of HMGR synthesis by intracellular cholesterol concentration occurs via the same SREBP pathway that regulates LDLR synthesis.

In the presence of replete sterol concentrations, cholesterol binds directly to the sterol sensing

domain of SCAP. This causes a conformational change in SCAP which results in the binding of the SCAP-SREBP complex to INSIGs, resident ER membrane proteins that serve as anchors (Yang et al., 2002). This process is responsible for the retention of the SCAP-SREBP complex within the ER. Transcription of the target genes declines and consequently the production of LDLR and HMGR mRNA ceases.

In summary, when the cell is low in cholesterol the SCAP-SREBP complex is active and free to move. In such a state nSREBP is formed and is able to reach the nucleus activating LDLR and HMGR mRNA transcription and thus both LDLR and HMGR synthesis, thereby increasing the cholesterol concentration in the cell. If conversely there are high cholesterol levels in the cell then SCAP-SREBP is unable to move and effectively inactive. Consequently both LDLR and HMGR mRNA transcription and LDLR and HMGR translation decreases, as illustrated in Figure 3.7.

3.5 A model of regulated cholesterol biosynthesis

We have, in Section 3.3, derived equations to describe genetic regulated protein synthesis. We now consider the derivation of a mathematical model which describes the mechanism of the synthesis of the protein HMGR, subsequent cholesterol synthesis and the regulation of this pathway via the action of SREBP. This is illustrated in Figure 3.8, which is an extension of Figure 3.4 as applied to cholesterol biosynthesis.

We are now in a position to derive the full system of ODEs describing the reactions of cholesterol biosynthesis (illustrated in Figure 3.8) reproduced as a reaction mechanism below, where the transcription factor SREBP is denoted by $\bar{S}$.

$$\begin{array}{ccccccc} \text{DNA} & \xrightarrow{\bar{\mu}_{mh}} & \bar{M}_h & \xrightarrow{\bar{\mu}_h} & \bar{H} & \xrightarrow{\bar{\mu}_c} & \bar{C}. \\ \uparrow & & \downarrow{\scriptstyle \bar{\delta}_{mh}} & & \downarrow{\scriptstyle \bar{\delta}_h} & & \downarrow{\scriptstyle \bar{\delta}_c} \\ \bar{S} & & \emptyset & & \emptyset & & \emptyset \end{array} \tag{3.51}$$

Here, HMGR mRNA ($\bar{M}_h$) is transcribed at a rate $\bar{\mu}_{mh}$ and degraded at a rate $\bar{\delta}_{mh}$. The mRNA

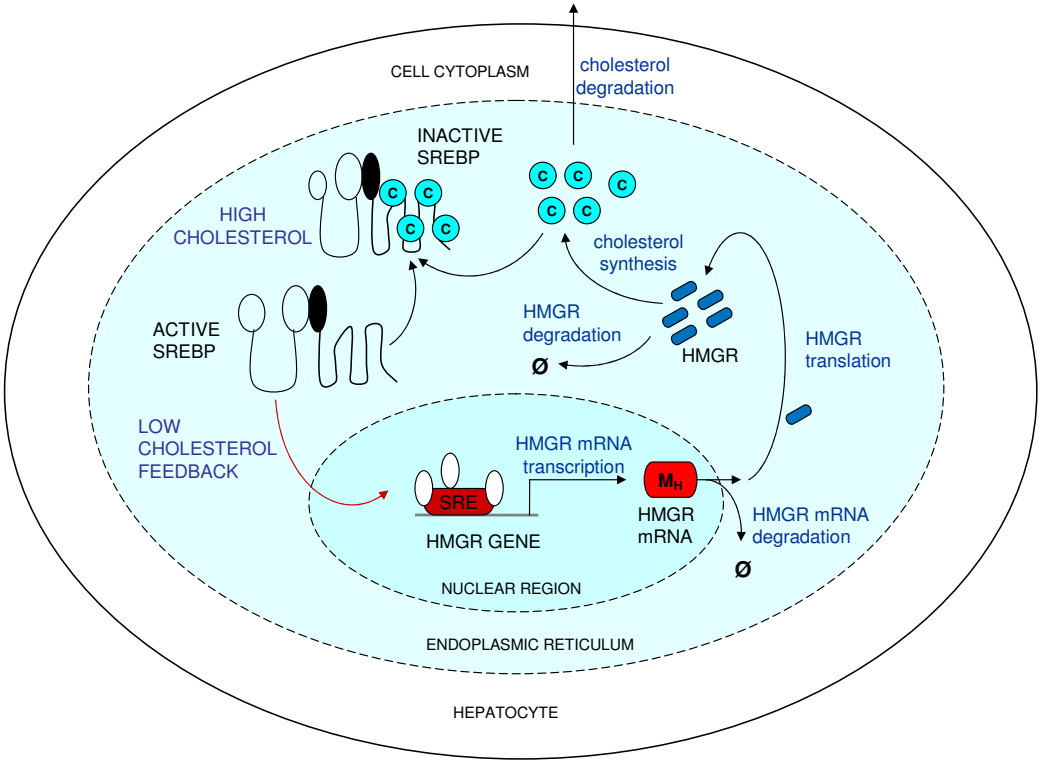

Fig. 3.8: A simplified overview of HMGR synthesis and regulation. The liver cell synthesises HMGR mRNA which in turn is translated into the enzyme HMGR. HMGR catalyses the synthesis of cholesterol which in turn influences its own transcription by interacting with the transcription factor SREBP; transcription increases when cholesterol is low in the cell and declines when cholesterol is high. (**SRE**: Sterol Regulatory Element; $\mathbf{M_h}$: HMGR mRNA; **C**: Cholesterol).

is translated at a rate $\bar{\mu}_h$ to create HMGR which subsequently produces cholesterol at a rate $\bar{\mu}_c$. HMGR degrades at rate $\bar{\delta}_h$ while cholesterol is used up at a rate $\bar{\delta}_c$.

In developing the reaction mechanism for cholesterol synthesis from HMGR, we use the fact that the HMGR reaction is the rate limiting (or slowest) step of the complete multistep pathway, and so this rate imposes an upper limit on the rate of the biosynthesis pathway as a whole, allowing its reduction into a single step mechanism.

Following the general derivation of Section 3.3, we can adapt the equations of system (3.47) to model the production of mRNA, $\bar{M}_h$, and HMGR protein, $\bar{H}$.

We apply the law of mass action to (3.51), and using the results of the previous section, obtain the system of equations

$$\frac{d\bar{m}_h}{dt} = \bar{\mu}_{mh}\left(\frac{\bar{s}^n}{(\bar{\kappa}_{mh})^n+\bar{s}^n}\right)-\bar{\delta}_{mh}\bar{m}_h, \tag{3.52a}$$

$$\frac{d\bar{h}}{dt} = \bar{\mu}_h\bar{m}_h-\bar{\delta}_h\bar{h}, \tag{3.52b}$$

$$\frac{d\bar{c}}{dt} = \bar{\mu}_c\bar{h}-\bar{\delta}_c\bar{c}, \tag{3.52c}$$

with initial conditions

$$\bar{m}_h(0)=\bar{m}_{h0}, \qquad \bar{h}(0)=\bar{h}_0, \qquad \bar{c}(0)=\bar{c}_0, \tag{3.53}$$

where $\bar{s}=[\bar{S}]$ and the parameter $\bar{\kappa}_{mh}$ reflects the binding efficiency between the transcription factor $\bar{s}$ and the HMGR gene promoter.

In system (3.52) the transcription factor $\bar{s}$ represents the active SREBP-SCAP complex (described in Section 3.4). To complete our model system we now go on to model the interaction between the active transcription factor SREBP, $\bar{s}$, and cholesterol, $\bar{c}$ by considering that the binding of cholesterol to active SREBP results in the transcription factor becoming inactive.

This is a simplified representation of the biological process of SREBP-SCAP complex retention in the wall of the ER when cholesterol binds to the sterol sensing domain of SCAP.

3.5.1 Modelling the interaction of SREBP and cholesterol

The final step in our cholesterol biosynthesis model derivation is to determine how the transcription factor interacts with cholesterol.

We know from Section 3.4 that SREBP is deactivated upon the binding of cholesterol, and we describe this reaction by

$$\bar{S}+q\bar{C}\underset{\bar{k}_d}{\overset{\bar{k}_a}{\rightleftharpoons}}\bar{SC}_q, \tag{3.54}$$

in which $\bar{k}_a$ describes the rate of transcription factor-cholesterol complex formation and the complex dissociates with rate $\bar{k}_d$. Here q represents the number of molecules of cholesterol, $\bar{C}$, that can bind to one molecule of active SREBP, $\bar{S}$.

We consider that SREBP, $\bar{S}$, can exist in one of two states, the active (or free) form, $\bar{S}$, which can initiate transcription, and the inactive form, $\bar{SC}_q$, which is bound to cholesterol. Applying the law of mass action to (3.54) leads to,

$$\frac{d\bar{s}}{dt} = \bar{k}_d\bar{s}_b - \bar{k}_a\bar{s}\bar{c}^q, \tag{3.55a}$$

$$\frac{d\bar{c}}{dt} = q\bar{k}_d\bar{s}_b - q\bar{k}_a\bar{s}\bar{c}^q, \tag{3.55b}$$

$$\frac{d\bar{s}_b}{dt} = \bar{k}_a\bar{s}\bar{c}^q - \bar{k}_d\bar{s}_b, \tag{3.55c}$$

with initial conditions

$$\bar{s}(0)=s_0, \qquad \bar{c}(0)=c_0, \qquad \bar{s}_b(0)=0, \tag{3.56}$$

where $\bar{s}=[\bar{S}]$, $\bar{c}=[\bar{C}]$ and $\bar{s}_b=[\bar{SC}_q]$.

We note that within system (3.55), the total concentration of cholesterol is conserved. This result is obtained on adding (3.55b) and (3.55c) giving

$$\frac{d\bar{c}}{dt}+q\frac{d\bar{s}_b}{dt}=0 \qquad \Rightarrow \qquad \bar{c}(t)+q\bar{s}_b(t)=c_0, \tag{3.57}$$

on using the initial conditions (3.56).

Furthermore, a conservation law for the transcription factor is obtained immediately on adding (3.55a) and (3.55c) to obtain

$$\frac{d\bar{s}}{dt}+\frac{d\bar{s}_b}{dt}=0 \qquad \Rightarrow \qquad \bar{s}(t)+\bar{s}_b(t)=s_0, \tag{3.58}$$

on using the initial conditions (3.56).

We assume that the binding reaction of active SREBP, $\bar{s}$, and cholesterol, $\bar{c}$, reaches equilibrium

rapidly and thus make a quasi-steady-state approximation in which $d\bar{s}_b/dt \approx 0$ such that,

$$\bar{k}_a \bar{s}\, \bar{c}^q - \bar{k}_d \bar{s}_b = 0, \tag{3.59}$$

from (3.55c). We can now use the conservation law in (3.58) and replace $\bar{s}_b$ with $(s_0 - \bar{s})$, to find

$$\bar{k}_a \bar{s}\, \bar{c}^{\ q} = \bar{k}_d (s_0 - \bar{s}), \tag{3.60}$$

which upon rearranging gives

$$\bar{s} = \frac{\bar{k}_d \bar{s}_0}{(\bar{k}_d + \bar{k}_a \bar{c}^{\ q})}. \tag{3.61}$$

Thus we have an expression for the concentration of active SREBP, $\bar{s}$, in terms of its initial concentration, $\bar{s}_0$, and cholesterol, $\bar{c}$,

$$\bar{s} = \frac{\bar{s}_0}{1 + \left(\dfrac{\bar{c}}{\bar{\kappa}_C}\right)^q}, \tag{3.62}$$

where the constant $\bar{\kappa}_c$ describes the binding affinity between $\bar{s}$ and $\bar{c}$ and is defined such that,

$$\bar{\kappa}_c = \left(\frac{\bar{k}_d}{\bar{k}_a}\right)^{1/q}. \tag{3.63}$$

We note that considering the concentration of variables in units of molecules/ml, and time in units of seconds, $\bar{k}_d$ has units of s^{-1} and $\bar{k}_a$ has units of ml ^{q} molecules^{-q} s^{-1}. Therefore, $\bar{\kappa}_c$ has units of molecules ml^{-1}.

Before deriving the full system of equations we take into account that, in comparison to enzymes and proteins, transcription factors are present in low intracellular concentrations (Sanguinetti et al., 2006).

Therefore, we will consider that the concentration of cholesterol required to bind to the active transcription factor, and the concentration of cholesterol resulting from the dissociation of the complex $\bar{s}_b$ will not cause any significant decrease or increase, respectively, in the total cell concentration of cholesterol.

Now, substituting the derived value of $\bar{s}$ in (3.62) into (3.52a) and rearranging we obtain

$$\frac{d\bar{m}_h}{dt} = \frac{\bar{\mu}_{mh}}{\left(1+\left(\frac{\bar{\kappa}_{mh}\left(1+(\bar{c}/\bar{\kappa}_c)^q\right)}{\bar{s}_0}\right)^n\right)} - \bar{\delta}_{mh}\bar{m}_h, \tag{3.64a}$$

$$\frac{d\bar{h}}{dt} = \bar{\mu}_h\bar{m}_h - \bar{\delta}_h\bar{h}, \tag{3.64b}$$

$$\frac{d\bar{c}}{dt} = \bar{\mu}_c\bar{h} - \bar{\delta}_c\bar{c}, \tag{3.64c}$$

which, with the initial conditions

$$\bar{m}_h(0) = \bar{m}_{h0}, \qquad \bar{h}(0) = \bar{h}_0, \qquad \bar{c}(0) = \bar{c}_0, \tag{3.65}$$

composes the system of equations derived to model the pathways of Figure 3.8.

The behaviour of active SREBP, $\bar{s}$, as a function of cholesterol concentration in equation (3.62), is illustrated in Figure 3.9. From Figure 3.9, we can see that if there is only one cholesterol binding site on SREBP, the concentration of $\bar{s}$ decreases hyperbolically as cholesterol concentration increases. As the number of binding sites increases, this behaviour changes to be sigmoidal. This allows active SREBP to switch between maximum state and zero within a definite range of cholesterol concentration. Experimental support for the derived mathematical form (3.62), of

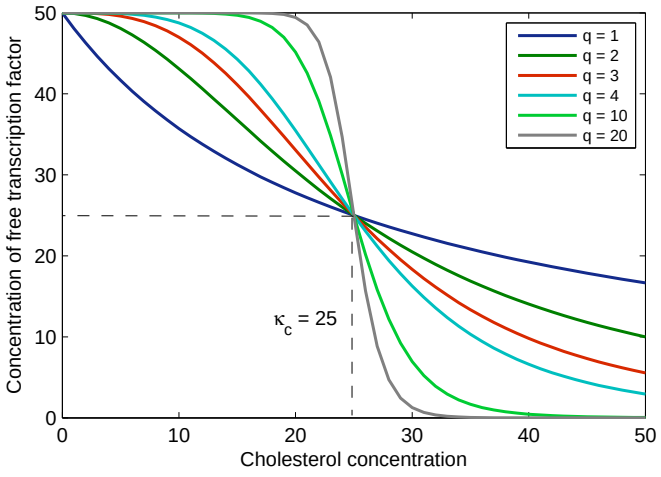

Fig. 3.9: Response of SREBP, $\bar{s}$, to variation in the number of cholesterol binding sites, q, with $\bar{s}_0 = 50$. Dashed line illustrates the value of $\bar{\kappa}_C$.

the interaction between $\bar{s}$ and $\bar{c}$, comes from the work of Radhakrishnan et al. (2004), whose results indicate a sigmoidal relationship between SREBP and ER cholesterol. Their later work, Radhakrishnan et al. (2008), one of the results of which is reproduced in Figure 3.10, further confirmed this relationship and demonstrated a Hill coefficient of 3.7 ± 0.23.

These experiments investigated the processing of nuclear SREBP2 in response to the concentration of cholesterol within the ER. Their results cannot be quantitatively matched, as in our equations SREBP response is modelled as a function of whole cell cholesterol concentration. However, Figure 3.10 confirms a qualitative fit of the sigmoidal nature of the interaction between SREBP and cholesterol.

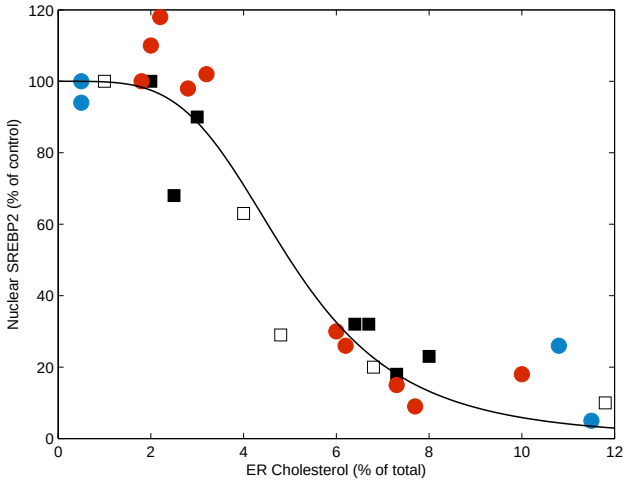

Fig. 3.10: Results of four experiments to determine the behaviour of nuclear SREBP2 in response to cholesterol concentration within the ER, (data reproduced from Figure 4c of Radhakrishnan et al. (2008)).

Using the assumption that the binding reaction (3.54) displays marked positive cooperativity (see Section 3.2), that is assuming all q molecules of cholesterol bind to SREBP simultaneously, we take a value of $q = 4$.

Thus in our model, we assume the binding of cholesterol to SREBP to be tetrameric, as have Radhakrishnan et al. (2004, 2008). The response of the function to changes in $\bar{\kappa}_c$ is illustrated in Figure 3.11 for the case $q = 4$.

We see that for smaller values of $\bar{\kappa}_C$ there is greater sensitivity in the response of SREBP to the concentration of cholesterol, and this sensitivity decreases as $\bar{\kappa}_C$ increases.

This can be understood by considering $\bar{\kappa}_c$ as equivalent to the concentration of cholesterol required to deactivate half of the total concentration of SREBP; the greater the value of $\bar{\kappa}_C$, the larger the concentration of cholesterol needed to deactivate SREBP, and therefore, the less sensitive the mechanism.

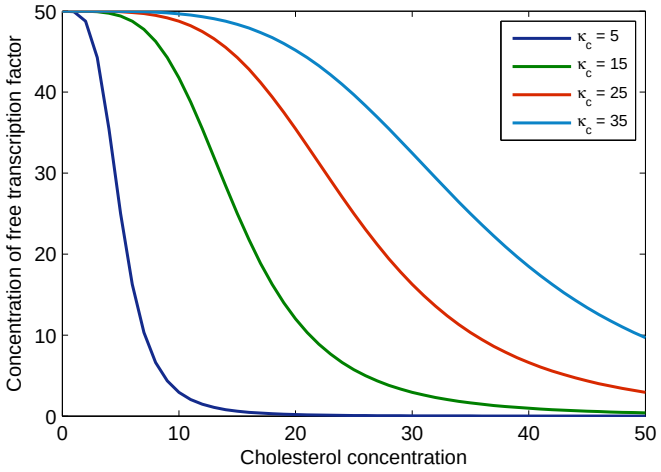

Fig. 3.11: Sensitivity of SREBP, $\bar{s}$, to various values of the binding affinity parameter, $\bar{\kappa}_C$, for the case $q = 4$ with $\bar{s}_0 = 50$.

The regulated cholesterol biosynthesis model

The equations describing regulated cholesterol biosynthesis are thus given by system (3.64) with $n = 3$ and $q = 4$. Thus the time evolution of the variables HMG-CoA reductase mRNA, $\bar{M}_h$, HMG-CoA reductase, $\bar{H}$ and cholesterol, $\bar{C}$ are governed by

$$\frac{d\bar{m}_h}{dt} = \frac{\bar{\mu}_{mh}\left(\bar{s}_0\,\bar{\kappa}_c{}^4\right)^3}{\left(\bar{s}_0\,\bar{\kappa}_c{}^4\right)^3 + \left(\bar{\kappa}_{mh}\left(\bar{\kappa}_c{}^4 + \bar{c}^{\,4}\right)\right)^3} - \bar{\delta}_{mh}\bar{m}_h, \tag{3.66a}$$

$$\frac{d\bar{h}}{dt} = \bar{\mu}_h\bar{m}_h - \bar{\delta}_h\bar{h}, \tag{3.66b}$$

$$\frac{d\bar{c}}{dt} = \bar{\mu}_c\bar{h} - \bar{\delta}_c\bar{c}, \tag{3.66c}$$

with the initial conditions

$$\bar{m}_h(0) = \bar{m}_{h0}, \qquad \bar{h}(0) = \bar{h}_0, \qquad \bar{c}(0) = \bar{c}_0. \tag{3.67}$$

Parameterisation of the above model system is discussed in the following section.

3.5.2 Model parameterisation

The next step in our model construction is the determination of parameter values. We use, wherever possible, data taken from human liver cells, or the HepG2 cell line, a liver cell line derived from a human hepatoblastoma cancer cell line that has been found to express a wide variety of liver-specific metabolic functions. If this data is unavailable, values from the closest possible counterpart, for example, human liver microsomes or Chinese hamster cells, have been used, (see Table 3.1).

Where no experimental data was available for particular parameters, the latter were approximated using calculations based on the biochemical reactions occurring; the main references for these calculations are given in Table 3.1. Further details and references pertaining to the specific calculations are to be found in Appendix B.1.

We note that there are as yet undetermined parameters in our model. Specifically, these are the parameters $\bar{\delta}_c$, $\bar{\kappa}_{mh}$ and $\bar{\kappa}_c$.

The rate of degradation of cholesterol, $\bar{\delta}_c$, is unlike the other degradation rates in the model, in that it is not a simple decay rate dependent on the half life of the molecule, as cholesterol cannot be degraded. Instead it is a measure of the extracellular or intracellular demands on the intracellular cholesterol concentration. As such, this rate is variable and so for numerical simulations we assign an initial value for $\bar{\delta}_c$ based on the values of $\bar{\delta}_{mh}$ and $\bar{\delta}_h$ and vary this parameter in the model investigation (see Chapter 5).

The binding affinity parameter, $\bar{\kappa}_{mh}$, is representative of the interaction between SREBP and

Parameter	Description	Value	Reference
$\bar{\mu}_{mh}$	HMGR mRNA transcription rate	5.36×10^6 molecules ml^{-1} s^{-1}	Goldstein and Brown (1984)
$\bar{\mu}_h$	HMGR translation rate	5.10×10^{-1} s^{-1}	Luskey and Stevens (1985)
$\bar{\mu}_c$	Cholesterol synthesis rate	4.33×10^{-2} s^{-1}	Tanaka et al. (1982)
$\bar{\delta}_{mh}$	HMGR mRNA degradation rate	4.48×10^{-5} s^{-1}	Wilson and Deeley (1995)
$\bar{\delta}_h$	HMGR degradation rate	6.42×10^{-5} s^{-1}	Brown et al. (1974)
$\bar{\kappa}_c$	Cholesterol-SREBP dissociation constant	undetermined	
$\bar{s}_0$	Total concentration of SREBP	8.21×10^{16} molecules ml^{-1}	Lange et al. (1999)
$\bar{\delta}_c$	Cholesterol utilisation rate	undetermined	
$\bar{\kappa}_{mh}$	SREBP-HMGR gene dissociation constant	undetermined	
Initial	**Description**	**Value**	
$\bar{m}_{h0}$	Initial HMGR mRNA concentration	3.00×10^{10} molecules ml^{-1}	Rudling et al. (2002)
$\bar{h}_0$	Initial HMGR concentration	9.04×10^{14} molecules ml^{-1}	Istvan et al. (2000)
$\bar{c}_0$	Initial cholesterol concentration,	1.89×10^{19} molecules ml^{-1}	Lange et al. (1999)

Table 3.1: Dimensional parameter values and initial conditions of the HMGR model.

the gene. Although this parameter has a biological interpretation, we note that it arises from the approximations and reductions that we have used to derive and simplify the model equations. Thus $\bar{\kappa}_{mh}$ may not have a direct biochemical interpretation and so we have not found any experimental data which allows calculation of this parameter.

The binding affinity parameter, $\bar{\kappa}_c$, describes the interaction between SREBP and cholesterol. Although this parameter has both an explicit biological and biochemical meaning, we have been unable to find an experimental value which allows us to approximate this parameter. The reasons for this are twofold.

Firstly, $\bar{s}$ in our model is assumed to react in response to whole cell cholesterol concentration, whereas in reality it is thought to respond to a much smaller pool of cholesterol that resides within the endoplasmic reticulum.

Secondly, both cholesterol and SCAP, which represents the binding region for cholesterol on SREBP, are both completely insoluble and so cannot be used in standard *in vitro* binding assays. Both the ligand and the binding protein must be added to assays in detergents and so cannot be analysed using the standard techniques for binding assays, (Radhakrishnan et al., 2004). These parameters will be considered in greater detail in Chapter 5.

Summary

In this chapter we have derived and parameterised an ODE model of intracellular cholesterol biosynthesis and genetic regulation. This model has been derived in a similar manner to a classic ODE model of genetic regulation developed by Goodwin (1963) and modified by Griffith (1968). However, we have explicitly proposed a novel two step feedback mechanism in which end product repression occurs via the inactivation of a specific transcription activator involved in the biological pathway of *de novo* synthesis. This repression is described using a Hill equation, and the repressor reaction mechanism has been derived from the biological processes underlying cellular cholesterol homeostasis. In the next chapter we explore the behaviour of the system using analytic techniques.

4

Analysis of The Cholesterol Biosynthesis Model

In the previous chapter we have derived an ODE model of the genetic regulation of cholesterol biosynthesis. In this chapter we consider an analytic investigation of the model, and determine that the model has only one physiologically valid steady state, which can exhibit different stability properties. The steady state may be stable, in which case either the system tends monotonically to this steady state or undergoes oscillatory convergence before reaching steady state. Alternatively the steady state may undergo a local Hopf bifurcation and exhibit limit cycle behaviour which gives rise to oscillatory solutions. Further analysis, by means of centre manifold theory, is performed on the limit cycle to obtain results on the nature of the limit cycle stability, and the physical properties, the amplitude and time period of the oscillations. We conclude

this chapter by considering the significance of the analytic conclusions made, both in relation to the biological phenomenon of homeostasis, and in reference to the work of Goodwin (1963) and Griffith (1968) discussed in Chapter 3.

4.1 Nondimensionalisation

Before proceeding to a complete analysis of the model, the equations of system (3.66) are nondimensionalised. To nondimensionalise, we rescale time with respect to the degradation rate of $\bar{m}_h$,

$$\tau = \bar{\delta}_{mh} t, \tag{4.1}$$

where τ represents nondimensional time. Variables describing concentration are rescaled with respect to the concentration of total (free and bound) SREBP, $\bar{s}_0$,

$$m_h = \frac{\bar{m}_h}{\bar{s}_0}, \qquad h = \frac{\bar{h}}{\bar{s}_0}, \qquad c = \frac{\bar{c}}{\bar{s}_0}, \tag{4.2}$$

where overbars denote the dimensional counterparts of the variables.

If the model system (3.66) is now formulated in terms of the rescaled variables (4.1) and (4.2), we obtain the following system of dimensionless equations

$$\frac{dm_h}{d\tau} = \frac{\mu_{mh}\,{\kappa_c}^{12}}{{\kappa_c}^{12} + \left(\kappa_{mh}\left({\kappa_c}^4 + c^4\right)\right)^3} - m_h, \tag{4.3a}$$

$$\frac{dh}{d\tau} = \mu_h m_h - \delta_h h, \tag{4.3b}$$

$$\frac{dc}{d\tau} = \mu_c h - \delta_c c, \tag{4.3c}$$

with nondimensional initial conditions

$$m_h(0) = \frac{\bar{m}_{h0}}{\bar{s}_0}, \qquad h(0) = \frac{\bar{h}_0}{\bar{s}_0}, \qquad c(0) = \frac{\bar{c}_0}{\bar{s}_0}. \tag{4.4}$$

The model in this form is dependent on the new nondimensional parameters

$$\begin{aligned} \mu_h &= \frac{\bar{\mu}_h}{\bar{\delta}_{mh}}, \qquad \mu_c = \frac{\bar{\mu}_c}{\bar{\delta}_{mh}}, \qquad \mu_{mh} = \frac{\bar{\mu}_{mh}}{\bar{s}_0 \bar{\delta}_{mh}}, \\ \kappa_{mh} &= \frac{\bar{\kappa}_{mh}}{\bar{s}_0}, \qquad \kappa_c = \frac{\bar{\kappa}_c}{\bar{s}_0}, \qquad \delta_c = \frac{\bar{\delta}_c}{\bar{\delta}_{mh}}, \qquad \delta_h = \frac{\bar{\delta}_h}{\bar{\delta}_{mh}}, \end{aligned} \tag{4.5}$$

where overbars denote the dimensional counterparts of the parameters. Here, μ_{mh}, μ_h and μ_c represent rates of synthesis of m_h, h and c respectively, δ_h and δ_c are the rates of degradation of h and c, and κ_{mh} and κ_c are association constants between s and the HMGR gene and s and c respectively. We now consider the steady state solutions of the system.

4.2 Steady state analysis

The steady states of system (4.3) are given by the solution of the following system

$$0 = \frac{\mu_{mh}\, {\kappa_c}^{12}}{{\kappa_c}^{12} + \left(\kappa_{mh}\left({\kappa_c}^4 + c_{ss}^4\right)\right)^3} - m_{hss}, \tag{4.6a}$$

$$0 = \mu_h m_{hss} - \delta_h h_{ss}, \tag{4.6b}$$

$$0 = \mu_c h_{ss} - \delta_c c_{ss}, \tag{4.6c}$$

where m_{hss}, h_{ss} and c_{ss} are the steady state values of m_h, h and c respectively. The form of this solution is now investigated.

From (4.6c) we have

$$h_{ss} = \frac{\delta_c}{\mu_c} c_{ss}, \tag{4.7}$$

and therefore from (4.6b) we see that

$$m_{hss} = \frac{\delta_h \delta_c}{\mu_h \mu_c} c_{ss} = \alpha c_{ss}, \tag{4.8}$$

where

$$\alpha = \frac{\delta_h \delta_c}{\mu_h \mu_c}. \tag{4.9}$$

Substituting this value of m_{hss} into (4.6a) we obtain

$$\alpha c_{ss} \left(1 + \left(\kappa_{mh}\left(1 + \left(\frac{c_{ss}}{\kappa_c}\right)^4\right)\right)^3\right) - \mu_{mh} = 0. \tag{4.10}$$

Expanding the powers then leads to

$$\left(\frac{\beta}{{\kappa_c}^{12}}\right) {c_{ss}}^{13} + \left(\frac{3\beta}{{\kappa_c}^8}\right) {c_{ss}}^9 + \left(\frac{3\beta}{{\kappa_c}^4}\right) {c_{ss}}^5 + (\alpha+\beta)\, c_{ss} - \mu_{mh} = 0, \tag{4.11}$$

where

$$\beta = \alpha \kappa_{mh}^3. \tag{4.12}$$

Since (4.11), a polynomial equation of degree thirteen and hence with thirteen roots, does not admit analytic solutions, we use the results of Descartes' rule of signs to deduce the nature of its roots (see Appendix C.1). As all parameters are real and positive valued, we can apply Descartes' rule of signs for positive roots (Theorem IV of Appendix C.1) which states that the number of positive real roots of (4.11) is either equal to the number of variations of signs in the coefficients of (4.13) or less than this by an even integer. We have

$$p(c_{ss}) \;=\; \left(\frac{\beta}{{\kappa_c}^{12}}\right) {c_{ss}}^{13} + \left(\frac{3\beta}{{\kappa_c}^8}\right) {c_{ss}}^9 + \left(\frac{3\beta}{{\kappa_c}^4}\right) {c_{ss}}^5 + (\alpha+\beta)\, c_{ss} - \mu_{mh} = 0. \tag{4.13}$$

It is clear that there is only one sign change in the sequence of coefficients of (4.13); therefore (4.11) has only one positive real root.

To calculate the number of negative real roots of (4.11) we apply Descartes' rule of signs for negative roots (Theorem V of Appendix C.1), where we consider the polynomial $q(c_{ss}) = p(-c_{ss})$ given by

$$q(c_{ss}) \;=\; -\left(\frac{\beta}{{\kappa_c}^{12}}\right) {c_{ss}}^{13} - \left(\frac{3\beta}{{\kappa_c}^8}\right) {c_{ss}}^9 - \left(\frac{3\beta}{{\kappa_c}^4}\right) {c_{ss}}^5 - (\alpha+\beta)\, c_{ss} - \mu_{mh} = 0. \tag{4.14}$$

There are no sign changes in the sequence of coefficients of (4.14) which indicates that $q(c_{ss})$ has no positive real roots. Consequently (4.11) has no real negative roots, and we conclude that the remaining twelve roots are six pairs of conjugate complex roots.

Therefore we conclude that system (4.3) has exactly one positive real root, corresponding to a physiologically valid fixed point of the system.

Let c^* be c_{ss}, the positive real root of (4.11). The physiologically valid fixed point of system (4.3) can thus be described by

$$(m_{hss}, h_{ss}, c_{ss}) = \left(\frac{\delta_h \delta_c}{\mu_h \mu_c} c^*, \frac{\delta_c}{\mu_c} c^*, c^* \right). \tag{4.15}$$

We now consider the stability of this fixed point by investigation of the eigenvalues of the linearised Jacobian matrix **J** of system (4.3), which is given by

$$\mathbf{J} = \begin{bmatrix} -1 & 0 & -\varphi \\ \mu_h & -\delta_h & 0 \\ 0 & \mu_c & -\delta_c \end{bmatrix}, \tag{4.16}$$

with

$$\varphi = -\left(\frac{\partial \phi}{\partial c} \right) \Big|_{c = c_{ss}}, \tag{4.17}$$

where

$$\phi = \frac{\mu_{mh} \, {\kappa_c}^{12}}{{\kappa_c}^{12} + \left(\kappa_{mh} \left({\kappa_c}^4 + c^4 \right) \right)^3}, \tag{4.18}$$

and so,

$$\varphi = -\left(\frac{\partial \phi}{\partial c} \right) \Big|_{c = c_{ss}} = \frac{12 \mu_{mh} {\kappa_{mh}}^3 {\kappa_c}^{12} {c_{ss}}^3 \left({\kappa_c}^4 + {c_{ss}}^4 \right)^2}{\left({\kappa_c}^{12} + \left(\kappa_{mh} \left({\kappa_c}^4 + {c_{ss}}^4 \right) \right)^3 \right)^2}. \tag{4.19}$$

We note that $\varphi \geq 0$ as all parameter values are positive and $c_{ss} \geq 0$ for physiologically valid parameter values.

The eigenvalues of **J** satisfy the characteristic equation

$$\lambda^3+(1+\delta_h+\delta_c)\lambda^2+(\delta_h+\delta_c+\delta_h\delta_c)\lambda+\left(\delta_h\delta_c+\mu_h\mu_c\varphi\right)=0, \tag{4.20}$$

which has three roots, λ_1, λ_2 and λ_3. Firstly we note that $\varphi \geq 0$ ensures all coefficients of (4.20) are positive and thus by Descartes' rule of signs there can be no purely positive real eigenvalues. There are then two cases for the roots of (4.20),

either three negative real eigenvalues,

or one negative real eigenvalue and a pair of complex conjugate eigenvalues.

The fixed point is stable iff the real parts of λ_1, λ_2 and λ_3 are negative. To determine for which conditions this occurs, we apply the Routh-Hurwitz criteria to (4.20). Routh-Hurwitz's criteria (see Appendix C.2) applied to a cubic equation

$$\lambda^3+a_2\lambda^2+a_1\lambda+a_0=0, \tag{4.21}$$

are satisfied if and only if $a_0>0$, $a_1>0$, $a_2>0$ and $a_1a_2-a_0>0$. That is, the necessary and sufficient condition for the roots of (4.20) to have negative real part requires

$$1+\delta_h+\delta_c > 0, \tag{4.22a}$$

$$\delta_h+\delta_c+\delta_h\delta_c > 0, \tag{4.22b}$$

$$\delta_h\delta_c+\mu_h\mu_c\varphi > 0, \tag{4.22c}$$

$$(1+\delta_h+\delta_c)(\delta_h+\delta_c+\delta_h\delta_c)-\left(\delta_h\delta_c+\mu_h\mu_c\varphi\right) > 0. \tag{4.22d}$$

Since all parameters are positive and real, condition (4.22a) and condition (4.22b) evidently hold, and further as $\varphi \geq 0$, condition (4.22c) also holds. Thus the stability of the roots is dependent on condition (4.22d), which is now considered in detail.

- **Case I** : $(1+\delta_h+\delta_c)(\delta_h+\delta_c+\delta_h\delta_c)-\left(\delta_h\delta_c+\mu_h\mu_c\varphi\right)>0$.

  In this case the steady state is stable. This implies that all three eigenvalues must have

negative real part. This encompasses two possibilities. Firstly, there may be three negative real eigenvalues in which case the equilibrium is a stable node. Secondly, there may be one negative real eigenvalue and a pair of complex conjugate eigenvalues with negative real part, which corresponds to the equilibrium being a stable focus or spiral.

- **Case II** : $(1+\delta_h+\delta_c)(\delta_h+\delta_c+\delta_h\delta_c)-\left(\delta_h\delta_c+\mu_h\mu_c\varphi\right)=0.$
  Substituting $(1+\delta_h+\delta_c)(\delta_h+\delta_c+\delta_h\delta_c)=\left(\delta_h\delta_c+\mu_h\mu_c\varphi\right)$ into (4.20), we now have the characteristic equation given by

$$\begin{aligned}\lambda^3+(1+\delta_h+\delta_c)\lambda^2+(\delta_h+\delta_c+\delta_h\delta_c)\lambda+(1+\delta_h+\delta_c)(\delta_h+\delta_c+\delta_h\delta_c) &= 0,\\ (\lambda+(1+\delta_h+\delta_c))\left(\lambda^2+(\delta_h+\delta_c+\delta_h\delta_c)\right) &= 0,\end{aligned}$$

  and so the characteristic equation has two conjugate roots $\lambda_{1,2}$ on the imaginary axis and one negative real eigenvalue λ_3 given by

$$\lambda_{1,2} = \pm i\sqrt{(\delta_h+\delta_c+\delta_h\delta_c)}, \tag{4.23}$$

$$\lambda_3 = -(1+\delta_h+\delta_c). \tag{4.24}$$

  The existence of a pair of pure imaginary eigenvalues means that we cannot determine the stability of the equilibrium using these means.

- **Case III** : $(1+\delta_h+\delta_c)(\delta_h+\delta_c+\delta_h\delta_c)-\left(\delta_h\delta_c+\mu_h\mu_c\varphi\right)<0.$
  In this case the steady state is unstable. This implies that at least one eigenvalue must have positive real part. As, from above, there can be no positive real eigenvalues it must be the case that there is one negative real eigenvalue and a pair of complex conjugate eigenvalues with positive real part and this will result in a saddle focus or spiral saddle.

Of particular interest is **Case II**, as here the possibility arises whereby the fixed point will lose stability as a result of a pair of complex conjugate eigenvalues crossing the imaginary axis.

This type of behaviour is a local bifurcation called a Hopf (or Poincare-Andronov-Hopf) bifurcation, and in the next section we will explore this bifurcation in greater detail.

4.2.1 Existence of the Hopf bifurcation

From the stability condition (4.22c) and the three cases described in the previous section, we can see that a variation in any single one of the parameters of system (4.3) may result in a loss of stability via complex conjugate eigenvalues crossing the imaginary axis. In this section we prove the existence of a Hopf bifurcation for two system parameters, μ_c and δ_c. The choice of a synthesis rate and a degradation rate as the critical bifurcation parameters is made on the assumption that it is, in biological terms, more feasible that this type of parameter will be subject to fluctuations, rather than κ_{mh} and κ_c which reflect more structural aspects of the chemical reactions occurring (they are, nevertheless, highly significant and are considered in greater detail in Chapter 5).

We begin by considering μ_c as the critical bifurcation parameter and analyse this case in detail to illustrate the proof, following which results are presented proving the existence for δ_c as the critical parameter.

According to the Hopf bifurcation theorem (Guckenheimer and Holmes, 1983), a bifurcation occurs for a critical value $\mu_c = \mu_c^*$, for which the following two conditions are fulfilled, at the equilibrium point $(m_{hss}, h_{ss}, c_{ss})$,

1. The matrix **J** has two complex eigenvalues

$$\lambda_{2,3} = \theta\left(\mu_c\right) \pm i\,\omega\left(\mu_c\right), \tag{4.25}$$

   in some neighbourhood of μ_c^* and for $\mu_c = \mu_c^*$ these eigenvalues are purely imaginary, that is,

$$\theta\left(\mu_c^*\right) = 0 \quad \text{and} \quad \omega\left(\mu_c^*\right) \neq 0. \tag{4.26}$$

   This non-hyperbolicity condition is a necessary condition for the Hopf bifurcation.

2. The relation

$$\left.\frac{d\,\theta\left(\mu_c\right)}{d\,\mu_c}\right|_{\mu_c = \mu_c^*} \neq 0, \tag{4.27}$$

holds in some neighbourhood of μ_c^*.

This is a sufficient condition for the Hopf bifurcation and is also known as the transversality or Hopf crossing condition. It ensures that the eigenvalues cross the imaginary axis with non zero speed and thus ensures the crossing of the complex conjugate pair at the imaginary axis is not tangent to the imaginary axis. If this is not the case we may observe, for example, the occurrence in which the eigenvalues move up to the imaginary axis and then reverse direction without crossing.

We notice that the first condition has already been shown to hold at the critical value of μ_c given by the solution of

$$\mu_c^* = \frac{1}{\mu_h \varphi}((1+\delta_h+\delta_c)(\delta_h+\delta_c+\delta_h\delta_c)-\delta_h\delta_c), \tag{4.28}$$

(where φ is given by (4.19)), together with the equation determining the equilibrium value of c_{ss} for μ_c^*,

$$\frac{{c_{ss}}^{13}}{{\kappa_c}^{12}} + 3\frac{{c_{ss}}^{9}}{{\kappa_c}^{8}} + 3\frac{{c_{ss}}^{5}}{{\kappa_c}^{4}} + \left(\frac{1}{\kappa_{mh}^3}+1\right)c_{ss} - \left(\frac{\mu_h\mu_{mh}}{\kappa_{mh}^3\delta_h\delta_c}\right)\mu_c^* = 0. \tag{4.29}$$

From the results of **Case II** of the previous section, we know that at this value of μ_c^* the characteristic polynomial (4.20) has two purely imaginary roots $\pm i\,\omega(\mu_c^*)$, given in (4.23), where

$$\omega(\mu_c^*) = \sqrt{(\delta_h+\delta_c+\delta_h\delta_c)} \neq 0. \tag{4.30}$$

To show that the second condition holds we use the Implicit Function Theorem. For each $\mu_c \in \mathbb{R}$ and the corresponding system (4.3), define

$$\mathrm{F}(\mu_c, \lambda) = p(\lambda), \tag{4.31}$$

as a function of two variables μ_c and λ, where $p(\lambda)$ is the characteristic polynomial of the system (4.3) defined by (4.20).

Let the complex eigenvalues $\lambda(\mu_c) = \theta(\mu_c) \pm i\,\omega(\mu_c)$ be roots of the characteristic polynomial.

Hence, for these eigenvalues we have

$$\mathrm{F}\left(\mu_c, \lambda\left(\mu_c\right)\right) = 0, \tag{4.32}$$

where (4.32) represents an implicit function of two variables μ_c and λ. The Implicit Function Theorem tells us that we may define μ_c as a function of λ near the point $\left(\mu_c^*, \lambda\left(\mu_c^*\right)\right)$, and the derivative of this function is given by

$$\frac{d\lambda}{d\mu_c}\left(\mu_c^*\right)\Big|_{\mu_c=\mu_c^*} = -\left(\left(\frac{\partial \mathrm{F}}{\partial \mu_c}\right)\Big/\left(\frac{\partial \mathrm{F}}{\partial \lambda}\right)\right)\Big|_{\mu_c=\mu_c^*}, \tag{4.33}$$

providing

$$\frac{\partial \mathrm{F}}{\partial \lambda} \neq 0. \tag{4.34}$$

We begin by computing the derivative of the function $\mathrm{F}\left(\mu_c, \lambda\left(\mu_c\right)\right)$ with respect to λ, and evaluating this at the critical point μ_c^*. Thus we have,

$$\begin{aligned}
&\frac{\partial \mathrm{F}}{\partial \lambda}\left(\mu_c, \lambda\right)\Big|_{(\mu_c,\lambda)=\left(\mu_c^*, \pm i\omega\left(\mu_c^*\right)\right)} \\
&= 3\lambda^2 + 2(1+\delta_h+\delta_c)\lambda + (\delta_h+\delta_c+\delta_h\delta_c)\Big|_{(\mu_c,\lambda)=\left(\mu_c^*, \pm i\omega\left(\mu_c^*\right)\right)}, \qquad (4.35)\\
&= 3\left(\pm i\omega\left(\mu_c^*\right)\right)^2 + 2(1+\delta_h+\delta_c)\left(\pm i\omega\left(\mu_c^*\right)\right) + (\delta_h+\delta_c+\delta_h\delta_c). \qquad (4.36)
\end{aligned}$$

Simplifying and using the fact that $\omega^2\left(\mu_c^*\right) = (\delta_h+\delta_c+\delta_h\delta_c)$ from (4.30), we obtain

$$\begin{aligned}
\frac{\partial \mathrm{F}}{\partial \lambda}\Big|_{\left(\mu_c^*, \pm i\omega\left(\mu_c^*\right)\right)} &= -3\omega^2\left(\mu_c^*\right) \pm 2i(1+\delta_h+\delta_c)\omega\left(\mu_c^*\right) + \omega^2\left(\mu_c^*\right), \qquad (4.37)\\
&= -2\omega^2\left(\mu_c^*\right) \pm 2i(1+\delta_h+\delta_c)\omega\left(\mu_c^*\right) \neq 0. \qquad (4.38)
\end{aligned}$$

Also, from the characteristic polynomial (4.20), we have

$$\frac{\partial \mathrm{F}}{\partial \mu_c}(\mu_c,\lambda)\Big|_{(\mu_c,\lambda)=(\mu_c^*,\pm i\omega(\mu_c^*))} = \mu_h\varphi, \tag{4.39}$$

where, we have previously noted that $\varphi \geq 0$. However, in the case $\varphi = 0$, the Jacobian matrix in (4.16) becomes

$$\mathbf{J} = \begin{bmatrix} -1 & 0 & 0 \\ \mu_h & -\delta_h & 0 \\ 0 & \mu_c & -\delta_c \end{bmatrix}, \tag{4.40}$$

which is lower triangular and hence has three negative real eigenvalues given by the entries of the leading diagonal, specifically $-1, -\delta_h$ and $-\delta_c$. This violates the requirement of condition 1 that the matrix **J** has two complex eigenvalues. Therefore we can conclude that in this case, $\varphi \neq 0$ and we need only be concerned with the strict inequality $\varphi > 0$.

Equations (4.38) and (4.39) together with (4.33) yield

$$\frac{d\lambda}{d\mu}(\mu_c^*) = \frac{1}{2\omega(\mu_c^*)}\left(\frac{\mu_h\varphi}{-\omega(\mu_c^*) \pm i(1+\delta_h+\delta_c)}\right). \tag{4.41}$$

Upon the rationalising the denominator of this complex fraction we obtain

$$\frac{d\lambda}{d\mu_c}(\mu_c^*) = \frac{1}{2\omega(\mu_c^*)}\left(\frac{-\omega(\mu_c^*)\mu_h\varphi}{\omega^2(\mu_c^*)+(1+\delta_h+\delta_c)^2}\right) + i\frac{1}{2\omega(\mu_c^*)}\left(\frac{\mp\mu_h\varphi(1+\delta_h+\delta_c)}{\omega^2(\mu_c^*)+(1+\delta_h+\delta_c)^2}\right),$$

and since $\varphi > 0$,

$$\frac{d\theta(\mu_c)}{d\mu_c}\Big|_{\mu_c=\mu_c^*} = \mathbb{R}\mathrm{e}\frac{d\lambda}{d\mu_c}(\mu_c^*) = \frac{1}{2}\left(\frac{-\mu_h\varphi}{\omega^2(\mu_c^*)+(1+\delta_h+\delta_c)^2}\right) < 0 \quad \neq 0, \tag{4.42}$$

and the second condition of the Hopf theorem is fulfilled. Thus we have proved the existence of a Hopf bifurcation at the critical value $\mu_c = \mu_c^*$.

Due to the dependence of the stability condition (4.22c) on all of the system parameters, it is in fact possible to illustrate existence of critical values at which a Hopf bifurcation may occur

for each system parameter. We are especially interested in where these bifurcations occur for those parameters which are as yet undetermined, and here, following the method above, we prove analytically for δ_c, a critical value exists and that for this critical value the two conditions of the Hopf theorem are satisfied at the equilibrium point. The effect of other parameters will be considered numerically, in Chapter 5.

To calculate the critical value $\delta_c = \delta_c^*$, we must solve the critical condition of **Case II** in terms of δ_c^*. In conjunction with this, we must find also find the equilibrium value of c_{ss} for this value of δ_c^*. Hence, the critical value δ_c^* for which a Hopf bifurcation may occur is given by the solution of the equation

$$(1+\delta_h)(\delta_c^*)^2 + (1+\delta_h)^2\delta_c^* + (1+\delta_h)\delta_h - \mu_h\mu_c\varphi = 0, \tag{4.43}$$

together with the equation determining the equilibrium value of c_{ss},

$$\delta_c^* \frac{{c_{ss}}^{13}}{{\kappa_c}^{12}} + 3\delta_c^* \frac{{c_{ss}}^{9}}{{\kappa_c}^{8}} + 3\delta_c^* \frac{{c_{ss}}^{5}}{{\kappa_c}^{4}} + \left(\frac{\delta_c^*}{\kappa_{mh}^3} + \delta_c^*\right) c_{ss} - \left(\frac{\mu_h\mu_{mh}\mu_c}{\kappa_{mh}^3\delta_h}\right) = 0. \tag{4.44}$$

The eigenvalues at this critical point are given by

$$\lambda_{1,2} = \pm i\sqrt{(\delta_h + \delta_c + \delta_h\delta_c^*)}, \tag{4.45}$$

$$\lambda_3 = -\left(1+\delta_h+\delta_c^*\right), \tag{4.46}$$

and so the first Hopf bifurcation condition holds.

Proceeding in the manner of the calculation for μ_c^*, we find

$$\left.\frac{d\theta(\delta_c)}{d\delta_c}\right|_{\delta_c=\delta_c^*} = \mathbb{R}\mathrm{e}\frac{d\lambda}{d\delta_c}(\delta_c^*) = \frac{1}{2}\left(\frac{\omega^2(\delta_c^*) + (1+\delta_h)(1+\delta_h+\delta_c^*) - \delta_h}{\omega^2(\delta_c^*) + (1+\delta_h+\delta_c^*)^2}\right) > 0, \tag{4.47}$$

and therefore the second condition of the Hopf theorem also holds.

Having proved the existence of a Hopf bifurcation in the dynamics of system (4.3) for one of the known and one of the, as yet, unknown parameters, we now consider the biological significance of this phenomenon. Hopf bifurcations show the birth or the demise of closed period orbits

known as limit cycles. The stability of the equilibrium point at a Hopf bifurcation is shifted from the original stationary solution to the periodic one. This loss of stability can occur generically in one of two ways.

In the **supercritical** Hopf bifurcation, a stable limit cycle is produced at the bifurcation, and a stable equilibrium point becomes unstable with increasing amplitude oscillations that are finally attracted by the stable limit cycle. At the critical value of the bifurcation parameter, μ_c^*, the limit cycle has zero amplitude. For values of μ_c slightly larger than the critical value, a small-amplitude limit cycle exists near the steady state solution from which the limit cycle has bifurcated. Thus the limit cycle is being *created* at the Hopf bifurcation point as μ_c is increased through μ_c^*. Although the steady state solution loses stability, the system remains in the neighbourhood of the equilibrium. This is also known as a **soft** loss of stability.

In the **subcritical** Hopf bifurcation, an unstable limit cycle, which exists before the bifurcation, becomes smaller and eventually disappears as it combines with a stable equilibrium point at the bifurcation. For values of μ_c slightly smaller than the critical value μ_c^*, a small-amplitude limit cycle exists near the steady state solution from which the limit cycle has bifurcated. Thus in this case, the limit cycle is being *destroyed* at the Hopf bifurcation point as μ_c is increased through μ_c^*. After the bifurcation, the equilibrium point becomes unstable resulting in diverging oscillations. In this case the system is moved away from the neighbourhood of the equilibrium. This is called a **hard** loss of stability.

Distinction between these two qualitatively different types of bifurcation is essential to understanding the genetic regulatory mechanism of system (4.3). If a system loses stability in a soft manner, the long time solution changes by a small amount since the limit cycle has small amplitude. Further, since the limit cycle is stable, any small perturbation from the closed trajectory causes the system to return to the limit cycle. This phenomenon can result in self sustained oscillations in the region of some equilibrium value. The resulting mechanism of control of the system to within narrow limits is the principle of the biological mechanism of homeostasis.

The focus of the next section is to determine which type of Hopf bifurcation the equation system (4.3) exhibits.

4.3 Analysis of the Hopf bifurcation

In this section we analyse the Hopf bifurcation whose existence was proved in Section 4.2. We use centre manifold reduction techniques to isolate the two dimensional manifold to which the dynamics of the bifurcation phenomena are restricted (Guckenheimer and Holmes, 1983). The stability properties of the limit cycles, their amplitudes and period are then determined using integral averaging (Chow and Mallett-Paret, 1977). We begin by outlining some of the theory to be used in order to motivate the analysis that follows.

Centre manifold theory allows us to isolate only those dimensions of the system on which the interesting dynamics occur. Since at a bifurcation, the number of eigenvalues of the system whose real part crosses zero is usually less than the dimension of the system, this isolation is effectively a reduction of the dimension of the system.

This subspace of the original state space is called a centre manifold, that is, a manifold tangent to the eigenvectors of the zero crossing eigenvalues at the bifurcation point. Since the other eigenvalue of the regulated cholesterol biosynthesis system has negative real part, the centre manifold is an attractor in the state space; thus it is sufficient to consider the dynamics on the centre manifold for the purposes of stability analysis. Before presenting the analysis we briefly review the centre manifold theorem and its implications. Further details may be found in Carr (1981) or Guckenheimer and Holmes (1983).

Theorem I (The centre manifold theorem)
Let $f \in C^r(\mathbb{R}^n)$ be a vector field on $\mathbb{R}^n$ vanishing at the origin ($f(0)=0$), and let $A = Df(0)$, where Df is the Jacobian matrix of f. Divide the eigenvalues, λ of A into three sets σ_s, σ_c and σ_u with

$$\mathbb{R}e\ \lambda < 0 \quad if \quad \lambda \in \sigma_s, \tag{4.48}$$

$$\mathbb{R}e\ \lambda = 0 \quad if \quad \lambda \in \sigma_c, \tag{4.49}$$

$$\mathbb{R}e\ \lambda > 0 \quad if \quad \lambda \in \sigma_u. \tag{4.50}$$

Let $\mathcal{E}^s, \mathcal{E}^c$ and $\mathcal{E}^u$ be the corresponding generalised eigenspaces. Then there exist stable and un-

stable invariant manifolds $\mathscr{W}^u \in C^r$ and $\mathscr{W}^s \in C^r$ tangent to $\mathscr{E}^u$ and $\mathscr{E}^s$ at 0 and a centre manifold $\mathscr{W}^c \in C^{r-1}$ tangent to $\mathscr{E}^c$ at 0. All manifolds are invariant for the flow of f. The stable and unstable manifolds are unique but the centre manifold is not necessarily unique.

The centre manifold theorem implies that at a bifurcation point (where $\sigma_c \neq \emptyset$), any ODE system can be written locally in coordinates $(x, y, z) \in \mathscr{W}^c \times \mathscr{W}^s \times \mathscr{W}^u$ on invariant manifolds as

$$\dot{x} = f(x), \tag{4.51}$$

$$\dot{y} = -y, \tag{4.52}$$

$$\dot{z} = z. \tag{4.53}$$

The flow on $\mathscr{W}^s$ is toward the stationary point and the motion on $\mathscr{W}^u$ is away from the stationary point, and thus the local behaviour can be understood by the solution of (4.51), that is by computing the *reduced* vector field f. This is the subject of the next section.

4.4 A centre manifold reduction for the Hopf bifurcation

In this section we wish to isolate the centre manifold of the equation system (4.3), that is, to compute the reduced vector field of system (4.3). This is a complex calculation, and so we begin by providing an outline of the structure of this section. To simplify the following analysis, the bifurcation point, μ_c^*, of system (4.3) is translated to the origin, and this translated system is separated into its linear and nonlinear components. Following this, the system is subjected to a coordinate transformation which will bring it into a canonical (simple) form, diagonalising the linear part of the translated system.

Calculation of the centre manifold of the translated system requires an explanation of the theory which underlies the approximation technique. This is explained with reference to the translated system. However, since we seek the stability properties of the limit cycle which bifurcates from the origin, we must consider how the system behaves under small perturbations from the bifurcation point. We present a method of approximation of the system for values close to the

bifurcation point, resulting in what is known as the suspended system, using which the required centre manifold flow is determined. The final part of the analysis is the determination of the stability and properties of the periodic solutions bifurcating from the origin. In order to simplify this, the centre manifold is expressed in polar coordinates, from which we obtain the solution describing the limit cycle of the system. Using this solution the stability properties, in addition to the amplitude and period properties, of the orbits are determined.

4.4.1 Coordinate transformations

We begin with system (4.3), which is written in the form

$$\dot{\mathbf{u}} = \mathbf{g}(\mathbf{u}, \mu_c) \qquad \text{where} \qquad \mathbf{u} = (m_h, h, c)^T, \tag{4.54}$$

for which the equilibrium value $\mathbf{u}^* = (m_h^*, h^*, c^*)$ and parameter value μ_c^* at the bifurcation point have been identified. Our first step is to translate the system to place the bifurcation point at the origin using

$$\mathbf{v} \equiv \mathbf{u} - \mathbf{u}^*, \qquad \rho \equiv \mu_c - \mu_c^*, \tag{4.55}$$

giving the system

$$\dot{\mathbf{v}} = \bar{\mathbf{g}}(\mathbf{v}, \rho), \tag{4.56}$$

with bifurcation point at $\mathbf{v}^* = 0$ and $\rho = 0$. Now let

$$v_1 = m_h - m_h^*, \qquad v_2 = h - h^*, \qquad v_3 = c - c^*, \qquad \rho = \mu_c - \mu_c^*, \tag{4.57}$$

and system (4.3) becomes

$$\frac{dv_1}{d\tau} = \frac{\mu_{mh}}{1 + \gamma_m \left(1 + \gamma_c (v_3 + c^*)^4\right)^3} - \left(v_1 + m_h^*\right), \tag{4.58a}$$

$$\frac{dv_2}{d\tau} = \mu_h v_1 - \delta_h v_2, \tag{4.58b}$$

$$\frac{dv_3}{d\tau} = \left(\rho + \mu_c^*\right) v_2 - \delta_c v_3. \tag{4.58c}$$

where

$$\gamma_m = (\kappa_{mh})^3 \qquad \text{and} \qquad \gamma_c = (1/\kappa_c)^4. \tag{4.59}$$

We recall from (4.6a) that

$$m_h^* = \frac{\mu_{mh}}{1+\gamma_m\left(1+\gamma_c(c^*)^4\right)^3}, \tag{4.60}$$

and so (4.58a) becomes

$$\frac{dv_1}{d\tau} = \frac{\mu_{mh}}{1+\gamma_m\left(1+\gamma_c(v_3+c^*)^4\right)^3} - \frac{\mu_{mh}}{1+\gamma_m\left(1+\gamma_c(c^*)^4\right)^3} - v_1. \tag{4.61}$$

If we let

$$f(v_3+c^*) = \frac{\mu_{mh}}{1+\gamma_m\left(1+\gamma_c(v_3+c^*)^4\right)^3}, \tag{4.62}$$

the first term of (4.58a) can be approximated by a Taylor expansion,

$$f(v_3+c^*) = f(c^*) + f'(c^*)v_3 + \frac{f''(c^*)}{2}v_3^2 + \dots . \tag{4.63}$$

Since

$$f(c^*) = \frac{\mu_{mh}}{1+\gamma_m\left(1+\gamma_c(c^*)^4\right)^3}, \tag{4.64}$$

equation (4.61) can be rewritten as

$$\frac{dv_1}{d\tau} = \sum_{n=1}^{\infty}\left(\frac{f^{(n)}(c^*)}{n!}(v_3)^n\right) - v_1. \tag{4.65}$$

Thus system (4.3) with the bifurcation point translated to the origin is approximated using

$$\frac{dv_1}{d\tau} = -v_1 - f_1 v_3 + f_2 v_3^2, \tag{4.66a}$$

$$\frac{dv_2}{d\tau} = \mu_h v_1 - \delta_h v_2, \tag{4.66b}$$

$$\frac{dv_3}{d\tau} = \left(\rho + \mu_c^*\right) v_2 - \delta_c v_3, \tag{4.66c}$$

where

$$f_1 = \frac{12\mu_{mh}\gamma_m\gamma_c(c^*)^3\left(1+\gamma_c(c^*)^4\right)^2}{\left(1+\gamma_m\left(1+\gamma_c(c^*)^4\right)^3\right)^2}, \tag{4.67}$$

and

$$f_2 = f_1\left(\frac{3}{c^*}+\frac{8\gamma_c(c^*)^3}{\left(1+\gamma_c(c^*)^4\right)}-\frac{24\gamma_m\gamma_c(c^*)^3\left(1+\gamma_c(c^*)^4\right)^2}{1+\gamma_m\left(1+\gamma_c(c^*)^4\right)^3}\right). \tag{4.68}$$

Next, the linear and nonlinear terms in $\overline{\mathbf{g}}(\mathbf{v},\rho)$ are separated and we obtain

$$\dot{\mathbf{v}} = \mathbf{M}\mathbf{v}+\mathbf{N}\rho+\mathbf{k}(\mathbf{v},\rho), \tag{4.69}$$

where

$$\mathbf{M} = \left(\frac{\partial\overline{\mathbf{g}}(\mathbf{v},\rho)}{\partial\mathbf{v}}\right)\Bigg|_{\mathbf{v}=0,\rho=0} \quad \text{and} \quad \mathbf{N} = \left(\frac{\partial\overline{\mathbf{g}}(\mathbf{v},\rho)}{\partial\rho}\right)\Bigg|_{\mathbf{v}=0,\rho=0}, \tag{4.70}$$

and $\mathbf{k}(\mathbf{v},\rho)$ contains the nonlinear terms. We note that for our system, $\mathbf{N}=0$ and thus the nonlinear system (4.66) under consideration can be written in matrix form as

$$\begin{bmatrix}\dot{v}_1\\ \dot{v}_2\\ \dot{v}_3\end{bmatrix} = \begin{bmatrix}-1 & 0 & -f_1\\ \mu_h & -\delta_h & 0\\ 0 & \rho+\mu_c^* & -\delta_c\end{bmatrix}\begin{bmatrix}v_1\\ v_2\\ v_3\end{bmatrix}+\begin{bmatrix}f_2v_3^2\\ 0\\ 0\end{bmatrix}, \tag{4.71}$$

that is in the form

$$\dot{\mathbf{v}} = \mathbf{M}\mathbf{v}+\mathbf{k}(\mathbf{v},\rho), \tag{4.72}$$

where $\mathbf{k}(\mathbf{v},\rho)$ is not dependent on ρ and is $\mathscr{O}\left(\mathbf{v}^2\right)$.

The matrix $\mathbf{M}$ has the characteristic equation given by

$$\lambda^3+(1+\delta_h+\delta_c)\lambda^2+(\delta_h+\delta_c+\delta_h\delta_c)\lambda+\left(\delta_h\delta_c+\mu_h\left(\rho+\mu_c^*\right)f_1\right)=0, \tag{4.73}$$

which from the results of Section 4.2 reduces to

$$\lambda^3+a_1\lambda^2+a_2\lambda+a_1a_2=0, \tag{4.74}$$

at the bifurcation point $(v_1, v_2, v_3, \rho) = (0,0,0,0)$. Here,

$$a_1 = 1+\delta_h+\delta_c, \tag{4.75}$$

$$a_2 = \delta_h+\delta_c+\delta_h\delta_c, \tag{4.76}$$

and equation (4.74) has roots given by

$$\lambda_1 = -i\sqrt{a_2} = -i\sqrt{\delta_h+\delta_c+\delta_h\delta_c}, \tag{4.77a}$$

$$\lambda_2 = +i\sqrt{a_2} = +i\sqrt{\delta_h+\delta_c+\delta_h\delta_c}, \tag{4.77b}$$

$$\lambda_3 = -a_1 = -1-\delta_h-\delta_c. \tag{4.77c}$$

We note that since there are no eigenvalues with positive real part, the unstable manifold is empty.

The next step of the calculation requires the transformation of system (4.72) evaluated at the bifurcation point into a **canonical** form which will preserve the qualitative dynamics of $\mathbf{M}$.

We achieve this by seeking a transformation matrix $\mathbf{P}$ such that

$$\mathbf{v} = \mathbf{P}\mathbf{z}, \qquad \mathbf{z} = \mathbf{P}^{-1}\mathbf{v}, \tag{4.78}$$

transforming system (4.69) into the form,

$$\dot{\mathbf{z}} = \mathbf{P}^{-1}\mathbf{M}\mathbf{P}\mathbf{z}+\mathbf{P}^{-1}\mathbf{k}(\mathbf{P}\mathbf{z}). \tag{4.79}$$

$\mathbf{P}$ is chosen to be a nonsingular linear transformation such that

$$\mathbf{P}^{-1}\mathbf{M}\mathbf{P} = \begin{bmatrix} \mathbf{M}^c & 0 \\ 0 & \mathbf{M}^s \end{bmatrix}, \tag{4.80}$$

where $\mathbf{M}^c$ and $\mathbf{M}^s$ are the blocks in canonical form whose diagonals contain the eigenvalues with $\mathbb{R}\mathrm{e}(\lambda) = 0$ and $\mathbb{R}\mathrm{e}(\lambda) < 0$ respectively. For system (4.69) the matrix $[\mathbf{M}^c]$ is the 2×2 matrix whose eigenvalues have zero real part and the matrix $[\mathbf{M}^s]$ is the 1×1 matrix whose eigenvalue has

negative real part.

Canonical forms of the Jacobian derivatives evaluated at bifurcation points for various types of bifurcation have been previously evaluated. Following Guckenheimer and Holmes (1983), we seek a **P** for system (4.69) such that

$$\mathbf{P}^{-1}\mathbf{M}\mathbf{P} = \begin{bmatrix} \begin{bmatrix} 0 & -\sqrt{a_2} \\ \sqrt{a_2} & 0 \end{bmatrix} & 0 \\ 0 & \begin{bmatrix} -a_1 \end{bmatrix} \end{bmatrix}. \tag{4.81}$$

P is constructed as the basis formed by the eigenvectors corresponding to the eigenvalues given by (4.77a)-(4.77c). To achieve the transformation of (4.81) we take

$$\mathbf{P} = \begin{bmatrix} \mathbb{R}\mathrm{e}\left(e_1^T\right) & \mathbb{I}\mathrm{m}\left(e_1^T\right) & e_3^T \end{bmatrix}. \tag{4.82}$$

Here e_1^T is the eigenvector corresponding to the imaginary eigenvalue $\lambda_1 = -i\sqrt{a_2}$,

$$e_1^T = \begin{bmatrix} -\dfrac{f_1}{1-i\sqrt{a_2}} & \dfrac{(-i\sqrt{a_2}-1)\mu_h f_1}{(1-i\sqrt{a_2})(1+i\sqrt{a_2})(\delta_h - i\sqrt{a_2})} & 1 \end{bmatrix}. \tag{4.83}$$

Cancelling common terms, and rationalising denominators results in

$$e_1 = \begin{bmatrix} -f_1(\delta_h - i\sqrt{a_2}) \\ -\mu_h f_1 \\ (1-i\sqrt{a_2})(\delta_h - i\sqrt{a_2}) \end{bmatrix} = \begin{bmatrix} -f_1\delta_h + i f_1\sqrt{a_2} \\ -\mu_h f_1 \\ -\delta_c(\delta_h+1) - i(1+\delta_h)\sqrt{a_2} \end{bmatrix}, \tag{4.84}$$

using the value of a_2 in (4.76).

Thus we have,

$$\mathbb{R}\mathrm{e}(e_1) = \begin{bmatrix} -f_1\delta_h \\ -\mu_h f_1 \\ -\delta_c(\delta_h+1) \end{bmatrix}, \qquad \mathbb{I}\mathrm{m}(e_1) = \begin{bmatrix} f_1\sqrt{a_2} \\ 0 \\ -(1+\delta_h)\sqrt{a_2} \end{bmatrix}. \tag{4.85}$$

The eigenvector e_3^T corresponds to the real eigenvalue $\lambda_3 = -1-\delta_h-\delta_c$ and is given by

$$e_3 = \begin{bmatrix} \dfrac{f_1}{\delta_h+\delta_c} & -\dfrac{\mu_h f_1}{(\delta_h+\delta_c)(1+\delta_c)} & 1 \end{bmatrix}. \tag{4.86}$$

Equation (4.85) together with (4.86) give the columns of the transformation matrix $\mathbf{P}$, where

$$\mathbf{P} = \begin{bmatrix} -f_1\delta_h & f_1\sqrt{a_2} & \dfrac{f_1}{\delta_h+\delta_c} \\ -\mu_h f_1 & 0 & -\dfrac{\mu_h f_1}{(\delta_h+\delta_c)(1+\delta_c)} \\ -\delta_c(\delta_h+1) & -(1+\delta_h)\sqrt{a_2} & 1 \end{bmatrix}, \tag{4.87}$$

and inverting (4.87) we obtain,

$$\mathbf{P}^{-1} = \begin{bmatrix} -\dfrac{1+\delta_h}{\psi f_1} & -\dfrac{(1+\delta_c)(a_1+\delta_h)}{\psi f_1\mu_h} & -\dfrac{1}{\psi} \\ \dfrac{a_2+\delta_c a_1}{\psi f_1\sqrt{a_2}} & -\dfrac{(1+\delta_c)\left(\delta_h^2-\delta_c\right)}{\psi f_1\mu_h\sqrt{a_2}} & -\dfrac{a_1}{\psi\sqrt{a_2}} \\ \dfrac{(1+\delta_h)(1+\delta_c)(\delta_h+\delta_c)}{\psi f_1} & -\dfrac{(1+\delta_h)(1+\delta_c)(\delta_h+\delta_c)^2}{\psi f_1\mu_h} & \dfrac{(1+\delta_c)(\delta_h+\delta_c)}{\psi} \end{bmatrix} \tag{4.88}$$

where $\psi = a_1^2 + a_2$ with a_1 and a_2 as in (4.75) and (4.76) respectively.

We note that the physical variables of the transformed system, $\mathbf{v}$, are related to the normal coordinates through the relation $\mathbf{v} = \mathbf{Pz}$. Using (4.87) we obtain

$$v_1 = -\delta_h f_1 x_1 + \left(f_1\sqrt{a_2}\right)x_2 + \left(\frac{f_1}{(\delta_h+\delta_c)}\right)y, \tag{4.89a}$$

$$v_2 = -\mu_h f_1 x_1 - \left(\frac{\mu_h f_1}{(\delta_h+\delta_c)(\delta_c+1)}\right)y, \tag{4.89b}$$

$$v_3 = -\delta_c(\delta_h+1)x_1 - (1+\delta_h)\sqrt{a_2}x_2 + y, \tag{4.89c}$$

which leads to,

$$\mathbf{k}(\mathbf{v},\rho)=\begin{bmatrix} f_2 v_3^2 \\ 0 \\ 0 \end{bmatrix} \quad \Rightarrow \quad \mathbf{k}(\mathbf{Pz})=\begin{bmatrix} f_2\left((\delta_h+1)(-\sqrt{a_2}x_2-\delta_c x_1)+y\right)^2 \\ 0 \\ 0 \end{bmatrix}. \tag{4.90}$$

Therefore using (4.88)

$$\mathbf{P}^{-1}\mathbf{k}(\mathbf{Pz}) = \frac{f_2}{f_1\left(a_1^2+a_2\right)}\begin{bmatrix} -(\delta_h+1)\left((\delta_h+1)(-\sqrt{a_2}x_2-\delta_c x_1)+y\right)^2 \\ \\ \dfrac{a_2+\delta_c a_1}{\sqrt{a_2}}\left((\delta_h+1)\left(-\sqrt{a_2}x_2-\delta_c x_1\right)+y\right)^2 \\ \\ (1+\delta_h)(1+\delta_c)(\delta_h+\delta_c)\left((\delta_h+1)(-\sqrt{a_2}x_2-\delta_c x_1)+y\right)^2 \end{bmatrix}, \tag{4.91}$$

which we write as

$$\mathbf{P}^{-1}\mathbf{k}(\mathbf{Pz}) = \begin{bmatrix} n_1 m_1 x_1^2+n_1 m_2 x_2^2+n_1 m_3 x_1 x_2+n_1 m_4 x_1 y+n_1 m_5 x_2 y+n_1 m_6 y^2 \\ n_2 m_1 x_1^2+n_2 m_2 x_2^2+n_2 m_3 x_1 x_2+n_2 m_4 x_1 y+n_2 m_5 x_2 y+n_2 m_6 y^2 \\ n_3 m_1 x_1^2+n_3 m_2 x_2^2+n_3 m_3 x_1 x_2+n_3 m_4 x_1 y+n_3 m_5 x_2 y+n_3 m_6 y^2 \end{bmatrix}, \tag{4.92}$$

with

$$\begin{aligned} n_1 &= -\frac{f_2(1+\delta_h)}{f_1\left(a_1^2+a_2\right)}, \quad n_2 = \frac{f_2(a_2+\delta_c a_1)}{f_1\sqrt{a_2}\left(a_1^2+a_2\right)}, \\ n_3 &= \frac{f_2(1+\delta_h)(1+\delta_c)(\delta_h+\delta_c)}{f_1\left(a_1^2+a_2\right)}, \end{aligned} \tag{4.93}$$

and

$$\begin{aligned} m_1 &= \delta_c^2(1+\delta_h)^2, & m_2 &= a_2(1+\delta_h)^2, \\ m_3 &= 2\sqrt{a_2}\delta_c(1+\delta_h)^2, & m_4 &= -2\delta_c(1+\delta_h), \\ m_5 &= -2\sqrt{a_2}(1+\delta_h), & m_6 &= 1. \end{aligned} \tag{4.94}$$

The successive application of coordinate transformations in this section has separated the bifurcating system into linear and nonlinear parts, with the linear part expressed in block diagonal form, bringing the system into the form of (4.79). We note that expression of the system in this form indicates that the centre manifold has been isolated from the stable manifold at leading order; the centre manifold is given by (x_1, x_2, y) with $y = 0$ and the stable manifold by $x_1 = x_2 = 0$ with $y \in \mathbf{R}$. We are now in a position to apply the centre manifold theorem and reduce the dimension of the system. In the following section, we begin with an explanation of the application of this technique.

4.4.2 Centre manifold theory

The previous calculations have separated the bifurcating system into linear and nonlinear parts, with the linear part expressed in block diagonal form, bringing the system into the form of (4.79). Next the vector $\mathbf{z}$ is separated into two vectors, $\mathbf{x} = (x_1, x_2)^T$ and $\mathbf{y}$,

$$\dot{\mathbf{x}} = \mathbf{A}\mathbf{x} + g\left(\mathbf{x}, \mathbf{y}, \rho\right), \tag{4.95a}$$

$$\dot{\mathbf{y}} = \mathbf{B}\mathbf{y} + l\left(\mathbf{x}, \mathbf{y}, \rho\right), \quad (\mathbf{x}, \mathbf{y}) \in \mathbb{R}^2 \times \mathbb{R}^1, \tag{4.95b}$$

$$\dot{\rho} = 0, \qquad \rho \in \mathbb{R}^1. \tag{4.95c}$$

where $\mathbf{x}$ corresponds to the purely imaginary eigenvalues of $\mathbf{M}$, and $\mathbf{y}$ to those eigenvalues with negative real part.

$\mathbf{A}$ and $\mathbf{B}$ are 2×2 and 1×1 matrices respectively, whose eigenvalues have zero real parts and negative real parts, and g and l vanish along with their partial first derivatives at the origin.

The addition of the trivial equation (4.95c) is in order that we may include the bifurcation parameter μ_c as part of the centre manifold. This allows us to obtain a centre manifold which stretches into the parameter space.

At $(\mathbf{x}, \mathbf{y}, \rho) = (0, 0, 0)$ there is a $(2+1)$-dimensional centre manifold tangent to $\mathscr{E}^c$ (the $y = 0$ space) and $\rho = 0$. Since the centre manifold $\mathscr{W}^c$ is tangent to both $\mathscr{E}^c$ and ρ, it can be represented

locally as the graph of a function of $\mathbf{x}$ and ρ

$$\mathscr{W}^c = \{(\mathbf{x},\mathbf{y})|\mathbf{y} = h(\mathbf{x},\rho)\}; \qquad h(\mathbf{0},0) = 0, \qquad Dh(\mathbf{0},0) = 0, \tag{4.96}$$

where $h : \mathbb{U} \to \mathbb{R}^1$ is defined on some neighbourhood $\mathbb{U} \subset \mathbb{R}^2$ of the origin. We consider the projection of $\mathbf{y} = h(\mathbf{x},\rho)$ onto $\mathscr{E}^c$ which is given by

$$\dot{\mathbf{x}} = \mathbf{A}\mathbf{x} + g(\mathbf{x}, h(\mathbf{x},\rho),\rho), \tag{4.97a}$$

$$\dot{\rho} = 0, \tag{4.97b}$$

where (4.97b) is trivial to solve and the local dynamics on the centre manifold are given by the solutions of (4.97a). (This is the flow of (4.51) restricted to $\mathscr{W}^c$, that is, the 'reduced' vector field that we wish to compute.) We now use the following theorem.

Theorem II (Carr (1981)a)

If the origin of $\mathbf{x} = \mathbf{0}$ *of (4.97a) is locally asymptotically stable (or unstable) then the origin of system (4.95) is also locally asymptotically stable (or unstable).*

Thus we see that calculating the centre manifold allows a simplified method of determining the stability of the original system. The centre manifold itself is given by the equation

$$y = h(\mathbf{x},\rho). \tag{4.98}$$

To obtain a functional form for h we substitute (4.98) into (4.95a), and apply the chain rule to obtain

$$\begin{aligned} y = h(\mathbf{x},\rho) \quad \Rightarrow \quad \dot{y} &= Dh(\mathbf{x},\rho)[\dot{\mathbf{x}},\dot{\rho}]^T, \\ &= Dh(\mathbf{x},\rho).\left[\mathbf{A}\mathbf{x} + g(\mathbf{x},h(\mathbf{x},\rho),\rho),\dot{\rho}\right]^T, \end{aligned} \tag{4.99}$$

where $Dh(\mathbf{x},\rho)$ is the Jacobian matrix of h. Using (4.95b) we also have that

$$\dot{y} = Bh(\mathbf{x},\rho) + l(\mathbf{x},h(\mathbf{x},\rho),\rho). \tag{4.100}$$

If we now define the operator $\mathscr{M}$ by

$$\mathscr{M}(h(\mathbf{x},\rho)) = Dh(\mathbf{x},\rho).\left[\mathbf{Ax}+g(\mathbf{x},h(\mathbf{x},\rho),\rho),\dot{\rho}\right]^T - Bh(\mathbf{x},\rho)-l(\mathbf{x},h(\mathbf{x},\rho),\rho), \tag{4.101}$$

with boundary conditions

$$h(\mathbf{0},0)=Dh(\mathbf{0},0)=0, \tag{4.102}$$

then the function h whose graph is the centre manifold of system (4.95), is a solution of the equation

$$\mathscr{M}(h(\mathbf{x},\rho))=0. \tag{4.103}$$

The solution for the partial differential equation in h above can be approximated arbitrarily closely as a Taylor series at $\mathbf{x}=0$ using the following theorem.

Theorem III (Carr (1981)b)

If a function $\Phi(x)$ *with* $\Phi(0)=D\Phi(0)=0$ *can be found such that* $\mathscr{M}(\Phi(x))=\mathscr{O}(|x|^p)$ *for some* $p>1$ *as* $|x|\to 0$ *then it follows that*

$$h(x)=\Phi(x)+\mathscr{O}(|x|^p)\ as\ |x|\to 0. \tag{4.104}$$

Before we compute $h(\mathbf{x},\rho)$, however, we note that the invariance properties of centre manifolds guarantee that any small solutions bifurcating from $(0,0,0)$ must lie in any centre manifold.

Thus we may follow the local evolution of bifurcating families of solutions in what is termed the suspended family of centre manifolds.

4.4.3 Calculation of the suspended system

To calculate the suspended form of (4.79), we must consider what happens to the matrix $\mathbf{P}^{-1}\mathbf{MP}$ in equation (4.81), for values of μ_c close to the bifurcation point μ_c^*.

That is, we consider what happens in the case where $0<\rho<<1$.

The characteristic equation ((4.73)) of the original system at the bifurcation point is given by

$$\lambda^3 + a_1\lambda^2 + a_2\lambda + \delta_h\delta_c + \left(\rho + \mu_c^*\right)\mu_h f_1 = 0, \tag{4.105}$$

$$\lambda^3 + a_1\lambda^2 + a_2\lambda + \delta_h\delta_c + \rho\mu_h f_1 + \mu_c^*\mu_h f_1 = 0, \tag{4.106}$$

with a_1 and a_2 given by equations (4.75) and (4.76). But at the critical point μ_c^*, we have that

$$a_1 a_2 = \delta_h\delta_c + \mu_c^*\mu_h f_1. \tag{4.107}$$

Therefore for the perturbed matrix $\tilde{\mathbf{M}}$, where $\rho \neq 0$, the characteristic equation is given by

$$\lambda^3 + a_1\lambda^2 + a_2\lambda + a_1 a_2 + \rho\mu_h f_1 = 0. \tag{4.108}$$

Let the eigenvalues of the perturbed matrix $\tilde{\mathbf{M}}$ be given by ω and let

$$\zeta = \rho\mu_h f_1. \tag{4.109}$$

Therefore we consider solutions of the equation

$$\omega^3 + a_1\omega^2 + a_2\omega + a_1 a_2 + \zeta = 0. \tag{4.110}$$

We calculate the eigenvalues ω using regular perturbation expansions of the form

$$\omega_1 = \lambda_1 + \zeta\omega_1^{(1)} + \mathcal{O}(\zeta^2), \tag{4.111a}$$

$$\omega_2 = \lambda_2 + \zeta\omega_2^{(1)} + \mathcal{O}(\zeta^2), \tag{4.111b}$$

$$\omega_3 = \lambda_3 + \zeta\omega_3^{(1)} + \mathcal{O}(\zeta^2), \tag{4.111c}$$

noting that in the case $\zeta = 0$, equation (4.110) reduces to the characteristic equation (4.74) with eigenvalues λ as in (4.77a) - (4.77c). The values of ω given in system (4.111) are substituted into (4.110) in turn and higher order terms (i.e. terms of $\mathcal{O}(\zeta^2)$, $\mathcal{O}(\zeta^3)$ etc.) are neglected. For ω_1 we find, to $\mathcal{O}(\zeta)$, that

$$1 - 2a_2\omega_1^{(1)} - 2ia_1\sqrt{a_2}\omega_1^{(1)} = 0, \tag{4.112}$$

and therefore

$$\omega_1^{(1)} = \frac{1}{2(a_2 + i a_1\sqrt{a_2})}. \tag{4.113}$$

Rationalising we find that

$$\omega_1^{(1)} = \frac{1}{2\left(a_2 + a_1^2\right)} - i\frac{a_1}{2\sqrt{a_2}\left(a_2 + a_1^2\right)}, \tag{4.114}$$

and therefore

$$\omega_1 = -i\sqrt{a_2} + \left(\frac{1}{2\left(a_2 + a_1^2\right)} - i\frac{a_1}{2\sqrt{a_2}\left(a_2 + a_1^2\right)}\right)\zeta + \mathcal{O}(\zeta^2). \tag{4.115}$$

In a similar manner we find

$$\omega_2 = i\sqrt{a_2} + \left(\frac{1}{2\left(a_2 + a_1^2\right)} + i\frac{a_1}{2\sqrt{a_2}\left(a_2 + a_1^2\right)}\right)\zeta + \mathcal{O}(\zeta^2). \tag{4.116}$$

For ω_3 we find

$$\omega_3 = -a_1 - \frac{1}{\left(a_2 + a_1^2\right)} + \mathcal{O}(\zeta^2). \tag{4.117}$$

For ease of the analysis that follows we express the eigenvalues calculated above as

$$\omega_1 = r'\zeta - \left(\sqrt{a_2} + \chi'\zeta\right) i, \tag{4.118a}$$

$$\omega_2 = r'\zeta + \left(\sqrt{a_2} + \chi'\zeta\right) i, \tag{4.118b}$$

$$\omega_3 = -a_1 + s'\zeta, \tag{4.118c}$$

where the coefficients r', χ' and s' are given by

$$r' = \frac{1}{2\left(a_2 + a_1^2\right)}, \tag{4.119a}$$

$$\chi' = \frac{a_1}{2\sqrt{a_2}\left(a_2 + a_1^2\right)}, \tag{4.119b}$$

$$s' = -\frac{1}{\left(a_2 + a_1^2\right)}. \tag{4.119c}$$

Thus for values of μ_c close to the bifurcation point μ_c^*, we approximate the matrix $\mathbf{P}^{-1}\mathbf{M}\mathbf{P}$ with

$$\tilde{\mathbf{P}}^{-1}\tilde{\mathbf{M}}\tilde{\mathbf{P}} = \begin{bmatrix} r'\zeta & -\left(\sqrt{a_2}+\chi'\zeta\right) & 0 \\ \sqrt{a_2}+\chi'\zeta & r'\zeta & 0 \\ 0 & 0 & -a_1+s'\zeta \end{bmatrix}. \tag{4.120}$$

The suspended system we require is given by

$$\dot{\mathbf{z}} = \tilde{\mathbf{P}}^{-1}\tilde{\mathbf{M}}\tilde{\mathbf{P}}\mathbf{z} + \mathbf{P}^{-1}\mathbf{k}(\mathbf{P}\mathbf{z}), \tag{4.121}$$

which, from (4.92), is given by the system below

$$\begin{aligned}
\dot{x}_1 &= r'\zeta x_1 - \left(\sqrt{a_2}+\chi'\zeta\right)x_2 + n_1m_1x_1^2 + n_1m_2x_2^2 + n_1m_3x_1x_2 && (4.122a)\\
&\quad + n_1m_4x_1y + n_1m_5x_2y + n_1m_6y^2, \\
\dot{x}_2 &= \left(\sqrt{a_2}+\chi'\zeta\right)x_1 + r'\zeta x_2 + n_2m_1x_1^2 + n_2m_2x_2^2 + n_2m_3x_1x_2 && (4.122b)\\
&\quad + n_2m_4x_1y + n_2m_5x_2y + n_2m_6y^2, \\
\dot{y} &= \left(-a_1+s'\zeta\right)y + n_3m_1x_1^2 + n_3m_2x_2^2 + n_3m_3x_1x_2 && (4.122c)\\
&\quad + n_3m_4x_1y + n_3m_5x_2y + n_3m_6y^2, \\
\dot{\rho} &= 0, && (4.122d)
\end{aligned}$$

where ζ is given in (4.109) and the coefficients n_i and m_i are found in system (4.93) and system (4.94) respectively.

4.4.4 Determination of the centre manifold

We seek a centre manifold of the form

$$\begin{aligned}
y &= h(\mathbf{x},\rho), \\
&= h(x_1,x_2,\rho), \\
&= \xi_1x_1^2 + \xi_2x_2^2 + \xi_3\rho^2 + \xi_4x_1x_2 + \xi_5x_1\rho + \xi_6x_2\rho + \mathscr{O}(3), && (4.123)
\end{aligned}$$

where the ξ_i are coefficients to be determined, and where, by $\mathscr{O}(3)$ we mean terms of orders $x_1^3, x_2^3, \rho^3, x_1^2 x_2 \ldots$

Using this approximation of h, together with (4.120) and (4.92), we have

$$Dh(\mathbf{x},\rho) = \left(\frac{\partial h}{\partial x_1}, \frac{\partial h}{\partial x_2}, \frac{\partial h}{\partial \rho}\right) = \begin{bmatrix} 2\xi_1 x_1 + \xi_4 x_2 + \xi_5 \rho \\ 2\xi_2 x_2 + \xi_4 x_1 + \xi_6 \rho \\ 2\xi_3 \rho + \xi_5 x_1 + \xi_6 x_2 \end{bmatrix}^T, \tag{4.124}$$

and

$$\begin{bmatrix} \mathbf{A} \begin{bmatrix} \dot{x}_1 \\ \dot{x}_2 \end{bmatrix} \\ \dot{\rho} \end{bmatrix} + \begin{bmatrix} g(x_1, h(x_1,x_2,\rho)) \\ g(x_2, h(x_1,x_2,\rho)) \\ 0 \end{bmatrix} = \begin{bmatrix} r'\zeta x_1 - \left(\sqrt{a_2} + \chi'\zeta\right) x_2 \\ \left(\sqrt{a_2} + \chi'\zeta\right) x_1 + r'\zeta x_2 \\ 0 \end{bmatrix} +$$

$$\begin{bmatrix} n_1 m_1 x_1^2 + n_1 m_2 x_2^2 + n_1 m_3 x_1 x_2 + n_1 m_4 x_1 h + n_1 m_5 x_2 h + n_1 m_6 h^2 \\ n_2 m_1 x_1^2 + n_2 m_2 x_2^2 + n_2 m_3 x_1 x_2 + n_2 m_4 x_1 h + n_2 m_5 x_2 h + n_2 m_6 h^2 \\ 0 \end{bmatrix}. \tag{4.125}$$

We know also that,

$$\begin{aligned} -Bh(\mathbf{x},\rho) - l(\mathbf{x}, h(\mathbf{x},\rho)) &= a_1 h - s'\zeta h - n_3 m_1 x_1^2 - n_3 m_2 x_2^2 - n_3 m_3 x_1 x_2 \\ &\quad - n_3 m_4 x_1 h - n_3 m_5 x_2 h - n_1 m_6 h^2. \end{aligned} \tag{4.126}$$

Using (4.124), (4.125) and (4.126) we calculate $\mathscr{M}(h(\mathbf{x},\rho))$.

The value of h in (4.123) is then substituted into $\mathscr{M}(h(\mathbf{x},\rho)) = 0$ and equating the powers of $x_1^2, x_2^2, x_1 x_2, \rho^2, x_1\rho$ and $x_2\rho$ we find that

$$\xi_3 = 0, \quad \xi_5 = 0, \quad \xi_6 = 0, \tag{4.127}$$

and furthermore we find the nontrivial values given by

$$\xi_4 = \frac{n_3 m_3 (a_1 - s'\zeta + 2r'\zeta) + 2n_3(m_1 - m_2)\left(\sqrt{a_2} + \chi'\zeta\right)}{(a_1 - s'\zeta + 2r'\zeta)^2 + 4\left(\sqrt{a_2} + \chi'\zeta\right)^2}, \tag{4.128a}$$

$$\xi_1 = \frac{n_3 m_1 - \xi_4\left(\chi'\zeta + \sqrt{a_2}\right)}{a_1 - s'\zeta + 2r'\zeta}, \tag{4.128b}$$

$$\xi_2 = \frac{n_3 m_2 + \xi_4\left(\chi'\zeta + \sqrt{a_2}\right)}{a_1 - s'\zeta + 2r'\zeta}, \tag{4.128c}$$

and thus the centre manifold we require is given by

$$y = \xi_1 x_1^2 + \xi_2 x_2^2 + \xi_4 x_1 x_2. \tag{4.129}$$

The reduced system which describes the suspended centre manifold flow of the system, and which determines stability, is given by

$$\dot{x}_1 = r'\zeta x_1 - \left(\sqrt{a_2} + \chi'\zeta\right) x_2 + J_1(x_1, x_2), \tag{4.130a}$$

$$\dot{x}_2 = \left(\sqrt{a_2} + \chi'\zeta\right) x_1 + r'\zeta x_2 + J_2(x_1, x_2), \quad (\dot{\rho} = 0), \tag{4.130b}$$

obtained by substituting y from (4.129) into equations (4.122a) and (4.122b), where,

$$\begin{aligned} J_1(x_1, x_2) = {} & n_1 m_1 x_1^2 + n_1 m_2 x_2^2 + n_1 m_3 x_1 x_2 + n_1 m_4 \xi_1 x_1^3 + \\ & (n_1 m_4 \xi_2 + n_1 m_5 \xi_4) x_1 x_2^2 + (n_1 m_4 \xi_4 + n_1 m_5 \xi_1) x_1^2 x_2 + n_1 m_5 \xi_2 x_2^3, \end{aligned} \tag{4.131a}$$

$$\begin{aligned} J_2(x_1, x_2) = {} & n_2 m_1 x_1^2 + n_2 m_2 x_2^2 + n_2 m_3 x_1 x_2 + n_2 m_4 \xi_1 x_1^3 + \\ & (n_2 m_4 \xi_2 + n_2 m_5 \xi_4) x_1 x_2^2 + (n_2 m_4 \xi_4 + n_2 m_5 \xi_1) x_1^2 x_2 + n_2 m_5 \xi_2 x_2^3, \end{aligned} \tag{4.131b}$$

on neglecting the higher order terms.

Having found the centre manifold, and reduced the original system of equations to two dimensions, we are now in a position to determine the stability of the bifurcation and to derive expressions for the amplitude and frequency of the resulting oscillations.

4.4.5 Averaging

If we introduce polar coordinates in the form

$$x_1 = \mathrm{R}\cos\theta, \qquad x_2 = \mathrm{R}\sin\theta, \tag{4.132}$$

we find that under this transformation

$$\dot{\mathrm{R}} = \frac{x_1\dot{x}_1 + x_2\dot{x}_2}{\mathrm{R}}, \qquad \mathrm{R}\dot{\theta} = \frac{x_1\dot{x}_2 - x_2\dot{x}_1}{\mathrm{R}}. \tag{4.133}$$

Using the above, system (4.130) can be written as

$$\dot{\mathrm{R}} = r'\zeta\mathrm{R} + J_1(\mathrm{R}\cos\theta, \mathrm{R}\sin\theta)\cos\theta + J_2(\mathrm{R}\cos\theta, \mathrm{R}\sin\theta)\sin\theta, \tag{4.134}$$

$$\mathrm{R}\dot{\theta} = \left(\sqrt{a_2} + \chi'\zeta\right)\mathrm{R} + J_2(\mathrm{R}\cos\theta, \mathrm{R}\sin\theta)\cos\theta - J_2(\mathrm{R}\cos\theta, \mathrm{R}\sin\theta)\sin\theta. \tag{4.135}$$

Equation (4.134) has the form

$$\dot{\mathrm{R}} = r'\zeta\mathrm{R} + \mathscr{A}_1(\theta)\mathrm{R}^2 + \mathscr{A}_2(\theta)\mathrm{R}^3, \tag{4.136}$$

where the functions $\mathscr{A}_1(\theta)$ and $\mathscr{A}_2(\theta)$ are 2π periodic in the angular coordinate θ and calculated using system (4.131), giving

$$\begin{aligned}\mathscr{A}_1(\theta) &= n_1m_1\cos^3\theta + (n_1m_2 + n_2m_3)\sin^2\theta\cos\theta + \\ &\quad (n_1m_3 + n_2m_1)\sin\theta\cos^2\theta + n_2m_2\sin^3\theta,\end{aligned} \tag{4.137}$$

$$\begin{aligned}\mathscr{A}_2(\theta) &= n_2m_5\xi_2 + (n_2m_4\xi_2 + n_1m_5\xi_2 + n_2m_5\xi_4)\sin\theta\cos\theta + \\ &\quad (n_2m_4\xi_4 - 2n_2m_5\xi_2 + n_1m_5\xi_4 + n_2m_5\xi_1 + n_1m_4\xi_2)\cos^2\theta + \\ &\quad (n_2m_5\xi_2 - n_2m_5\xi_1 + n_1m_4\xi_1 - n_1m_5\xi_4 - n_1m_4\xi_2 - n_2m_4\xi_4)\cos^4\theta + \\ &\quad (n_1m_4\xi_4 - n_2m_4\xi_2 + n_2m_4\xi_1 - n_1m_5\xi_2 - n_2m_5\xi_4 + n_1m_5\xi_1)\sin\theta\cos^3\theta.\end{aligned} \tag{4.138}$$

If (4.136) is averaged over one cycle in θ, we obtain an equation with constant coefficients,

$$\dot{\mathrm{R}} = r'\zeta\mathrm{R} + \mathscr{B}_1\mathrm{R}^2 + \mathscr{B}_2\mathrm{R}^3, \tag{4.139}$$

where

$$\mathscr{B}_1 = \frac{1}{2\pi}\int_0^{2\pi} \mathscr{A}_1(\theta)d\theta, \tag{4.140}$$

and

$$\mathscr{B}_2 = \frac{1}{2\pi}\int_0^{2\pi} \mathscr{A}_2(\theta)d\theta. \tag{4.141}$$

Substituting (4.137) into (4.140) and evaluating, we find that the integral yields even trigonometric powers and thus evaluates to zero. Substituting (4.138) into (4.141) and evaluating the integral, we find

$$\mathscr{B}_2 = \frac{1}{8}(3n_1m_4\xi_1 + n_1m_4\xi_2 + n_1m_5\xi_4 + n_2m_4\xi_4 + n_2m_5\xi_1 + 3n_2m_5\xi_2), \tag{4.142}$$

where the ξ_i are found in system (4.128). And so, the averaged form of (4.134) is given by

$$\dot{\mathrm{R}} = r'\zeta\mathrm{R} + \mathscr{B}_2\mathrm{R}^3. \tag{4.143}$$

Similar averaging can be performed for (4.135) which has the form

$$\dot{\theta} = \left(\sqrt{a_2} + \chi'\zeta\right) + \mathscr{U}_1\mathrm{R} + \mathscr{U}_2\mathrm{R}^2, \tag{4.144}$$

where under the assumption $\mathrm{R} \neq 0$, the functions $\mathscr{U}_1(\theta)$ and $\mathscr{U}_2(\theta)$ are 2π periodic.

The integral of $\mathscr{U}_1(\theta)$ between the limits 0 and 2π evaluates to zero and the function $\mathscr{U}_2(\theta)$ is given by

$$\begin{aligned}\mathscr{U}_2(\theta) \;=\; & (n_2m_5\xi_2 - n_1m_4\xi_2 - n_1m_5\xi_4)\sin\theta\cos\theta - n_1m_5\xi_2 + \\ & (n_1m_4\xi_4 - n_2m_4\xi_2 + n_2m_4\xi_1 - n_1m_5\xi_2 - n_2m_5\xi_4 + n_1m_5\xi_1)\cos^4\theta + \\ & (2n_1m_5\xi_2 - n_1m_4\xi_4 + n_2m_5\xi_4 - n_1m_5\xi_1 + n_2m_4\xi_2)\cos^2\theta + \\ & (n_1m_4\xi_2 + n_2m_4\xi_4 - n_1m_4\xi_1 - n_2m_5\xi_2 + n_1m_5\xi_4 + n_2m_5\xi_1)\cos^3\theta\sin\theta.\end{aligned} \tag{4.145}$$

Therefore, the averaged form of (4.144) is given by the equation

$$\dot{\theta} = \left(\sqrt{a_2} + \chi'\zeta\right) + \mathscr{V}_2\mathrm{R}^2, \tag{4.146}$$

where

$$\mathscr{V}_2 = \frac{1}{2\pi}\int_0^{2\pi} \mathscr{U}_2(\theta)d\theta. \tag{4.147}$$

The system of equations (4.143) and (4.146) exhibits the same stability properties as the system in polar coordinates given by equations (4.139) and (4.144), (Chow and Mallett-Paret, 1977). This stability is studied next.

4.4.6 Limit cycle analysis

As (4.143) separates from (4.146), we can see that the nonzero solutions of $\mathtt{R}$ in (4.143), given by

$$\mathtt{R}^2 = \frac{-r'}{\mathscr{B}_2}\zeta, \tag{4.148}$$

are circles where $\mathtt{R}$ is constant. This is the equilibrium solution corresponding to a periodic solution or limit cycle in the coordinates x_1 and x_2. As r' is always positive (see (4.119a)), the existence of these periodic solutions depends on the value of $\mathscr{B}_2$, given in (4.142). Specifically

- if $\mathscr{B}_2 < 0$, periodic solutions exist for $\zeta > 0$ that is $\mu_c > \mu_c^*$,
- if $\mathscr{B}_2 > 0$, periodic solutions exist for $\zeta < 0$ that is $\mu_c < \mu_c^*$.

The Floquet exponent of (4.143) in the vicinity of (4.148) is given by $-2r'\zeta$, and therefore

- if periodic solutions exist for $\zeta > 0$ they are stable, and
- if periodic solutions exist for $\zeta < 0$ they are unstable.

The results outlined above allow us to determine the stability of any limit cycle generated as a result of μ_c passing through a critical value μ_c^*. The first (stable) case is referred to as the supercritical Hopf bifurcation, whilst the second (unstable) case is the subcritical Hopf bifurcation, (Glendinning, 1994).

The determination of the stability coefficient $\mathscr{B}_2$ is dependent on the coefficients ξ_i in system (4.128), n_i in system (4.93), and m_i in system (4.94). Therefore $\mathscr{B}_2$ is dependent on the magnitude of the values of the parameters appearing in the system. In Chapter 5, we evaluate $\mathscr{B}_2$ with the set of parameters detailed in Table 5.1 for μ_c as the bifurcation parameter, and show that since $\mathscr{B}_2 < 0$, a stable limit cycle is generated for μ_c greater than the critical value μ_c^*. Thus the Hopf bifurcation dependent on μ_c is *supercritical*.

4.4.7 Limit cycle properties

To calculate the period, T, of these limit cycles, we use the fact that the angular frequency $\dot{\theta}$ is equivalent to $2\pi/\mathrm{T}$. Substituting (4.148) in (4.146), we find

$$\begin{aligned} \mathrm{T} &= \frac{2\pi}{\left(\sqrt{a_2}+\chi'\zeta\right)+\tfrac{1}{2}\mathrm{R}^2} = \frac{2\pi\mathscr{B}_2}{\sqrt{a_2}\mathscr{B}_2+\zeta\left(\chi'\mathscr{B}_2-\tfrac{1}{2}r'\right)}, \\ &= \frac{\dfrac{2\pi\mathscr{B}_2}{\sqrt{a_2}\mathscr{B}_2}}{1+\dfrac{\zeta}{\sqrt{a_2}\mathscr{B}_2}\left(\chi'\mathscr{B}_2-\tfrac{1}{2}r'\right)}, \end{aligned} \tag{4.149}$$

and so we have an estimate for the period of oscillations given by

$$\mathrm{T} \approx \frac{2\pi}{\sqrt{a_2}}\left(1-\frac{\chi'\mathscr{B}_2-\tfrac{1}{2}r'}{\sqrt{a_2}\mathscr{B}_2}\zeta\right)+\mathscr{O}(\zeta^2). \tag{4.150}$$

The amplitude of the limit cycles is computed using the equations of system (4.89) to obtain an expression in terms of the original variables. In system (4.89) the variable v_3 represents the concentration of cholesterol, c, where

$$v_3 = -\delta_c(\delta_h+1)x_1-\left((1+\delta_h)\sqrt{a_2}\right)x_2+y, \tag{4.151}$$

and on substituting the values of x_1, x_2 and y from equations (4.132) and (4.129) we obtain

$$\begin{aligned} v_3 = &-\mathrm{R}\delta_c(\delta_h+1)\cos\theta-\mathrm{R}\left((1+\delta_h)\sqrt{a_2}\right)\sin\theta \\ &+\mathrm{R}^2\xi_1\cos^2\theta+\mathrm{R}^2\xi_2\sin^2\theta+\mathrm{R}^2\xi_4\sin\theta\cos\theta. \end{aligned} \tag{4.152}$$

Rearranging and using trigonometric identities, we find v_3 in (4.152) can be written as

$$\frac{\mathrm{R}^2(\xi_1+\xi_2)}{2}+\mathrm{R}(1+\delta_h)\left(\sqrt{a_2}\sin\theta-\delta_c\cos\theta\right)+\left(\frac{\mathrm{R}^2(\xi_1+\xi_2)}{2}\right)\cos 2\theta+\left(\frac{\mathrm{R}^2\xi_4}{2}\right)\sin 2\theta,$$

which on further manipulation becomes

$$\begin{aligned}\frac{\mathrm{R}^2(\xi_1+\xi_2)}{2} &+ \left(\mathrm{R}(1+\delta_h)\sqrt{a_2+\delta_c^2}\right)\sin\left(\theta+\tan^{-1}\left(\frac{\delta_c}{\sqrt{a_2}}\right)\right)\\ &+ \left(\frac{\mathrm{R}^2\sqrt{\xi_4^2+(\xi_1-\xi_2)^2}}{2}\right)\sin\left(2\theta+\tan^{-1}\left(\frac{\xi_1-\xi_2}{\xi_4}\right)\right).\end{aligned} \tag{4.153}$$

The maximum amplitude of the expression above, obtained on substituting values of the relevant coefficients and reading the amplitude of the resulting wave, is then used to approximate the amplitude of the oscillations in cholesterol concentration from numerical simulation of the equations in system (3.66).

The analytic values relating to the amplitude and period of the limit cycle calculated in this section, along with the results which determine stability will be verified with numerical solutions to the regulated cholesterol biosynthesis model presented in Chapter 5. Before doing so, we consider the implications of the analysis presented in this chapter on the biological processes modelled in this thesis.

4.5 Biological implications of the model analysis

We have developed a mathematical model that describes the genetic regulation of cholesterol biosynthesis within the cell. Biologically, many variables are kept tightly controlled within a narrow range around a certain optimal level. In particular intracellular cholesterol concentration is always maintained to within a fairly narrow range of values; this is termed homeostasis. Homeostasis literally means *same state* and it refers to the process of keeping an internal environment in a steady state either with or without changes in the external environment. Broadly speaking, there are two schools of thought on how homeostatic mechanisms function.

The first and more traditional of these is the focus on static stability. Deviations from a fixed steady point are corrected by placing parameters within normal ranges to restore the steady point. This type of behaviour is exhibited by our model in the case where the system eventually reaches a steady state value, either monotonically or via oscillatory convergence to steady state. This is the behaviour described in **Case I** of Section 4.2.

The second is the consideration of dynamic stable states, such as oscillatory behaviour, described in **Case II** of Section 4.2. All homeostatic mechanisms use negative feedback to maintain a constant value (often called the set point). Negative feedback describes the situation whereby a change occurring in a system automatically intitates a corrective mechanism, which reverses the original change and brings the system back towards the set point. Generally, the bigger the change occurring, the bigger the corrective mechanism.

Therefore, in a system controlled by negative feedback, the set level is never perfectly maintained, but constantly oscillates about the set point. An efficient homeostatic system minimises the size of the oscillations, although if variation is not present both corrective mechanisms would try to operate at once. This is especially true in enzyme controlled homeostatic mechanisms where there is a significant time lag before the corrective mechanism can be activated due to the time it takes for protein synthesis to commence.

Furthermore, there are possible functional advantages to oscillatory homeostatic mechanisms; it could be that limiting the time during which cholesterol concentration is necessarily elevated within the cell (e.g. due to increased demand from the plasma membrane) may decrease the risk of cytotoxicity that could result due to this high concentration. Additionally, increasing cell cholesterol levels in this manner may incur less demand on cellular energy supplies than sustained elevation.

Oscillatory behaviour has also been demonstrated in other biological homeostatic systems, for example, in the regulation of intracellular calcium levels (Carafoli, 1987; Berridge et al., 2003). Closely associated with calcium oscillations is the periodic release of insulin by β-cells in the pancreas where insulin is synthesised (Aspinwall et al., 1999).

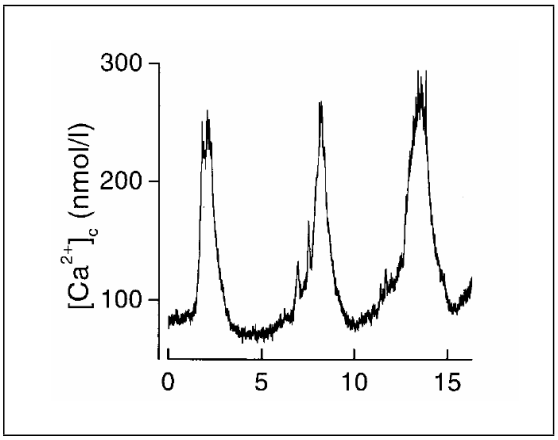

Fig. 4.1: Ca^{2+} oscillations induced by glucose in a single β-cell. The horizontal axis represents time in minutes. Illustration reproduced from Figure 1 of Gilon et al. (2002).

Figure 4.1 illustrates the periodic response of β-cell calcium concentration in response to insulin stimulation by glucose. Insulin oscillations are believed to be significant in preventing downregulation of insulin receptors in cells.

This behaviour maintains insulin sensitivity and protects against the development of insulin resistance; loss of this periodicity is a precursor to the development of Type II diabetes.

Oscillatory behaviour has also been shown to exist in enzyme synthesis. Glycolytic oscillations represent the best known example of periodic behaviour, due to the action of the regulatory enzyme phosphofructokinase (Ghosh and Chance, 1964). Oscillations have also been exhibited as a result of end product repression in heme (a component of haemoglobin) biosynthesis (Waxman et al., 1966).

There is, therefore, biological precedence for periodicity in systems of regulated enzyme synthesis; thus the existence of limit cycle behaviour in our model of regulated cholesterol biosynthesis via the synthesis of HMGR may be significant.

However, there is as yet very little experimental data concerning cholesterol biosynthesis without any interference from extra or intracellular pathways, one of the reasons being the highly complex network of reactions within which *de novo* synthesis falls.

4.6 Comparison with Griffith's model

In this section we consider some implications our model has on one of the classic models of regulated gene expression developed by Goodwin (1965) and modified by Griffith (1968). Hopf bifurcations have been shown to exist in Griffith's modification to Goodwin's classic negative feedback model discussed in Section 3.2, given by

$$\frac{dx_1}{dt} = \frac{\alpha_1}{1+\beta x_3^m} - k_1 x_1, \tag{4.154}$$

$$\frac{dx_2}{dt} = \alpha_2 x_1 - k_2 x_2, \tag{4.155}$$

$$\frac{dx_3}{dt} = \alpha_3 x_2 - k_3 x_3. \tag{4.156}$$

Previous analysis on these equations have shown that for a three variable system, the cooperativity of feedback, that is the Hill coefficient, must be very high ($m > 8$), (Griffith, 1968; Murray, 1977). As such, genetic regulatory systems modelled using this framework have been considered unsatisfactory. Biologically, this corresponds to an unphysiologically high number of repressor molecules required to bind to a gene in order to cause deactivation. Experimental results indicate that the number of transcription factor binding sites on a gene is rarely higher than four.

We now consider the effects of cooperativity and number of gene binding sites in respect to our model. In order to do this, we make some simplifying assumptions. First, we assume that $\delta_{mh} = \delta_h = \delta_c = \delta$ in system (3.66). Secondly, we alter the nondimensionalisation of the system for ease of calculation

$$\tau = \bar{\mu}_h t \qquad m_h = \frac{\bar{m}_h}{\bar{s}_0}, \qquad h = \frac{\bar{h}}{\bar{s}_0}, \qquad c = \frac{\bar{c}}{\bar{s}_0}, \tag{4.157}$$

which results in the following system of equations, where n and q are considered generally

$$\frac{dm_h}{d\tau} = \frac{\mu_{mh}}{1+\gamma_m\left(1+\gamma_c c^q\right)^n} - \delta m_h, \tag{4.158a}$$

$$\frac{dh}{d\tau} = m_h - \delta h, \tag{4.158b}$$

$$\frac{dc}{d\tau} = \mu_c h - \delta c, \tag{4.158c}$$

where $\gamma_m = \kappa_{mh}^n$ and $\gamma_c = \left(\kappa_c^q\right)^{-1}$. We note that the conclusions made previously in this chapter about the steady states of the system apply here also; thus system (4.158) has one physiologically valid, positive real root, given by the solution of

$$\frac{1}{1+\gamma_m\left(1+\gamma_c c_{ss}^{\,q}\right)^n} = \vartheta c_{ss}, \tag{4.159}$$

where

$$\vartheta = \frac{\delta^3}{\mu_c \mu_{mh}}. \tag{4.160}$$

The Jacobian matrix, **J**, of system (4.158), is given by

$$\mathbf{J} = \begin{bmatrix} -\delta & 0 & -\mu_{mh}\,\Lambda \\ 1 & -\delta & 0 \\ 0 & \mu_c & -\delta \end{bmatrix}, \tag{4.161}$$

where

$$\begin{aligned} \Lambda &= -\frac{\partial}{\partial c}\left(\frac{1}{1+\gamma_m\left(1+\gamma_c c_{ss}^{\,q}\right)^n}\right)_{c=c_{ss}}, \\ &= \frac{nq\gamma_m\gamma_c c_{ss}^{\,q-1}\left(1+\gamma_c c_{ss}^{\,q}\right)^{n-1}}{\left(1+\gamma_m\left(1+\gamma_c c_{ss}^{\,q}\right)^n\right)^2}. \end{aligned} \tag{4.162}$$

We note that Λ from (4.162) can be rewritten as,

$$\Lambda = nq\gamma_m\gamma_c\vartheta^2 c_{ss}^{\,q+1}\left(1+\gamma_c c_{ss}^{\,q}\right)^{n-1}, \tag{4.163a}$$

$$= nq\gamma_c\vartheta c_{ss}^{\,q}\left[\vartheta c_{ss}\gamma_m\left(1+\gamma_c c_{ss}^{\,q}\right)^{n-1}\right], \tag{4.163b}$$

and also from (4.159), we have

$$1-\vartheta c_{ss} = \vartheta c_{ss}\gamma_m\left(1+\gamma_c c_{ss}^{\,q}\right)^n. \tag{4.164}$$

Using the above and (4.159) we may rewrite Λ in (4.163b) as

$$\Lambda = nq\vartheta(1-\vartheta c_{ss})\frac{\gamma_c {c_{ss}}^q}{1+\gamma_c {c_{ss}}^q}. \tag{4.165}$$

Thus the characteristic equation of the Jacobian in (4.161) can now be written as

$$(\lambda+\delta)^3 + \mu_{mh}\mu_c\Lambda = 0, \tag{4.166}$$

where

$$\mu_{mh}\mu_c\Lambda = \delta^3 nq(1-\vartheta c_{ss})\frac{\gamma_c {c_{ss}}^q}{1+\gamma_c {c_{ss}}^q}. \tag{4.167}$$

Using the result above, the characteristic equation (4.166) becomes

$$(\lambda+\delta)^3 + \delta^3 nq(1-\vartheta c_{ss})\frac{\gamma_c {c_{ss}}^q}{1+\gamma_c {c_{ss}}^q} = 0, \tag{4.168}$$

the solutions of which provide the eigenvalues which characterise the stability of the system.

These eigenvalues are given by

$$\lambda_1 = -\delta - \delta\left(nq(1-\vartheta c_{ss})\frac{\gamma_c {c_{ss}}^q}{1+\gamma_c {c_{ss}}^q}\right)^{1/3}, \tag{4.169}$$

$$\lambda_{2,3} = -\delta + \delta\left(nq(1-\vartheta c_{ss})\frac{\gamma_c {c_{ss}}^q}{1+\gamma_c {c_{ss}}^q}\right)^{1/3}\left(\cos\frac{\pi}{3} \pm i\sin\frac{\pi}{3}\right). \tag{4.170}$$

The fixed point of this system is stable if and only if $\mathbb{R}\mathrm{e}(\lambda_{2,3}) < 0$, that is if and only if

$$-\delta + \delta\left(nq(1-\vartheta c_{ss})\frac{\gamma_c {c_{ss}}^q}{1+\gamma_c {c_{ss}}^q}\right)^{\frac{1}{3}}\frac{1}{2} < 0. \tag{4.171}$$

Since δ is a positive real parameter, the inequality (4.171) is dependent on

$$-1 + \frac{1}{2}\left(nq(1-\vartheta c_{ss})\frac{\gamma_c {c_{ss}}^q}{1+\gamma_c {c_{ss}}^q}\right)^{1/3}, \tag{4.172}$$

which can be rewritten as

$$nq(1-\vartheta c_{ss})\frac{\gamma_c c_{ss}^{\,q}}{1+\gamma_c c_{ss}^{\,q}} < 8. \tag{4.173}$$

At the Hopf bifurcation point, equality holds and so

$$nq(1-\vartheta c_{ss})\frac{\gamma_c c_{ss}^{\,q}}{1+\gamma_c c_{ss}^{\,q}} = 8. \tag{4.174}$$

From (4.159) we may calculate

$$1-\vartheta c_{ss} \quad = \quad 1-\frac{1}{1+\gamma_m\left(1+\gamma_c c_{ss}^{\,q}\right)} \quad = \quad \frac{\gamma_m\left(1+\gamma_c c_{ss}^{\,q}\right)}{1+\gamma_m\left(1+\gamma_c c_{ss}^{\,q}\right)}, \tag{4.175}$$

and thus we know $0<1-\vartheta c_{ss}<1$. Similarly, we also know

$$0<\frac{\gamma_c c_{ss}^{\,q}}{1+\gamma_c c_{ss}^{\,q}}<1. \tag{4.176}$$

Therefore we find

$$nq=\frac{8}{(1-\vartheta c_{ss})\left(\frac{\gamma_c c_{ss}^{\,q}}{1+\gamma_c c_{ss}^{\,q}}\right)}>8. \tag{4.177}$$

Hence, we find from (4.177), that for the possibility of a Hopf bifurcation to arise it is necessary that $nq>8$. At first glance it may seem that we have simply reproduced similar criteria as for oscillatory solutions to occur in the Goodwin model equations, but there are significant differences in our model. Here, the exponent describing cooperativity in the reaction is a product of two factors, the number of cholesterol molecules able to bind to a molecule of SREBP, ($q=4$) and the number of binding sites for SREBP on the HMGR gene ($n=3$) which gives $nq=12$, thus allowing for the possibility of limit cycles.

Previous work has suggested that oscillatory solutions of Goodwin's model equations are unfeasible due to the unphysiological degree of cooperativity required. However the analysis above indicates that the model we have constructed can reproduce oscillatory behaviour without being biologically unsound. Specifically, our inclusion of an end product repressor coupled with

the action of a transcription factor creates a feedback mechanism containing two steps. The Hill coefficients of each of these steps are biologically valid, and have been supported by experimental evidence. Thus our model reduces the restrictive cooperativity constraint that Griffith's model imposes. We have also shown that the simplicity of the Goodwin model equations, and therefore the number of parameters required to be determined, need not be compromised in order to create a genetic regulatory model capable of producing oscillations.

We note briefly that other modifications of Goodwin's model equations have also been postulated to allow for the possibility of oscillations without unreasonable constraints on cooperativity. Bliss et al. (1982) proposed a model based on the Goodwin equations which undergoes a transition to oscillations under more reasonable conditions. In their model the feedback step is no longer cooperative, and the linear degradation of the end product is replaced by a Michaelis-Menten function. The latter is appropriate in the case when the end product is consumed in an enzyme catalysed reaction described by Michaelis-Menten kinetics; the presence of the additional nonlinear term in the rate law of the last component of the reaction chain is sufficient to cause oscillation. In deriving the regulated model of cholesterol biosynthesis, we have explicitly modelled the efflux of cholesterol as a single term. However, as one of the major reactions intracellular cholesterol participates in is its esterification, mediated by the enzyme ACAT, this modification is applicable to our model.

In Goodwin's equations and the modified models of both Griffith (1968) and Bliss et al. (1982), it is assumed implicitly that there are no time delays in the processes of transcription, translation, or end product repression. However, there are delays in transcription and translation associated with mRNA and protein processing following synthesis. Furthermore, delays in the feedback term are also likely to be present as the end product must move into the nucleus to bind with transcription factors and subsequently interact with the regulatory sites of the gene. MacDonald (1977) analyzed a generalisation of Goodwin's equations incorporating time lags in the production of one biochemical component of the model based on the history of another chemical component, resulting in a system of delay differential equations. This system has been shown to generate oscillations in two variables, compared with the minimum of three variables required using Griffith's modification. Again, this modification is also applicable to our model

since we have also ignored the effect of time delays occurring in genetic processes.

We have demonstrated the possibility of oscillatory behaviour in a model of gene expression regulation by improving the equations developed by Goodwin (1965) to provide a more realistic physiological framework to the mathematical equations.

Summary

In this chapter we have analysed the model of regulated cholesterol biosynthesis which was developed in Chapter 2. We have shown that this model may admit oscillatory solutions, and the transition to periodic behaviour can occur under biologically feasible conditions, as compared with other models derived in a similar manner. The oscillatory behaviour occurring was shown to be the result of a supercritical Hopf bifurcation; thus the oscillations generated are stable with small amplitude. The significance of these periodic solutions in the context of biological homeostasis has been discussed, and although there is no suitable experimental data available for direct comparison, the possibility that this type of behaviour for regulated cholesterol biosynthesis may be correct is high. The conclusions made thus far, however, have been based on mathematical analysis alone. In the following chapter we will solve our model numerically to investigate parameter spaces for oscillatory and non-oscillatory solutions and investigate whether or not these regions of parameter space are physiologically valid. Numerical solutions will also be used to determine both the effect and range of values for the three undetermined parameters in the system, δ_c, κ_m and κ_c.

5

Numerical Analysis of The Cholesterol Biosynthesis Model

In this chapter we present numerical solutions to the cholesterol biosynthesis ODE model (system (3.66)) derived in Chapter 3 and nondimensionalised in Chapter 4 (system (4.3)). The numerical results of the first half of this chapter show simulations in which μ_c is considered the critical parameter, and the solutions presented are used to verify the analytical conclusions made in Chapter 4. The second half of this chapter contains results which investigate the response of the system to model parameters. In particular we investigate the effects of the three undetermined system parameters, δ_c, κ_{mh} and κ_c, using the results obtained to isolate regions of steady state and oscillatory behaviour in the parameter space.

The model was simulated using the Matlab stiff differential equation solver ODE 15s, (Hunt et al., 2006), which uses a backward differentiation formula (also known as Gear's Method) of order 5. The characteristics of bifurcations and limit cycles of the system were explored using the Matlab numerical continuation package MatCont (Dhooge et al., 2003). MatCont is a collection of numerical algorithms implemented as a Matlab Toolbox, for the detection and continuation of equilibria, limit cycles and bifurcations in differential equations.

5.1 Nondimensional model parameter values

The set of nondimensional parameters and initial conditions used to investigate the model are listed in Table 5.1; further details on the calculations of the dimensional parameters may be found in Appendix B.1. The parameters of Table 5.1 result from the nondimensionalisation described by equations (4.1) and (4.2), which leads to the parameters in (4.5). In the case of the three undetermined parameters δ_c, κ_{mh} and κ_c, we estimate starting values for these based on their biological function. We recall from Section 3.3 that $\bar{\kappa}_{mh}$ is representative of the concentra-

Parameter	**Description**	**Nondimensional Value**
μ_{mh}	Rate of HMGR mRNA transcription	1.46×10^{-6}
μ_h	Rate of HMGR translation	1.14×10^{4}
μ_c	Rate of cholesterol production (HMGR activity)	9.67×10^{2}
δ_h	Rate of HMGR degradation	1.43
κ_c	Dissociation constant between cholesterol and SREBP	100
δ_c	Rate of cholesterol degradation	1.00
κ_{mh}	Dissociation constant between SREBP and HMGR gene	1.00
Initial Condition	**Description**	**Nondimensional Value**
$m_h(0) = m_{h0}$	Initial HMGR mRNA concentration	3.65×10^{-7}
$h(0) = h_0$	Initial HMGR concentration	1.10×10^{-2}
$c(0) = c_0$	Initial cholesterol concentration	2.30×10^{2}

Table 5.1: Nondimensional parameter and initial values of the HMGR model.

tion of $\bar{s}$ required for half of the genes to be active. Therefore as a starting point we set $\bar{\kappa}_{mh}$ to be $\mathcal{O}(\bar{s}_0)$. From (4.5) we have an initial nondimensional value of $\kappa_{mh} = 1$. We estimate a value for $\bar{\kappa}_c$ using similar reasoning, noting that $\bar{\kappa}_c$ is representative of the concentration of $\bar{c}$ producing half occupation in the binding reaction of $\bar{c}$ and $\bar{s}$. Therefore as an initial estimate we set $\bar{\kappa}_c$ to

be $\mathcal{O}(\bar{c}) = c_0$. From (4.5) we have an initial nondimensional value of $\kappa_c = 1 \times 10^2$. Finally, to assign an initial estimate for $\bar{\delta}_c$ we consider that this value will be of the same order of magnitude as δ_{mh} and δ_h. Therefore as an initial estimate we set $\bar{\delta}_c$ to be $\mathcal{O}(\bar{\delta}_{mh})$. From (4.5) we have an initial nondimensional value of $\delta_c = 1$. These values will be varied in order to gauge their effect on the response of the system.

5.2 Model results for μ_c as a bifurcation parameter

Having, in Section 4.2, analysed the different dynamical responses of the system with respect to μ_c, we begin by presenting results of the system where all parameters are fixed except for μ_c which we vary. The analysis of the previous section tells us that we may expect to see at least three types of equilibrium, the stable node, the stable focus and a limit cycle, corresponding to monotonic convergence to steady state, oscillatory convergence to steady state and pure oscillatory system behaviour respectively. This is confirmed by the numerical results presented below. For the system parameters detailed in Table 5.1, we find that the solution trajectories tend directly to the stable equilibrium point (see Figure 5.1). To confirm that the system is tending to a steady state smoothly, a phase space portrait was constructed (i.e. a plot in the three-dimensional variable space, where each trajectory corresponds to a different set of initial conditions). This can be seen in Figure 5.4(a), where the trajectory travels directly to the fixed point of the system. This is a stable node equilibrium point corresponding to three negative real eigenvalues of the linearised Jacobian matrix of the system.

We also note the behaviour of the system response in Figure 5.1. Initially, all three variables decrease in concentration, the effect of the degradation terms in the equation. However, after a short delay, the decrease in cholesterol concentration feeds back to the regulation term in the mRNA equation, and at $\tau \approx 1$ mRNA concentration starts to rise. This is followed by a similar delayed increase in HMGR concentration at $\tau \approx 1.7$.

As μ_c is increased by at least one order of magnitude there is a distinct change of system behaviour. Concentrations of variables exhibit oscillations that decay and are eventually com-

pletely damped to a steady state value. As illustrated in Figure 5.2, when μ_c is increased by greater amounts, the time taken for the initial oscillatory behaviour to decay fully increases. This is a stable focus equilibrium point where the decaying oscillations are governed by the existence of a pair of complex conjugate eigenvalues. The third eigenvalue of this system is real and negative, and results in the equilibrium being stable. This corresponds to the phase space portrait of Figure 5.4(b) where the solution trajectory spirals in toward the equilibrium point.

Still further increases in the magnitude of μ_c result in the equilibrium point eventually losing stability altogether, as predicted by the analysis of the previous chapter. Here, μ_c reaches its critical value μ_c^*, and the real parts of the complex conjugate pair of eigenvalues of the linearised Jacobian matrix cross the imaginary axis. As they do so, they become a pair of pure imaginary eigenvalues, at which point a periodic trajectory is generated. This is exhibited in the results of Figure 5.3. The equilibrium point loses stability and becomes a limit cycle due to the Hopf bifurcation determined in Section 4.2. This limit cycle behaviour is illustrated in Figure 5.4(c).

Based on the numerical results presented in Figure 5.3, we expect a bifurcation point to exist for μ_c somewhere in the region of $\approx \mathcal{O}(10^5)$. Analytic calculation of the bifurcation point, that is, the solution of the simultaneous equations (4.28) and (4.29), provides an exact value for the critical value μ_c^*. Numerical computation of the critical bifurcation values are illustrated in Figure 5.5. The values obtained using both methods are in excellent agreement and are found in Table 5.2, together with analytically and numerically determined eigenvalues at the bifurcation point in Table 5.3.

Parameter	**Analytic Value**	**Numerical Value**
μ_c^*	433785.42	433786.01
c_{ss}	124.48	124.48

Table 5.2: Analytic and numerical solutions for bifurcation value of μ_c^* and c_{ss}.

Eigenvalue	**Analytic Value**	**Numerical Value**
λ_1	-1.966	-1.966
λ_2	1.966	1.966
λ_3	-3.433	-3.433

Table 5.3: Analytic and numerical values of eigenvalues at bifurcation point, μ_c^*.

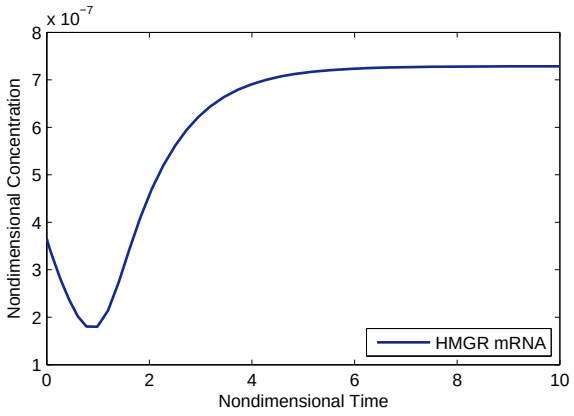

(a)

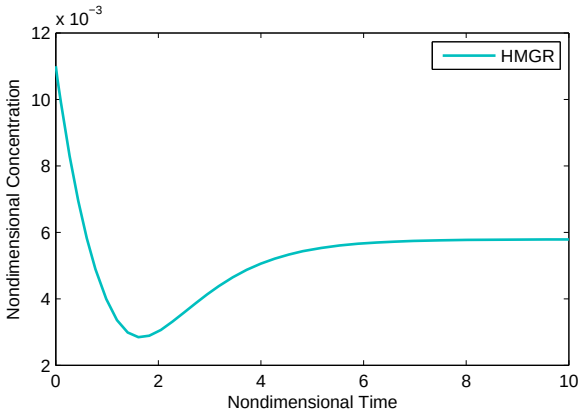

(b)

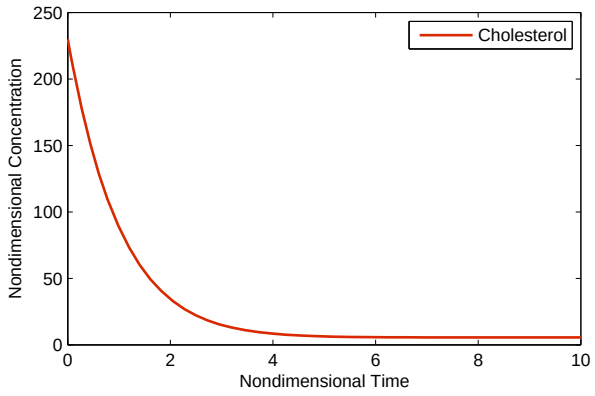

(c)

Fig. 5.1: Solution trajectories tending directly to a stable equilibrium point with nondimensional values of $\kappa_{mh} = 1, \kappa_c = 100, \delta_c = 1$ and $\mu_c = 9.67 \times 10^2$ (Figure 5.1(a): mRNA; Figure 5.1(b): HMGR and Figure 5.1(c): cholesterol).

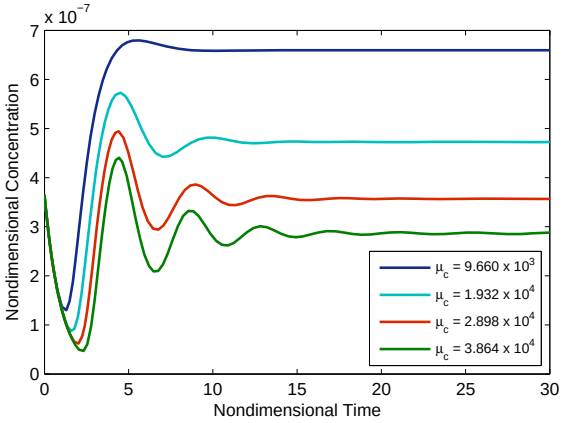

(a)

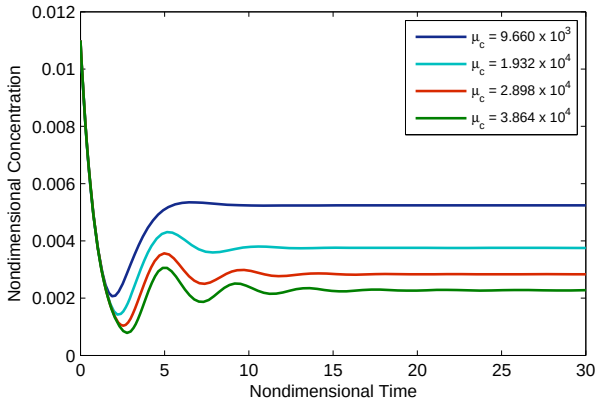

(b)

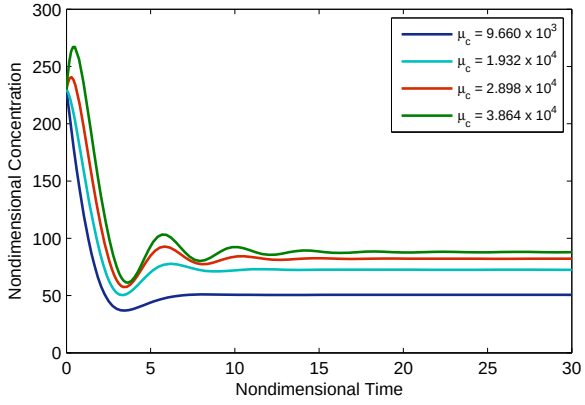

(c)

Fig. 5.2: Solution trajectories undergoing oscillatory convergence to a stable equilibrium. As μ_c increases the oscillatory decay occurs for longer times before reaching steady state (Figure 5.2(a): mRNA; Figure 5.2(b): HMGR and Figure 5.2(c): cholesterol).

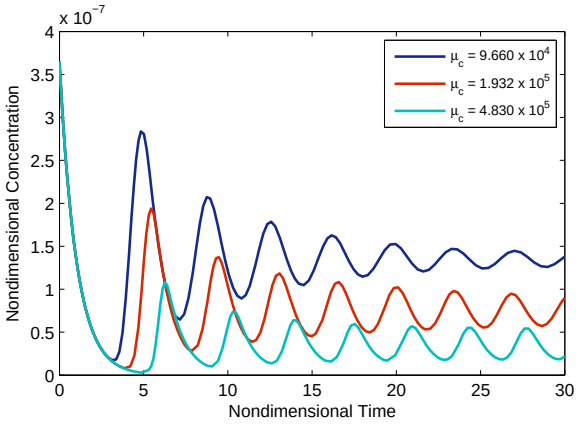

(a)

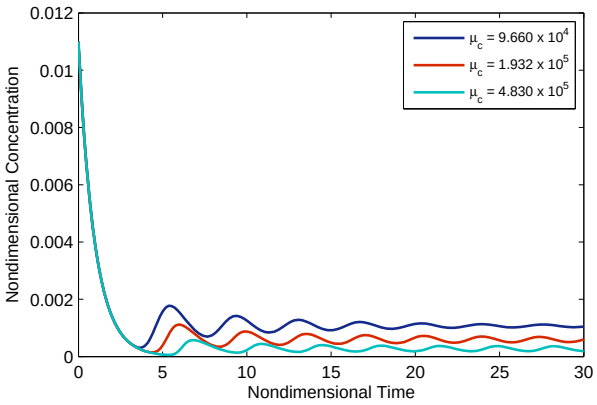

(b)

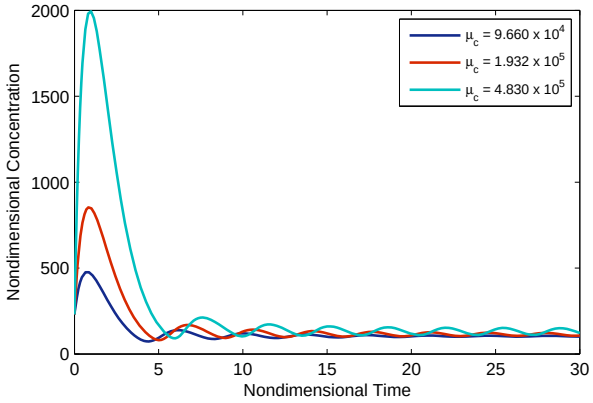

(c)

Fig. 5.3: Solution trajectories displaying oscillatory behaviour. Continued increases in μ_c eventually result in the system exhibiting sustained oscillations (Figure 5.3(a): mRNA; Figure 5.3(b): HMGR and Figure 5.3(c): cholesterol).

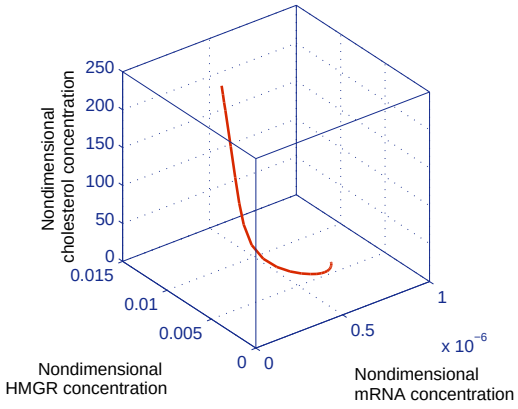

(a)

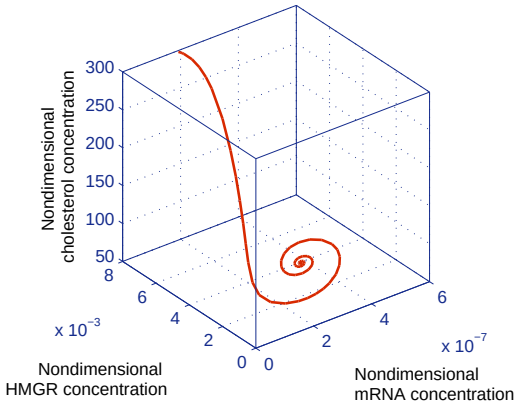

(b)

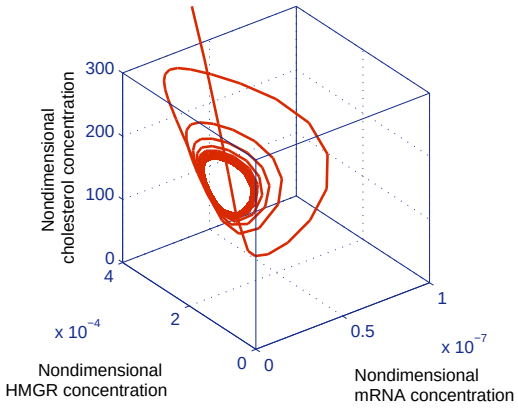

(c)

Fig. 5.4: Phase space portraits illustrating the types of different dynamical behaviour. Figure 5.4(a): Stable node with $\mu_c = 9.660 \times 10^2$; Figure 5.4(b): Stable focus with $\mu_c = 3.864 \times 10^4$ and Figure 5.4(c): Limit cycle with $\mu_c = 4.830 \times 10^5$.

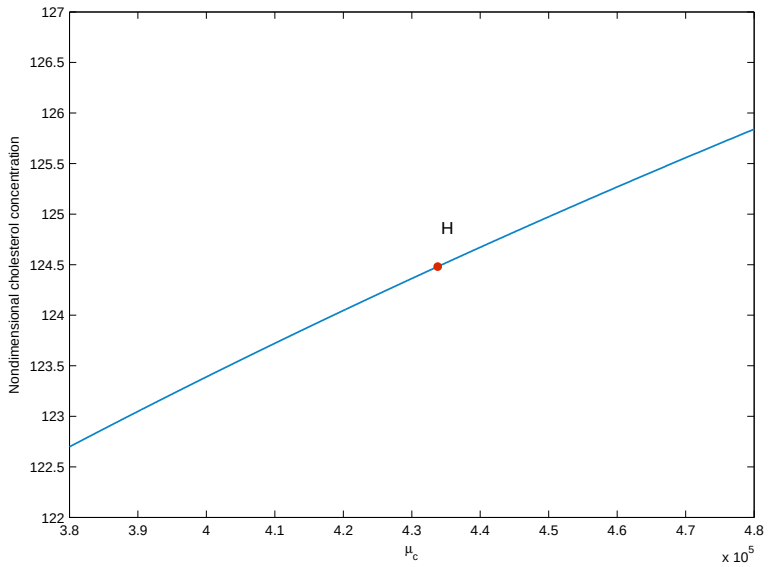

Fig. 5.5: Equilibrium manifold in the μ_c, c plane, with all parameter values other than μ_c as detailed in Table 5.1. As μ_c is increased the system undergoes a Hopf bifurcation (represented by H) at some critical value μ_c^* for a corresponding value of c_{ss}.

Having demonstrated numerically the generation of a limit cycle for the bifurcation point μ_c^* as detailed in Table 5.2, we now investigate whether the simulations match the analysis of Section 4.4.6 and Section 4.4.7. For the case $\mu_c = 1.00005\mu_c^*$, the cubic coefficient $\mathscr{B}_2$ (equation (4.142)) which dictates the nature of the resulting limit cycles is negative and is given by $\mathscr{B}_2 = -0.01491$. Thus from the analysis of the previous section we predict that a supercritical bifurcation occurs at this value of μ_c^*. That is, we may expect to see an oscillatory response approaching zero when $\mu_c < \mu_c^*$ and stable limit cycles bifurcating when $\mu_c > \mu_c^*$.

Figure 5.6 illustrates the family of limit cycles generated at the Hopf bifurcation when varying μ_c with all other parameters held at the values given in Table 5.1. When μ_c crosses its bifurcation value, μ_c^*, and increases, a stable limit cycle is expelled from the bifurcation point which grows in amplitude. To confirm these limit cycles are stable, the convergence to the numerically computed limit cycle of trajectories using different initial conditions, when $\mu_c > \mu_c^*$ is illustrated in Figure 5.7.

Analytically predicted approximations of the time period and amplitude, compared with estimates obtained from the numerical solution for the evolution of c, are presented in Table 5.4.

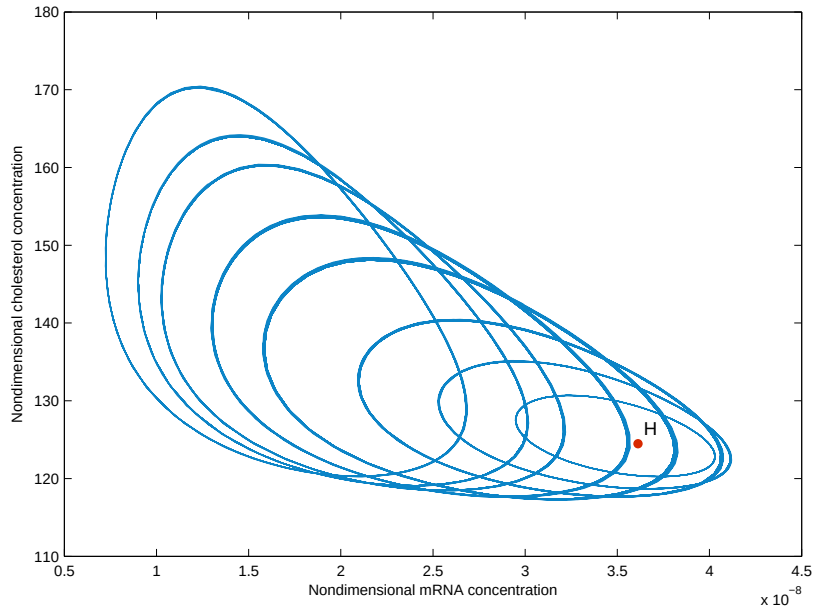

Fig. 5.6: Family of limit cycles bifurcating from the Hopf bifurcation point of Figure 5.5, in the (m_h, c) plane, as μ_c is varied. Limit cycles of increasing amplitude are generated as μ_c becomes progressively greater than μ_c^*.

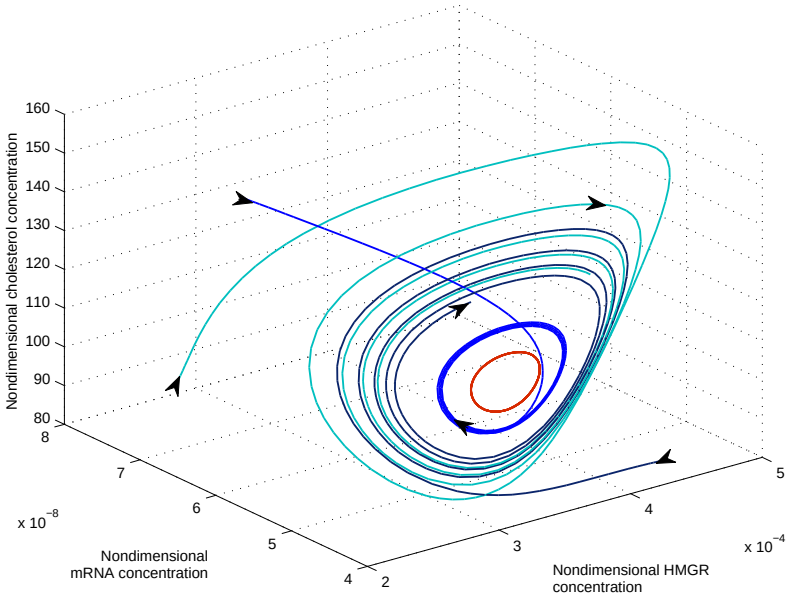

Fig. 5.7: Phase space plot of differing initial conditions illustrating trajectories converging to the limit cycle when $\mu_c > \mu_c^*$.

The numerical and analytical values of the limit cycle properties show reasonable agreement; the reason for discrepancy may lie in the use and calculation of the approximation of the eigenvalues near the bifurcation point in the determination of the analytic period (calculated using the matrix (4.120)).

Property	Analytic Value	Numerical Value
Period	3.168	3.344
Amplitude	16.105	16.269

Table 5.4: Analytic and numerical limit cycle properties of c when $\mu_c = 1.00005\mu_c^*$.

Oscillatory solutions for the case $\mu_c = 1.05\mu_c^*$ are illustrated in Figure 5.8 where the concentration of h has been rescaled, and the results displayed for a non zero initial time, to allow for clearer comparison. We note that the concentrations are out of phase, and as to be expected, the maximum in the enzyme HMGR follows the maximum in mRNA. The maximum in cholesterol concentration follows after both. Thus the system demonstrates a homeostatic mechanism

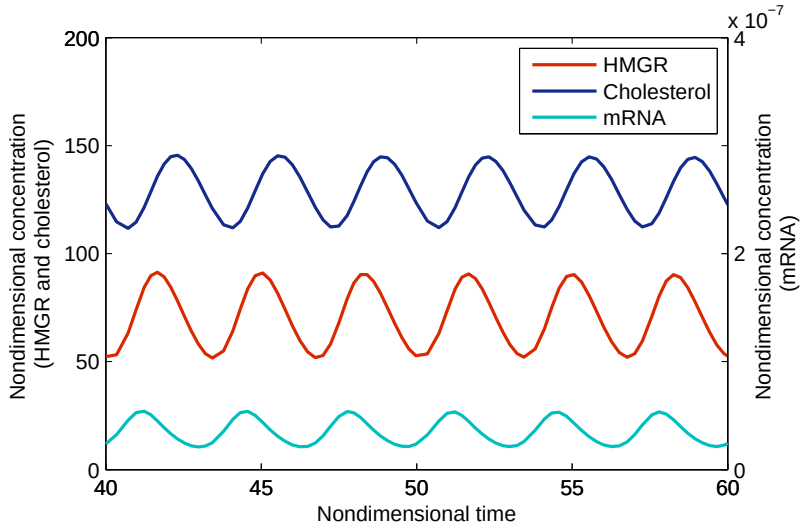

Fig. 5.8: Time evolution of system variables for $\mu_c = 1.05\mu_c^*$. Note that h has been rescaled in order to allow for phase comparison. The left hand y-axis corresponds to the nondimensional concentration of c and h; the right hand y-axis represents the nondimensional concentration of m.

whereby increases in cholesterol feed back to mRNA which then responds. As mRNA synthesis is decreased, less enzyme is created and cholesterol production falls. This information is once again relayed to mRNA and the system cycles in this manner, keeping cholesterol concentration

restricted between upper and lower bounds, as determined by the parameter values.

Thus far the analyses of Chapter 4, with respect to μ_c as a bifurcation parameter have been confirmed. We now go on to investigate the response of the system to the remaining model parameters using local sensitivity analysis. By varying a single parameter at a time whilst keeping all other parameters constant, we find that there exist critical values for all model parameters at which the cholesterol biosynthesis model undergoes a supercritical Hopf bifurcation, that is, at which a stable limit cycle is generated. Of particular interest in the model are the three parameters for which values could not be determined from the experimental data. The results of the system behaviour in response to these values is now presented.

5.3 Model results for δ_c as a bifurcation parameter

We begin by considering the parameter δ_c. This undetermined parameter is the rate of cholesterol degradation, equivalent to the efflux of cholesterol from the cell. We examine the effects of varying this parameter on the system, and consider the following two cases

i) the **nonoscillatory** system with $\mu_c = 9.67 \times 10^2$,

ii) the **oscillatory** system with $\mu_c = 4.55 \times 10^5$,

where all other parameters, except for δ_c, are kept constant with the values given in Table 5.1.

The results of varying δ_c on the nonoscillatory system can be seen in Figure 5.9. Here we see that greater values of δ_c result in lower steady states of cholesterol which are reached progressively faster as cholesterol depletion from the cell is increased (Figure 5.9(b)). This is reflected in differing speeds of response in the mRNA concentration, the faster cholesterol is lost from the cell, the more rapid the response of mRNA (Figure 5.9(a)).

The effect of varying δ_c on the oscillatory system is seen in Figure 5.10 demonstrating interesting results. (Only results for mRNA concentration are provided here; the other two variables

of the system (HMGR and cholesterol) display qualitatively similar behaviour.) It is clear that within the range of values investigated, oscillatory behaviour can be lost by either increasing or decreasing δ_c to a sufficient degree. That is, the system can regain stability in two directions; suggesting that for the oscillatory system, there exist two Hopf bifurcation points for δ_c as the bifurcation parameter. This is confirmed by the numerically computed continuation of the equilibrium of δ_c illustrated in Figure 5.11.

The reason for the existence of two bifurcation points is seen explicitly in Figure 5.12, which plots the course of one of the complex eigenvalues of the Jacobian matrix of the cholesterol biosynthesis system as δ_c varies. Following the first crossing of the imaginary axis, the eigenvalue changes direction and recrosses the axis, resulting in the second bifurcation point. This is confirmed analytically from the solutions of equations (4.43) and (4.44); results are displayed in Table 5.5.

	Parameter	Analytic Value	Numerical Value
First Hopf	δ_c^*	0.702	0.702
Point	$c_{(ss)}$	130.657	130.656
Second Hopf	δ_c^*	1.174	1.174
Point	$c_{(ss)}$	123.778	123.778

Table 5.5: Analytic and numerical solutions of bifurcation values for δ_c and c_{ss}.

Figure 5.13 illustrates that between the two bifurcation points, there exists a family of stable limit cycles. In this case, a supercritical bifurcation occurs at the first Hopf point at $\delta_c = 0.702$; periodic solutions exist for $\delta_c > 0.702$. At the second Hopf point, at $\delta_c = 1.174$, we see that periodic solutions exist for $\delta_c < 1.174$. These conclusions were confirmed by investigating the behaviour of trajectories for the interval $0.702 < \delta_c < 1.174$; in all cases examined, the trajectories converged to the numerically computed limit cycle.

We note these results indicate the system is extremely sensitive to δ_c, as the range of values in which periodic solutions are obtained for this parameter is very narrow. This will not affect cellular behaviour under conditions where cell cholesterol efflux is fairly constant; however, even a small perturbation from its resting value, will result in a significant change in the behaviour of the system.

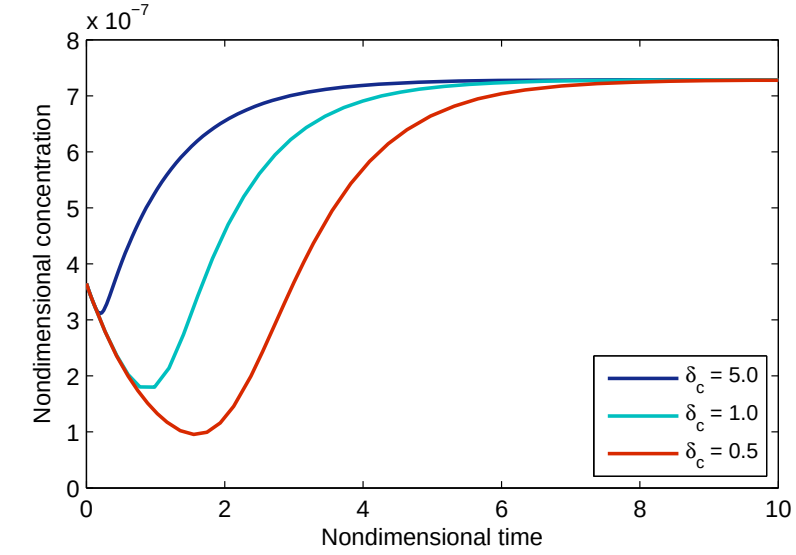

(a)

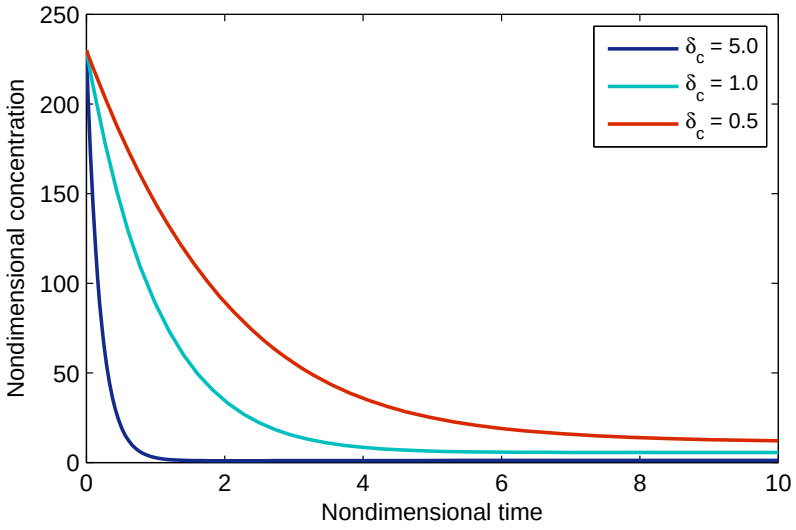

(b)

Fig. 5.9: Variation of stable cholesterol biosynthesis system (with $\mu_c = 9.67 \times 10^2$) showing continued stability in response to altering the value of δ_c. Figure 5.9(a): mRNA concentration; Figure 5.9(b): cholesterol concentration.

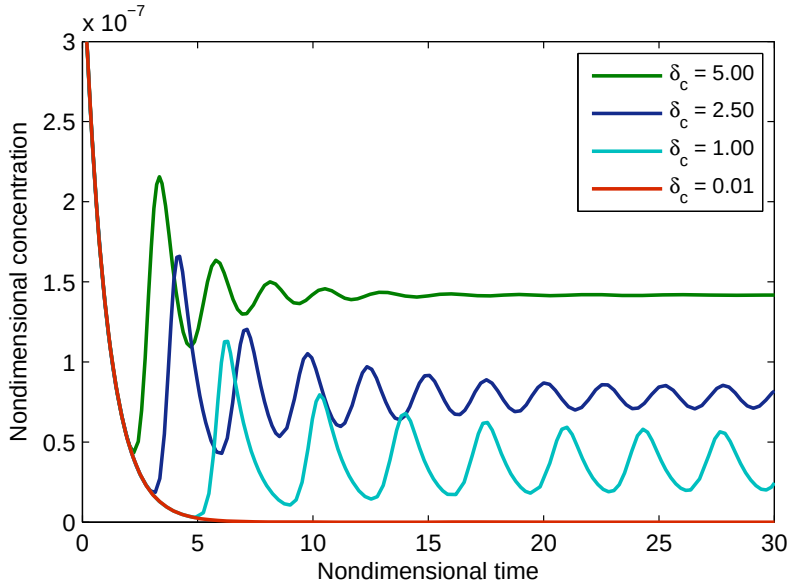

Fig. 5.10: Variation of the oscillatory cholesterol biosynthesis system (with $\mu_c = 4.55 \times 10^5$); response of mRNA concentration, from oscillatory convergence to steady state to oscillatory then nonoscillatory behaviour, to the variation of δ_c.

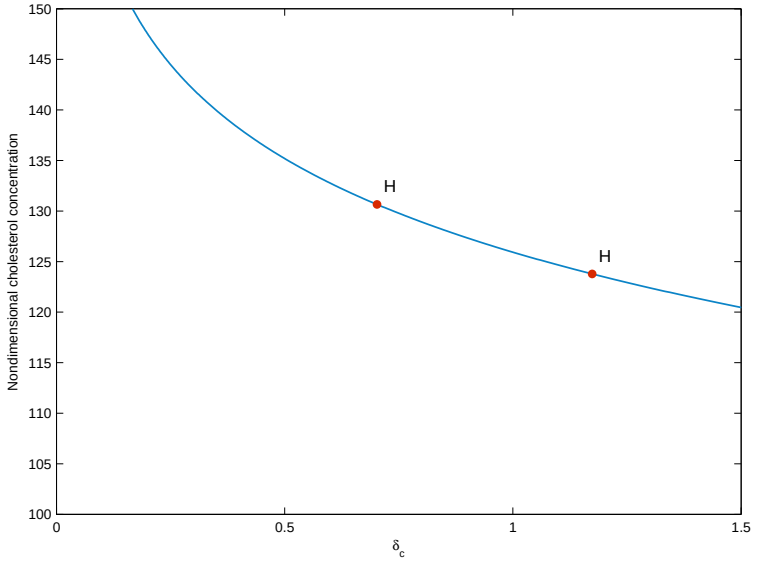

Fig. 5.11: Equilibrium manifold in the δ_c, c plane, with parameters $\kappa_c = 100$ and $\mu_c = 4.55 \times 10^5$. H represents a Hopf bifurcation point.

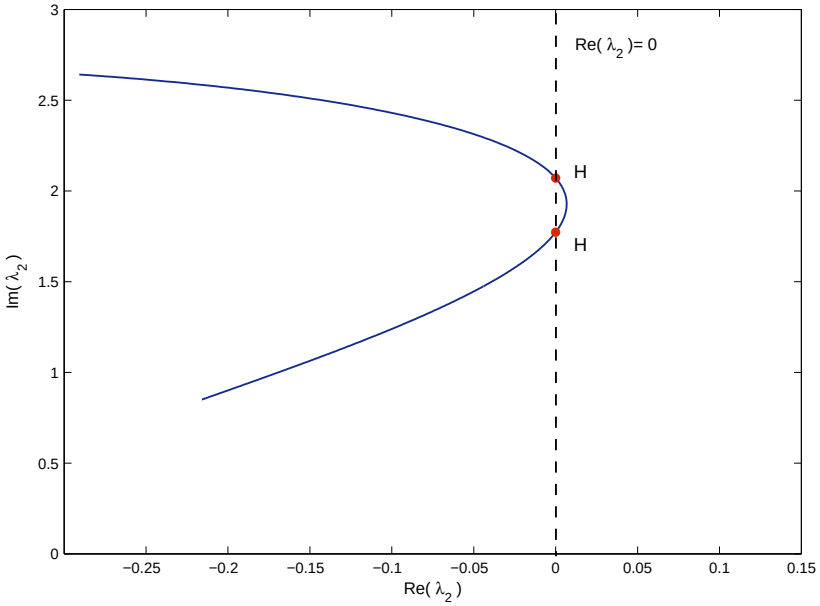

Fig. 5.12: Behaviour of the complex eigenvalue λ_2 with δ_c as a bifurcation parameter.

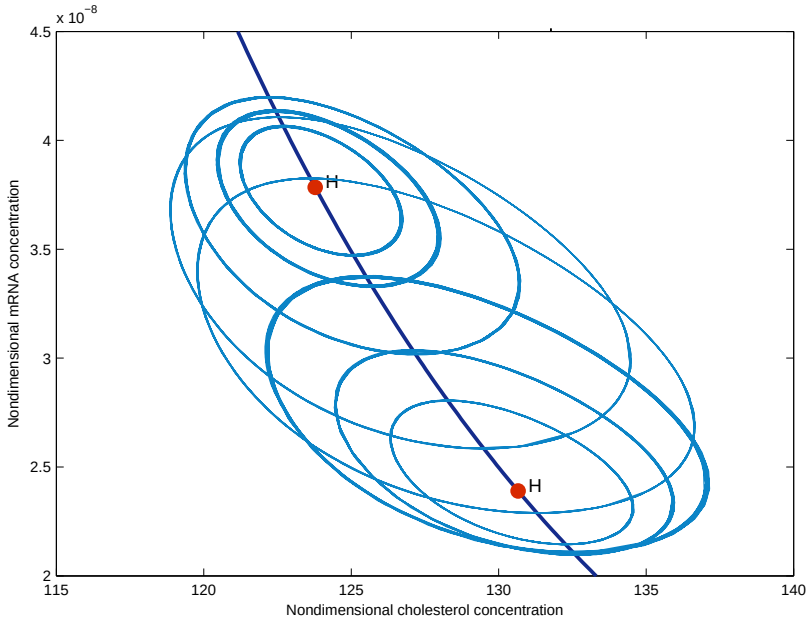

Fig. 5.13: Family of limit cycles bifurcating between the two Hopf bifurcation points of Figure 5.11, in the (m_h, c) plane, where each limit cycle corresponds to differing values of δ_c within the bifurcatory region.

5.4 Model results for κ_{mh} and κ_c as bifurcation parameters

In this section we will consider the effect of the two remaining undetermined parameters κ_{mh} and κ_c, investigating the nonoscillatory and oscillatory cases detailed at the beginning of Section 5.3.

We begin by examining the effect of κ_{mh}, which represents the dissociation constant between the transcription factor s and the HMGR gene. Simulation results on the nonoscillatory system have elucidated the system's response to this parameter and we summarise the main findings. For $\kappa_{mh} > 1$, as cholesterol concentration decreases so does mRNA synthesis, whereas for values of $\kappa_{mh} \leq 1$, a decrease in cholesterol concentration causes a resultant increase in the synthesis of mRNA. Intuitively, it is the latter behaviour require the model to exhibit, as we require the cell to create more cholesterol in response to its depletion in the intracellular environment.

A dissociation constant is the measure of the propensity of a complex to separate (dissociate) reversibly into component molecules. The smaller the dissociation constant the higher the affinity between the component molecules of the complex, thus the model simulations suggest the tighter the binding between the transcription factor and the gene, the better the negative feedback regulation occurring due to cholesterol concentration.

When κ_{mh} is varied for the oscillatory system, we find that for $\kappa_{mh} \approx 2$ a bifurcation occurs and the oscillatory behaviour is lost; this persists for all $\kappa_{mh} > 2$. For $\kappa_{mh} \leq 1$, no change in dynamic behaviour was found. Continued reductions in the value of κ_{mh} lead to the conclusion that either the system possesses periodic solutions for all $\kappa_{mh} \leq 1$ or that the value of κ_{mh} at which another qualitative change in behaviour occurs is too small for machine precision.

We next investigate the effect of κ_c, which represents the dissociation constant between the transcription factor s and cholesterol c. Beginning with the nonoscillatory case, we find that decreasing κ_c gradually alters the stability of the equilibrium, with solutions ranging from stable steady state, to those with oscillatory convergence to steady state and eventually to periodic solutions. Still further reductions in the value of κ_c results in continued generation of periodic solutions. In addition, as κ_c becomes smaller the delay before the onset of oscillations increases.

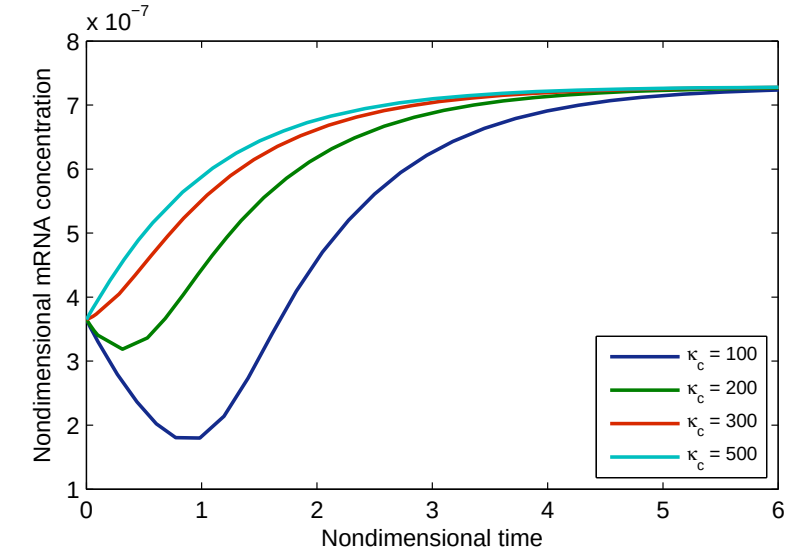

(a)

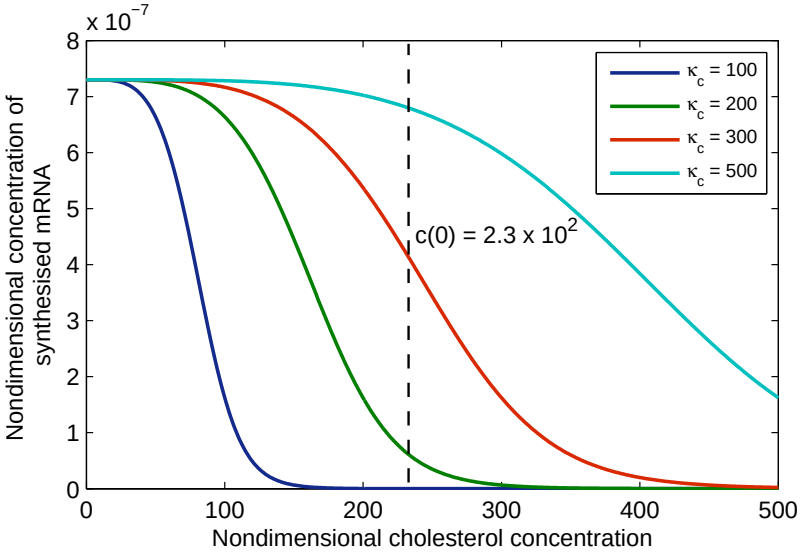

(b)

Fig. 5.14: The effect of increasing κ_c on the stable steady state system with $\kappa_{mh} = 1$ and $\delta_c = 1$. Figure 5.14(a) shows the response of mRNA. Figure 5.14(b)shows how the rate of mRNA synthesis is affected by cholesterol concentration and by varying values of κ_c. The line $c(0) = 230$ is the initial concentration of cholesterol used in the model simulations.

Increasing κ_c up to values of 1×10^{12} has no effect on the dynamical behaviour of the system. In this case the system always exhibits behaviour which tends to a stable steady state; only the final steady state values differ. However, increasing κ_c is interesting in that it shows the effect that the

switching response mechanism in the mRNA equation has on the system.

Figure 5.14(a) illustrates the initial behaviour of mRNA concentration as κ_c is changed. We can see that as κ_c increases the evolution of mRNA changes from an initial decrease followed by an increase, to an immediately increasing response. This can be explained by considering the synthesis term for mRNA given by

$$m_{h(\mathtt{synth})} = \frac{\mu_{mh}\ {\kappa_c}^{12}}{{\kappa_c}^{12} + \left(\kappa_{mh}\left({\kappa_c}^4 + c^4\right)\right)^3}, \tag{5.1}$$

which is plotted in Figure 5.14(b) for the values of κ_c corresponding to those in Figure 5.14(a). We can see that altering κ_c alters the position at which the initial concentration of cholesterol falls on the synthesis switch function.

The behaviour of mRNA responds to where on this switch cholesterol concentration falls. The further away from the maximal rate of synthesis at initial time, the greater the effect of mRNA degradation on mRNA concentration, resulting in the primary decrease seen for $\kappa_c = 100$ and $\kappa_c = 200$. Eventually cholesterol concentration falls low enough to increase the mRNA synthesis rate to greater than that of degradation, causing the secondary increase.

Having characterised the essential features of the three undetermined system parameters δ_c, κ_{mh}, and κ_c, we now wish to try and determine the regions of parameter space in which the differing types of dynamical behaviour occur.

This is problematic with three unknowns to investigate; therefore our approach has been to obtain two dimensional parameter space plots, and track how these plots alter as the third parameter is varied. Results of this are found in Figure 5.15.

In this figure, bounded regions in the (κ_{mh}, δ_c) parameter space are illustrated for steadily decreasing values of κ_c. Values of κ_{mh} and δ_c which fall within these regions will result in the system exhibiting periodic solutions (the oscillatory solution regions in Figure 5.15).

Values in the parameter space which fall outside of this region result in solutions which have

a stable steady state; this includes both monotonic and oscillatory convergence to the steady state. Distinguishing between the two types of stable solutions has not been possible; cases of monotonic and oscillatory convergence to steady state are distributed nonuniformly around the oscillatory regions. The results of Figure 5.15 show as κ_c decreases, the range of values for both

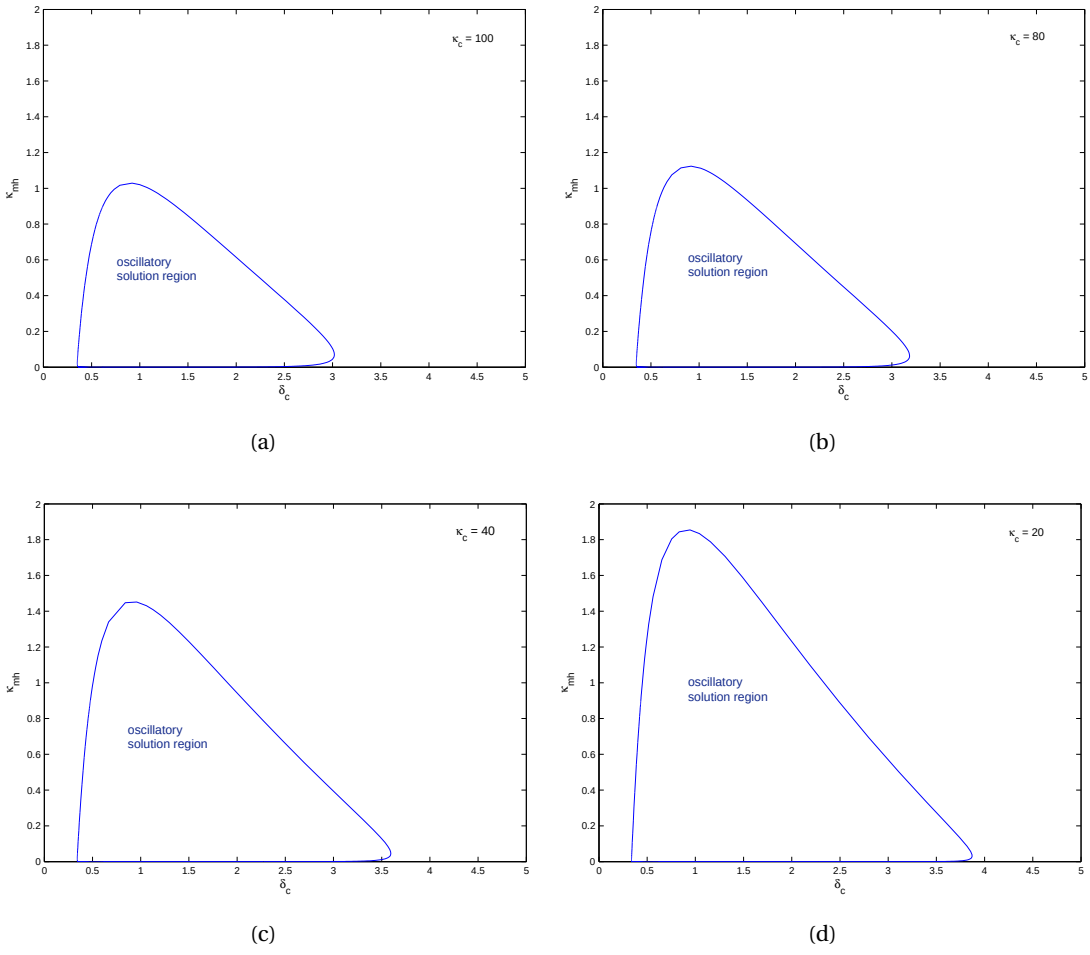

Fig. 5.15: Regions in the κ_{mh}, δ_c parameter space as κ_c is varied. Parameter values falling within the bounded region result in the system producing only periodic solutions (oscillatory solution region). Parameter values falling outside of the bounded region correspond to the system displaying stable behaviour, either tending directly to or exhibiting decaying oscillations to a stable steady state. Figure 5.15(a) : $\kappa_c = 100$; Figure 5.15(b) : $\kappa_c = 80$; Figure 5.15(c) : $\kappa_c = 40$; Figure 5.15(d) : $\kappa_c = 20$.

κ_{mh} and δ_c, in which periodic solutions exist, increases. This range is far greater for the response in κ_{mh} than for the response in δ_c.

Summary

In this chapter we have presented numerical solutions for the model of regulated cholesterol biosynthesis which was derived in Chapter 3. These solutions have confirmed the analytic conclusions which were formed in Chapter 4 regarding the appearance of and the stability of the Hopf bifurcation, together with the physical properties of the limit cycle generated by this bifurcation. In particular, the numerical simulations have allowed the exploration of and evaluation of system behaviour for parameters which were unable to be determined from experimental data.

In the final part of this thesis we integrate the model of cholesterol biosynthesis and its genetic regulation with an existing model of LDL uptake by hepatocytes. In doing so, we wish to investigate whether the inclusion of the genetic regulatory processes in the LDL uptake model captures important behaviour that may not be seen in the existing model, where the intracellular processes are simplified.

6

An Integrated Model of Liver Cell LDL Uptake and Genetic Regulation

Chapter 2 highlighted the lack of mathematical models describing LDL receptor mediated uptake with adequate description of the genetic processes occurring. In this chapter we will adapt an existing model of LDL RME developed by Wattis et al. (2008) to include these mechanisms. We extend this model by including ODEs, developed in Section 3.5.1, which describe the pathway of regulated cholesterol biosynthesis. We also apply the ideas of genetic regulation developed in Section 3.3 to the mechanism of LDLR synthesis. In doing so we will create an integrated model of LDL RME which describes the pathways occurring at both the cellular and subcellular level.

This chapter begins with a brief description of the Wattis et al. model following which we derive

the integrated model. Numerical solutions of the model are presented and discussed in the context of LDL uptake and intracellular cholesterol homeostasis.

6.1 The Wattis model of LDL receptor mediated uptake

In this section we provide a brief description of the model developed by Wattis et al. (2008). This model describes the process of hepatic LDLR mediated LDL uptake, as reviewed in Section 2.1.3, and is based on a system of nonlinear ODEs which describe the evolution of spatially averaged concentrations of LDL and cholesterol. The focus of the model is on the dynamics of LDL adhesion, internalization, and receptor regulation; the biological processes modelled are summarized in Figure 6.1. The model contains two quantities which describe the attachment of LDL

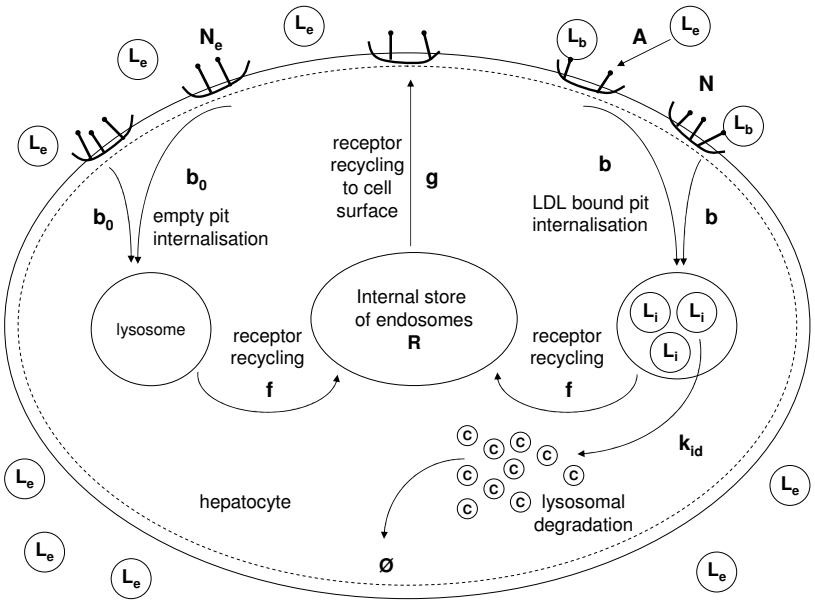

Fig. 6.1: Pictorial view of LDL endocytosis in a hepatocyte as modelled by Wattis et al. (2008). LDL binds to cell surface receptors clustered in coated pits, is internalised and subsequently degraded to release cholesterol. Receptors are either degraded or recycled to the cell surface. See text for variables and Table 6.1 for parameters.

particles to coated pits on the cell surface; coated pits containing bound LDL particles (N) and coated pits completely free of LDL particles (N_e). The model also explicitly accounts for LDL

particles in the extracellular medium (L_e), surface bound LDL particles (L_b), and internalised LDL particles (L_i), the intracellular cholesterol concentration, (C), and the number of pits per unit volume in the cell's internal store (R).

Quantitative validation of this model with the experimental results of Goldstein et al. (1979) is illustrated in Figure 2.9 of Chapter 2. The classical results of Goldstein et al. were obtained using *in vitro* assays, where an amount of lipoprotein containing radiolabelled LDL is added to cell culture medium following which the movement of radiolabelled LDL into the cell is tracked over time. However, as comparison with this experimental data is not the the purpose of our model, we focus on the reduced system given below, in which we consider the case of a single delivery of LDL to the system. This leads to the following equations

$$\begin{aligned}
\frac{d\bar{n}_e}{d\bar{t}} &= \bar{g}\bar{r} - \bar{A}p_m\bar{l}_e\bar{n}_e - \bar{b}_0\bar{n}_e, && \text{(6.1a)}\\
\frac{d\bar{n}}{d\bar{t}} &= \bar{A}p_m\bar{l}_e\bar{n}_e - \bar{b}\bar{n}, && \text{(6.1b)}\\
\frac{d\bar{r}}{d\bar{t}} &= \frac{\bar{k}_s}{\bar{K}+\bar{c}} + f\bar{b}\bar{n} + f\bar{b}_0\bar{n}_e - \bar{g}\bar{r}, && \text{(6.1c)}\\
\alpha\frac{d\bar{l}_e}{d\bar{t}} &= -\bar{A}\bar{l}_e\left(p_m\bar{n} + p_m\bar{n}_e - \bar{l}_b\right), && \text{(6.1d)}\\
\frac{d\bar{l}_b}{d\bar{t}} &= \bar{A}\bar{l}_e\left(p_m\bar{n} + p_m\bar{n}_e - \bar{l}_b\right) - \bar{b}\bar{l}_b, && \text{(6.1e)}\\
\frac{d\bar{l}_i}{d\bar{t}} &= \bar{b}\bar{l}_b - \bar{k}_{id}\bar{l}_i, && \text{(6.1f)}\\
\frac{d\bar{c}}{d\bar{t}} &= \eta\bar{k}_{id}\bar{l}_i - \bar{\delta}_c(\bar{c}-\bar{c}_e), && \text{(6.1g)}
\end{aligned}$$

with the initial conditions

$$\begin{aligned}
\bar{n}(0) &= \bar{n}_0\nu_p, \qquad \bar{n}_e(0) = \bar{n}_0 - \sum_{p=1}^{p_m}\bar{n}_0\nu_p \quad (1\le p\le p_m), \qquad \bar{r}(0)=0, && \text{(6.2)}\\
\bar{l}_e(0) &= \bar{l}_0, \qquad \bar{l}_b = \sum_{p=1}^{p_m} p\,\bar{n}_0\nu_p, \qquad \bar{l}_i(0)=0, \qquad \bar{c}(0)=\theta\bar{c}_e \quad (0<\theta<1),
\end{aligned}$$

where ν_p is the fraction of pits with p labelled LDL particles already bound at $t=0$ and θ is a fraction which describes the initial cholesterol concentration relative to the equilibrium cholesterol concentration c_e. The concentration of LDL particles present in the external medium is $\bar{l}_0$ while pits on the cell surface are present at the maximum level $\bar{n}_0$. Here, lowercase letters denote

concentrations of variables. Parameter values of the model are listed in Table 6.1.

We note that the first term of (6.1c) describes *de novo* synthesis of pits, regulated by the two constants $\bar{k}_s$ and $\bar{K}$. This gives a lower pit production rate when the cell's internal cholesterol level is high and a higher production rate when $\bar{c}$ is low. The values of k_s and K are chosen so that pit production is equal to 10% of its maximum value when $\bar{c} = \bar{c}_e$.

Parameter	Description	Value
p_m	Maximum number of receptors per pit	200
α	Volume ratio of extracellular to cellular media	1.50×10^4
$\bar{A}$	Rate of LDL binding to a receptor	6.64×10^{-17} ml molecules^{-1} s^{-1}
$\bar{g}$	Rate of release of pits from store	1.08×10^{-2} s^{-1}
$\bar{b}$	Rate of internalisation of LDL-bound pits	4.60×10^{-3} s^{-1}
$\bar{b}_0$	Rate of internalisation of empty pits	6.10×10^{-3} s^{-1}
$\bar{c}_e$	Intracellular cholesterol concentration	2.65×10^{19} molecules ml^{-1}
$\bar{K}$	Cholesterol regulation of pit production	2.94×10^{18} molecules ml^{-1}
$\bar{k}_s$	Rate of production of new pits	4.87×10^{27} molecules^2 ml^{-2} s^{-1}
$\bar{f}$	Fraction of internalised pits recycled	$[0.7, 1]$
$\bar{k}_{id}$	Rate of degradation of LDL to cholesterol	2.00×10^{-4} s^{-1}
$\bar{\eta}$	Number of cholesterol molecules per LDL	3.40×10^3
$\bar{\delta}_c$	Timescale of cholesterol regulation	3.30×10^{-3} s^{-1}
$\bar{n}_0$	Concentration of pits	1.81×10^{11} molecules ml^{-1}
$\bar{l}_0$	Initial concentration of extracellular LDL	1.17×10^{13} molecules ml^{-1}

Table 6.1: Dimensional parameter values of the reduced Wattis et al. (2008) model.

The results of simulations using the model described by system (6.1) are shown in Figure 6.2 for typical experimental initial conditions, in which the cell has been deprived of LDL, with θ taken to be 0.7. These initial conditions are defined in Table 6.2.

Variable	Description	Initial Condition
$\bar{n}(0)$	Concentration of bound LDL containing pits	0
$\bar{n}_e(0)$	Concentration of empty pits	1.81×10^{11} molecules ml^{-1}
$\bar{l}_e(0)$	Initial concentration of extracellular LDL	1.17×10^{13} molecules ml^{-1}
$\bar{l}_i(0)$	Initial concentration of internalised LDL	0
$\bar{l}_b(0)$	Initial concentration of bound LDL	0
$\bar{r}(0)$	Initial concentration of pits in the internal store	0
$\bar{c}(0)$	Initial concentration of intracellular cholesterol	1.17×10^{13} molecules ml^{-1}

Table 6.2: Initial conditions of the reduced Wattis et al. (2008) model.

In Figure 6.2 we see that at initial times, as extracellular LDL, l_e binds to receptors on the cell surface, the concentration of pits containing LDL, n increases rapidly. This is accompanied by a similarly rapid, opposing response in the concentration of empty pits, n_e, which decreases. We can see in the bottom right hand panel of Figure 6.2 that bound LDL, l_b, increases quickly and this is followed by an increase in internalised LDL, l_i. As pits on the cell surface become occupied with l_b, this slower response of l_i results in n overshooting its steady state value. The high initial concentration of l_e, corresponding to a large single dose of extracellular LDL, is the reason why very little change is seen in l_e.

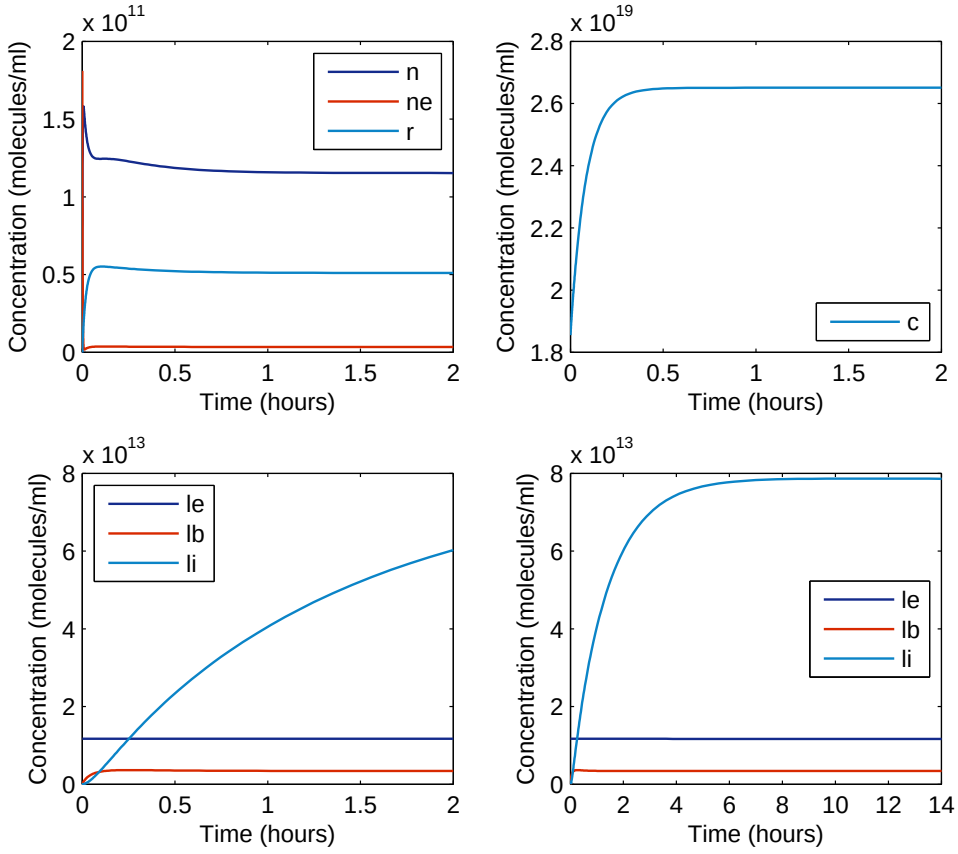

Fig. 6.2: Results of pit related, LDL related and cholesterol concentrations of the reduced (Wattis et al., 2008) RME model, system (6.1). Top left: concentrations of occupied, empty and internal pits ($\bar{n}, \bar{n}_e, \bar{r}$) over two hours; top right: concentration of intracellular cholesterol ($\bar{c}$) over two hours; bottom left: concentration of extracellular, bound and internalised LDL ($\bar{l}_e, \bar{l}_b, \bar{l}_i$), over two hours; bottom right: concentration of extracellular, bound and internalised LDL ($\bar{l}_e, \bar{l}_b, \bar{l}_i$), over fourteen hours.

The results of Figure 6.2 also illustrate that most of the system variables reach steady state in approximately two hours, however, internalised LDL, $\bar{l}_i$, takes significantly longer to equilibrate. The bottom right hand figure of Figure 6.2 demonstrates that l_i does not reach equilibrium until at least twelve hours later. This has been shown, in Wattis et al. (2008), to be due to the fact that the intracellular cholesterol level is predominantly determined by its rate of regulation, $\bar{\delta}_c$.

We also see that cholesterol concentration regains its equilibrium level within approximately half an hour of LDL entry to the cell. Biologically, as the cell has been deprived of cholesterol, *de novo* cholesterol synthesis will be at a maximal rate within the cell. As LDL cholesterol enters, the cell should move toward switching off the energy consuming biosynthesis reaction. This process is regulated at the genetic level, and experimental evidence suggests that the repression of HMGR synthesis via cessation of HMGR mRNA synthesis occurs on a timescale of approximately 24 hours (Molowa and Cimis, 1989). Further experimental evidence suggests that the LDL mediated suppression of cellular cholesterol synthesis can take from approximately 12 to well over 20 hours (Liscum and Faust, 1987; Liscum et al., 1989). Thus this rapid time to steady state for intracellular cholesterol concentration seems to be too fast.

In the next section we describe the extension of the LDL RME model presented here. The additional pathways will provide missing information on cholesterol biosynthesis and both the regulation of HMGR synthesis, as well as that of LDLR. It is hoped this will result in a model that is better able to model the experimental evidence regarding intracellular cholesterol concentration mentioned above. In doing so, the model will be able to provide a better description of the behaviour of intracellular cholesterol within the cell. Therefore, it will also allow the investigation of how the genetic pathways which control cellular processes influence the uptake of LDL, and the effect of these mechanisms on the long time behaviour of the model variables.

6.2 Model extension

Figure 6.3 summarises the biological mechanisms to be included in this integrated model and Figure 6.4 summarises the kinetic parameters of the integrated model. The equations describ-

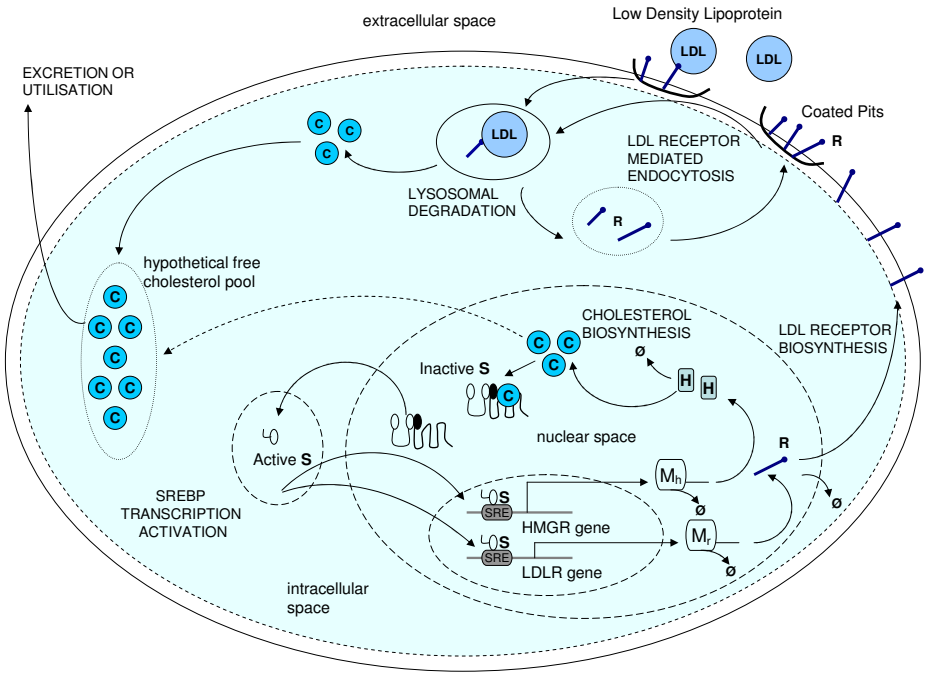

Fig. 6.3: Biological mechanisms of integrated cellular and subcellular LDL RME model. The model describes binding, internalisation and degradation of LDL, in conjunction with the genetic regulation of both LDLR and cholesterol biosynthesis via the HMGR pathway. Both genetic processes are controlled by negative feedback from the concentration of intracellular cholesterol.

ing cholesterol biosynthesis were previously derived in Chapter 3. To complete our model, we now derive the equations required to describe the synthesis of the LDLR protein. The reaction mechanism being considered is given by

$$\begin{array}{ccccc} \text{DNA} & \xrightarrow{\bar{\mu}_{mr}} & \bar{M}_r & \xrightarrow{\bar{\mu}_r} & \bar{R}, \\ \vdots & & \downarrow{\scriptstyle \bar{\delta}_{mr}} & & \downarrow{\scriptstyle \bar{\delta}_r} \\ \bar{S} & & \emptyset & & \emptyset \end{array} \tag{6.3}$$

where $\bar{S}$ is the transcription factor SREBP responsible for the regulation of LDLR mRNA transcription in the manner described in Chapter 3. LDLR mRNA ($\bar{M}_r$) is transcribed with rate $\bar{\mu}_{mr}$ and degraded with rate $\bar{\delta}_{mr}$. LDLR is translated with rate $\bar{\mu}_r$ and degraded at a rate $\bar{\delta}_h$.

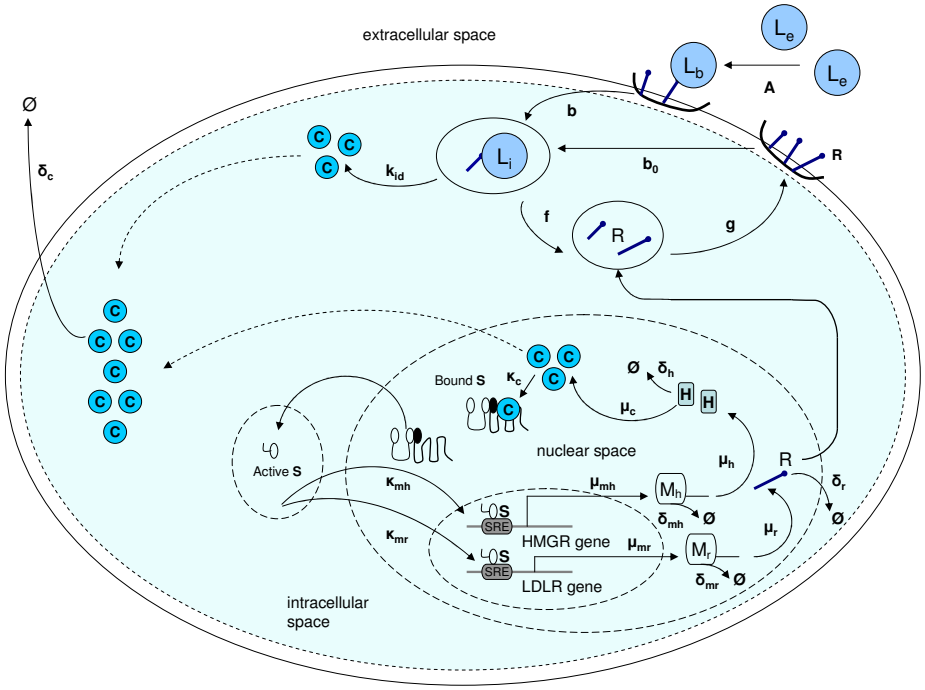

Fig. 6.4: Parameters of integrated cellular and subcellular LDL RME model.

Following the general derivation of Section 3.3, we can adapt the equations of system (3.47) to model the production of $\bar{M}_r$ and $\bar{R}$ as given in the mechanism (6.3). We obtain the following system of equations with $\bar{m}_r = [\bar{M}_r]$ and $\bar{r} = [\bar{R}]$,

$$\frac{d\bar{m}_r}{dt} = \bar{\mu}_{mr}\left(\frac{\bar{s}^w}{(\bar{\kappa}_{mr})^w + \bar{s}^w}\right) - \bar{\delta}_{mr}\bar{m}_h, \tag{6.4a}$$

$$\frac{d\bar{r}}{dt} = \bar{\mu}_r\bar{m}_r - \bar{\delta}_r\bar{r}, \tag{6.4b}$$

with initial conditions

$$\bar{m}_r(0) = \bar{m}_{r0}, \qquad \bar{r}(0) = \bar{r}_0, \tag{6.5}$$

where the parameter $\bar{\kappa}_{mr}$ reflects the binding efficiency between the transcription factor $\bar{s}$ and the HMGR gene promoter. Here, w is the number of binding sites for $\bar{s}$ on the LDLR gene. We use the information that in the case of the LDLR gene, there exists only one binding site for SREBP within its sterol regulatory element (Smith et al., 1990), and so $w = 1$. Furthermore, we know

from the underlying biology described in Section 3.4, that SREBP functions in the same manner for both the LDLR and HMGR gene. Hence we may apply the derivations of Section 3.5.1 to system (6.4), and arrive at the following system of equations describing regulated LDLR synthesis,

$$\frac{d\bar{m}_r}{dt} = \frac{\bar{\mu}_{mr}\left(\bar{s}_0\,\bar{\kappa}_c{}^4\right)}{\left(\bar{s}_0\,\bar{\kappa}_c{}^4\right)+\left(\bar{\kappa}_{mr}\left(\bar{\kappa}_c{}^4+\bar{c}^{\,4}\right)\right)} - \bar{\delta}_{mr}\bar{m}_r, \tag{6.6}$$

$$\frac{d\bar{r}}{dt} = \bar{\mu}_r\bar{m}_r - \bar{\delta}_r\bar{r}, \tag{6.7}$$

with the initial conditions

$$\bar{m}_r(0)=\bar{m}_{r0}, \qquad \bar{r}(0)=\bar{r}_0. \tag{6.8}$$

We are now in a position to derive the full integrated system, and note that extending the original model system (6.1) in this way will result in alterations to the equations describing both c and r.

The full integrated system is given by

$$\beta\frac{d\bar{m}_h}{dt} = \frac{\bar{\mu}_{mh}\left(\bar{s}_0\,\bar{\kappa}_c{}^4\right)^3}{\left(\bar{s}_0\,\bar{\kappa}_c{}^4\right)^3+\left(\bar{\kappa}_{mh}\left(\bar{\kappa}_c{}^4+\bar{c}^{\,4}\right)\right)^3} - \bar{\delta}_{mh}\bar{m}_h, \tag{6.9a}$$

$$\beta\frac{d\bar{m}_r}{dt} = \frac{\bar{\mu}_{mr}\left(\bar{s}_0\,\bar{\kappa}_c{}^4\right)}{\left(\bar{s}_0\,\bar{\kappa}_c{}^4\right)+\left(\bar{\kappa}_{mr}\left(\bar{\kappa}_c{}^4+\bar{c}^{\,4}\right)\right)} - \bar{\delta}_{mr}\bar{m}_r, \tag{6.9b}$$

$$\frac{d\bar{n}_e}{dt} = \bar{g}\bar{r} - \bar{A}p_m\bar{l}_e\bar{n}_e - \bar{b}_0\bar{n}_e, \tag{6.9c}$$

$$\frac{d\bar{n}}{dt} = \bar{A}p_m\bar{l}_e\bar{n}_e - \bar{b}\bar{n}, \tag{6.9d}$$

$$\frac{d\bar{r}}{dt} = \bar{\mu}_r\bar{m}_r + f\bar{b}\bar{n} + f\bar{b}_0\bar{n}_e - \bar{\delta}_r\bar{r} - \bar{g}\bar{r}, \tag{6.9e}$$

$$\alpha\frac{d\bar{l}_e}{dt} = -\bar{A}\bar{l}_e\left(p_m\bar{n}+p_m\bar{n}_e-\bar{l}_b\right), \tag{6.9f}$$

$$\frac{d\bar{l}_b}{dt} = \bar{A}\bar{l}_e\left(p_m\bar{n}+p_m\bar{n}_e-\bar{l}_b\right) - \bar{b}\bar{l}_b, \tag{6.9g}$$

$$\frac{d\bar{l}_i}{dt} = \bar{b}\bar{l}_b - \bar{k}_{id}\bar{l}_i, \tag{6.9h}$$

$$\frac{d\bar{h}}{dt} = \bar{\mu}_h\bar{m}_h - \bar{\delta}_h\bar{h}, \tag{6.9i}$$

$$\frac{d\bar{c}}{dt} = \bar{\mu}_c\bar{h} + \bar{\eta}\bar{k}_{id}\bar{l}_i - \bar{\delta}_c\bar{c}, \tag{6.9j}$$

with initial conditions

$$\begin{aligned}
\bar{n}(0) &= \bar{n}_0 v_p \quad (1 \le p \le p_m), \qquad \bar{n}_e(0) = \bar{n}_0 - \sum_{p=1}^{p_m} \bar{n}_0 v_p, \qquad \bar{r}(0) = 0, \qquad (6.10)\\
\bar{l}_e(0) &= \bar{l}_0, \qquad \bar{l}_b = \sum_{p=1}^{p_m} p\,\bar{n}_0 v_p, \qquad \bar{l}_i(0) = 0, \qquad \bar{c}(0) = \theta\,\bar{c}_0 \quad (0 < \theta < 1),\\
\bar{m}_h(0) &= \bar{m}_{h0}, \qquad \bar{m}_r(0) = \bar{m}_{r0}, \qquad \bar{h}(0) = \bar{h}_0.
\end{aligned}$$

In the system above the equations describing the evolution of HMGR mRNA, $\bar{M}_h$, and HMGR, $\bar{H}$, are those previously explained and derived in Chapter 3 given by equations (3.66a) and (3.66b).

We have also introduced the parameter β to describe the ratio of the nuclear to cytoplasmic volume of the cell. A commonly cited value for the volume of a cell nucleus is 10% of the total cell volume (Alberts et al., 2008), and so we take $\beta = 0.1$. The effect of this parameter will be investigated later in this chapter.

The new parameter values introduced are estimated from information in the literature and details of their calculations can be found in Appendix B.2. The initial conditions of system (6.9) are stated in Table 6.3. The parameter values of system (6.9) are stated in Table 6.4 and Table 6.5.

Variable	Description	Dimensional Value	Nondimensional Value
$\bar{n}_0$	Concentration of pits	1.81×10^{11} molecules ml^{-1}	2.20×10^{-6}
$\bar{l}_0$	Initial concentration of extracellular LDL	1.17×10^{13} molecules ml^{-1}	1.43×10^{-6}
$\bar{m}_{h0}$	Initial HMGR mRNA concentration	3.00×10^{10} molecules ml^{-1}	3.65×10^{-7}
$\bar{m}_{r0}$	Initial HMGR mRNA concentration	4.80×10^{10} molecules ml^{-1}	5.84×10^{-7}
$\bar{h}_0$	Initial HMGR concentration	9.04×10^{14} molecules ml^{-1}	1.10×10^{-2}
$\bar{c}_0$	Initial cholesterol concentration,	1.89×10^{19} molecules ml^{-1}	2.30×10^{2}

Table 6.3: Dimensional and nondimensional initial conditions of integrated LDL model.

We note that there are three parameters given as control parameters for the model, κ_c, δ_c, κ_{mh}. These are the parameter values that were the subject of the latter half of Chapter 5.

Using the information gained from the numerical analysis of Section 5.3 and Section 5.4, we will consider two cases for these parameters. The first case results in limit cycles in the regulated

Parameter	Description	Dimensional Value
p_m	Maximum number of receptors per pit	200
α	Volume ratio of extracellular to cellular media	1.5×10^4
β	Volume ratio of nuclear to cellular media	0.1
$\bar{f}$	Fraction of internalised pits recycled	$[0.7, 1]$
$\bar{\eta}$	Number of cholesterol molecules per LDL	3.4×10^3

Table 6.4: Dimensionless parameter values of the integrated LDL model.

Parameter	Description	Dimensional Value	Nondimensional Value
$\bar{A}$	Rate of LDL binding to a receptor	6.64×10^{-17} ml mol^{-1} s^{-1}	1.185×10^3
$\bar{g}$	Rate of release of pits from store	1.08×10^{-2} s^{-1}	2.34
$\bar{b}$	Rate of internalisation of LDL-bound pits	4.60×10^{-3} s^{-1}	1.00
$\bar{b}_0$	Rate of internalisation of empty pits	6.10×10^{-3} s^{-1}	1.32
$\bar{f}$	Fraction of internalised pits recycled	$[0.7, 1]$	$[0.7, 1]$
$\bar{k}_{id}$	Rate of degradation of LDL to cholesterol	2.00×10^{-4} s^{-1}	4.30×10^{-2}
$\bar{s}_0$	Total concentration of SREBP	8.21×10^{16} mol ml^{-1}	1.00
$\bar{\mu}_{mh}$	Rate of HMGR mRNA transcription	1.67×10^8 mol ml^{-1} s^{-1}	1.42×10^{-8}
$\bar{\mu}_{mr}$	Rate of LDLR mRNA transcription	4.56×10^6 mol ml^{-1} s^{-1}	1.21×10^{-8}
$\bar{\mu}_h$	Rate of HMGR translation	5.10×10^{-1} s^{-1}	1.11×10^2
$\bar{\mu}_r$	Rate of LDLR translation	5.10×10^{-1} s^{-1}	1.11×10^2
$\bar{\mu}_c$	Rate of cholesterol production (HMGR activity)	4.33×10^{-2} s^{-1}	9.41
$\bar{\delta}_{mh}$	Rate of HMGR mRNA degradation	4.48×10^{-5} s^{-1}	9.74×10^{-3}
$\bar{\delta}_{mr}$	Rate of LDLR mRNA degradation	1.75×10^{-4} s^{-1}	3.80×10^{-2}
$\bar{\delta}_h$	Rate of HMGR degradation	6.42×10^{-5} s^{-1}	1.40×10^{-2}
$\bar{\delta}_r$	Rate of LDLR degradation	1.34×10^{-5} s^{-1}	2.91×10^{-3}
$\bar{\kappa}_c$	Dissociation constant between cholesterol and SREBP	control parameter	control parameter
$\bar{\delta}_c$	Rate of cholesterol degradation	control parameter	control parameter
$\bar{\kappa}_{mh}$	Dissociation constant between SREBP and HMGR gene	control parameter	control parameter
$\bar{\kappa}_{mr}$	Dissociation constant between SREBP and LDLR gene	undetermined	undetermined

Table 6.5: Dimensional and nondimensional parameter values of the integrated LDL model. Here the unit mol represents molecules. Control parameters and undetermined parameters are discussed in the text.

cholesterol biosynthesis system, while the second nonoscillatory case causes stable behaviour.

We approximate the value of the remaining undetermined parameter, κ_{mr}, in a similar manner to the approximation of κ_c in Section 5.1. Thus we consider that $\bar{\kappa}_{mr}$ is representative of the concentration of $\bar{s}$ required for half of the genes to be active. Therefore as a starting point we set $\bar{\kappa}_{mr}$ to be $\mathcal{O}(\bar{s}_0)$.

6.2.1 Nondimensionalisation

All concentration variables are rescaled with respect to $\bar{s}_0$, the total concentration of SREBP transcription factor within the cell, and time is rescaled with respect to $\bar{b}$, the internalisation rate of LDL containing pits. Here τ is nondimensional time.

$$\begin{aligned} \tau &= \bar{b}t, \quad n_e = \frac{\bar{n}_e}{\bar{s}_0}, \quad n = \frac{\bar{n}}{\bar{s}_0}, \quad l_e = \frac{\bar{l}_e}{\bar{s}_0}, \\ l_b &= \frac{\bar{l}_b}{\bar{s}_0}, \quad l_i = \frac{\bar{l}_i}{\bar{s}_0}, \quad m_h = \frac{\bar{m}_h}{\bar{s}_0}, \quad m_r = \frac{\bar{m}_r}{\bar{s}_0}, \\ h &= \frac{\bar{h}}{\bar{s}_0}, \quad r = \frac{\bar{r}}{\bar{s}_0}, \quad \text{and} \quad c = \frac{\bar{c}}{\bar{s}_0}. \end{aligned} \tag{6.11}$$

This results in the following system of nondimensional equations

$$\beta \frac{dm_h}{d\tau} = \frac{\mu_{mh}\, {\kappa_c}^{12}}{{\kappa_c}^{12} + \left(\kappa_{mh}\left({\kappa_c}^4 + c^{\,4}\right)\right)^3} - \delta_{mh} m_h, \tag{6.12a}$$

$$\beta \frac{dm_r}{d\tau} = \frac{\mu_{mr}\, {\kappa_c}^4}{{\kappa_c}^4 + \left(\kappa_{mr}\left({\kappa_c}^4 + c^{\,4}\right)\right)} - \delta_{mr} m_r, \tag{6.12b}$$

$$\frac{dn_e}{d\tau} = gr - Ap_m l_e n_e - b_0 n_e, \tag{6.12c}$$

$$\frac{dn}{d\tau} = Ap_m l_e n_e - n, \tag{6.12d}$$

$$\frac{dr}{d\tau} = \mu_r m_r + fn + fb_0 n_e - \delta_r r - gr, \tag{6.12e}$$

$$\alpha \frac{dl_e}{d\tau} = -Al_e\left(p_m n + p_m n_e - l_b\right), \tag{6.12f}$$

$$\frac{dl_b}{d\tau} = Al_e\left(p_m n + p_m n_e - l_b\right) - l_b, \tag{6.12g}$$

$$\frac{dl_i}{d\tau} = l_b - k_{id} l_i, \tag{6.12h}$$

$$\frac{dh}{d\tau} = \mu_h m_h - \delta_h h, \tag{6.12i}$$

$$\frac{dc}{d\tau} = \mu_c h + \eta k_{id} l_i - \delta_c c, \tag{6.12j}$$

with the nondimensional initial conditions

$$n(0) = 0, \qquad r(0)=0, \qquad l_b(0)=0, \qquad l_i(0)=0, \tag{6.13}$$

$$l_e(0) = \frac{l_0}{s_0}, \qquad n_e(0)=\frac{n_0}{s_0}, \qquad c(0)=\frac{c_0}{s_0},$$

$$m_h(0) = \frac{m_{h0}}{s_0}, \qquad m_r(0)=\frac{m_{r0}}{s_0}, \qquad h(0)=\frac{h_0}{s_0},$$

making the assumption that $v_p = 0$, that is, all pits on the cell surface are free of LDL at $\tau = 0$.

This produces the new nondimensional parameters,

$$A = \frac{\bar{A}\ \bar{s}_0}{\bar{b}}, \qquad b_0=\frac{\bar{b}_0}{\bar{b}}, \qquad k_{id}=\frac{\bar{k}_{id}}{\bar{b}}, \qquad g=\frac{\bar{g}}{\bar{b}}, \tag{6.14}$$

$$\mu_r = \frac{\bar{\mu}_r}{\bar{b}}, \qquad \mu_h=\frac{\bar{\mu}_h}{\bar{b}}, \qquad \mu_c=\frac{\bar{\mu}_c}{\bar{b}}, \qquad \mu_{mh}=\frac{\bar{\mu}_{mh}}{\bar{s}_0\bar{b}},$$

$$\kappa_{mr} = \frac{\bar{\kappa}_{mr}}{\bar{s}_0}, \qquad \kappa_{mh}=\frac{\bar{\kappa}_{mh}}{\bar{s}_0}, \qquad \kappa_c=\frac{\bar{\kappa}_c}{\bar{s}_0}, \qquad \mu_{mr}=\frac{\bar{\mu}_{mr}}{\bar{s}_0\bar{b}},$$

$$\delta_c = \frac{\bar{\delta}_c}{\bar{b}}, \qquad \delta_h=\frac{\bar{\delta}_h}{\bar{b}}, \qquad \delta_r=\frac{\bar{\delta}_r}{\bar{b}}, \qquad \delta_{mr}=\frac{\bar{\delta}_{mr}}{\bar{b}}, \qquad \delta_{mh}=\frac{\bar{\delta}_{mh}}{\bar{b}},$$

which are described in Table 6.5. The nondimensional initial conditions are stated in Table 6.3. We now go on to consider numerical solutions of the system (6.12).

6.3 Integrated model results for the oscillatory case

In this section we investigate model solutions for the system (6.12), in which the control parameters, δ_c, κ_{mh} and κ_c, are known to cause oscillatory behaviour in the cholesterol biosynthesis model given by system (4.3); the parameter values used can be found in Table 6.6. The model was simulated using Matlab as described previously in Chapter 5.

δ_c	κ_{mr}	κ_{mh}	κ_c
9.74×10^{-3}	1	1	20

Table 6.6: Oscillatory case for the control parameter values.

We begin by simulating the model for a two hour period to examine the behaviour of the model at initial times. The results of this can be seen in Figure 6.5.

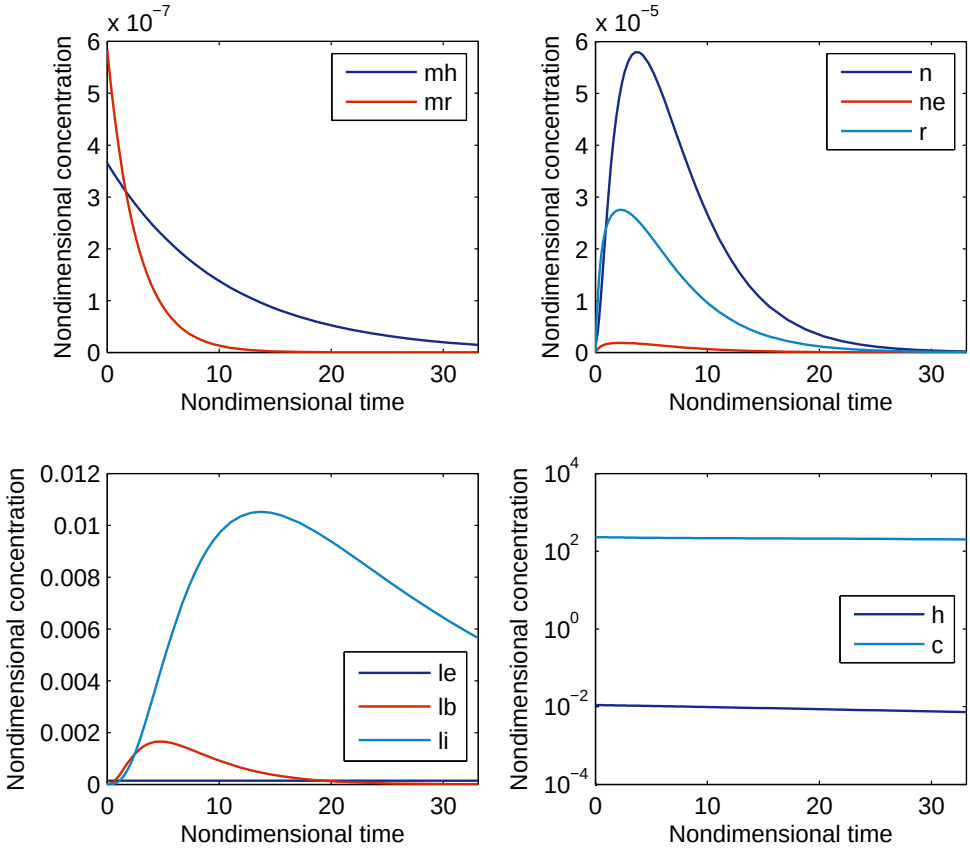

Fig. 6.5: Integrated model results for the oscillatory case over 2 hours. Top left: concentrations of HMGR and LDLR mRNA (m_h,m_r); top right: concentration of occupied, empty and internal pits (n, n_e, r); bottom left: concentrations of extracellular, bound and internalised LDL (l_e, l_b, l_i); bottom right: cholesterol and HMGR enzyme concentration (c, h).

We see that both the concentrations of HMGR mRNA and LDLR mRNA are initially decreasing. As can be seen in the bottom right hand figure, there is very little change in cholesterol concen-

tration, c, close to $\tau = 0$; thus here the degradation mechanism is dominating and both mRNA concentrations are declining. The binding of extracellular LDL, l_e to the receptors on the cell surface results in an increase in the concentration of bound LDL, l_b, which is accompanied by a large increase in the concentration of pits containing LDL, n. This increase in n is explained by the preceding increase in receptor synthesis driven by the nonzero initial concentration of LDLR mRNA. The increase in the concentration of l_b on the cell surface contributes to the large incoming concentration of l_i which can be seen in the bottom left hand figure. However, cholesterol concentration remains fairly constant following the increase in l_i. The contribution to intracellular cholesterol is offset by the decreasing concentration of HMGR, h, which reduces the contribution of cholesterol biosynthesis.

The subsequent decrease in l_i that is visible in Figure 6.5 follows a similar decrease in the concentration of n, which itself is a result of the decrease in r. Reduced receptor synthesis results in reduced cell surface receptor concentration leading to reduced LDL internalisation. The decrease in r is a direct consequence of the decreasing concentration of m_r, which is a direct result of the cholesterol concentration remaining fairly constant.

The results of Figure 6.5 also suggest that the concentrations of the receptor related variables, n, n_e, r, seem to tend towards a steady state of zero. This seems unlikely given that extracellular LDL has remained fairly constant, thus there is l_e available for uptake, and the declining levels of HMGR suggest that the cell will need to bolster its cholesterol concentration. To clarify the exact nature of the evolution of variables, we consider long time solutions where the system is simulated until all variables reach steady state as illustrated in Figure 6.6. This occurs on a dimensional timescale of approximately 60 hours or 2.5 days.

We see in the bottom right hand figure of Figure 6.6 that there is a continued decrease in h. Coupled with the drop in incoming LDL, cholesterol concentration begins to fall. Decreasing cholesterol concentration activates the feedback mechanism controlling the synthesis of m_r and synthesis is switched on. This upregulation in m_r concentration results in increased synthesis of r and hence an increase in cell surface receptors, n. This is accompanied by an increase in l_i which eventually settles to a steady state following the equilibration of r and n. What is clear from these results is that a corrective mechanism exists whereby the receptor variables exhibit

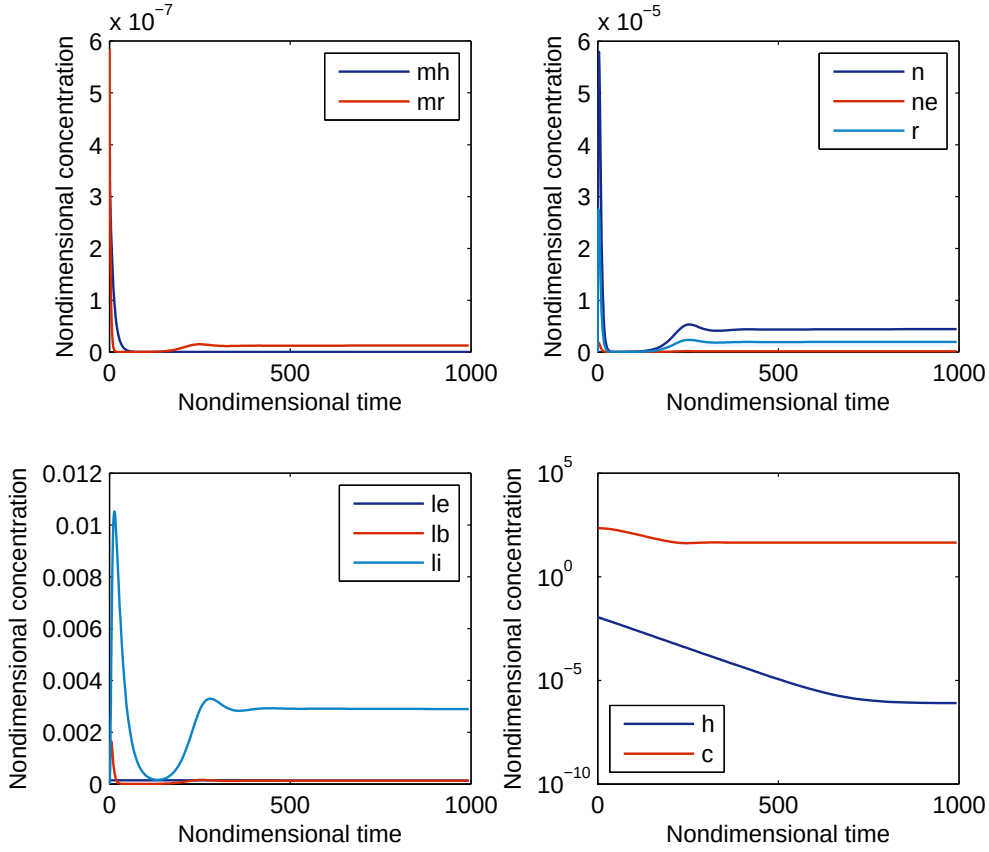

Fig. 6.6: Integrated model results for the oscillatory case run to steady state with a final time of approximately sixty hours. Top left: concentrations of HMGR and LDLR mRNA (m_h,m_r); top right: concentration of occupied, empty and internal pits (n, n_e, r); bottom left: concentrations of extracellular, bound and internalised LDL (l_e, l_b, l_i); bottom right: cholesterol and HMGR enzyme concentration (c, h).

over and undershooting behaviour before settling to steady state; this evolution is mirrored by l_i. This type of behaviour is common in systems controlled by negative feedback mechanisms where the cell is attempting to maintain certain concentrations, in this case c, within the cell, and has been discussed in Chapter 4.

We also note, in the top left hand figure of Figure 6.6 that there is no upregulation in the concentration of HMGR mRNA, m_h. To understand why, we consider the action of the transcription factor, s. The falling cholesterol concentration seen in the bottom right hand figure of Figure 6.6 results in a decrease in the concentration of s that is bound to c. There is a subsequent increase

in free or active s which is then available to enhance transcription. However, there is only one binding site on the LDLR gene that must be bound by s before LDLR mRNA transcription can be initiated, compared to three binding sites on the HMGR gene, and so m_r synthesis is activated first.

The availability of extracellular LDL ensures that the decline in cholesterol concentration is halted as a result of the increased internalisation of LDL. This increase in l_i is a direct consequence of increased receptor synthesis due to the activation of the genetic pathway which controls this process. As c is no longer decreasing, the increase in active s stops and so s does not reach a high enough concentration to bind the three binding sites on the HMGR gene, and HMGR mRNA transcription is not activated.

This suggests a cellular mechanism whereby, in order to supplement falling intracellular cholesterol levels, LDL uptake is activated rather than cholesterol biosynthesis. This result has biological significance, as cholesterol biosynthesis requires more energy than LDL uptake (Stryer et al., 2002), and preferential activation of the LDL uptake pathway relative to cholesterol biosynthesis could enable the cell to conserve energy stores.

6.3.1 Sensitivity analysis for the oscillatory case

In this section we present the results of local sensitivity analysis on the model system (6.12). Each parameter was varied whilst keeping all other constant at the values given in Table 6.6 and Table 6.5.

The results of the analyses using parameters pertaining to the LDL uptake pathway demonstrate that the model behaves in a similar manner to varying the same parameters in the reduced Wattis et al. model (system (6.12)). For example, reducing the rate at which LDL is degraded to cholesterol, that is decreasing the parameter k_{id} causes an initial decrease in cholesterol c. This is followed by an upregulation in most other system variables. Lower c feeds back to both HMGR mRNA and LDL mRNA and increases their synthesis. This results in upregulated receptor synthesis which increases the number of bound pits on the cell surface, and decreases the number

of empty pits leading to increased l_i. These processes are followed by an eventual increase in c.

The next set of results we present are the results of local sensitivity analyses on the parameters which define the genetic component of the model and will allow us to determine how this component exerts its control on the other cellular pathways. These parameters were chosen because they illustrate the differences in dynamic behaviour of the system which occur as a direct result of the new genetic processes that have been incorporated into the model, and therefore provide new insight.

The numerical results we show here are for the parameters κ_{mh}, κ_{mr}, and δ_c, which have been specifically chosen as they best represent the effect of the genetic regulatory pathways and illustrate interesting results. The other new parameters introduced behaved in an obvious manner. As an example, increasing the rate of synthesis of HMGR mRNA, μ_{mh}, had no significant effect on the dynamic behaviour of the system, but resulted in higher steady state values of model variables.

In the results that follow, we do not display the simulations for all model variables; those variables shown are chosen on the basis of how useful they are in explaining the effect of the parameter variations on the system's response. Thus variables for which no significant response was seen have not been presented. Where variables exhibited similar responses, one such variable was chosen as representative. All cases were simulated until they reached a steady state.

We begin by considering the effect of κ_{mh}, and find that increasing this parameter results in no, or no significant change to the behaviour of the system. The results for decreasing κ_{mh} can be seen in Figure 6.7, and they show that smaller values of this parameter confer greater sensitivity on the cell to cholesterol concentration (not illustrated as there is only a slight decrease in c for all decreases in κ_{mh}). The smallest value of κ_{mh} illustrated in Figure 6.7 causes a huge upregulation in HMGR mRNA, and consequently HMGR for a relatively small decrease in cholesterol concentration.

Here the low κ_{mh}, or low dissociation constant between s and the HMGR gene, implies that there is a high binding affinity between the two, and hence a small concentration of s is enough

to cause a response in HMGR mRNA. As a result of this l_i reaches a lower steady state value as κ_{mh} decreases; this is the response of the cell to the increased input to cholesterol from the biosynthesis reaction.

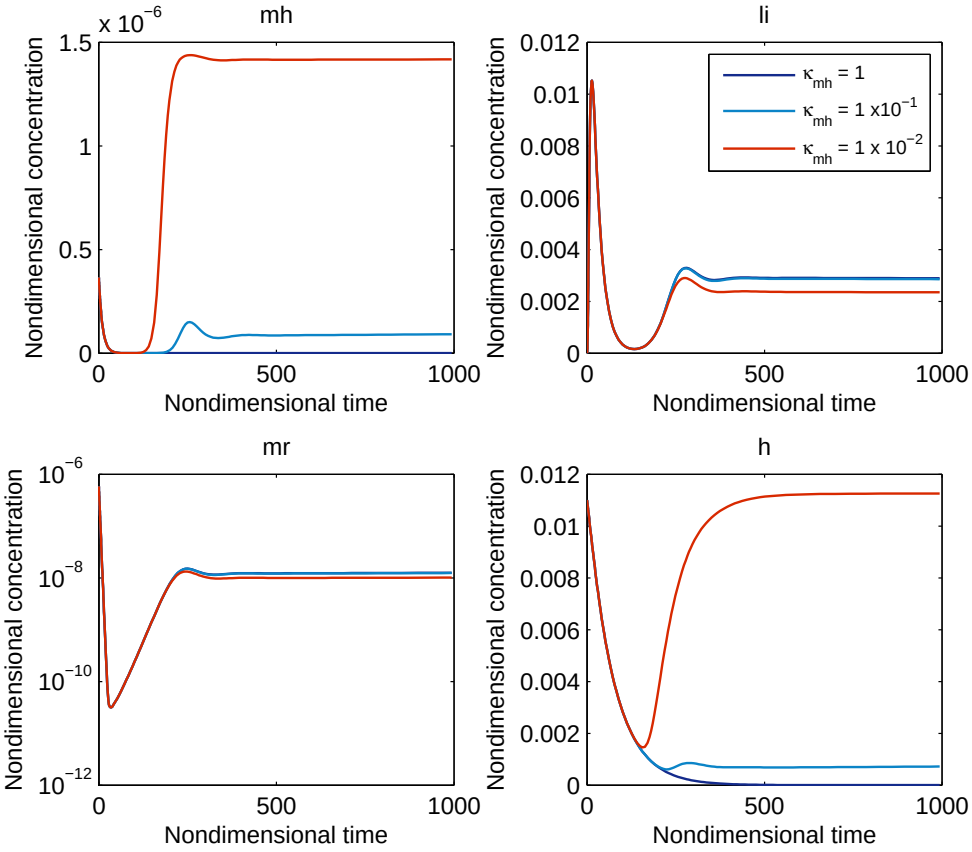

Fig. 6.7: Sensitivity of integrated model to decreasing κ_{mh} for oscillatory case. Top left: concentration of HMGR mRNA (m_h); top right: concentration of internalised LDL (l_i); bottom left: concentration of LDLR mRNA (m_r); bottom right: HMGR enzyme concentration (h).

The effect of increasing κ_{mr} is seen in Figure 6.8. Increasing κ_{mr} is equivalent to decreasing the binding affinity between s and the LDLR gene. Consequently receptor synthesis decreases, explaining the reduction in the concentration of LDL being internalised. This reduces the amount of cholesterol incoming to the cell, and as a consequence we see upregulation in both HMGR mRNA and HMGR.

Decreasing κ_{mr} results in the opposite behaviour; LDLR mRNA responds rapidly to declining cholesterol concentration, receptor synthesis and therefore, the concentration of LDL occupied cell surface receptors (n) increases, and so more LDL is internalised, as illustrated in Figure 6.9.

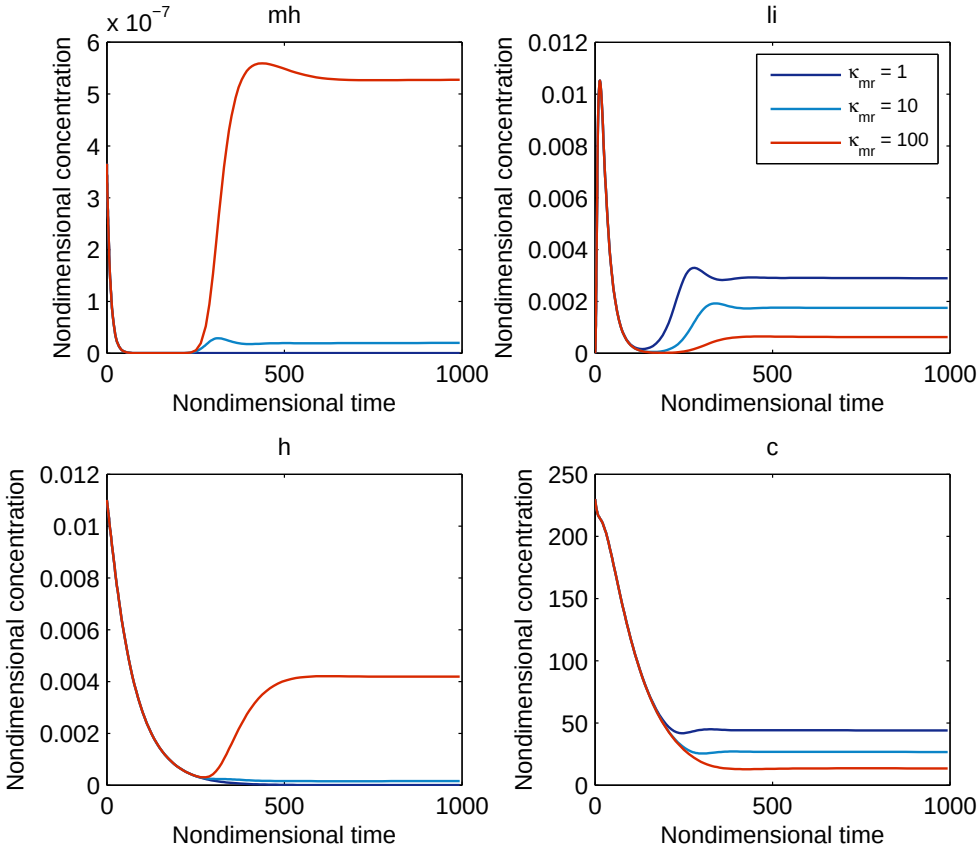

Fig. 6.8: Sensitivity of integrated model to increasing κ_{mr} for oscillatory case. Top left: concentration of HMGR mRNA (m_h); top right: concentration of internalised LDL (l_i); bottom left: HMGR enzyme concentration (h); bottom right: cholesterol concentration (c).

The final parameter we illustrate is δ_c. Interesting responses occur for increasing this parameter as can be seen in Figure 6.10. The overall behaviour of the variables is as would be expected as cholesterol is taken out of the system. As cholesterol concentration declines by greater amounts, both LDLR mRNA and HMGR mRNA are upregulated. As a consequence, much larger amounts of LDL are internalised.

However, we see that for the values of δ_c illustrated, there is a distinct region wherein variable

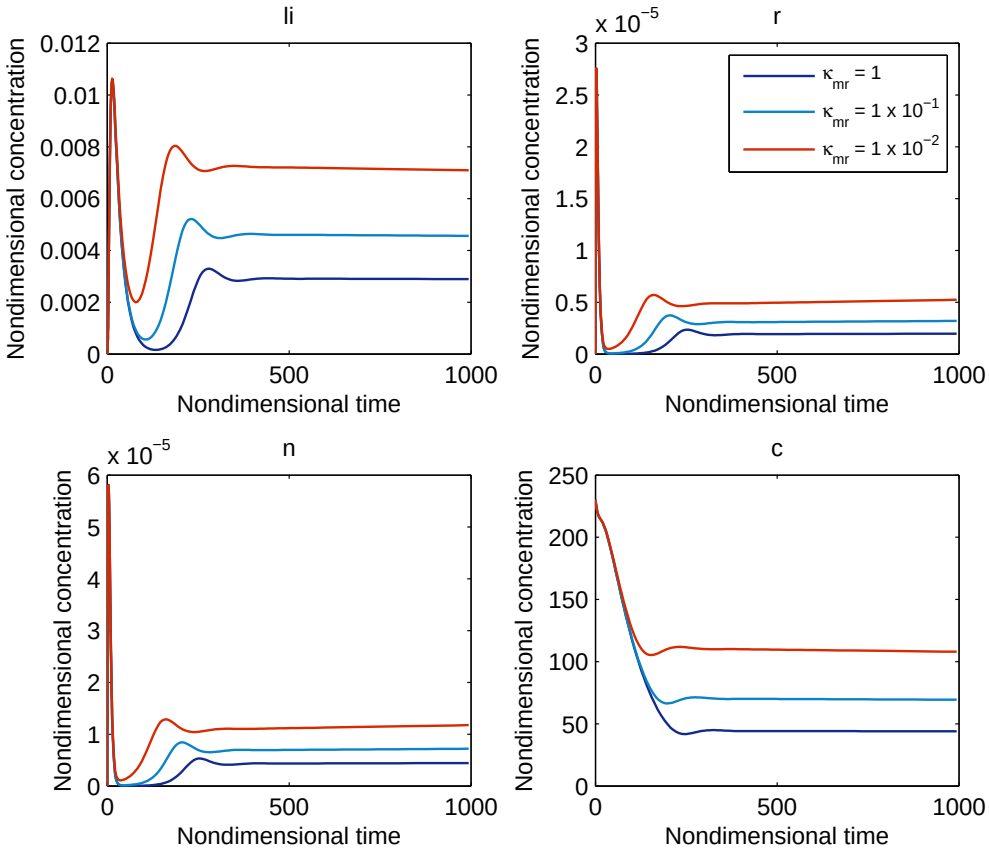

Fig. 6.9: Sensitivity of integrated model to decreasing κ_{mr} for oscillatory case. Top left: concentration of internalised LDL (l_i); top right: concentration of internal receptors (r); bottom left: concentration of occupied pits (n); bottom right: cholesterol concentration (c).

concentrations undergo damped oscillations whilst reaching a steady state, surrounded by regions where the variables tend monotonically to a steady state.

In this case, increasing the rate δ_c results in a rapid loss of cholesterol from the cell. This dramatic change in cholesterol concentration results in a rapid increase in the concentration of unbound transcription factor which immediately activates the feedback mechanism to mRNA concentrations. As seen in the top left hand figure of Figure 6.10, HMGR mRNA undergoes a fairly quick upregulation. The corresponding upregulation which occurs in LDLR mRNA concentration, results in similar increases in receptor concentrations and consequently, in the concentration of l_i as seen in the top right hand illustration in Figure 6.10.

The resulting contribution to the cellular cholesterol concentration results in opposing feedback to mRNA which is then downregulated causing corresponding decreases in the concentrations of their protein products and hence also for l_i. This eventually results in cholesterol concentration declining once again, and the system cycles in this manner resulting in damped oscillations until a steady state is reached as is visible in Figure 6.10.

Interestingly, no similar damped oscillations are seen in HMGR concentration, h. This may suggest that the estimated rate of translation μ_h is too small for the oscillatory behaviour in m_h to be conferred upon the evolution of h.

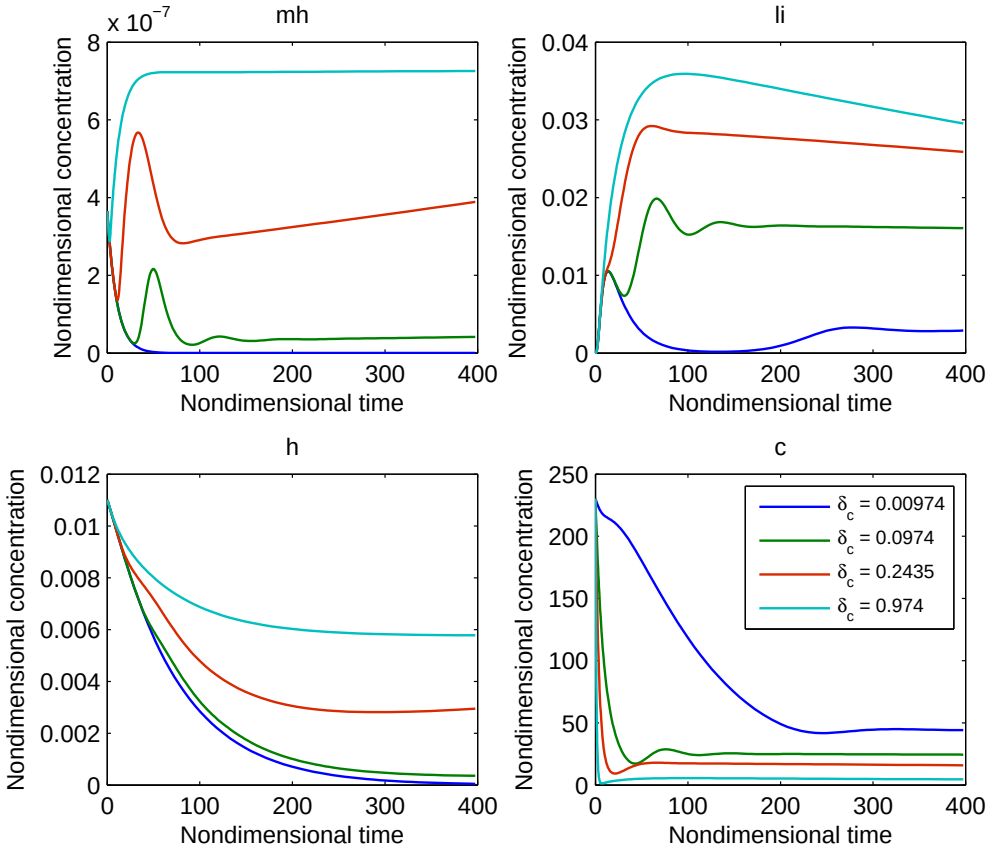

Fig. 6.10: Sensitivity of integrated model to increasing δ_c for oscillatory case. Top left: concentration of HMGR mRNA (m_h); top right: concentration of internalised LDL (l_i); bottom left: HMGR enzyme concentration (h); bottom right: cholesterol concentration (c).

6.4 Integrated model results for the nonoscillatory case

In this section we now go on to consider model solutions for the integrated model, in which the control parameters, δ_c, κ_{mh} and κ_c, do not cause oscillatory behaviour in the cholesterol biosynthesis model given by system (4.3); these parameter values can be found in Table 6.7. We

δ_c	κ_{mr}	κ_{mh}	κ_c
9.74×10^{-3}	1	1	100

Table 6.7: Nonoscillatory case for control parameter values.

simulate the model as before for a two hour period and until the system reaches a steady state. The results of this can be seen in Figure 6.11. We can see that the short time behaviour for the nonoscillatory case is qualitatively very similar to that of the oscillatory case. However, some subtle differences are present and we now discuss the reasons for these.

Essentially, the difference between the sets of parameter values for the two cases lies in the value of κ_c, the dissociation constant for the reaction between cholesterol and the transcription factor. In the nonoscillatory case, κ_c is greater. As discussed previously in Chapter 3, smaller values of κ_c confer greater sensitivity in the response of the transcription factor to the concentration of cholesterol.

Thus, while the cholesterol concentration, c, in the bottom right hand panels of Figure 6.11 and Figure 6.5 is qualitatively identical, in the oscillatory case transcription factor is more sensitive to c and hence exists in a larger bound or inactive concentration than in the nonoscillatory case (Figure 6.11).

This explains the difference in the LDLR mRNA concentrations seen in the top left hand panels of Figure 6.11 and Figure 6.5. In Figure 6.5 where $\kappa_c = 20$, m_r drops to zero, whereas in Figure 6.11 where $\kappa_c = 100$ and a higher concentration of active transcription factor is present, m_r plateaus at a nonzero value over the course of two hours.

Following the elucidation of the initial behaviour, the nonoscillatory system was simulated until a steady state was reached. These results are shown in Figure 6.12 where we can see that the

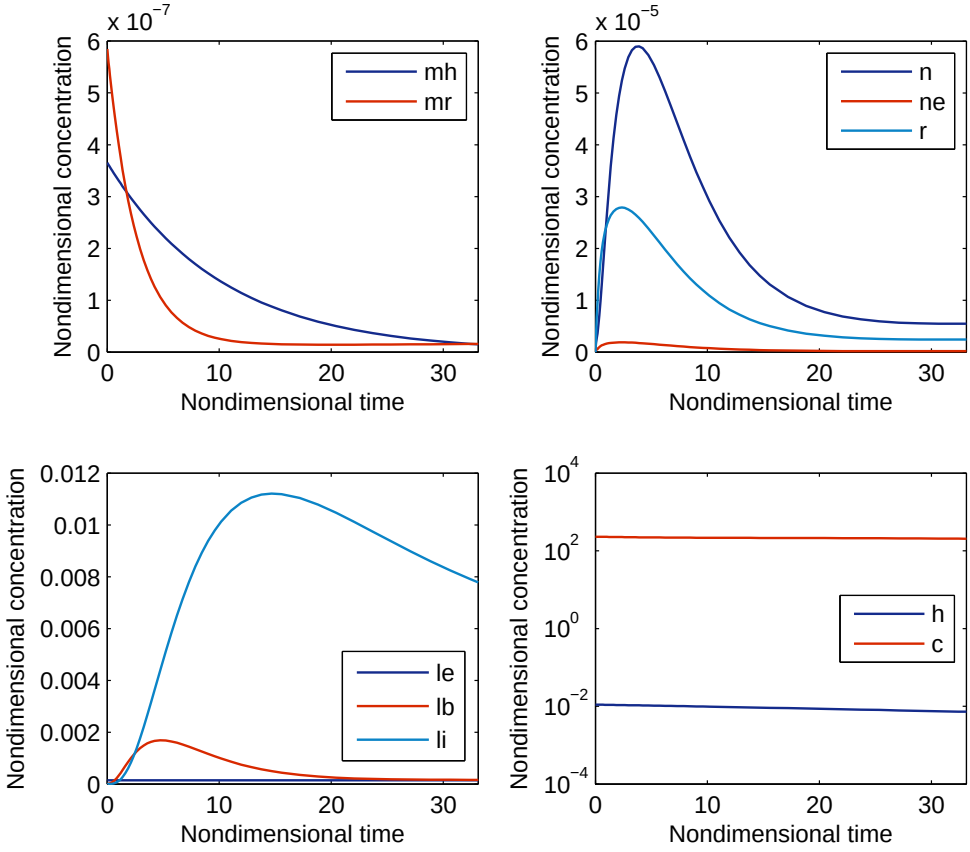

Fig. 6.11: Integrated model results for the nonoscillatory case over 2 hours. Top left: concentrations of HMGR and LDLR mRNA (m_h,m_r); top right: concentration of occupied, empty and internal pits (n, n_e, r); bottom left: concentrations of extracellular, bound and internalised LDL (l_e, l_b, l_i); bottom right: cholesterol and HMGR enzyme concentration (c, h).

system takes approximately forty days to reach a complete steady state. In this case the cell continues to respond to the extracellular LDL concentration, l_e until it is completely depleted. Following this, l_b, and after a short delay, l_i, also drop to zero, followed by a similar decrease in the number of pits containing bound LDL, n.

The net effect of this is a drop in the intracellular cholesterol concentration which is not supplemented by the presence of a steady concentration of h. This seems to suggest that the estimate of μ_c, the rate of cholesterol synthesis from h is too small.

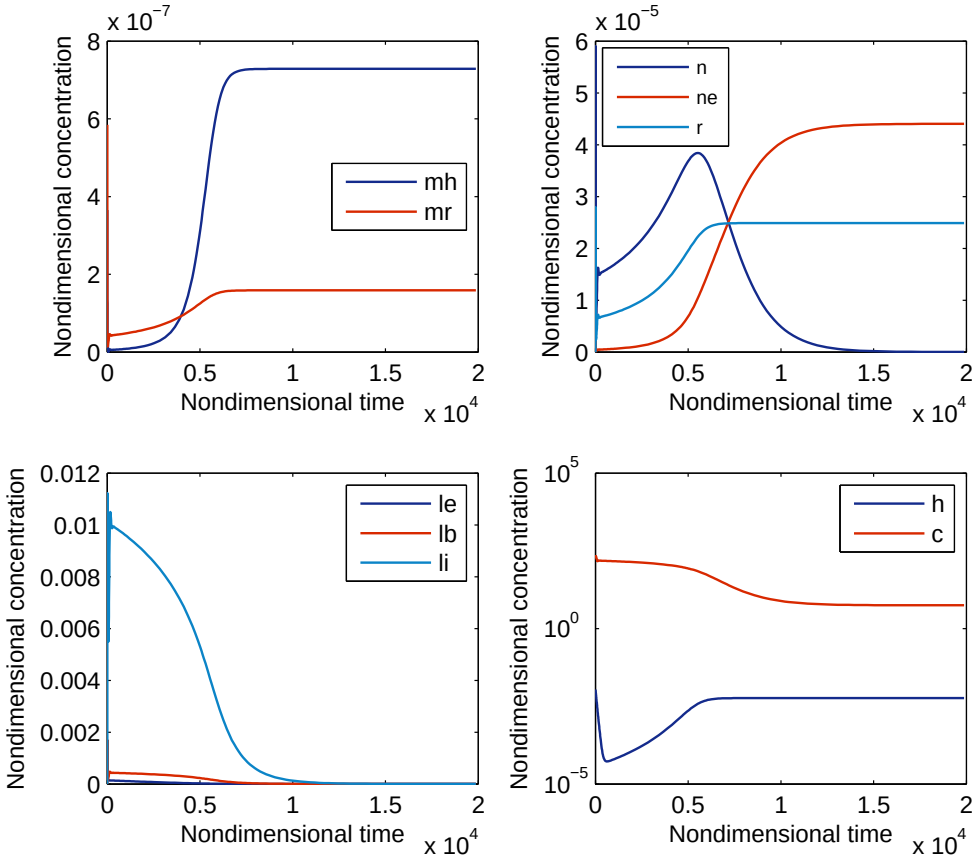

Fig. 6.12: Integrated model results for the nonoscillatory case run to steady state. Top left: concentrations of HMGR and LDLR mRNA (m_h,m_r); top right: concentration of occupied, empty and internal pits (n, n_e, r); bottom left: concentrations of extracellular, bound and internalised LDL (l_e, l_b, l_i); bottom right: cholesterol and HMGR enzyme concentration (c, h).

6.4.1 Sensitivity analysis for the nonoscillatory case

In this section we present the results of local sensitivity analysis on the nonoscillatory case. Reasons for the choice in both parameter values and variable responses illustrated are as given in Section 6.3.1. The effect of κ_c was explained previously when considering the difference between the results of the oscillatory and nonoscillatory cases.

We found no significant changes in response to alterations in κ_{mh}, which describes the dissociation constant between transcription factor and the HMGR gene, for any of the system variables.

As discussed above, in the nonoscillatory case, the larger value of κ_c implies that there is less sensitivity of the transcription factor to the concentration of cholesterol within the cell. This lower sensitivity results in the strength of κ_{mh} becoming redundant, and thus no significant change in behaviour is seen. Increasing κ_{mr} gave similar results as for the oscillatory case, but with higher final steady state values.

The effect of decreasing κ_{mr} for the nonoscillatory case is seen in Figure 6.13. Decreasing κ_{mr} is equivalent to increasing the binding affinity between s and the LDLR gene. Variables related to LDLR mRNA, m_r, thus become very sensitive to increases in cellular cholesterol. However, in this case, increases in cholesterol concentration result in a higher steady state value of LDLR mRNA. This results in a higher concentration of synthesised and cell surface receptors; consequently the cellular response to increasing cholesterol concentration is to increase LDL uptake. Hence, for the nonoscillatory case we can state that κ_{mr} must be ≥ 1, since we require a cellular response whereby LDL uptake is reduced for high intracellular concentrations.

We now consider the parameter δ_c for which results are illustrated in Figure 6.14. Again we see similar results as for the oscillatory case, with increased output of cellular cholesterol resulting in increased input from the LDL uptake pathway. However, the damped oscillations observed in the oscillatory case are no longer seen. This is explained by the lower sensitivity of transcription factor to intracellular cholesterol, caused by the larger value of κ_c. This results in lowered sensitivity of mRNA response; the overall slowing down of the regulatory process causes the damping behaviour to be much less pronounced.

6.4.2 The effect of nuclear size on the nonoscillatory system

In this section we investigate the effect of β on the system. β describes the change in volume that occurs between the nucleus and the cytoplasm. We vary this value from 0.1 through to 0.2. It is important to note that higher values of β do not have any physiological meaning, for example, $\beta = 0.5$ suggests that nuclear volume is half of total cell volume. The value of $\beta = 0.1$ is obtained from the estimate of nuclear volume being approximately 10% of the whole cell volume. Hepatic cells are known to exhibit the phenomenon of double nuclei, and hence $\beta = 0.2$

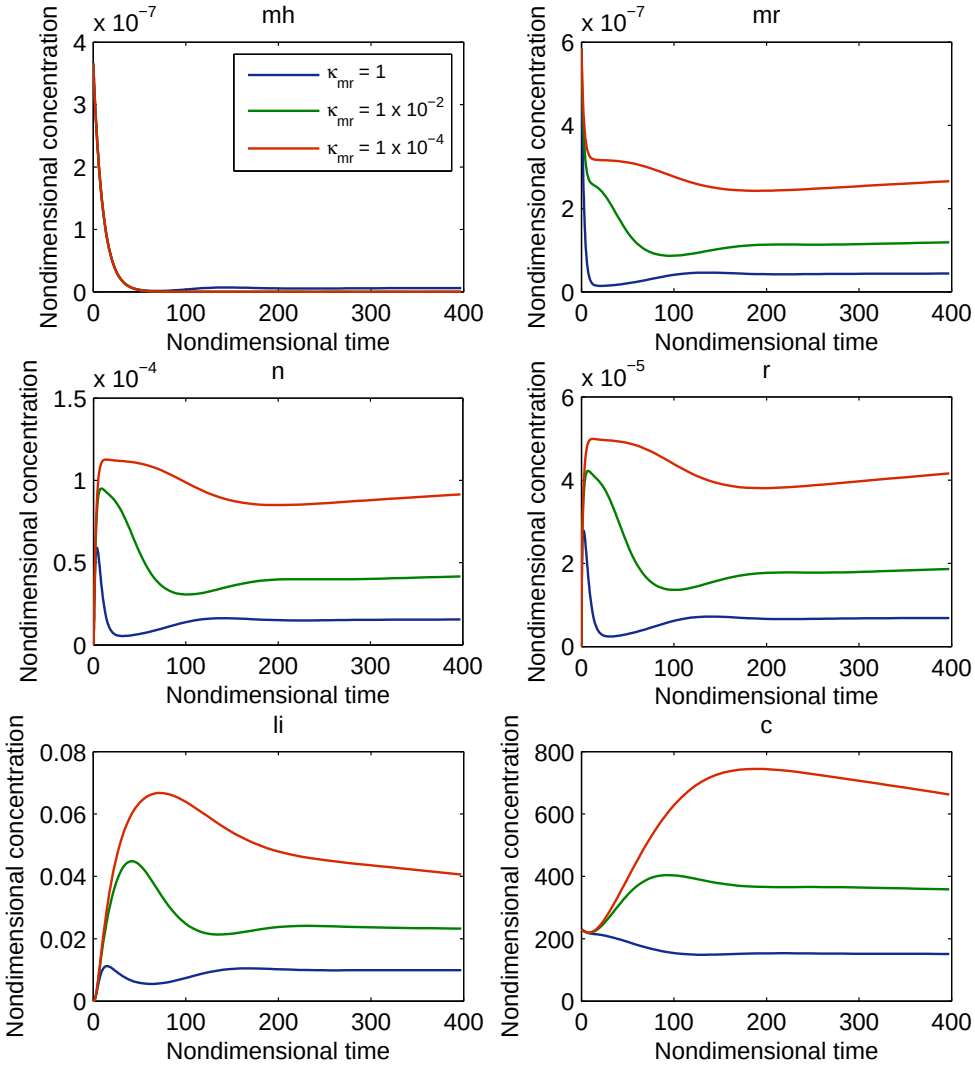

Fig. 6.13: Sensitivity of integrated model to decreasing κ_{mr} for nonoscillatory case. Top left: concentration of HMGR mRNA (m_h); top right: concentration of LDLR mRNA (m_r); centre left: concentration of occupied pits (n); centre right: concentration of internal receptors (r); bottom left: concentration of internalised LDL (l_i); bottom right: cholesterol concentration (c).

is also physiologically valid. Finally, we consider the case $\beta = 1$; this is equivalent to modelling the cell as one whole compartment, that is, we do not consider the nucleus as a separate region of the cell. The results of this sensitivity analysis can be seen in Figure 6.15. Results obtained for both cases were qualitatively similar; we present only the results of the nonoscillatory case.

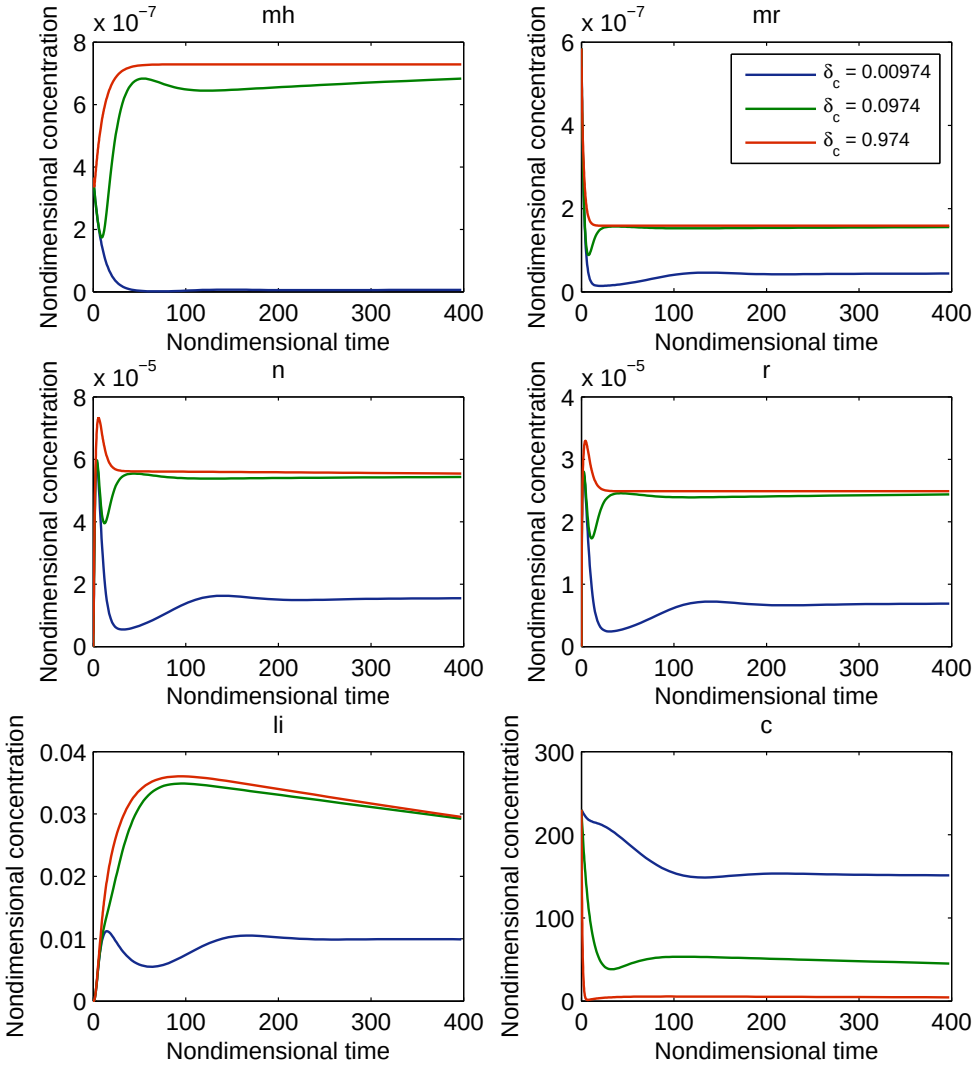

Fig. 6.14: Sensitivity of integrated model to δ_c for nonoscillatory case. Top left: concentration of HMGR mRNA (m_h); top right: concentration of HMGR enzyme (h); centre left: concentration of occupied pits (n); centre right: concentration of internal receptors (r); bottom left: concentration of internalised LDL (l_i); bottom right: cholesterol concentration (c).

It is clear that as β increases, the response in HMGR mRNA, m_h, becomes slower. Concurrently, the response in LDLR mRNA, m_r, begins to exhibit damped oscillations, which persist for longer as β increases. Corresponding damped oscillations are seen in r (top right in Figure 6.15; note the logarithmic scale on the y axis here to illustrate the changes better) and consequently in the

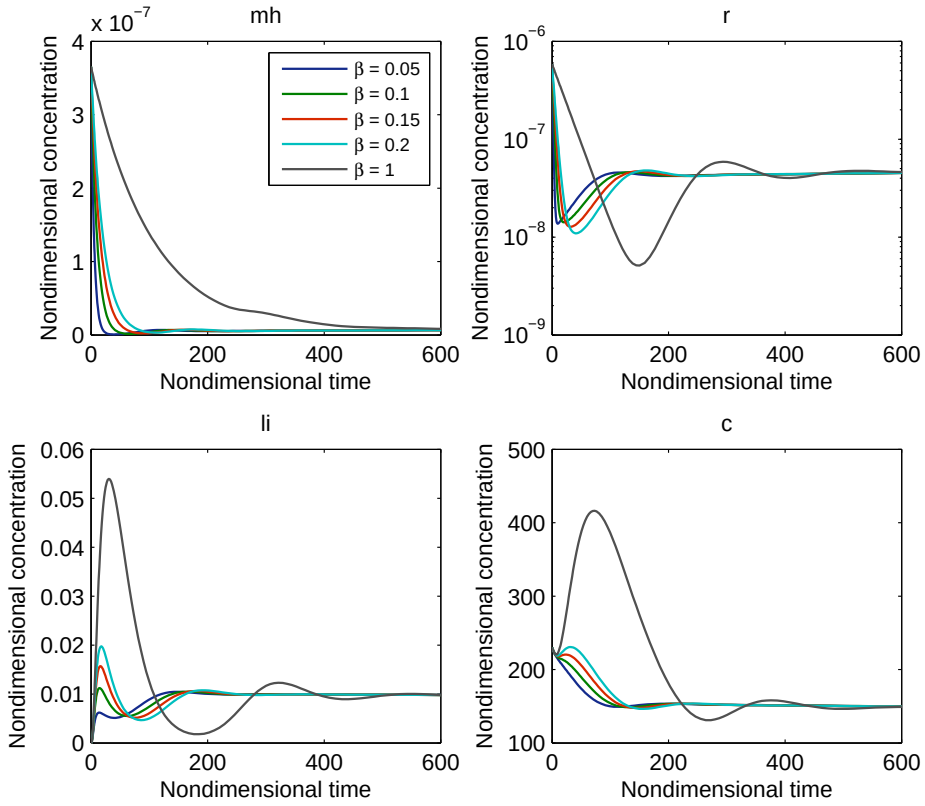

Fig. 6.15: Sensitivity of the nonoscillatory integrated model case to β over 24 hours. Top left: HMGR mRNA concentration (m_h); top right: concentration of internal receptors (r); bottom left: concentration of internalised LDL (l_i); bottom right: cholesterol concentration (c).

concentration of LDL internalised, l_i, by the cell (bottom left in Figure 6.15) which is propagated to cholesterol concentration (bottom right in Figure 6.15). We suggest a possible reason for this based on previous discussions within this chapter in which it was stated that the HMGR gene responds to cell cholesterol changes more slowly than LDLR, owing to the number of transcription factor binding sites. It may be possible that the even slower or *delayed* response in m_h for the case $\beta = 1$ drives the oscillatory convergence to steady state, as time delays are known to produce oscillatory behaviour (see Section 4.5).

We also compare the response of m_h for $\beta = 0.1$ and $\beta = 1$, with experimental data from the work of Molowa and Cimis (1989) to compare the qualitative behaviour of the time evolution of this variable, as seen in Figure 6.16. As is clear from this figure, it is the case $\beta = 1$ which gives

a better qualitative fit. Although the qualitative fit in this case is somewhat unsatisfactory, we note possible reasons for this. Firstly, the experimental results of Molowa and Cimis measure a particular type of mRNA (hybridisable mRNA) which is known to be more stable than 'ordinary' mRNA. Hence the gradient of mRNA decay in the experimental results may be slower than the actual rate of decay.

Secondly, comparison with experimental results suggest that the system as a whole is responding too rapidly. In fact, there are delays inherently present in the system which are unaccounted for by our ODE model. This is discussed further in Chapter 7. Finally, the experimental results indicate a basal expression of approximately 45% of control HMGR mRNA.

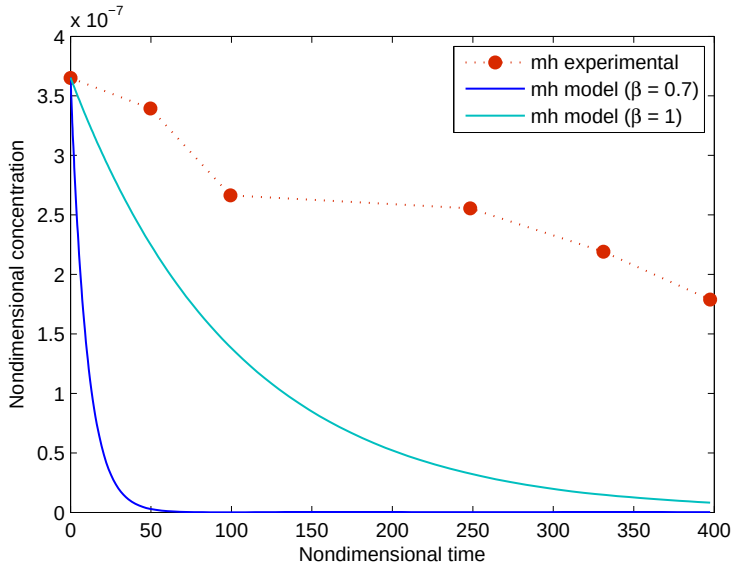

Fig. 6.16: Comparison of model results for m_h in the case $\beta = 0.1$ and $\beta = 1$ with experimental results of Molowa and Cimis (1989) describing the time course of HMGR mRNA repression.

Many genes have a nonzero minimal expression level, called the basal expression level. Thus for the HMGR gene, basal transcription describes HMGR mRNA transcription rate in the absence of transcription factor. Our model has not accounted for this; we have considered a system in which transcription factor *must* be present for the system reactions to function. To include this mechanism would involve adapting the regulated function which describes the synthesis of mRNA.

As an example, for HMGR mRNA, we have

$$m_{h(\texttt{synth})} = \mu_{mh0} + \frac{\mu^*_{mh}\,{\kappa_c}^{12}}{{\kappa_c}^{12} + \left(\kappa_{mh}\left({\kappa_c}^4 + c^{\,4}\right)\right)^3}, \tag{6.15}$$

where μ_{mh0} is the basal expression rate, and μ^*_{mh} is the expression rate which is modulated by transcription factor.

In this section and the previous one, we have illustrated the effect of adding genetic regulatory pathways to an existing model of LDL binding, uptake and internalisation developed by Wattis et al. (2008). The behaviour of the Wattis et al. model suggests that most variables reach steady state after two hours and, after approximately 12 hours, all variables are at steady state. The results presented here demonstrate that if the genetic regulation pathways which control LDL uptake are explicitly modelled, significantly different behaviour occurs.

The cellular response is that of a corrective mechanism, with key variables, for example both internal receptors, r, cell surface receptors, n, and internalised LDL, l_i exhibiting overshooting and undershooting behaviour before settling to steady state. Thus we suggest that the dynamic features of cellular cholesterol homeostasis, which is the governing mechanism behind all the processes being modelled, control long time cellular responses. In this long time cellular behaviour, model variables do not reach a steady state either rapidly or directly. Instead, evolution to steady state is slower and demonstrates adjustment to the cell's demands.

The results presented thus far raise the possibility that oversimplification of important subcellular processes can obscure dynamic behaviour of the cell. However, the conclusions we have made are based on qualitative results only. In order to validate our model, we are lacking in experimental data. This is due in part to the difficulty of conducting binding studies over long times, and also due to the difficulty in experimental measurement of genetic variables such as mRNA. Quantitative validation of the model requires further experimental work in these areas to generate the data needed. However, the qualitative conclusions we have made are both useful and interesting. In the next section, we extend these ideas to consider cellular response to disease states.

6.5 Parameters pertaining to familial hypercholesterolaemia

Thus far we have investigated the effect of parameters related to the genetic control mechanisms we introduced to the LDL uptake model in order to create the integrated model. In this section we will investigate the effect of certain parameters which correspond to the genetic causes of the disease familial hypercholesterolaemia (FH), characterised by increased total plasma cholesterol and plasma LDL cholesterol.

By altering specific model parameters we can quantitatively represent the effect of genetic mutations responsible for FH and demonstrate the reasons whereby this condition results in elevated plasma cholesterol. This is important for understanding the high incidence of CHD amongst FH sufferers. We can also use the integrated model to illustrate how current strategies for treatment of this disease are effective.

6.5.1 Familial hypercholesterolaemia

FH is a genetic disorder primarily attributable to a mutation in the gene for the LDL receptor and, as previously mentioned, is characterised by high levels of plasma LDL cholesterol. The gene for the LDLR is located on chromosome 19 and numerous mutations have been identified in the DNA of individuals affected with this disorder (Dammerman and Breslow, 1995). Five categories of functional LDLR defects (defects that result in a loss of LDLR function) resulting from LDLR gene mutations have been identified (Hobbs et al., 1990); these classes are summarised in Table 6.8. The third column of Table 6.8 highlights which model parameter is directly affected by the mutation (see Figure 6.4 for reference).

The only LDLR defect our system is not able to model is the Class II mutation as our ODE model does not compartmentalise the cell into subcellular organelles other than the nucleus. Therefore we do not take into account transport processes between these structures.

Defective LDLR classes can also be categorised more simply as **receptor-negative** in which either

Class	Description	Parameter
I (Receptor Negative)	LDLR not synthesised.	μ_{mr}
II (Receptor Defective)	LDLR not transported to the Golgi apparatus.	
III (Receptor Defective)	LDLR does not bind properly to LDL particles.	A
IV (Receptor Defective)	Bound surface receptors are not properly internalised.	b
V (Receptor Defective)	Receptors do not recycle properly.	f

Table 6.8: LDLR mutation classes.

no protein is produced or the protein that is produced has little or no function, and **receptor-defective**, in which a mutant protein that retains some residual receptor function is produced.

The clinical phenotype is more severe for homozygotes (those FH individuals who have inherited two defective LDLR genes) than for heterozygotes (those with only one mutated gene); the former group frequently suffer fatal CHD by their third decade of life unless treated. The rarity of homozygotes means the more frequent heterozygous condition has the greater impact on public health (Austin et al., 2004).

Traditionally, models simulating FH do not distinguish between mutation classes, however, the processes included in our model will allow us to investigate the difference between some of the mutations resulting in FH. We present here results to illustrate the effects of two classes of LDLR mutations. These classes have been chosen on the basis that one mutation affects a parameter related to the genetic processes; the other mutation affects a parameter related to the LDL RME process.

6.5.2 Class I familial hypercholesterolaemia

We first consider the Class I case where receptors are not synthesised, for a heterozygous individual. In this case, we begin by varying the rate of LDLR transcription, μ_{mr}, and investigate whether the model responds correctly. The results are illustrated in Figure 6.17.

As expected, if no receptors are synthesised at all, ($\mu_{mr} = 0$) the concentration of m_r in the system drops to zero. This results in no LDL being internalised; biologically this will result in a build up of LDL levels in the plasma. The resulting decline in intracellular cholesterol levels

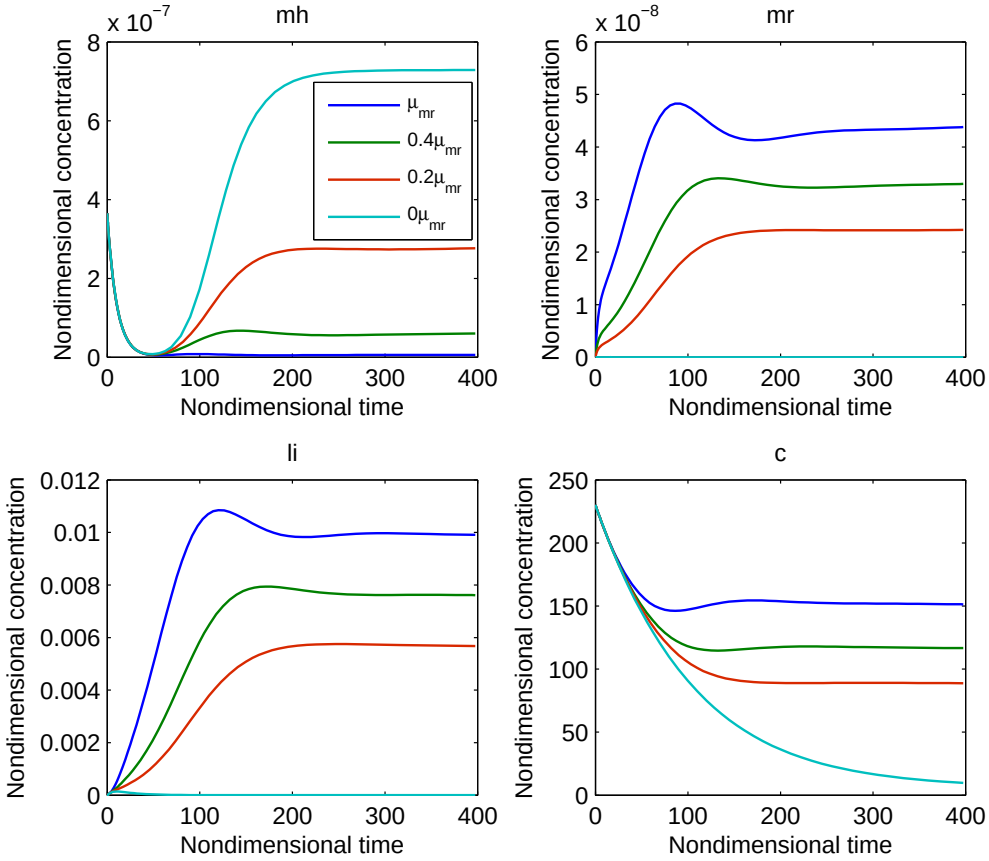

Fig. 6.17: Response of the integrated model to μ_{mr} (Class I FH) over 24 hours. Top left: HMGR mRNA concentration (m_h); top right: LDLR mRNA concentration (m_r); bottom left: concentration of internalised LDL (l_i); bottom right: cholesterol concentration (c).

results in a large upregulation of HMGR mRNA. Simulations over a longer time illustrate that this upregulation increases the concentration of HMGR within the cell, and this is followed by an increase in cholesterol.

Successively increasing μ_{mr}, the rate of receptor synthesis, results in successively increasing levels of LDLR mRNA, m_r, and the concentration of LDL internalised, l_i, increases accordingly. Using the model parameters we have estimated, the results suggest that a 10 fold reduction in the rate of transcription μ_{mr} can lead to a three fold reduction in the concentration of internalised LDL. This corresponds biologically to increased uptake from the plasma, and hence lower LDL plasma cholesterol levels.

6.5.3 Class V familial hypercholesterolaemia

The Class V mutation can be investigated by varying the recycling parameter, f, and the results of this simulation are shown in Figure 6.18.

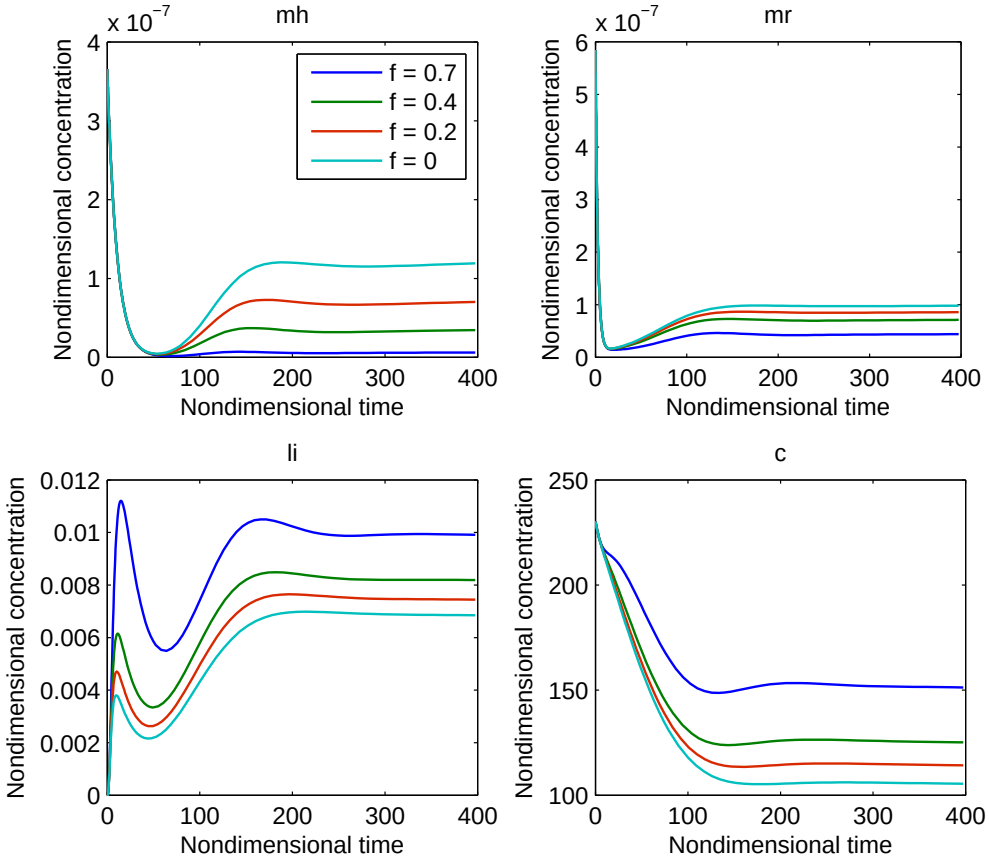

Fig. 6.18: Response of the integrated model to f (Class V FH) over 24 hours. Top left: HMGR mRNA concentration (m_h); top right: LDLR mRNA concentration (m_r); bottom left: concentration of internalised LDL (l_i); bottom right: cholesterol concentration (c).

These results illustrate that as the amount of receptors recycled decreases, the concentration of internalised LDL also decreases, as there are now fewer receptors on the cell surface available for LDL to bind. This reduces the concentration of cholesterol within the cell, and as a consequence both LDLR mRNA and HMGR mRNA are upregulated. From Figure 6.18 we see that when no receptors are recycled, the concentration of internalised LDL drops by 30%. This is a much less

significant drop compared to that seen for a reduction in receptor synthesis.

Comparison with the results of Figure 6.17 demonstrates that the effect of the Class I mutation is much more damaging than the effect of the Class V mutation. Even in the case where no receptors are being recycled ($f = 0$), LDLR mRNA is still being synthesised. Therefore the option of LDL uptake is still available to the cell, in direct contrast with the case where $\mu_{mr} = 0$. The model results therefore confirm the physiological finding that the receptor negative defect causes more severe effects, in terms of LDL uptake and corresponding plasma cholesterol levels, than receptor defective mutations.

Having used the results presented thus far to verify that the model reproduces appropriate biological behaviour, we use the Class V defect to provide insight into the action of two most commonly used treatments for high plasma cholesterol levels. These therapies and how their effects may be simulated with the model are summarised below.

- **Bile acid sequestrants**

  The liver is the major site for bile acid synthesis. This is the only pathway for cholesterol excretion from the body. However, a significant proportion of these bile acids are returned to the liver, via the intestine, in a process termed the enterohepatic cycle. Bile acid sequestrants bind bile acids in the intestine, removing them from the enterohepatic circulation via faecal elimination. The resulting loss of cholesterol from the liver cell stimulates the upregulation of LDLR synthesis and increases uptake from the plasma. We simulate this effect by increasing δ_c.

- **Statins**

  Statins (or HMGR inhibitors) are a class of drug used to lower cholesterol levels by inhibiting the HMGR enzyme. Statins act by competitively inhibiting HMGR. Because statins have a similar molecular structure to HMG-CoA (the substrate for the HMGR enzyme reaction) they take the place of HMG-CoA in the enzyme and reduce the rate by which it is able to produce mevalonate, the next molecule in the cascade that eventually produces cholesterol (see Section 2.2.1). Thus cholesterol synthesis is reduced. When the cell can no longer produce cholesterol, negative feedback from falling intracellular cholesterol levels

results in an upregulation of LDLR synthesis, increasing LDL uptake from the plasma. We simulate this effect by setting $\mu_c = 0$.

The results of Figure 6.19 demonstrates the action of bile acid sequestrants, where we have shown only the response in internalised LDL, l_i as it is the best indicator of LDL uptake from the plasma. The blue lines in Figure 6.19 correspond to the parameter values of Table 6.5 and Table 6.7 in the case where $f = 0$ (dark blue line) and $f = 0.7$ (light blue line). The red line corresponds to the response of the system to a two and a half fold increase in δ_c for the case $f = 0$ in which no receptors are recycled.

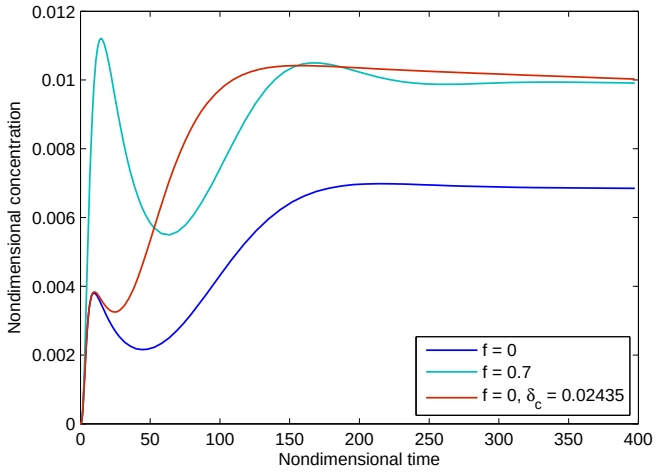

Fig. 6.19: Internalised LDL response from the integrated model to f and changes in δ_c as an illustration of the effect of bile acid sequestrant treatment.

As we can see, this increase in δ_c approximately restores internalised LDL to levels corresponding to the normal working of the receptor recycling pathway.

We now repeat this simulation, this time setting $\mu_c = 0$. We see in Figure 6.20 that this has very little effect on internalised LDL. This is, however, an incorrect response since we know from experimental data that this is one of the most effective methods of reducing plasma cholesterol levels. This may suggest that the rate of μ_c estimated for the purposes of our model is inaccurate.

In fact, the *in vitro* estimates used may not be reliable. Enzyme concentration is usually the most significant difference between routine *in vitro* assays and *in vivo* conditions, as it is well

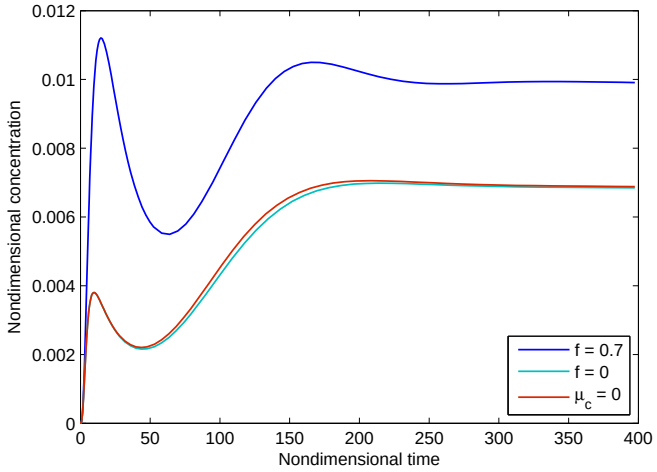

Fig. 6.20: Internalised LDL response from the integrated model to f and inhibition of μ_c as an illustration of the effect of statin treatment.

known that many intracellular enzymes are present *in vivo* at much higher concentrations than used *in vitro*. Another reason for the possible inaccuracy of *in vitro* data is the disruption of organelles and compartments in which the *in vivo* enzyme resides, which may lead to the release of activators or inhibitors that can artificially affect enzymatic activity.

To examine whether this was the case, the simulation of Figure 6.20 was repeated, this time setting the initial value of μ_c to be one hundred fold bigger than its estimated value as given in Table 6.5. Results are presented in Figure 6.21, where the upregulatory effect on internalised LDL on setting $\mu_c = 0$ can now be seen clearly (green line).

Summary

In this chapter we have used a model of genetic regulation that was derived in Chapter 3 and incorporated this into an existing model of LDL receptor mediated uptake developed by Wattis et al. (2008). This has created an integrated model of both the cellular and subcellular processes responsible for LDL RME and its regulation which is governed by cholesterol homeostasis. We have shown in this chapter, that for short times the model can reproduce the results of a reduced form of the Wattis et al. model. However, for long times the integrated model displays signifi-

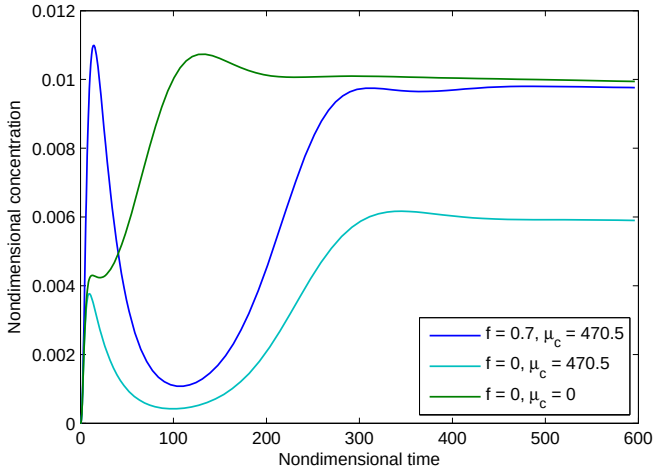

Fig. 6.21: Internalised LDL response from the integrated model to f and changes in μ_c as an illustration of the effect of statin treatment. In this simulation the initial value of μ_c was set at a larger level than for previous simulations.

cantly different behaviour. This behaviour illustrates the existence of a corrective mechanism which adjusts the long time concentration of internalised LDL in order to maintain the cellular cholesterol concentration.

Model simulations have been shown to accurately reproduce qualitative behaviour of genetic mutations causing FH, and the action of therapeutic strategies used in the treatment of this condition.

7

Discussion

The primary achievement of this work has been the development and investigation of an ODE model of gene expression regulation by a two step mechanism of end product repression mediated by a transcription factor.

Integration of this model with an existing model of the mechanism of hepatic LDL uptake has illustrated the importance of including subcellular pathways when modelling processes occurring at the cellular level.

In this chapter we summarise the findings of the work carried out in this thesis and suggest areas for further work both in terms of mathematical modelling and biological experiment.

7.1 Summary

The impact of CHD and the broader spectrum of CVD has been described by the World Health Organisation as a global epidemic. Of the many modifiable risk factors which can lead to the development and enhance the progression of CHD, high plasma cholesterol levels have long been recognised as one of the more significant causes. Understanding the reason for elevated levels of plasma cholesterol is crucial to developing strategies for its treatment.

In Chapter 2 the biological processes involved in the development of CHD were discussed, and the correlation between risk of development of this disease and plasma cholesterol levels was highlighted. In this chapter, we introduced the function of lipoproteins as the carriers of cholesterol within the plasma and outlined the pathways by which lipoproteins are metabolised. Central to this metabolic pathway is lipoprotein uptake by the liver; it is this clearance which controls plasma cholesterol levels.

Mathematical models have been widely used in an attempt to clarify the specific mechanisms of this process. Our review of the mathematical literature indicated that while processes occurring at the cellular level have been well characterised, less well explored are the subcellular mechanisms which govern these processes. Cholesterol concentration within cells is strictly maintained, and uptake of extracellular cholesterol exists in a fine balance with intracellular *de novo* synthesis; these processes are controlled by intracellular cholesterol concentration.

The main aim of this thesis was summarised as the development of a model to describe the pathway of *de novo* synthesis and its regulation by cell cholesterol content.

In Chapter 3, a three variable ODE model of regulated gene expression describing cholesterol biosynthesis within the cell was developed. The chapter began with an overview of the biological background necessary to understand the pathways being modelled and a brief review of mathematical approaches to gene regulation modelling.

The first gene regulation system to be studied in detail was that responsible for the control of lactose metabolism in *Escherichia coli*, the *lac* operon studied in the classical work of Jacob and

Monod (1961). This work led Goodwin (1963) and later, Griffith (1968), to the mathematical study of systems containing genes and gene products controlled by inhibitory or negative feedback loops. The derivation of the model in this thesis followed this modelling framework.

The full ODE system was derived from the biochemical reactions describing gene transcription factor interaction, using the law of mass action. We showed by means of quasi-steady state assumptions and conservation laws that these equations can be modelled with Hill type functions. The specific reaction mechanism modelled is illustrated below

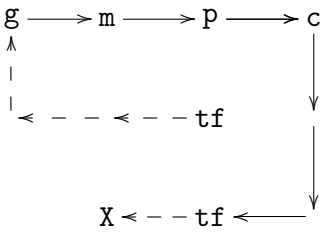

(7.1)

where g denotes the gene, m denotes mRNA, p is protein, c represents cholesterol, the end product of the reaction, and tf is the transcription factor that activates the process. In the presence of excess end product, tf binds to c and activation is halted (X). The ODE model described a general case in which multiple transcription factor binding sites are available on the gene. The reaction between cholesterol and the transcription factor was also described by a Hill function which modelled the repressive effect of this binding. Thus we created an ODE model in which the overall repressive effect of cholesterol on genetic regulation occurs as the result of repression of an activation mechanism.

The regulated cholesterol biosynthesis model we developed in Chapter 3 was analysed in Chapter 4. Using centre manifold theory the three-dimensional model was reduced to two variables. Averaging of this two-dimensional model, with respect to a critical bifurcation parameter, allowed the determination of the stability of the limit cycle generated. The analysis further allowed measurement of the physical properties, the amplitude and time period, of the resulting oscillations.

We demonstrated that limit cycles could be generated by the ODE system for a variation in any system parameter as a result of supercritical Hopf bifurcations. Thus the model produces only

small amplitude, stable oscillations. Such dynamic behaviour is of biological relevance when considering the mechanism of homeostasis, whereby the cell acts to maintain a certain value within a narrow range.

Griffith (1968) proved analytically, for his ODE model of genetic regulation, that the Hill coefficient had to be greater than eight in order for his model to generate oscillations. However, we have proved that such a high Hill coefficient, which is biologically infeasible, is not necessary. Our two step repression mechanism results in two Hill functions with physiologically valid Hill coefficients; this interaction is sufficient for oscillatory behaviour.

The results discussed above were confirmed numerically in Chapter 5, and demonstrated that the centre manifold analysis provides accurate approximations of both the stability and physical properties (amplitude and period of oscillation) of the limit cycles obtained. Chapter 5 also contained local sensitivity analysis to determine the behaviour of the model with respect to all model parameter values, including those that were unable to be determined from the experimental literature. Results illustrated greater model sensitivity to parameters such as synthesis and degradation rates which are more likely to fluctuate. Sensitivity to degradation rates were more significant than the sensitivity to synthesis rates. The model was less sensitive to the κ parameters which represent binding affinities; these parameters are biologically unlikely to undergo a change in value.

In Chapter 6, the model of genetic regulation was used to adapt and extend a simplified version of an LDL uptake model developed by Wattis et al. (2008). Although experimental data is lacking for quantitative comparison, investigation of the qualitative behaviour of the model suggested that the lack of rigorous modelling of intracellular processes masks possible long time behaviour of the system. In the original Wattis et al. model, most variables reached a steady state value within two hours. Our integrated model showed that over longer simulation time periods it is possible for the cellular responses to result in a corrective behaviour by which variables describing receptor concentrations and internalised LDL overshoot and undershoot before reaching steady state; depending on parameter values this could take from between one to three days.

This integrated model was then used to illustrate system behaviour for two cases of genetic mu-

tations causing familial hypercholesterolaemia. The model illustrated correct responses of declining LDL internalisation as the relevant parameters decreased in value, mimicking parameter ranges for heterozygous sufferers with one faulty gene. We were able to illustrate restoration of LDL internalisation by varying parameters corresponding to current pharmaceutical treatments for high plasma cholesterol levels.

7.2 Conclusions and further work

In this section we discuss the model results in the context of lipoprotein uptake models and suggest areas for both further work and model improvement.

The model of regulated *de novo* cholesterol biosynthesis derived in Chapter 3 was based on a number of assumptions in order to allow the use of an ODE modelling formalism. These assumptions are outlined below and possible model improvements or related areas for further work are suggested.

- **The cellular environment is essentially homogeneous.**
  This assumption relates to the use of the law of mass action, which assumes that reactions are taking place in a homogeneous, well mixed environment. While this assumption is applicable to the chemical solutions typical of *in vitro* experiments, its validity is tenuous when one considers the intracellular environment. Such environments are well structured and highly compartmented (see Figure 3.1), and are characterised by a high total macromolecular content, known as macromolecular crowding (Minton, 2001).

- **Reactions are continuous and deterministic.**
  Molecular reactions are discrete random processes; it is impossible to be completely certain at which the time a reaction within a volume will occur. In macroscopic systems, which contain large numbers of interacting molecules, the randomness of this behaviour averages out so that the overall state of the system becomes highly predictable; this allows the use of deterministic, continuous approaches.
  However, the validity of this assumption becomes strained in small scale *in vivo* reaction

environments, such as those described above. Furthermore, genetic variables such as mRNA are present in low concentration within the cell. In this case the probability that two molecules will undergo a biochemical reaction decreases, and discrete or stochastic effects are introduced. These effects can be highly important; cells are intrinsically noisy and low reactant numbers can lead to significant statistical fluctuations in both molecule numbers and reaction rates (Isaacs et al., 2003; Cai et al., 2006).

A possible improvement would be to consider the use of stochastic modelling, and thus account for the fluctuations in the system. Such an approach considers discrete numbers of molecules of n reacting species, and studies the evolution of the state vector $\mathbf{x}(t) = (x_1(t), \ldots, x_n(t))$, where $\mathbf{x}_i(t)$ denotes the number of molecules of a given species, i, in the system at time t.

The idea behind the approach is to calculate the probability distribution $P(\mathbf{x}, t|x_0, t_0)$, that is, the probability that, given $\mathbf{x}(t_0) = x_0$, at time t, $\mathbf{x}(t)$ will contain x_1 molecules of species 1, x_2 molecules of species 2, and so on.

Calculation of this probability distribution requires solution of the chemical master equation; typical methods for its solution are stochastic simulation algorithms (Gillespie, 1977, 1976).

To simplify the modelling process itself, and reduce the number of parameters required, gene expression was modelled using the reaction mechanism below

$$\text{DNA} \xrightarrow{\text{transcription}} \text{mRNA} \xrightarrow{\text{translation}} \text{protein.} \tag{7.2}$$

A more accurate description of the process is the mechanism below

$$\text{DNA} \xrightarrow{\text{transcription}} \xrightarrow{\text{processing}} \text{mRNA} \xrightarrow{\text{translation}} \tag{7.3}$$

$$\xrightarrow{\text{processing}} \xrightarrow{\text{post translational modification}} \text{protein.} \tag{7.4}$$

There are multiple mechanistic reactions involved in the processes of transcription and translation. These processes do not occur instantaneously, and may have considerable delays associated with them. A more suitable approach to modelling these pathways may be the use of delay

differential equations, taking the form

$$\frac{dm}{dt} = \mu_m f(p(t-\tau_m)) - \delta_m, \tag{7.5}$$

$$\frac{dp}{dt} = \mu_p m(t-\tau_p) - \delta_p, \tag{7.6}$$

where τ_m represents the transcriptional delay associated with the production of mRNA, m and τ_p represents the translational delay which occurs during the production of protein, p.

The inclusion of delays is significant, as comparison with experimental data in Chapter 6 illustrated that the genetic regulatory processes in the model seemed to respond too rapidly.

The results of the nonlinear ODE model derived to model regulated *de novo* cholesterol synthesis suggest that homeostatic mechanisms may well be dynamic, constantly fluctuating around a set point, as opposed to a static mechanism where a single value is maintained. However, no experimental evidence exists for cholesterol biosynthesis. One reason is the highly complex metabolic network in which this pathway exists; isolation of one section of the network is highly difficult and, consequently, the availability of experimental data for comparison with the model results is sparse.

Determination of the precise nature of the dynamic behaviour of this pathway is necessary. Oscillatory dynamic behaviour (although seen in some biological systems) is traditionally thought to be indicative of a disease state, for example, insulin and diabetes. This work raises the possibility that for cholesterol biosynthesis, periodic behaviour may be the norm.

Circadian (24 hour) rhythms in cholesterol synthesis have been previously demonstrated in biological investigations and are thought to be a response to regular feeding (Mayer, 1976; Jones and Schoeller, 1990). The results of Chapter 5 suggest an approximate period of 20 hours which is close to circadian rhythm. It may be possible that this response to feeding may be entrainment of the feeding cycle with an underlying circadian rhythm in cholesterol biosynthesis. To confirm or disprove these conjectures requires further experimental work in this area.

With little available data for quantitative validation, determination of accurate values for the kinetic processes and structural parameters is paramount. The difficulty of obtaining good es-

timates for model parameters was demonstrated in Chapter 6 where simulations of the integrated model illustrated that the value used for the rate of cholesterol biosynthesis was too low. Other model parameters were also difficult to evaluate, especially structural parameters such as binding affinities. This is due not only to a lack of experimental data, but also to simplifying assumptions made in deriving the governing ODEs. Many of the parameter values derived in Appendix B.1 were calculated using experimental data dating to two or more decades ago. The advent of newer, more sophisticated techniques in the intervening period could provide much more accurate parameter estimates and this needs to undertaken if accurate models of LDL uptake are to be created.

A primary motivation for this work was the mechanism of action of statins, currently the most commonly used pharmaceutical treatment for lowering plasma cholesterol levels. Statins act on the cholesterol biosynthesis pathway, by inhibiting HMGR and so reducing the level of synthesis. The resultant decline in cell cholesterol levels upregulates receptor synthesis, cell surface receptors, and subsequently LDL uptake from the plasma.

Therefore, any model of LDL uptake which aims to make conclusions about mechanisms for increasing this uptake should also include this pathway. The integrated model results in Chapter 6 have illustrated that the modelling of this pathway, and the coordinate regulation of the receptor pathway, provided useful information on the dynamics of long time LDL uptake by the cell, and enabled us to create a model that can replicate qualitative behaviour of both diseased states and their treatment. This treatment could be more thoroughly explored in the case of statins. In the model, cholesterol biosynthesis is a linear function of HMGR concentration; a more appropriate formulation would be to model the action of the enzyme using Michaelis-Menten kinetics; the action of statins could then be investigated in depth, by integrating the effect of competitive inhibition into the Michaelis-Menten rate law.

Throughout this work we have considered the total concentration of cholesterol within the cell to be free cholesterol. Cholesterol actually exists in two forms within the cell, free and esterified, as discussed in Chapter 2. A useful extension to the integrated model would be to consider the two forms as two variables and model the acyl-CoA cholesterol acyltransferase (ACAT) catalysed esterification of cholesterol explicitly.

Esterified cholesterol provides a valuable nontoxic mode of cholesterol storage within the cell, and LDL uptake is known to stimulate the ACAT pathway. Extra capacity for cholesterol in the cell may have an effect on LDL uptake; new therapeutic strategies based on ACAT inhibitors are currently being developed and trialled (Heinonen, 2002; Insull Jr et al., 2001). Further development of the model to include the ACAT-regulated pathway would allow for the investigation of the cellular response to this treatment, and an evaluation of whether this could lead to excess, toxic unesterified cholesterol in the cell.

In conclusion, it is hoped that the importance of the combined modelling of cellular processes (LDL binding, internalisation and uptake) and subcellular processes (regulation of cholesterol biosynthesis and *de novo* receptor synthesis), as demonstrated in this thesis, will be utilised in future work. We have provided scope for both future experimental work and mathematical modelling, which may be applied to better understanding of, and therefore improving therapeutic strategies for, high plasma cholesterol levels.

A

DNA Transcription Factor Interaction

In this appendix we carry out a singular perturbation analysis, using the approach of Murray (2002), for the equations describing the interaction of DNA and transcription factor as derived in Section 3.3.

We consider the binding reaction

$$\bar{D} + n\,\bar{T}_f \underset{\bar{k}_r}{\overset{\bar{k}_f}{\rightleftharpoons}} \bar{T}_c, \tag{A.1}$$

where $\bar{D}$ represents DNA, $\bar{T}_f$ represents transcription factor, n the number of molecules of $\bar{T}_f$ that must bind to $\bar{D}$ for the reaction to occur, and $\bar{T}_c$ is the complex they form on reaction.

Using the law of mass action we can describe (A.1) using the following system of ODEs.

$$\frac{d\bar{d}}{d\bar{t}} = \bar{k}_r \bar{t}_c - \bar{k}_f \bar{t}_f{}^n \bar{d}, \tag{A.2a}$$

$$\frac{d\bar{t}_f}{d\bar{t}} = n\bar{k}_r \bar{t}_c - n\bar{k}_f \bar{t}_f{}^n \bar{d}, \tag{A.2b}$$

$$\frac{d\bar{t}_c}{d\bar{t}} = \bar{k}_f \bar{t}_f{}^n \bar{d} - \bar{k}_r \bar{t}_c, \tag{A.2c}$$

with the initial conditions

$$\bar{t}_f(0) = t_0, \qquad \bar{d}(0) = d_0, \qquad \bar{t}_c(0) = 0. \tag{A.3}$$

Here $\bar{d} = [D\bar{N}A]$, $\bar{t}_f = [\bar{T}]$ and $\bar{t}_c = [\bar{T}_c]$ where square brackets denote concentration.

We note that within system (A.2), the total concentration of transcription factor is conserved. This conservation law is obtained from (A.2b) and (A.2c) to give

$$\frac{d\bar{t}_f}{d\bar{t}} + n\frac{d\bar{t}_c}{d\bar{t}} = 0 \quad \Rightarrow \quad \bar{t}_f(\bar{t}) + n\bar{t}_c(\bar{t}) = t_0, \tag{A.4}$$

on using the initial conditions (A.3).

We note also that the number of genes within a cell is always constant. This conservation law comes immediately on adding (A.2a) and (A.2c) to obtain

$$\frac{d\bar{d}}{d\bar{t}} + \frac{d\bar{t}_c}{d\bar{t}} = 0 \quad \Rightarrow \quad \bar{d}(\bar{t}) + \bar{t}_c(\bar{t}) = d_0, \tag{A.5}$$

on using the initial conditions (A.3). Thus the ODE system reduces to only two equations, for $\bar{t}_f$ and $\bar{t}_c$,

$$\frac{d\bar{t}_f}{d\bar{t}} = n\bar{k}_r \bar{t}_c - n\bar{k}_f \bar{t}_f{}^n (d_0 - \bar{t}_c), \tag{A.6a}$$

$$\frac{d\bar{t}_c}{d\bar{t}} = \bar{k}_f \bar{t}_f{}^n (d_0 - \bar{t}_c) - \bar{k}_r \bar{t}_c, \tag{A.6b}$$

with the initial conditions

$$\bar{t}_f(0) = t_0, \qquad \bar{t}_c(0) = 0. \tag{A.7}$$

We nondimensionalise system (A.6) using the rescalings

$$\tau = \bar{k}_f d_0 {t_0}^{n-1} t, \qquad t_f = \frac{\bar{t}_f}{t_0}, \qquad t_c = \frac{\bar{t}_c}{d_0}, \tag{A.8}$$

where overbars indicate dimensional variables and τ is nondimensional time.

The nondimensionalised system is given by

$$\frac{dt_f}{d\tau} = -n{t_f}^n + nt_c{t_f}^n + n\left(\frac{\bar{k}_r}{\bar{k}_f {t_0}^n}\right)t_c, \tag{A.9}$$

$$\frac{dt_c}{d\tau} = \frac{t_0}{d_0}{t_f}^n - \frac{t_0}{d_0}t_c{t_f}^n - \frac{t_0}{d_0}\left(\frac{\bar{k}_r}{\bar{k}_f {t_0}^n}\right)t_c. \tag{A.10}$$

We now let the nondimensional parameters appearing in the above system be written as

$$\gamma = \frac{\bar{k}_r}{\bar{k}_f {t_0}^n} \qquad \text{and} \qquad \epsilon = \frac{d_0}{t_0}, \tag{A.11}$$

and note that since the concentration of genes within a cell is much less than that of the concentration of transcription factor, ($d_0 << t_0$), we can see that $\epsilon << 1$.

The nondimensionalised system now becomes

$$\frac{dt_f}{d\tau} = -n{t_f}^n + nt_c{t_f}^n + n\gamma t_c, \tag{A.12a}$$

$$\epsilon\frac{dt_c}{d\tau} = {t_f}^n - t_c{t_f}^n - \gamma t_c, \tag{A.12b}$$

with the initial conditions

$$t_f(0) = 1, \qquad t_c(0) = 0. \tag{A.13}$$

We now seek a regular Taylor expansion solution to t_f and t_c in the form

$$t_f(\tau;\epsilon) = \sum_{m=0} \epsilon^m t_f^{(m)}(\tau) \qquad \text{and} \qquad t_c(\tau;\epsilon) = \sum_{m=0} \epsilon^m t_c^{(m)}(\tau). \tag{A.14}$$

We substitute the above into (A.12a) and (A.12b) and then equate powers of ϵ.

The outer solution, valid for $\tau > 0$, of system (A.12) is given by

$$O(1) \quad \begin{cases} \dfrac{dt_f^{(0)}}{d\tau} &= -n\left(t_f^{(0)}\right)^n + nt_c^{(0)}\left(t_f^{(0)}\right)^n + n\gamma t_c^{(0)}, \\ \\ 0 &= \left(t_f^{(0)}\right)^n - t_c^{(0)}\left(t_f^{(0)}\right)^n - \gamma t_c^{(0)}, \end{cases} \tag{A.15}$$

with the initial conditions

$$t_f^{(0)}(0) = 1, \qquad t_c^{(0)}(0) = 0. \tag{A.16}$$

Solving system (A.15) we find

$$t_c^{(0)} = \frac{\left(t_f^{(0)}\right)^n}{\left(t_f^{(0)}\right)^n + \gamma} \quad \Rightarrow \quad \frac{dt_f^{(0)}}{d\tau} = 0, \tag{A.17}$$

and so

$$t_c^{(0)} = \frac{\left(t_f^{(0)}\right)^n}{\left(t_f^{(0)}\right)^n + \gamma}, \quad t_f^{(0)} = K, \tag{A.18}$$

where K is an arbitrary constant.

However the solution (A.18) is not uniformly valid for all $\tau \geq 0$ since $t_c^{(0)}(0) \neq 0$. To find the solution valid near $\tau = 0$ we use the following transformations

$$\sigma = \frac{\tau}{\epsilon}, \quad t_f(\tau;\epsilon) = u(\sigma;\epsilon), \quad t_c(\tau;\epsilon) = v(\sigma;\epsilon), \tag{A.19}$$

under which the equations of system (A.12) become

$$\frac{du}{d\sigma} = -\epsilon n u^n + \epsilon n v u^n + \epsilon n \gamma v, \tag{A.20}$$

$$\frac{dv}{d\sigma} = u^n - v u^n - \gamma v, \tag{A.21}$$

with the initial conditions

$$u(0) = 1, \qquad v(0) = 0. \tag{A.22}$$

Thus the inner solution, valid for $0 \leq \tau << 1$, of system (A.12) is given by

$$O(1) \quad \begin{cases} \dfrac{du^{(0)}}{d\sigma} &= 0, \\ \\ \dfrac{dv^{(0)}}{d\sigma} &= \left(u^{(0)}\right)^n - v^{(0)}\left(u^{(0)}\right)^n - \gamma v^{(0)}. \end{cases} \tag{A.23}$$

The solution of system (A.23) is given by

$$u^{(0)}(\sigma) = 1, \qquad v^{(0)}(\sigma) = \frac{1}{1+\gamma}\left(1 - e^{-(1+\gamma)\sigma}\right). \tag{A.24}$$

We require that

$$\lim_{\sigma\to\infty}\left[u(\sigma;\epsilon), v(\sigma;\epsilon)\right] \quad = \quad \lim_{\tau\to 0}\left[t_f(\tau;\epsilon), t_c(\tau;\epsilon)\right], \tag{A.25}$$

thus

$$\lim_{\sigma\to\infty} v^{(0)}(\sigma) \quad = \quad \frac{1}{1+\gamma} \quad = \quad \lim_{\tau\to 0} t_c^{(0)}(\tau), \tag{A.26}$$

$$\Rightarrow \quad t_c^{(0)}(0) \quad = \quad \frac{1}{1+\gamma} \quad = \quad \frac{\left(t_f^{(0)}\right)^p}{\left(t_f^{(0)}\right)^p + \gamma}, \tag{A.27}$$

$$\Rightarrow \quad t_f^{(0)}(0) \quad = \quad 1 \quad \Rightarrow \quad K \quad = \quad 1. \tag{A.28}$$

In summary to $O(1)$ for small ϵ

$$t_f(\tau;\epsilon) \quad = \quad t_f^{(0)}(\tau) + O(\epsilon), \qquad t_f^{(0)}(\tau) = 1, \tag{A.29}$$

$$t_c(\tau;\epsilon) \quad = \quad v^{(0)}(\sigma) + O(\epsilon), \qquad v^{(0)}(\sigma) = \frac{1}{1+\gamma}\left(1 - e^{-(1+\gamma)\sigma}\right), \qquad 0 < \tau << 1, \tag{A.30}$$

$$= \quad t_c^{(0)}(\tau) + O(\epsilon), \qquad t_c^{(0)}(0) = \frac{\left(t_f^{(0)}\right)^p}{\left(t_f^{(0)}\right)^p + \gamma}, \qquad 0 < \epsilon << \tau. \tag{A.31}$$

The rapid change in the DNA-transcription factor complex $t_c(\tau,\epsilon)$ takes place in dimensional times $\tau = O(\epsilon)$ which is very small.

The relevant solution is then the $O(1)$ outer solution, $t_f^{(0)}(\tau)$ and $t_c^{(0)}(\tau)$ in (A.18), obtained from the system (A.12) on setting $\epsilon = 0$ and satisfying only the initial condition on $t_f(\tau)$, the transcription factor concentration.

Thus the reaction for the complex $t_c(\tau)$ is so fast it is essentially in a steady state. We can then make the quasi-steady state hypothesis that

$$\epsilon \frac{d\,t_c}{d\,\tau} \approx 0. \tag{A.32}$$

B

Parameter Values

This appendix is concerned with the calculations of the parameter values used within the models derived and discussed in this thesis. Note that the experimental data found in the literature have been converted so that we consider numbers of molecules, with volumes in ml, and time in units of s^{-1}.

B.1 Parameter values of the HMGR system

In this section we detail the calculations used to estimate parameters pertaining to the biosynthesis of cholesterol and its regulation. These are the parameters which have previously been considered in Section 3.5.2 and detailed in Table 3.1.

B.1.1 Rate of transcription $\bar{\mu}_{mh}$

To produce an estimate for the transcription rate we assume that any time delays involved in the initiation of transcription, promoter clearance and elongation are negligible. We also assume that no abortive transcripts are produced. We know that liver cells are somatic cells, therefore the majority are diploid, that is they contain two genes per cell. We make the assumption that all liver cells are diploid and ignore the existence of both tetraploidy and double nuclei that can be present within some liver cells. From Darzacq et al. (2007), we find that in a typical mammalian gene, 14000 base pairs can be transcribed in 20 minutes which gives a rate of 12 bases per second.

We use these assumptions, to provide a rough estimate of the rate of transcription, equivalent to the number of mRNA molecules produced per cell per unit time.

One human HMG-CoA reductase mRNA transcript is 4475 bases long (Goldstein and Brown, 1984). To transcribe one molecule of HMG-CoA reductase mRNA, from one gene, assuming a rate of 12 bases per second, takes

$$\frac{4475 \text{ bases}}{12 \text{ bases/s}} = 372.92 \text{ s} . \tag{B.1}$$

Then per gene, this equates to

$$\frac{1}{372.92 \text{ s}} = 2.68 \times 10^{-3} \text{ molecules HMGR mRNA s}^{-1} . \tag{B.2}$$

Therefore one gene can synthesise 2.68×10^{-3} molecules of HMG-CoA reductase mRNA per second. Since a liver cell contains two genes, we have 5.36×10^{-3} molecules HMG-CoA reductase mRNA being synthesised per cell per second.

Given an average cell volume of 1pl, (1×10^{-12} l $= 1 \times 10^{-9}$ ml), we have a rate of HMGR transcription is given by,

$$\bar{\mu}_{mh} = \frac{5.36 \times 10^{-3} \text{ molecules s}^{-1}}{1 \times 10^{-9} \text{ ml}} = 5.36 \times 10^{6} \text{ molecules ml}^{-1} \text{ s}^{-1} . \tag{B.3}$$

Thus we take a value

$$\bar{\mu}_{mh} = 5.36 \times 10^6 \text{ molecules ml}^{-1} \text{ s}^{-1} . \tag{B.4}$$

B.1.2 Rate of translation $\bar{\mu}_h$

To calculate an estimate of the rate of translation, we again outline our assumptions. Firstly, we ignore any effects that are caused by the transport of mRNA from the nucleus to its localisation in the cytoplasm. We also ignore the effects of protein folding on transcriptional regulation as well as biochemical interactions amongst proteins. Finally we assume that any time delays in the elongation phase of protein synthesis are negligible.

We then use the *in vivo* estimate from Slobin (1991) that the translation rate for eukaryotic cells is 6 amino acids per second, where one amino acid contains 3 nucleotides or bases. From Granner and Weil (2006) we find that many ribosomes can translate the same mRNA molecule simultaneously. Because of their large size, ribosomes cannot attach to an mRNA any closer than 35 nucleotides apart. This detail allows us to create a rough estimate of the rate of transcription, equivalent to proteins synthesised per unit time from mRNA.

A human HMG-CoA reductase mRNA transcript contains 888 amino acids, (Luskey and Stevens, 1985). For one ribosome to transcribe one molecule of HMG-CoA reductase protein, from one HMG-CoA reductase mRNA, assuming a translation rate of 6 amino acids per second, takes

$$\frac{888 \text{ amino acids}}{6 \text{ amino acids/s}} = 148 \text{ s} . \tag{B.5}$$

Then per ribosome, this equates to

$$\frac{1 \text{ molecule}}{148 \text{ s}} = 6.76 \times 10^{-3} \text{ molecules s}^{-1} . \tag{B.6}$$

Thus, 6.76×10^{-3} molecules of HMG-CoA reductase protein being synthesised per second per ribosome.

Given that the coding region of the HMG-CoA reductase mRNA is 888 amino acids $\times 3 = 2664$

nucleotides long, and a ribosome can attach every 35 nucleotides, we have 76.11 ribosomes attached per mRNA molecule. Therefore, per HMG-CoA reductase mRNA molecule we have,

$$6.76 \times 10^{-3} \text{ molecules s}^{-1} \text{ ribosome}^{-1} \times 76.11 \text{ ribosomes} \quad = \quad 0.51 \text{ molecules s}^{-1}. \tag{B.7}$$

That is, there are 0.51 molecules of HMG-CoA reductase protein being synthesised per second. We take as an approximation of the rate of HMGR translation,

$$\bar{\mu}_h \quad = \quad 0.51 \text{ s}^{-1}. \tag{B.8}$$

B.1.3 HMG-CoA reductase activity $\bar{\mu}_c$

From Tanaka et al. (1982) for human liver microsomes, we find a value of 52 pmol mevalonate formed per minute per mg protein. This must now be converted into a turnover number.

The turnover number (K_{cat}) of an enzyme is the maximum number of substrate molecules that an enzyme can convert to product per mole of catalytic site of the enzyme per unit time. The activity of an enzyme is the moles of substrate converted per unit time and is a measure of the quantity of active enzyme present and the specific activity is the activity of an enzyme per mg of total protein, i.e. a measure of enzyme efficiency.

HMG-CoA reductase is a tetrameric protein, composed of monomers arranged in two dimers. Each dimer has two active sites, (Istvan et al., 2000) and $M_r = 99906$ Dalton . The Dalton, (Da), (alternatively *atomic mass unit*) is a unit of mass used to express atomic and molecular masses. It is defined so that one mole of a substance with atomic or molecular mass 1 Da will have a mass of precisely 1 g.

Therefore the full HMG-CoA reductase molecule is an enzyme containing 4 active sites with a molecular mass $M_r = 2 \times 99906 = 199812$ Da , i.e. 1 mole HMG-CoA reductase has a mass of 199812 g. The reaction catalysed by HMG-CoA reductase is given by

$$\text{HMG-CoA} + 2\text{NADPH} + 2\text{H}^+ \longrightarrow \text{mevalonate} + 2\text{NADP}^+ + \text{CoASH} \tag{B.9}$$

which indicates a stoichiometry of one mole mevalonate being produced from one mole HMG-CoA. (Note we have assumed in our model that all other substrates of this reaction are present in excess).

The specific activity of the enzyme, (52×10^{-12} mol per minute per mg protein) is equivalent to

$$\begin{aligned} 52 \times 10^{-12} \times N_A &= 52 \times 10^{-12} \text{ mol min}^{-1} \text{ mg}^{-1} \times 6.022 \times 10^{23} \text{ molecules mol}^{-1}, \\ &= 3.13 \times 10^{13} \text{ molecules min}^{-1} \text{ mg}^{-1}, \end{aligned} \tag{B.10}$$

where

$$N_A = 6.022 \times 10^{23} \text{ molecules mol}^{-1}, \tag{B.11}$$

is the Avogadro Constant which describes the number of 'elementary entities' (usually atoms or molecules) in one mole.

We take the assumption of Segel (1993) that there are approximately 1000 different enzymes in a cell. Thus the moles of enzyme in 1mg of protein is equivalent to

$$\left(\frac{1 \times 10^{-3} \text{ g}}{199812 \text{ g mol}^{-1} \times 1000} \right) = 5.00 \times 10^{-12} \text{ mol}, \tag{B.12}$$

and given 4 active sites per HMG-CoA reductase enzyme, there are 2.00×10^{-11} moles of enzyme active sites in 1mg of protein.

Thus, given the specific activity of an enzyme, 52×10^{-12} mol min^{-1} mg^{-1}, we have

$$\frac{52 \times 10^{-12} \text{ mol min}^{-1} \text{ mg}^{-1}}{2.00 \times 10^{-11} \text{ mol mg}^{-1}} = 2.60 \text{ min}^{-1}. \tag{B.13}$$

And so the turnover number for HMG-CoA reductase is given by,

$$\bar{\mu}_{ch} = 4.33 \times 10^{-2} \text{ s}^{-1}. \tag{B.14}$$

B.1.4 Degradation rates $\bar{\delta}_{mh}$, $\bar{\delta}_h$

The calculation of degradation rates of proteins and mRNAs are based on their half-lives, $t_{1/2}$, derived from an exponential decay model. For a decay constant δ, the rate of degradation of the variable is given by

$$\delta = \frac{\ln 2}{t_{1/2}}. \tag{B.15}$$

From Wilson and Deeley (1995), we have a half-life of $t_{1/2} = 4.3$ hr for HMG-CoA reductase mRNA, measured in Hep G2 cells and so

$$\bar{\delta}_{mh} = \frac{\ln 2}{15480\text{ s}} = 4.48 \times 10^{-5}\text{ s}^{-1}. \tag{B.16}$$

From Brown et al. (1974), we have a half-life of $t_{1/2} = 3$ hr for the HMG-CoA reductase protein, measured in human fibroblast cells and so

$$\bar{\delta}_h = \frac{\ln 2}{10800\text{ s}} = 6.42 \times 10^{-5}\text{ s}^{-1}. \tag{B.17}$$

B.1.5 Concentration of total activator $\bar{s}_0$

In general, transcription factors have low gene expression, and are therefore present in relatively low concentrations within the cell, (Sanguinetti et al., 2006). Since we have simplified the SREBP signalling pathway, we make some assumptions to obtain an estimate for this value. We know that the majority of cellular cholesterol is located within the plasma membrane of the cell, and its concentration is governed by multiple regulatory proteins regulated in the endoplasmic reticulum, (ER), which are themselves under the control of a small regulatory pool of ER cholesterol, (Lange et al., 1999). We therefore assume that the concentration of s_0 is of the order of this concentration, which allows small changes in the cellular cholesterol pool, to be magnified in the transcription factor pathway. From Lange et al. (1999), we have an average of 0.45 nmol ER cholesterol/mg cell protein.

Taking Avogadro's number, $N_A = 6.022 \times 10^{23}$, and the assumption that one cell has approximately 300 pg of cell protein and a volume of 1 pl; 1 mg of cell protein is thus equivalent to 0.0033 ml, we obtain

$$\begin{aligned} \bar{s}_0 &= \frac{0.45 \times 10^{-9} \text{ mol} \times 6.022 \times 10^{23} \text{molecules mol}^{-1}}{0.0033 \text{ ml}}, \\ &= 8.21 \times 10^{16} \text{ molecules ml}^{-1}. \end{aligned} \tag{B.18}$$

B.1.6 Initial conditions $\bar{m}_{h0}, \bar{h}_0, \bar{c}_0$

To calculate the initial conditions for the model, we make the assumption that to begin with the cell is functioning at a normal capacity, i.e. the cholesterol concentration within the cell is at or near its equilibrium level.

From Lange et al. (1999), we take a value of resting cholesterol for the cell of 40 μg cell cholesterol/mg cell protein. Using the molecular weight of cholesterol, $M_r = 386.65$ g and the fact that 1 mg of cell protein is equivalent to 0.0033 ml, we obtain

$$\begin{aligned} \bar{c}_0 &= \frac{40 \times 10^{-6} \text{ g} \times 6.022 \times 10^{23} \text{ molecules mol}^{-1}}{386.65 \text{ g mol}^{-1} \times 0.0033 \text{ ml}}, \\ &= 1.89 \times 10^{19} \text{ molecules ml}^{-1}. \end{aligned} \tag{B.19}$$

To calculate the initial condition for HMGR mRNA we use information from Rudling et al. (2002), which details copy numbers of mRNA found in human liver cells under basal conditions. We take a value of 30 copies of HMGR mRNA per cell, i.e. per 1×10^{-9} ml. This gives

$$\bar{m}_{h0} = \frac{30 \text{ molecules}}{1 \times 10^{-9} \text{ ml}} = 3.0 \times 10^{10} \text{ molecules ml}^{-1}. \tag{B.20}$$

To approximate the initial concentration of HMGR enzyme within a cell, we use the fact that one liver cell contains roughly 300 pg cell protein, and has a volume of 10^{-9} ml. Using the molecular weight of HMGR, $M_r = 199812$ g mol^{-1} (Istvan et al., 2000), we calculate that the number of

moles of HMGR is

$$\frac{300\times10^{-12}\text{ g}}{199812\text{ g mol}^{-1}}=1.50\times10^{-15}\text{ mol per cell}. \tag{B.21}$$

Thus we have 1.50×10^{-15} mol per 10^{-9} ml which is equivalent 1.50×10^{-6} mol ml^{-1} or $1.50\times10^{-6}\times N_A=9.04\times10^{17}$ molecules/ml. Taking into account that a cell contains on average a thousand different enzymes (Segel, 1993) we have

$$\bar{h}_0=9.04\times10^{14}\text{ molecules ml}^{-1}. \tag{B.22}$$

B.2 Parameter values of LDLR synthesis

In this section we detail the calculations used to estimate parameters pertaining to the biosynthesis of the low density lipoprotein receptor and its regulation. These are the parameters which have previously been considered in Section 6.2 and detailed in Table 6.5.

B.2.1 Rate of transcription $\bar{\mu}_{mr}$

The estimate for the transcription rate of LDLR is produced using the same assumptions and initial information as for the estimation of the HMGR transcription rate. We proceed in a similar manner.

One human LDL Receptor mRNA transcript is 5265 bases long [1]. To transcribe one molecule of LDLR mRNA, from one gene, assuming a rate of 12 bases per second, takes

$$\frac{5265\text{ bases}}{12\text{ bases/s}} \quad = \quad 438.75\text{ s}. \tag{B.23}$$

Then per gene, this equates to

$$\frac{1}{438.75\text{ s}} \quad = \quad 2.28\times10^{-3}\text{ molecules LDLR mRNA s}^{-1}. \tag{B.24}$$

[1] www.nbci.nlm.nih.gov/Genomes

Therefore one gene can synthesise 2.28×10^{-3} molecules of LDLR mRNA per second. Since a liver cell contains two genes, we have 4.56×10^{-3} molecules LDLR mRNA being synthesised per cell per second.

Given an average cell volume of 1pl, (1×10^{-12} l $= 1 \times 10^{-9}$ ml), we have a rate of LDLR transcription is given by,

$$\bar{\mu}_{mr} = \frac{4.56 \times 10^{-3} \text{ molecules s}^{-1}}{1 \times 10^{-9} \text{ ml}} = 4.56 \times 10^{6} \text{ molecules ml}^{-1} \text{ s}^{-1} . \tag{B.25}$$

Thus we take a value

$$\bar{\mu}_{mr} = 4.56 \times 10^{6} \text{ molecules ml}^{-1} \text{ s}^{-1} . \tag{B.26}$$

B.2.2 Rate of translation $\bar{\mu}_r$

To calculate an estimate of the rate of translation, we again use similar assumptions as for the HMGR calculation, and estimate in the same manner.

A human LDL Receptor mRNA transcript contains 839 amino acids, (Soutar and Knight, 1990). For one ribosome to transcribe one molecule of LDLR protein, from one LDLR mRNA, assuming a translation rate of 6 amino acids per second, takes

$$\frac{839 \text{ amino acids}}{6 \text{ amino acids/s}} = 139.83 \text{ s} . \tag{B.27}$$

Then per ribosome, this equates to

$$\frac{1 \text{ molecule}}{139.83 \text{ s}} = 7.15 \times 10^{-3} \text{ molecules s}^{-1} . \tag{B.28}$$

Thus, 7.15×10^{-3} molecules of LDLR are protein being synthesised per second per ribosome.

Given that the coding region of the LDLR mRNA is 839 amino acids $\times 3 = 2517$ nucleotides long, and a ribosome can attach every 35 nucleotides, we have 71.91 ribosomes attached per mRNA

molecule. Therefore, per LDLR mRNA molecule we have,

$$7.15\times10^{-3}\text{ molecules s}^{-1}\text{ ribosome}^{-1}\times 71.91\text{ ribosomes} \quad = \quad 0.51\text{ molecules s}^{-1}. \tag{B.29}$$

That is there are 0.51 molecules of LDLR protein synthesised per second. We take as an approximation of the rate of LDLR translation,

$$\bar{\mu}_r \quad = \quad 0.51\text{ s}^{-1}. \tag{B.30}$$

B.2.3 Degradation rates $\bar{\delta}_{mr}$, $\bar{\delta}_r$

The calculation of degradation rates of proteins and mRNAs are based on their half-lives, $t_{1/2}$ and is derived as for HMGR.

From Vargas et al. (2009), we have a half-life of $t_{1/2} = 66$ min for LDLR mRNA, measured in Hep G2 cells and so

$$\bar{\delta}_{mr} \quad = \quad \frac{\ln 2}{3960\text{ s}} = 1.75\times10^{-4}\text{ s}^{-1}. \tag{B.31}$$

From Graadt van Roggen et al. (1995), we have a half-life of $t_{1/2} = 14.4$ hr for the LDLR protein, measured in human fibroblast cells and so

$$\bar{\delta}_r \quad = \quad \frac{\ln 2}{51840\text{ s}} = 1.34\times10^{-5}\text{ s}^{-1}. \tag{B.32}$$

B.2.4 Initial conditions $\bar{m}_{r0}$

To calculate the initial condition for HMGR mRNA we use information from Rudling et al. (2002), which details copy numbers of mRNA found in human liver cells under basal conditions. We take a value of 48 copies of HMGR mRNA per cell, i.e. per 1×10^{-9} ml. This gives

$$\bar{m}_{r0} = \frac{48\text{ molecules}}{1\times10^{-9}\text{ ml}} = 4.8\times10^{10}\text{ molecules ml}^{-1}. \tag{B.33}$$

C

Mathematical Results

In this appendix we provide the details of mathematical theorems and stability results which were used in Chapter 4 of this thesis.

C.1 Descartes' rule of signs

Descartes' rule of signs is used to find zeros of polynomial functions that are not factorable. In particular, it can be used to determine the number of possible positive and negative real zeros, and the number of possible nonreal zeros, of a polynomial function arranged in order of highest to lowest power, that is in standard form (Murray, 2002).

Theorem IV (Descartes' rule of signs I)

Let $p(x)$ be any polynomial with real coefficients. The number of positive, real roots of $p(x)=0$ is either equal to the number of variations of sign in the coefficients of $p(\lambda)$ or else is less than this number by an even integer. A zero coefficient is not counted as a change of sign.

Theorem V (Descartes' rule of signs II)

Let $p(\lambda)$ be any polynomial with real coefficients and let the polynomial $q(\omega)=p(-\lambda)$. The number of negative, real roots of $p(\lambda)=0$ is either equal to the number of variations of sign in the coefficients of $q(\omega)$ or else is less than this number by an even integer. A zero coefficient is not counted as a change of sign.

As an example, consider the application of Theorem IV to a cubic polynomial given by

$$p(\lambda) \;=\; a_3\lambda^3 + a_2\lambda^2 - a_1\lambda + a_0 \;=\; 0, \tag{C.1}$$

where $a_i > 0$ for all $i = 0, 1, 2$. We note that there are two sign changes in the sequence of coefficients, and so the polynomial has either two or zero real, positive roots.

Now using Theorem V, we have

$$q(\omega) \;=\; p(-\lambda) \;=\; -a_3\lambda^3 + a_2\lambda^2 + a_1\lambda + a_0 \;=\; 0, \tag{C.2}$$

where one change of sign in the coefficient sequence indicates (C.2) has only one positive real root and consequently (C.1) has exactly one negative real root.

C.2 The Routh-Hurwitz stability criterion

The Routh-Hurwitz stability criterion is an algebraic procedure for determining whether a polynomial has any zeros in the right half plane, that is, a method for determining whether or not a linear system is stable, by examining the location of the roots of the charcteristic equation of the system (Murray, 2002).

The method does not indicate the relative degree of stability or instability; it simply determines the necessary and sufficient conditions for stability.

C.2.1 Routh-Hurwitz stability of a cubic polynomial

We consider this method for the general form of a cubic characteristic equation, described by

$$A(\lambda) = a_n\lambda^3 + a_{n-1}\lambda^2 + a_{n-2}\lambda + a_{n-3} = 0. \tag{C.3}$$

A necessary (but not sufficient) condition for $A(\lambda)$ to be Hurwitz, i.e., for all of its roots to have strictly negative real part, is that all polynomial coefficients be nonzero and positive. If any coefficient is zero or negative, then there is at least one root in the closed right-half plane. If this condition is satisfied, the Routh-Hurwitz array for (C.3) may be computed as follows

$$\begin{vmatrix} a_n & a_{n-2} & a_{n-4} \\ a_{n-1} & a_{n-3} & a_{n-5} \\ b_1 & b_2 & b_3 \\ c_1 & c_2 & c_3 \end{vmatrix}, \tag{C.4}$$

where the a_i are the polynomial coefficients and the other coefficients are calculated using,

$$b_1 = -\left(\frac{1}{a_{n-1}}\right)(a_n a_{n-3} - a_{n-2}a_{n-1}), \tag{C.5a}$$

$$b_2 = -\left(\frac{1}{a_{n-1}}\right)(a_n a_{n-5} - a_{n-4}a_{n-1}), \tag{C.5b}$$

$$b_3 = -\left(\frac{1}{a_{n-1}}\right)(a_n a_{n-7} - a_{n-6}a_{n-1}), \tag{C.5c}$$

$$c_1 = -\left(\frac{1}{b_1}\right)(a_{n-1}b_2 - a_{n-3}b_1), \tag{C.5d}$$

$$c_2 = -\left(\frac{1}{b_1}\right)(a_{n-1}b_3 - a_{n-5}b_1), \tag{C.5e}$$

$$c_3 = -\left(\frac{1}{b_1}\right)(a_{n-1}b_4 - a_{n-7}b_1). \tag{C.5f}$$

The necessary and sufficient condition that all roots of (C.3) have negative real parts is that all the elements of the first column of the Routh-Hurwitz array have the same sign. If there are sign

changes in these elements, then the number of roots with nonnegative real parts is equal to the number of changes of sign.

Thus the characteristic equation given by,

$$a_3\lambda^3 + a_2\lambda^2 + a_1\lambda + a_0 = 0, \tag{C.6}$$

has the nonzero Routh-Hurwitz coefficients given by

$$b_1 = -\left(\frac{1}{a_2}\right)(a_3a_0 - a_1a_2), \tag{C.7}$$

$$c_1 = -\left(\frac{1}{b_1}\right)(a_20 - a_0b_1) = a_0, \tag{C.8}$$

and the Routh-Hurwitz array is given by

$$\begin{vmatrix} a_3 & a_1 & 0 \\ a_2 & a_0 & 0 \\ -\left(\frac{a_3a_0 - a_1a_2}{a_2}\right) & 0 & 0 \\ a_0 & 0 & 0 \end{vmatrix}. \tag{C.9}$$

And so, all roots of (C.6) have negative real parts if and only if the following relations hold

$$a_0 > 0, \qquad a_1 > 0, \qquad a_2 > 0, \qquad a_3 > 0, \tag{C.10}$$

together with the condition

$$-\left(\frac{a_3a_0 - a_1a_2}{a_2}\right) > 0, \tag{C.11}$$

$$\Rightarrow \quad a_3a_0 - a_1a_2 < 0, \tag{C.12}$$

$$\Rightarrow \quad a_1a_2 - a_3a_0 > 0. \tag{C.13}$$

Glossary of Biological Terms

- **Catabolism**
  General term for the enzyme catalysed reactions in a cell by which complex molecules are degraded to simpler ones with release of energy.
- **Cytoplasm**
  Contents of a cell that are contained within its plasma membrane but, in the case of eukaryotic cells, outside the nucleus.
- ***De novo* synthesis**
  De novo is a Latin phrase meaning from the beginning. *De novo* synthesis refers to the synthesis of complex molecules from simple molecules.
- **Endocytosis**
  Uptake of material into a cell by invagination of the plasma membrane and its internalisation in a membrane-bounded vesicle.
- **Endoplasmic reticulum**
  Labyrinthine compartment in the cytoplasm of eukaryotic cells, where lipids are synthesised and membrane bound proteins and secretory proteins are made.
- **Enzyme**
  Protein that catalyses a specific chemical reaction.
- **Eukaryote**
  Organism composed of one or more cells that have a distinct nucleus.
- **Feedback inhibition**
  The process in which a product of a reaction feeds back to inhibit a previous reaction in the same pathway.
- **Gene**
  Region of DNA that carries information for a discrete hereditary characteristic, usually corresponding to a single protein.
- **Gene expression**
  Production of an observable molecular product (RNA or protein) by a gene.

- **Hepatocyte**
  The major cell type in the liver.
- **Homeostasis**
  The property of a system, either open or closed, which regulates its internal environment in order to maintain a stable, constant condition.
- ***In vitro***
  Taking place in an isolated cell free extract, as opposed to a living cell. Sometimes used to distinguish between cell culture studies from studies in intact organisms.
- ***In vivo***
  Taking place in an intact cell or organism.
- **Messenger RNA**
  RNA molecule that specifies the amino acid sequence of a protein.
- **Metabolism**
  The sum total of the chemical processes that take place in living cells.
- **Nucleus**
  Prominent membrane bounded organelle in eukaryotic cells containing DNA.
- **Plasma**
  The liquid component of blood in which the blood cells of whole blood are normally suspended.
- **Promoter**
  Nucleotide sequence in DNA to which RNA polymerase binds to initiate transcription.
- **Transcription**
  Copying of one strand of DNA into a complementary RNA sequence.
- **Transcriptional activator**
  Gene regulatory protein that binds to a specific DNA sequence to activate the transcription of a gene.
- **Transcription factor**
  Any protein required to initiate or regulate transcription in eukaryotic cells.
- **Translation**
  Process by which the sequence of nucleotides in a mRNA molecule directs the incorporation of amino acids into protein.

Bibliography

M. Adiels, C. Packard, M. J. Caslake, P. Stewart, A. Soro, et al. A new combined multicompartmental model for apolipoprotein B-100 and triglyceride metabolism in VLDL subfractions. *Journal of Lipid Research*, **46**(1):58–67, 2005.

B. Alberts, A. Johnson, J. Lewis, M. Raff, K. Roberts, and P. Walter, editors. *Molecular Biology of the Cell*. Garland Science, New York, Fifth edition, 2008.

C. A. Aspinwall, J. R. T. Lakey, and R. T. Kennedy. Insulin-stimulated insulin secretion in single pancreatic beta cells. *Journal of Biological Chemistry*, **274**(10):6360–6365, 1999.

E. August, K. H. Parker, and M. Barahona. A dynamical model of lipoprotein metabolism. *Bulletin of Mathematical Biology*, **69**:535–542, 2007.

M. A. Austin, C. M. Hutter, R. L. Zimmern, and S. E. Humphries. Familial hypercholesterolemia and coronary heart disease: A HuGE association review. *American Journal of Epidemiology*, **160**(5):421–429, 2004.

W. F. Beltz, Y. A. Kesaniemi, B. V. Howard, and S. M. Grundy. Development of an integrated model for analysis of the kinetics of apolipoprotein B in plasma very low density lipoproteins, intermediate density lipoproteins, and low density lipoproteins. *The Journal of Clinical Investigation*, **76**(2):575–585, 1985.

M. J. Berridge, M. D. Bootman, and H. LLewelyn-Roderick. Calcium signalling : Dynamics, homeostasis and remodelling. *Nature Reviews Molecular Cell Biology*, **4**:517–529, 2003.

R. D. Bliss, P. R. Painter, and A. G. Marr. Role of feedback inhibition in stabilizing the classical operon. *Journal of Theoretical Biology*, **97**(2):177–193, 1982.

K. Bloch. The biological synthesis of cholesterol. *Science*, **150**:19–28, 1965.

S. Bornholdt. Boolean network models of cellular regulation: prospects and limitations. *Journal of the Royal Society Interface*, **5**:S85–S94, 2008.

British Heart Foundation. BHF Coronary Heart Disease Statistics Chapter Thirteen (Economic Costs), 2008a. [online] `http://www.heartstats.org/temp/2008.Chaptersp13.pdf`.

British Heart Foundation. BHF Coronary Heart Disease Statistics Chapter One (Mortality), 2008b. [online] http://www.heartstats.org/temp/2008.Chaptersp1.pdf.

M. S. Brown and J. L. Goldstein. The SREBP pathway: Regulation of cholesterol metabolism by proteolysis of a membrane bound transcription factor. *Cell*, **89**:331–340, 1997.

M. S. Brown and J. L. Goldstein. Receptor mediated endocytosis: Insights from the lipoprotein receptor system. *Proceedings of the National Academy of Sciences*, **76**:3330–3337, 1979.

M. S. Brown, S. E. Dana, and J. L. Goldstein. Regulation of 3-hydroxy-3-methylglutaryl coenzyme A reductase activity in cultured human fibroblasts. Comparison of cells from a normal subject and from a patient with homozygous familial hypercholesterolemia. *Journal of Biological Chemistry*, **249**(3):789–796, 1974.

L. Cai, N. Friedman, and X. S. Xie. Stochastic protein expression in individual cells at the single molecule level. *Nature*, **440**:358–362, 2006.

E. Carafoli. Intracellular calcium homeostasis. *Annual Review of Biochemistry*, **56**(1):395–433, 1987.

J. Carr. *Applications of Centre Manifold Theory*. Springer-Verlag, New York, 1981.

M. Chetiveaux, K. Ouguerram, Y. Zair, P. Maugere, I. Falconi, et al. New model for kinetic studies of HDL metabolism in humans. *European Journal of Clinical Investigation*, **34**(4):262–267, 2004.

M. C. Cheung and J. J. Albers. Distribution of high density lipoprotein particles with different apoprotein composition: Particles with A-I and A-II and particles with A-I but no A-II. *Journal of Lipid Research*, **23**(5):747–753, 1982.

S. N. Chow and J. Mallett-Paret. Integral averaging and bifurcation. *Journal of Differential Equations*, **26**:112–159, 1977.

P. W. Chun, A. J. Espinosa, C. W. Lee, R. B. Shireman, and E. E. Brumbaugh. Low density lipoprotein receptor regulation. Kinetic models. *Biophysical Chemistry*, **21**:185–200, 1985.

M. Dammerman and J. L. Breslow. Genetic basis of lipoprotein disorders. *Circulation*, **91**(2): 505–512, 1995.

X. Darzacq, Y. Shav-Tal, V. de Turris, Y. Brody, S. M. Shenoy, et al. In vivo dynamics of RNA polymerase II transcription. *Nature Structural and Molecular Biology*, **14**:796 – 806, 2007.

M. J. Davies, P. D. Richardson, and N. Woolf. Risk of thrombosis in human atherosclerotic plaques: role of extracellular lipid, macrophage and smooth muscle cell content. *British Heart Journal*, **69**:377–381, 1993.

A. Dhooge, W. Govaerts, and Y. A. Kuznetsov. Matcont : A Matlab package for numerical bifurcation analysis of ODEs. *ACM Transactions on Mathematical Software*, **29**(2):141–164, 2003.

D. Eberlé, B. Hegarty, P. Bossard, P. Ferré, and F. Foufelle. SREBP transcription factors: Master regulators of lipid homeostasis. *Biochimie*, **86**:839–848, 2004.

H. Echavarria-Heras. Convective flow effects in receptor-mediated endocytosis. *Mathematical Biosciences*, **89**(1):9–27, 1988.

European Heart Network. European Cardiovascular Disease Statistics Chapter One (Mortality), 2008. [online] `http://www.heartstats.org/temp/ESspweb08chapter.1.pdf`.

E. Falk. Pathogenesis of atherosclerosis. *Journal of the American College of Cardiology*, **7**(8): Suppl.C7–C12, 2006.

Framingham Heart Study. The Framingham Heart Study, 1948. [online] `http://www.framinghamheartstudy.org/`.

H. Gao, W. Shi, and L. B. Freund. Mechanics of receptor-mediated endocytosis. *Proceedings of the National Academy of Sciences, USA*, **102**(27):9469–9474, 2005.

M. Gex-Fabry and C. DeLisi. Receptor-mediated endocytosis: a model and its implications for experimental analysis. *American Journal of Physiology : Regulatory, Integrative and Comparative Physiology*, **247**(5):R768–779, 1984.

A. Ghosh and B. Chance. Oscillations of glycolytic intermediates in yeast cells. *Biochemical and Biophysical Research Communications*, 16(2):174 – 181, 1964.

D. T. Gillespie. Exact stochastic simulation of coupled chemical reactions. *The Journal of Physical Chemistry*, **81**(25):2340–2361, 1977.

D. T. Gillespie. A general method for numerically simulating the stochastic time evolution of coupled chemical reactions. *Journal of Computational Physics*, **22**(4):403 – 434, 1976.

P. Gilon, M. A. Ravier, J. C. Jonas, and J. C. Henquin. Control mechanisms of the oscillations of insulin secretion in vitro and in vivo. *Diabetes*, **51**(S1):S145–S151, 2002.

L. Glass and S. A. Kauffman. The logical analysis of continuous, non-linear biochemical control networks. *Journal of Theoretical Biology*, **39**(1):103 – 129, 1973.

P. Glendinning. *Stability, Instability and Chaos : An Introduction to the Theory of Nonlinear Differential Equations*. Cambridge University Press, UK, 1994.

I. J. Goldberg. Lipoprotein lipase and lipolysis: central roles in lipoprotein metabolism and atherogenesis. *Journal of Lipid Research*, **37**(4):693–707, 1996.

B. Goldstein, C. Wofsy, and G. Bell. Interactions of low density lipoprotein receptors with coated pits on human fibroblasts: Estimate of the forward rate constant and comparison with the diffusion limit. *Proceedings of the National Academy of Sciences, USA*, **78**(9):5695–5698, 1981.

B. Goldstein, R. Griego, and C. Wofsy. Diffusion-limited forward rate constants in two dimensions. Applications to the trapping of cell surface receptors by coated pits. *Biophysical Journal*, **46**:537–586, 1984.

B. Goldstein, C. Wofsy, and H. Echavarria-Heras. Effect of membrane flow on the capture of receptors by coated pits. Theoretical results. *Biophysical Journal*, **53**:405–414, 1988.

J. L. Goldstein and M. S. Brown. The low density lipoprotein pathway and its relation to atherosclerosis. *Annual Review of Biochemistry*, **46**:897–930, 1977.

J. L. Goldstein and M. S. Brown. Progress in understanding the LDL receptor and HMG-CoA reductase, two membrane proteins that regulate the plasma cholesterol. *Journal of Lipid Research*, **25**:1450–1461, 1984.

J. L. Goldstein, R. G. W. Anderson, and M. S. Brown. Coated pits, coated vesicles and receptor mediated endocytosis. *Nature*, **279**:679–685, 1979.

J. L. Goldstein, M. S. Brown, R. G. W. Anderson, D. W. Russell, and W. J. Schneider. Receptor-mediated endocytosis: Concepts emerging from the LDL receptor system. *Annual Review of Cell Biology*, **1**:1–39, 1985.

B. C. Goodwin. *Temporal Organization in Cells; A Dynamic Theory of Cellular Control Processes.* Academic Press, London, 1963.

B. C. Goodwin. Oscillatory behaviour of enzymatic control processes. *Advances in Enzyme Regulation*, **3**:425–439, 1965.

J. F. Graadt van Roggen, D. R. van der Westhuyzen, G. A. Coetzee, A. D. Marais, K. Steyn, et al. FH Afrikaner-3 LDL receptor mutation results in defective LDL receptors and causes a mild form of familial hypercholesterolemia. *Arteriosclerosis, Thrombosis, and Vascular Biology*, **15** (6):765–772, 1995.

I. Graham, D. Atar, K. Borch-Johnsen, G. Boysen, G. Burell, et al. European guidelines on cardiovascular disease prevention in clinical practice. Fourth joint task force of the European society of cardiology and other societies on cardiovascular disease prevention in clinical practice. *European Heart Journal*, **28**:2375–2414, 2007.

D. K. Granner and P. A. Weil. Protein synthesis and the genetic code. In R. K. Murray, D. K. Granner, and V. W. Rodwell, editors, *Harper's Illustrated Biochemistry*, chapter 37, pages 365 – 379. McGraw Hill Medical, USA, Twentyseventh edition, July 2006.

J. S. Griffith. Mathematics of cellular control processes I. Negative feedback to one gene. *Journal of Theoretical Biology*, **20**:202–208, 1968.

R. Grima and S. Schnell. A systematic investigation of the rate laws in intracellular environments. *Biophysical Chemistry*, **124**:1–10, 2006.

S. M. Grundy, J. I. Cleeman, C. N. B. Merz, H. Bryan Brewer Jr, L. T. Clark, et al. Implications of recent clinical trials for the national cholesterol education program adult treatment panel III guidelines. *Circulation*, **110**:227–239, 2004.

J. Guckenheimer and P. Holmes. *Nonlinear Oscillations, Dynamical Systems and Bifurcations of Vector Fields*. Springer-Verlag, New York, 1983.

H. J. Harwood Jr and L. D. Pellarin. Kinetics of low-density lipoprotein receptor activity in Hep-G2 cells: Derivation and validation of a Briggs-Haldane-based kinetic model for evaluating receptor-mediated endocytotic processes in which receptors recycle. *Biochemical Journal*, **323**:649–659, 1997.

T. M. Heinonen. Inhibition of acyl coenzyme a-cholesterol acyltransferase : A possible treatment of atherosclerosis? *Current Atherosclerosis Reports*, **4**:65–70, 2002.

A. V. Hill. The combinations of haemoglobin with oxygen and with carbon monoxide I. *Biochemical Journal*, **7**(5):471–480, 1913.

T. L. Hill. *Cooperativity Theory in Biochemistry*. Springer, New York, 1985.

H. H. Hobbs, D. W. Russell, M. S. Brown, and J. L. Goldstein. The LDL receptor locus in familial hypercholesterolemia: Mutational analysis of a membrane protein. *Annual Review of Genetics*, **24**(1):133–170, 1990.

J. D. Horton, J. L. Goldstein, and M. S. Brown. SREBPs : Activators of the complete program of cholesterol and fatty acid synthesis in the liver. *Journal of Clinical Investigation*, **109**(9): 1125–1131, 2002.

B. R. Hunt, R. L. Lipsman, J. M. Rosenberg, and K. R. Coombes. *A Guide to Matlab : For Beginners and Experienced Users*. Cambridge University Press, Cambridge, Second edition, 2006.

W. Insull Jr, M. Koren, J. Davignon, D. Sprecher, H. Schrott, et al. Efficacy and short-term safety of a new ACAT inhibitor, avasimibe, on lipids, lipoproteins, and apolipoproteins, in patients with combined hyperlipidemia. *Atherosclerosis*, **157**:137–144, 2001.

F. J. Isaacs, J. Hasty, C. R. Cantor, and J. J. Collins. Prediction and measurement of an autoregulatory genetic module. *Proceedings of the National Academy of Sciences, USA*, **100**(13):7714 – 7719, 2003.

E. S. Istvan, M. Palnitkar, S. K. Buchanan, and J. Deisenhofer. Crystal structure of the catalytic portion of human HMG-CoA reductase : Insights into regulation of activity and catalysis. *EMBO Journal*, **19**(5):819–830, 2000.

F. Jacob and J. Monod. Genetic regulatory mechanisms in the synthesis of proteins. *Journal of Molecular Biology*, **3**(3):318–356, 1961.

P. J. Jones and D. A. Schoeller. Evidence for diurnal periodicity in human cholesterol synthesis. *Journal of Lipid Research*, **31**(4):667–673, 1990.

S. Kauffman, C. Peterson, B. Samuelsson, and C. Troein. Random Boolean network models and the yeast transcriptional network. *Proceedings of the National Academy of Sciences, USA*, **100** (25):14796–14799, 2003.

S. A. Kauffman. Metabolic stability and epigenesis in randomly constructed genetic nets. *Journal of Theoretical Biology*, **22**(3):437 – 467, 1969.

J. Keizer, J. Ramirez, and E. Peacock-Lopez. The effect of diffusion on the binding of membrane bound receptors to coated pits. *Biophysical Journal*, **47**:79–88, 1985.

G. Kervizic and L. Corcos. Dynamical modeling of the cholesterol regulatory pathway with Boolean networks. *BMC Systems Biology*, **2**:99, 2008.

H. Knoblauch, H. Schuster, F. C. Lust, and J. Reich. A pathway model of lipid metabolism to predict the effect of genetic variability on lipid levels. *Journal of Molecular Medicine*, **78**(9): 507–515, 2000.

Y. Lange, J. Ye, M. Rigney, and T. L. Steck. Regulation of endoplasmic reticulum cholesterol by plasma membrane cholesterol. *Journal of Lipid Research*, **40**:2264–2270, 1999.

L. Liscum and J. R. Faust. Low density lipoprotein (LDL)-mediated suppression of cholesterol synthesis and LDL uptake is defective in Niemann-Pick type C fibroblasts. *Journal of Biological Chemistry*, **262**(35):17002–17008, 1987.

L. Liscum, R. M. Ruggiero, and J. R. Faust. The intracellular transport of low density lipoprotein-derived cholesterol is defective in Niemann-Pick type C fibroblasts. *Journal of Cell Biology*, **108**(5):1625–1636, 1989.

K. L. Luskey and B. Stevens. Human 3-hydroxy-3-methylglutaryl coenzyme A reductase. Conserved domains responsible for catalytic activity and sterol-regulated degradation. *Journal of Biological Chemistry*, **260**(18):10271–10277, 1985.

N. MacDonald. Time lag in a model of a biochemical reaction sequence with end product inhibition. *Journal of Theoretical Biology*, **67**(3):549–556, 1977.

D. Mayer. The circadian rhythm of synthesis and catabolism of cholesterol. *Archives of Toxicology*, **36**:267–276, 1976.

H. H. McAdams and A. Arkin. Stochastic mechanisms in gene expression. *Proceedings of the National Academy of Sciences, USA*, **94**(3):814–819, 1997.

J. S. Millar and C. J. Packard. Heterogeneity of apolipoprotein B-100 containing lipoproteins: what we have learnt from kinetic studies. *Current Opinion in Lipidology*, **9**(3):197–202, 1998.

A. P. Minton. The influence of macromolecular crowding and macromoleculer confinement on biochemical reactions in physiological media. *Journal of Biological Chemistry*, **276**(14):10577–10580, 2001.

D. T. Molowa and G. M. Cimis. Co-ordinate regulation of low density lipoprotein receptor and 3-hydroxy-3-methylglutaryl-CoA reductase and synthase gene expression in HepG2 cells. *Biochemical Journal*, 260(3):731–736, 1989.

J. D. Murray. *Lectures on Nonlinear Differential Equation Models in Biology*. Clarendon Press, Oxford, 1977.

J. D. Murray. *Mathematical Biology I : An Introduction*. Springer-Verlag, New York, Third edition, 2002.

N. B. Myant. *The Biology of Cholesterol and Related Steroids*. William Heinemann Medical Books, London, 1981.

A. Nicoll and B. Lewis. Evaluation of the roles of lipoprotein lipase and hepatic lipase in lipoprotein metabolism: in vivo and in vitro studies in man. *European Journal of Clinical Investigation*, **10**(6):487–495, 1980.

S. O. Olofsson, L. Asp, and J. Boren. The assembly and secretion of apolipoprotein B-containing lipoproteins. *Current Opinion in Lipidology*, **10**(4):341–346, 1999.

T. F. Osborne. Transcriptional control mechanisms in the regulation of cholesterol balance. *Critical Reviews in Eukaryotic Gene Expression*, **5**(3&4):317–335, 1995.

C. J. Packard and J. Shepherd. Lipoprotein heterogeneity and apolipoprotein B metabolism. *Arteriosclerosis, Thrombosis, and Vascular Biology*, **17**:3542–3556, 1997.

C. J. Packard, A. Munro, A. R. Lorimer, A. M. Gotto, and J. Shepherd. Metabolism of apolipoprotein B in large triglyceride-rich very low density lipoproteins of normal and hypertriglyceridemic subjects. *Journal of Clinical Investigation*, **74**(6):2178–2192, 1984.

C. J. Packard, T. Demant, J. P. Stewart, D. Bedford, M. J. Caslake, et al. Apolipoprotein B metabolism and the distribution of VLDL and LDL subfractions. *Journal of Lipid Research*, **41**(2):305–318, 2000.

K. G. Parhofer, P. Hugh, R. Barrett, D. M. Bier, and G. Schonfeld. Determination of kinetic parameters of apolipoprotein B metabolism using amino acids labeled with stable isotopes. *Journal of Lipid Research*, **32**(8):1311–1323, 1991.

E. Peacock-Lopez and J. A. Ramirez. The effect of diffusion on the trapping of membrane-bound receptors by localized coated pits. *Biophysical Chemistry*, **25**(2):117 – 125, 1986.

A. Radhakrishnan, L. P. Sung, H. J. Kwon, M. S. Brown, and J. L. Goldstein. Direct binding of cholesterol to the purified membrane region of SCAP : Mechanism for a sterol-sensing domain. *Molecular Cell*, **15**(2):259–268, 2004.

A. Radhakrishnan, J. L. Goldstein, J. G. McDonald, and M. S. Brown. Switch-like control of SREBP-2 transport triggered by small changes in ER cholesterol : A delicate balance. *Cell Metabolism*, **8**(6):512–521, 2008.

A. V. Ratushny. Mathematical modelling of receptor mediated endocytosis of low density lipoproteins and their degradation in lysosomes. In *Proceedings of the 5th Conference on Bioinformatics of Genome Regulation and Structure*, pages 151–155, Novosibirsk, Russia, 2006. Vol. 2.

T. G. Redgrave. Chylomicron metabolism. *Biochemical Society Transactions*, **32**(1):79–82, 2004.

R. Ross. Atherosclerosis - an inflammatory disease. *New England Journal of Medicine*, **340**:115–126, 1999.

M. Rudling, B. Angelin, L. Stahle, E. Reihner, S. Sahlin, et al. Regulation of hepatic low density lipoprotein receptor, 3-hydroxy-3-methylglutaryl coenzyme A reductase, and cholesterol 7α-hydroxylase mRNAs in human liver. *Journal of Clinical Endocrinology*, **87**(9):4307–4313, 2002.

G. Sanguinetti, N. D. Lawrence, and M. Rattray. Probabilistic inference of transcription factor concentrations and gene-specific regulatory activities. *Bioinformatics*, **22**:2775–2781, 2006.

S. Schnell and T. E. Turner. Reaction kinetics in intracellular environments with macromolecular crowding: simulations and rate laws. *Progress in Biophysics and Molecular Biology*, **85**:235–260, 2004.

I. H. Segel. *Enzyme Kinetics. Behavior and Analysis of Rapid Equilibrium and Steady State Enzyme Systems*. Wiley-Interscience, USA, 1993.

L. A. Segel, editor. *Modelling Dynamic Phenomena in Molecular and Cellular Biology*. Cambridge University Press, Cambridge, 1984.

K. Simons and E. Iknonen. How cells handle cholesterol. *Science*, **290**:1721–1726, 2000.

L. I. Slobin. Polypeptide chain elongation. In H. Trachsel, editor, *Translation in Eukaryotes*, chapter 6, pages 149 – 176. CRC Press, Boca Raton, Florida, First edition, July 1991.

J. R. Smith, T. F. Osborne, J. L. Goldstein, and M. S. Brown. Identification of nucleotides responsible for enhancer activity of sterol regulatory element in low density lipoprotein receptor gene. *Journal of Biological Chemistry*, 265(4):2306 – 2310, 1990.

P. Smolen, D. A. Baxter, and J. H. Byrne. Effects of macromolecular transport and stochastic fluctuations on dynamics of genetic regulatory systems. *American Journal of Physiology: Cell Physiology*, **277**(4):C777–790, 1999.

R. Somogyi and C. Sniegoski. Modelling the complexity of genetic networks: understanding multigenic and pleiotropic regulation. *Complexity*, **1**:45–63, 1996.

A. K. Soutar and B. L. Knight. Structure and regulation of the LDL-receptor and its gene. *British Medical Bulletin*, **46**(4):891–916, 1990.

J. Stamler, D. Wentworth, and J. D. Neaton. Is relationship between serum cholesterol and risk of premature death from coronary heart disease continuous and graded? Findings in 356 222 primary screenees of the multiple risk factor intervention trial (MRFIT). *Journal of the American Medical Association*, **256**(20):2823–2828, 1986.

L. Stryer, J. M. Berg, and J. L. Tymoczko. *Biochemistry*. W.H.Freeman, USA, 2002.

I. Tabas. Free cholesterol-induced cytotoxicity. A possible contributing factor to macrophage foam cell necrosis in advanced atherosclerosis lesions. *Trends in Cardiovascular Medicine*, **7** (7):256–263, 1997.

I. Tabas. Lipids and atherosclerosis. In D. E. Vance and J. E. Vance, editors, *Biochemistry of Lipids, Lipoproteins and Membranes*, chapter 21, pages 579–604. Elsevier Science, Amsterdam, Fifth edition, 2008.

A. R. Tall. Plasma high density lipoproteins. Metabolism and relationship to atherogenesis. *Arteriosclerosis, Thrombosis, and Vascular Biology*, **86**(2):379–384, 1990.

R. D. Tanaka, P. A. Edwards, S. F. Lan, E. M. Knoppel, and A. M. Fogelman. Purification of 3-hydroxy-3-methylglutaryl coenzyme A reductase from human liver. *Journal of Lipid Research*, **23**(4):523–530, 1982.

R. K. Tangirala, W. G. Jerome, N. L. Jones, D. M. Small, W. J. Johnson, et al. Formation of cholesterol monohydrate crystals in macrophage-derived foam cells. *Journal of Lipid Research*, **35**: 93–104, 1994.

G. A. Truskey, C. K. Colton, and P. F. Davies. Kinetic analysis of receptor mediated endocytosis and lysosomal degradation in cultured cells. *Annals of the New York Academy of Sciences*, **435**: 349–351, 1984.

S. M. Vallett, H. B. Sanchez, J. M. Rosenfeld, and T. F. Osborne. A direct role for sterol regulatory element binding protein in activation of 3-hydroxy-3-methylglutaryl coenzyme A reductase gene. *Journal of Biological Chemistry*, **271**(21):12247 – 12253, 1996.

M. M. J. van Greevenbroek and T. W. A. de Bruin. Chylomicron synthesis by intestinal cells in vitro and in vivo. *Atherosclerosis*, **141**(Suppl. 1):S9–S16, 1998.

N. B. Vargas, B. Y. Brewer, T. B. Rogers, and G. M. Wilson. Protein kinase C activation stabilizes LDL receptor mRNA via the JNK pathway in HepG2 cells. *Journal of Lipid Research*, **50**(3): 386–397, 2009.

J. A. D. Wattis, B. O'Malley, H. Blackburn, L. Pickersgill, J. Panovska, H. M. Byrne, and K. G. Jackson. Mathematical model for low density lipoprotein (LDL) endocytosis by hepatocytes. *Bulletin of Mathematical Biology*, **70**:2303–2333, 2008.

A. D. Waxman, A. Collins, and D. P. Tschudy. Oscillations of hepatic delta-aminolevulinic acid synthetase produced by heme. *Biochemical and Biophysical Research Communications*, **24** (5):675 – 683, 1966.

H. S. Wiley and D. D. Cunningham. The endocytotic rate constant. A cellular parameter for quantitating receptor mediated endocytosis. *Journal of Biological Chemistry*, **257**(8):4222–4229, 1982.

H. S. Wiley and C. D. D. A steady state model for analyzing the cellular binding, internalization and degradation of polypeptide ligands. *Cell*, **25**(2):433–440, 1981.

G. M. Wilson and R. G. Deeley. An episomal expression vector system for monitoring sequence specific effects on mRNA stability in human cell lines. *Plasmid*, **33**(3):198–207, 1995.

World Health Organisation. The World Health Report 2002. Reducing Risks, Promoting Healthy Life, 2002. [online] `http://www.who.int/whr/2002/en/whr02_en.pdf`.

T. Yang, P. J. Espenshade, M. E. Wright, Y. Daisuke, Y. Gong, et al. Crucial step in cholesterol homeostasis: Sterols promote binding of SCAP to INSIG-1, a membrane protein that facilitates retention of SREBPs in ER. *Cell*, **110**(4):489–500, 2002.

P. L. Yeagle. Modulation of membrane function by cholesterol. *Biochimie*, **73**:1303–1310, 1991.

F. Yuan, S. Weinbaum, R. Pfeffer, and S. Chien. A mathematical model for the receptor mediated cellular regulation of the low density lipoprotein metabolism. *Journal of Biomechanical Engineering*, **113**:1–10, 1991.